UNIVERSITY OF LIVERPOOL

Characterising mesothelial cell cultures derived from the murine omentum

This thesis is submitted in accordance with the requirements of the University of Liverpool for the degree of Doctor in Philosophy

November 2016

Sumaya Dauleh

Declaration

This thesis is the result of my own work. The material contained within this thesis has not been presented, nor is it currently being presented wholly, or in part, for any other degree or qualification.

Sumaya Dauleh

This research was undertaken at the Department of Cellular and Molecular Physiology at the University of Liverpool.

Contents

Glossary of common abbreviations

AtMCs Adipose tissue derived mesothelial cells
Bmi1 Proto-Oncogene, Polycomb Ring Finger
Bra Brachyury
Cdh1 E-cadherin
CFDA SE Carboxyfluorescein diacetate succinimidyl ester
d Days
Dmp1 Dentin matrix protein
E/M state Intermediate state
eControl Whole embryonic rudiment control
EGF Epidermal growth factor
EGFR Epidermal growth factor
EGFRi Epidermal growth factor inhibitor
EMT Epithelial to mesenchymal transition
E-state Epithelial state
FCS Fetal calf serum
Gapdh Glyceraldehyde 3-phosphate dehydrogenase
GFP Green fluorescent protein
h Hours
Krt8 cytokeratin 8
MCs Mesothelial cells
MM Metanephric mesenchyme
MMT mesothelial to mesenchymal transition
mRNA Messenger ribonucleic acid
Msln Mesothelin
M-state Mesenchymal state
OMC Omentum cultures
OMT Omentum tissue
Pax2 Paired Box 2
PD Peritoneal dialysis
PDE Peritoneal dialysis effluents
PMCs Pleural mesothelial cells
PNA Peanut agglutinin
PPARγ Peroxisome proliferator-activated receptor
rControl Reaggregated rudiment control
RPMCs Rat peritoneal mesothelial cells
siSnail2 siRNA Snail2
Six2 SIX Homeobox 2
siZeb1 siRNA Zeb1
siZeb1+2 siRNA Zeb1 + Zeb2
siZeb2 siRNA Zeb2
Sox2 SRY (Sex-Determining Region Y)-Box 2 Protein
Sox9 SRY (Sex-Determining Region Y)-Box 9 Protein
Sparc Secreted Protein Acidic And Cysteine Rich
TGF-β Transforming growth factor β
TβRI Transforming growth factor β receptor I
TβRi Transforming growth factor β receptor I inhibitor
TβRII Transforming growth factor β receptor II
UB ureteric bud
UtMCs uterine derived mesothelial cells
Vim Vimentin
Wt1 Wilms tumor 1
ZO1 zona occuldens protein 1
αSMA α smooth muscle actin

Abstract

Mesothelial cells have been described to possess progenitor characteristics and contribute to regeneration through differentiation. However, it is not clear what the effects of prolonged culture have on the mesothelial cell properties and relative plasticity; as long-term cultures have not yet been established as a result of early senescence. Understanding the effects of time in culture is crucial for the development of novel therapies.

In this thesis, we demonstrated that mesothelial cell cultures isolated from murine omentum could be cultured for more than 40 passages and showed relatively stable population doubling times. While initially, the cells did down-regulated the expression of mesothelial markers *Wilm's tumor protein 1* (*Wt1*) and *mesothelin* and epithelial genes; their mesenchymal profile was maintained. This along with the increased *Snail2* expression suggested the cells were progressing through the mesothelial to mesenchymal (MMT) transdifferentiation programme. TGF-β and more recently EGF are known mediators of MMT. Targeting signalling through these receptors with small molecule inhibitors LY364947 and PD153035, slowed the rate of gap closure, *in vitro* and increased zonula occludens 1 accumulation at cell-cell contacts. Which seemed to be mediated through the MEK5/ERK5 pathway. Furthermore, siRNA-mediated transient knockdown of Zeb1 and Zeb2 transcription factors also achieved attenuated the rate of migration.

Next, we moved onto to accessing the progenitor properties of the mesothelial cells with time in culture. The expression of stem cells markers *Bmi1* (*Proto-Oncogene, Polycomb Ring Finger*), *Sox9* ((*Sex Determining Region Y*)-*Box 9*) and *CD34* were

downregulated with repeated passaging. However, the low passage mesothelial cells exhibited clonogenicity and could differentiate into osteoblasts and adipocytes. Finally, in an embryonic kidney rudiment assay, we could show that the mesothelial cells co-existed with the embryonic kidney cells and allowed renal structures to form in their presence.

Ultimately, we have demonstrated that the mesothelial cells from the omentum maintain some mesothelial characteristics with prolonged culturing. The cells showed clonogenic and multi-lineage potential and expressed a number of stem cell genes. The MMT programme is complex and could be partly reversed by targeting TGF-βR1 and EGFR tyrosine kinases, which along with transiently silencing the Zeb transcriptional factors seem likely key targets in ameliorating pathological fibrosis.

Chapter 1 Introduction

Synopsis

The mesothelium is a monolayer of mesothelial cells that line the surface of internal organs, and cavity walls. As well as having roles in providing a frictionless barrier and immunomodulatory functions, studies have also suggested that mesothelial cells have progenitor properties. They have been shown to transdifferentiate from a more epithelial state to a myofibroblastic cell via a phenomenon known as mesothelial to mesenchymal transition and aid in the wound healing process. Furthermore, mesothelial cells have been demonstrated to have the ability to differentiate along other cell lineages including osteocytes and adipocytes. These multipotential properties may be advantageous in treating debilitating fibrosis and sclerosis that arise from insult to the mesothelium induced through surgical and non-surgical methods. In the third chapter, we will address the effects of culturing on mesothelial characteristics. Then in the fourth chapter of this thesis will attempt to address the progenitor properties of mesothelial cells and the influence of cell passage on these characteristics. Before finally presenting work which aimed to elucidate the regulatory MMT networks that control the status of the mesothelial cells. The findings from this thesis could help develop strategies that could harness the regulatory MMT networks.

This chapter will provide an overview of the current literature on aspects relevant to the subsequent experiments described in the forthcoming chapters. Particular emphasis will be placed on the relation between mesothelial progenitor properties and their contribution to regeneration and development within *in vitro* and *ex vivo* settings. We will also review relevant literature on the cellular and molecular mechanisms that contribute to wound repair following insult to mesothelium with

emphasis on the role of MMT in modulating this and evidence for its pathological contributions.

1.1 Mesothelium structure and functions

1.1.1 Morphology of the mesothelium

The mesothelium is a membrane composed of a monolayer of specialized epithelial-like mesothelial cells that are situated on a thin basement membrane and line the walls of the coelomic cavities (pleural, pericardial, and peritoneal) and the surfaces of visceral organs (Figure 1.1) (Herrick and Mutsaers, 2004, Lua and Asahina, 2016).

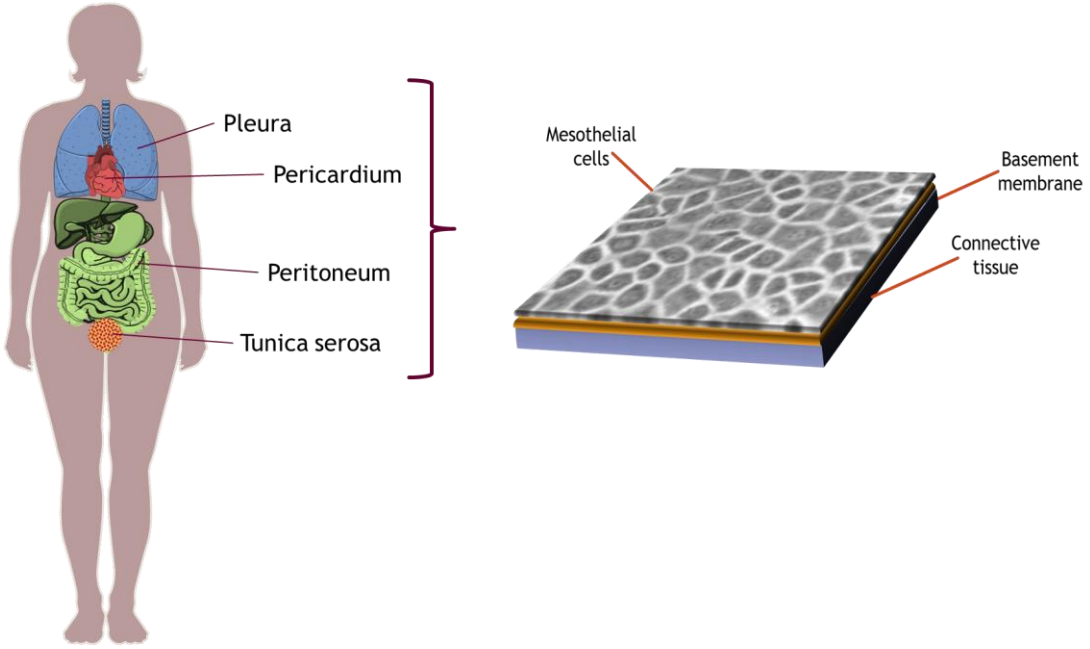

Figure 1.1 Mesothelial membrane. The mesothelium is composed of a monolayer of epithelial-like cells that sit on a thin basement membrane and line the surfaces of internal organs and cavity walls.

Microscopically, mesothelial cells from different serosal sites and different mammalian species are considered morphologically similar (Lachaud et al., 2015, Herrick and Mutsaers, 2004). However, ultrastructurally the mesothelial cells located at the parietal and visceral sites differ (Mutsaers and Wilkosz, 2007, Lachaud et al., 2015). The parietal mesothelium lining the coelomic cavities are a flattened sheet of larger mesothelial cells and have a lower abundance of intracellular organelles (Mutsaers et al., 2015). By contrast, the mesothelial cells located on the visceral organs (visceral mesothelium), are more densely compacted and have a higher intracellular organelle content which suggests a more active metabolic cell state (Mutsaers and Wilkosz, 2007, Lachaud et al., 2015). The differences between the visceral and the parietal mesothelial cells are summarized in table 1.1.

Table 1.1: A summary of the ultrastructural differences between the visceral and parietal mesothelial cells (Michailova et al., 1999, Yung and Chan, 2007)

	Visceral mesothelium	Parietal mesothelium
Overall Morphology	Cuboidal	Flatter, longer cells
Nucleus	Rounded	Elongated
Mitochondria	+++++	++
RER (Rough endoplasmic reticulum)	+++++	+
Golgi body	Well developed	Poorly developed
Vesicles	++++	++
Microfilaments	+++++	+++
Metabolic cell state	Active	Resting

1.1.2 Mesothelial cell barrier function

Previously, the mesothelium was postulated to just function as a protective barrier against abrasions and provide a frictionless surface for intracoelomic movement (Lachaud et al., 2015, Lua and Asahina, 2016, Mutsaers and Wilkosz, 2007). The mesothelium maintains the lubricated non-adhesive barrier through its ability to secrete surfactants, proteoglycans, and glycosaminoglycans that are electrochemically entrapped between their microvilli (Lachaud et al., 2015, Mutsaers et al., 2015)

However, the mesothelium is now recognized as having more diverse physiological functions (Mutsaers and Wilkosz, 2007). It serves as a semi-permeable membrane barrier that maintains homeostatic osmolarity and ionic activity between the fluid filled serosal cavities and the blood vessels and lymphatic systems that run in the submesothelial connective tissues. This function is mediated through the presence of aquaporin (AQP) and transmembrane ATPase pumps (Lachaud et al., 2015, Mutsaers and Wilkosz, 2007, Yung and Chan, 2007). Whereby the knockout of AQP1 in mice showed significantly reduce transcellular water transport (Zhang et al., 2016).

1.1.3 Mesothelial cells modulate inflammation

The mesothelium is also the first line of defense for the serosa from insult induced by surgery, and continuous exposure to bio-incompatible and infectious agents (Herrick and Mutsaers, 2007). Mesothelial cells have the capacity to modulate inflammation through immunosuppressive mechanisms and the ability to recruit innate immune cells (Eigenbrod et al., 2008a, Lachaud et al., 2015). For example, in response to IL-1α stimulation released by neighboring necrotic cells, the mesothelial

cells secrete CXCL1, a neutrophil recruiting chemokine, through the activation of the IL-1R/MyD88/NFκB (interleukin 1 receptor/ Myeloid differentiation primary response gene 88/ nuclear factor-kappaB) pathway (Eigenbrod et al., 2008a). Mesothelial cells have also been demonstrated to modulate the pro-inflammatory response by suppressing the proliferation of γδ T cells through the secretion of TGF-β (transforming growth factor β) (Lin et al., 2013).

Finally, a new player in the modulation of mammalian immunity has emerged. Arginase-1 is an enzyme that metabolizes L-arginine to L-ornithine and its presence is associated with the suppression of T cell responsiveness as well as increasing tissue regeneration (Kitayama et al., 2014, Munder, 2009). CD90+/CD45- mesothelial cells derived from peritoneal fluid highly expressed this enzyme and significantly reduced T cell proliferation, *in vitro* (Kitayama et al., 2014).

Overall mesothelial cells show the capacity to ameliorate and contribute to inflammatory-induced fibrosis following insult from infectious agents, trauma and chemical agents (Mutsaers and Wilkosz, 2007, Yung and Chan, 2007). The mechanisms by which this is orchestrated are diverse and complex and are summarized in table 1.2.

Table 1.2: A summary of the proteins secreted by mesothelial cells in regulation of inflammation

Molecules	Stimulus	Biological function	Reference
Cytokines			
IL-1α/β	LPS, TNF-α, IL-1α	Amplification of the initial inflammatory response regulates growth and cytokine release by mesothelial cells	(Douvdevani et al., 1994)
IL-6	Peritoneal dialysis effluents (PDE) effluents , IL -1β and IL-1α	Promotes of B-cell differentiation and immunoglobulin production and is a reliable predictor of peritoneal solute transport rate	(Witowski et al., 1996, Cho et al., 2014)
IL-15	PD effluents , IL-2 and IFN-γ	A potent T-cell activator (CD4+, CD8+, and B and natural killer cells)	(Hausmann et al., 2000)
Chemokines			
IL-8	PDE, TNF-α, IL-1β, IFN-γ	Leukocyte chemotaxis during peritonitis	(Topley et al., 1993, Man et al., 2003)
MCP-1			
RANTES			
CXCL1	PDE, IL-1α	Neutrophil recruitment via IL-1R/MyD88	(Eigenbrod et al., 2008b)
Growth Factors			
TGF-β	IL-1β	Master regulator of fibrosis	(Offner et al., 1996)
bFGF	IL-1β	Promotes PAI-1 expression which functions to suppress fibrinolysis	(Cronauer et al., 1999)
HB-EGF	IL-1, TNF-α	Promotes mesothelial cell migration and adhesion through MMT and therefore has a role in fibrosis	(Faull et al., 2001)
HGF	Autocrine secretion	Promotes mesothelial cell motility and proliferation during wound repair	(Warn et al., 2001)
ECM Molecules			
Collagen I	PDE, IL-1 β, IL-13, TNF-α, EGF, PDGF, TGF-β	Laid down during tissue remodelling process by ECM producing myofibroblasts. They are markers of fibrosis	(Strippoli et al., 2016)
Collagen III			
Collagen IV			
Fibronectin			
Elastin			
Vitronectin			

1.1.4 Mesothelial cell response to injury

Soft tissue repair is essentially composed of four overlapping phases; bleeding, inflammation, proliferation and remodelling (Foley-Comer et al., 2002b). Under physiological conditions in the serosa, there is a fine balance between fibrin deposition and breakdown and the mesothelial cells are known contributors to fibrinolysis (Mutsaers et al., 2015). The mesothelium is the main source of tPA (tissue plasminogen activator) in the serosa (Eigenbrod et al., 2008a, Lin et al., 2013). tPA activates the serine protease plasmin that in turn degrades fibrin (Falk et al., 2000, Rougier et al., 1998). An imbalance in the fibrinolysis through the presence of inflammatory mediators TGFβ, TNFα and IL-1 promote serosal adhesions by depleting tPA mRNA and protein levels and stimulating plasminogen activator inhibitor-1 expression in mesothelial cells resulting in increased overall fibrin deposition (Falk et al., 2000, Rougier et al., 1998). The mesothelial cells also contribute to the deposition of a number of extracellular matrix (ECM) molecules that have important roles in serosal membrane function and repair (Herrick and Mutsaers, 2004, Mutsaers et al., 2015). The rate of ECM deposition can be further stimulated by the presence of peritoneal effluents and a number of growth factors and cytokines highlighted in table 1.2 (Herrick and Mutsaers, 2004, Mutsaers et al., 2015). Moreover, the turnover of ECM is regulated by mesothelial cells through the synthesis of matrix-degrading metalloproteinase (MMPs) and tissue inhibitors of metalloproteinases (TIMPs) (Mutsaers et al., 2015). A more detailed description of the role of mesothelial cells in injury and disease is provided later, in the context of molecular mechanisms (section 1.4).

As well as synthesizing and releasing a number of proteases, basement membrane molecules and signaling factors to aid repair to the serosa; free floating mesothelial also contribute to the wound healing process through implantation and proliferation (Foley-Comer et al., 2002b). Using a testicular thermal injury rat model, labeled mesothelial cells were injected into the wounded serosa and monitored for incorporation 3, 5 and 8 days post-injury through confocal imaging. The mesothelial cells showed evidence of implantation and proliferation in the serosa through the expression of the tight junction-associated protein, zonula occludens-1 (ZO1) and proliferating cell nuclear antigen (Foley-Comer et al., 2002b). Similarly, Chen and colleagues showed through inducible genetic fate mapping that the injured peritoneum was repaired and replaced by intrinsic surviving Wt1-RFP^{+} mesothelial cells, and not by submesothelial fibroblasts (Chen et al., 2014).

1.2 Mesothelial to mesenchymal transition

Mesothelial cells originate from the mesoderm however they show characteristics analogous to both mesenchymal and epithelial cells (see figure 1.3) (Foley-Comer et al., 2002b). Recent evidence suggests that the mesothelial cells can undergo phenotypic changes following activation from an epithelial-like state to a more mesenchymal morphology in a process similar to EMT (epithelial to mesenchymal transition) and EndMT (endothelial to mesenchymal transition). The process has been coined mesothelial to mesenchymal transition (MMT) in mesothelial cells (Liu et al., 2015, Mutsaers et al., 2015). This led to the notion that a population of mesothelial progenitor cells exists within the mesothelium which constitutes the proposed origin of myofibroblasts during organogenesis and peritoneal fibrosis (Lachaud et al., 2015, Liu et al., 2015, Mutsaers et al., 2015).

1.2.1 What is MMT?

MMT is a dynamic cellular process that occurs during development, tissue repair, fibrosis and metastasis (Liu et al., 2015, Pez-Cabrera, 2014). MMT is characterized by the gradual loss of cell-cell adhesion networks through the repression of adherence and tight junctional proteins; E-cadherin (Cdh1) and ZO1 respectively (Liu et al., 2015, Mutsaers et al., 2015). This, in turn, results in mesothelial cell detachment from the basal lamina and a loss in apical-basal cell polarity and a gain in front-back polarity following cytoskeletal rearrangement (Liu et al., 2015, Mutsaers et al., 2015). The end result is a Vim/ αSMA expressing transdifferentiated myofibroblastic mesothelial cell with migratory and invasive capacity (Liu et al., 2015, Mutsaers et al., 2015) (Figure 1.2).

MMT is activated by a diverse number of proangiogenic and morphogenic growth factors (TGFβ, EGF, bFGF and PDGF-bb) and by exposure to bio-incompatible peritoneal dialysis (PD) fluids through receptor-mediated signaling (Liu et al., 2015, Mutsaers et al., 2015). These, in turn, activate a plethora of intracellular signaling effectors that orchestrate mesothelial transdifferentiation (Pez-Cabrera, 2014) (Figure 1.2).

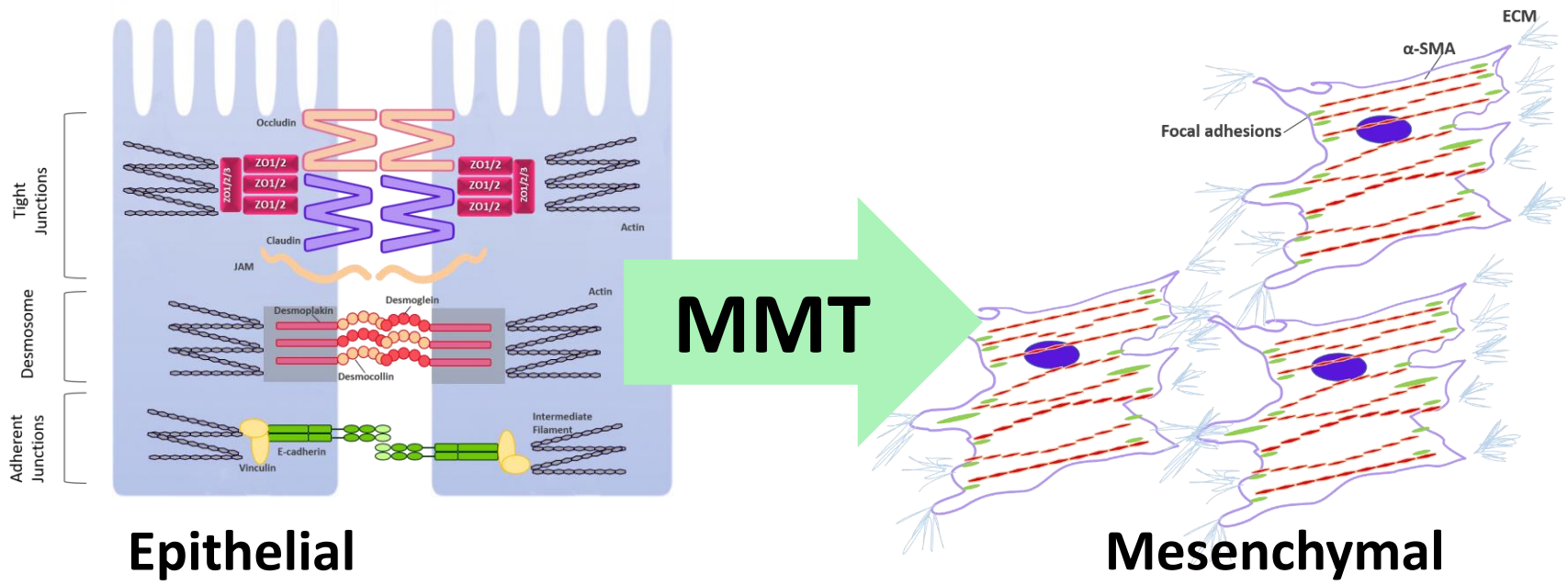

Inducers of MMT	Proteins Activated	Proteins Upregulated	Proteins Downregulated	Cellular Changes
• TGF-β • EGF • IL-1 • IL-6 • HB-EGF • HGF	• MAPK • PI3-K • NFκB • Smad2/3	• αSMA • Vim • Cdh2 • Snail1/2 • Twist1 • Zeb1/2 • Fibronectin • Collagen I/III • MMP2/9 • PAI-1	• Cdh1 • Cytokeratins • Claudins • Occludins • Desmoplakins • ZO1 • tPA	• Gain a front back polarity • Increased migration and invasion • Reduced fibrinolysis • Increased ECM deposition

Figure 1.2: A summary of the biochemical and morphological changes associated with MMT following stimulation.

1.2.2 MMT spectrum

Mesothelial cells isolated from peritoneal effluents have revealed that MMT is not a binary process, rather it houses a whole spectrum of intermediate cell states that simultaneously co-express epithelial and mesenchymal characteristics at varying degrees (Figure 1.3) (Lee et al., 2014, Zhang et al., 2013, Li and Kang). It also rarely results in the complete loss of epithelial genes (Lee et al., 2014, Zhang et al., 2013, Li and Kang). Yáñez-Mó and colleagues described three MMT state phenotypes; epithelial-like (E-state), intermediate (E/M state) and fibroblastic-like (M-state), in mesothelial cells isolated from the effluents of peritoneal dialysis patients (Yáñez-Mó et al., 2003). The length of exposure to PD fluids (dwelling time) seemed to influence the relative progression through the MMT (Lee et al., 2014). Patients exposed to PD >6 months had significantly lower Cdh1 and higher Vim, fibronectin and collagen 1 protein and mRNA expression compared to patients that had just started PD treatment (Zhang et al., 2013). Logistic regression analysis further supported these findings and showed that persistent PD treatment for 24 h induced the highest rate of full MMT, characterized by reduced *Cdh1*mRNA and protein (Lee et al., 2014).

Moreover, the MMT spectrum was also reported in healthy mesothelial cells derived from adipose and uterine tissues (Lachaud et al., 2014, Lachaud et al., 2013). Over the course of the 15 d culture period in a high glucose medium supplemented with EGF, the mesothelial cells initially showed a cobblestone-like morphology and accordingly expressed high intercellular levels of β-catenin, ZO1 and E-cadherin (Lachaud et al., 2014, Lachaud et al., 2013). By 3 – 5 d the mesothelial cells displayed transitional E/M morphologies characterized by disrupted ZO1 localization and

increased WT1 and αSMA expression (Lachaud et al., 2014, Lachaud et al., 2013). At 15 d the cells adopted the M-state phenotype and that was consistent with increased expression of αSMA and Vim and a reduction in all epithelial and mesothelial markers including Wt1 and mesothelin (Lachaud et al., 2014, Lachaud et al., 2013). These gradual changes in the protein and mRNA expression are summarized in figure 1.3.

Mesothelial cell phenotypes

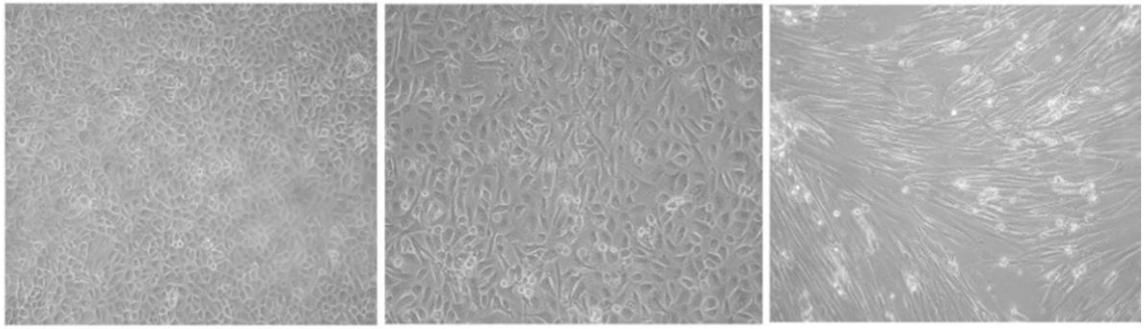

Biochemical marker expression	E state	E/M state	M state
E-cadherin	+++	+	-
Cytokeratin	+++	++	+/-
ZO1	+	++	+/-
β-Catenin	++	+++	+
Fibronectin	+/-	+	+++
Vimentin	+	++	+++
α Smooth muscle actin	-	+/-	+++
Collagen 1	+/-	+	+++
Snail1	-	+/-	+++
Wt1	+	++	-
Mesothelin	++	+++	+

Figure 1.3: MMT spectrum of transitory states. The MMT transdifferentiation programme produces cells that reside in a spectrum of intermediate states, where they progressively lose epithelial genes and gradually gain mesenchymal features. These intermediate states are associated with plasticity (MMT transitionary mesothelial cells images were taken from (Abelardo Aguilera, 2013, Lachaud et al., 2014, Lachaud et al., 2013).

The E/M state of EMT provides relative benefits over complete transdifferentiation into a myofibroblastic cell, as it allows cells to move collectively and is a hallmark of tissue remodeling during embryonic development, wound repair and metastasis (Jolly et al., 2015b, Savagner, 2015). This increases the efficiency of epithelial cell migration as it removes the need for all cells to identify and respond to an external stimulus (Jolly et al., 2015b, Savagner, 2015).

The E/M phase has also been associated with stemness (Jolly et al., 2015b, Savagner, 2015). Lachaud and colleagues showed through RT-PCR and western blotting that UtMCs transiently upregulated the expression of stem and progenitor genes Nanog, Sox2 and c-Kit during the E/M phase of MMT, and this expression was reduced once the cells had fully differentiated into myofibroblasts (Figure 1.4A-C) (Lachaud et al., 2013). Overall the E/M state is a developing concept that still needs to be better characterized in mesothelial cells (Figure 1.4D).

MMT is also reversible (mesenchymal to mesothelial transition) during the early stages of transdifferentiation when the MMT signal is removed or through the presence of a number of signaling and scaffolding proteins (Vargha et al., 2006, Pez-Cabrera, 2014). When E-state and M-state mesothelial cells were cultured for 7 days in the presence of MMT-inducing TGF-β or the antifibrotic cytokine bone morphogenic protein 7 (Bmp7), respectively, they showed a reversal in cell morphologies (Vargha et al., 2006). Furthermore, transfection with an adenoviral BMP-7 vector or treatment with BMP-7 peptide reversed the M-state morphology and attenuated peritoneal fibrosis in animal models of PD (Yu et al., 2009). Moreover, HGF (hepatocyte growth factor) treatment protected the peritoneum from PD-

induced damage by counteracting TGF-β1 signaling (Yu et al., 2009, Loureiro et al., 2010, Liu et al., 2015). Caveolin 1 (Cav1) has recently been identified as a regulator of MMT (Strippoli et al., 2015). This putative scaffolding protein has diverse physiological functions, including the regulation of cholesterol homeostasis, cell adhesion, and vesicular trafficking. $Cav1^{-/-}$ mice showed thickened peritoneal membranes, increased fibrosis and heightened activation of the Mek-Erk1/2-Snail1 pathway, under both basal and peritoneal dialysis treated conditions (Strippoli et al., 2015). Overexpression of Cav1 protein in HPMC isolated from the effluents of PD patients reversed MMT (Strippoli et al., 2015).

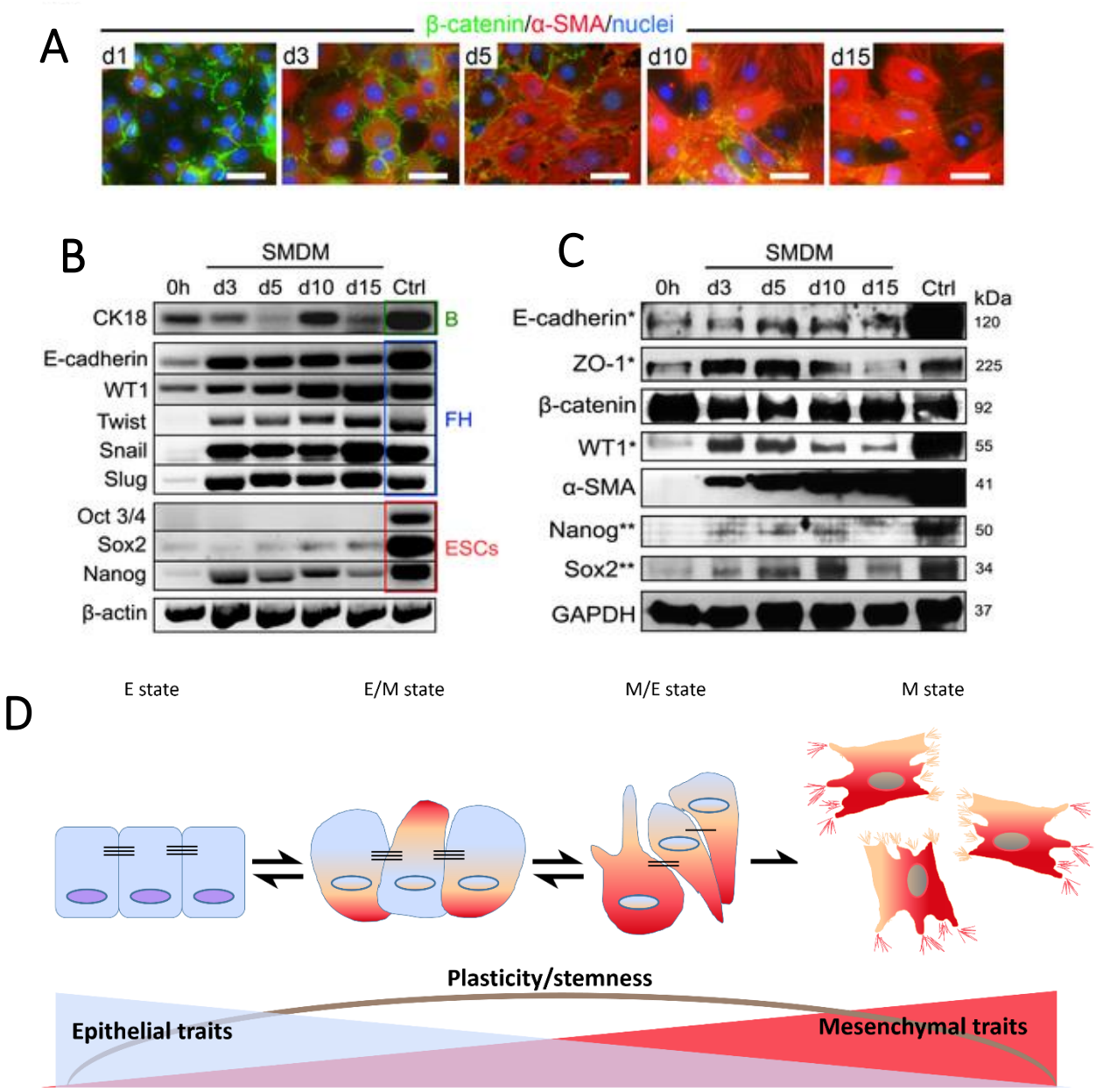

Figure 1.4: UtMCs cultured in smooth muscle differentiating medium transdifferentiate via MMT and temporally upregulate stem/ progenitor markers. A) Time course staining showing the gradual gain in αSMA and loss of β-catenin as the cells progress through the MMT program. B) RT-PCR products analysis and C) western blot analysis of time course study for mesothelial (cytokeratin-18 (CK-18), WT1, E-cadherin), MMT (Twist, Snail, Slug) and pluripotent (Oct 3/4, Sox2, Nanog) marker. During the MMT programme the UtMCs temporally upregulated the expression of Sox2, Nanog, and Wt1. D) MMT is not a binary process and the E/M and M/E states are associated with stemness (Figure A-C was taken from (Lachaud et al., 2013).

1.3 Signalling pathways regulating MMT

TGF-β and EGF initiate downstream signaling events through their own respective receptors, however, recent reports show that many of the downstream components of their signaling pathways may be shared (Figure 1.5) (Jia and Souchelnytstkyi, 2011). Understanding the mechanisms by which TGF-β and EGF interact to induce MMT is important for the development of the reversal of pathological MMT.

1.3.1 TGF-β induced MMT

TGF-β is regarded as the master molecule of the fibrotic process in all organs as it is the main signaling pathway activated and perpetuated during the wound healing process (Strippoli et al., 2016). Therefore its involvement in the promotion of MMT is not surprising. The TGF-β ligand exerts its functions by binding to the constitutively active TGF-β receptor II (TβRII) which subsequently recruits, and activates the type I receptor (TβRI/ ALK5) (Xu et al., 2009, Strippoli et al., 2016). The activated TβRI then mediates downstream signaling through serine/ threonine kinase activity, by binding and phosphorylating members of the Smad and non-Smad signaling proteins (Xu et al., 2009, Strippoli et al., 2016).

The TGF-β/Smad signaling cascade induces MMT following phosphorylation of Smad2 and/or Smad3 signaling mediators. These form a heteromultimeric complex with Smad4 and translocate into the nucleus where to directly bind DNA and activate downstream gene targets that act to repress Cdh1 and upregulate αSMA/ Vim expression (Xu et al., 2009, Strippoli et al., 2016). Biopsies from patients receiving continuous ambulatory peritoneal dialysis (CAPD) showed sub-mesothelial thickening and increased TGF-β/Smad2/3 signaling (Duan et al., 2014). However, the roles of Smad2 and Smad3 in MMT differ (Xu et al., 2009). The peritoneum of Smad3

knockout mice was resistant to fibrosis following prolonged treatment with peritoneal dialysis effluents (Duan et al., 2014). Similarly, Smad3 deficient peritoneal mouse cells also showed resistance to MMT following TGF-β stimulation (Duan et al., 2014). In contrast, the transient knockdown of Smad2 promoted MMT by upregulating αSMA and collagen I expression and repressing Cdh1 in a time-dependent manner. It also resulted in exacerbated fibrosis in Smad2 conditional knockout mice (Duan et al., 2014).

While the Smad protein complexes can directly regulate MMT alone, their activity is low in comparison to other transcription factors (Heldin et al., 2012, Strippoli et al., 2016). Rather the majority of their EMT/MMT regulatory transcriptional activity occurs in tandem with other MMT- transcription factors (MMT-TF), co-activators and co-repressors (Heldin et al., 2012, Strippoli et al., 2016). Therefore, the Smad signaling pathway is not the only means for TGF-β induced MMT (Javelaud and Mauviel, 2005). Pathways including the mitogen-activated protein kinase (MAPK)(Xu et al., 2003), NFκB and the phosphoinositide 3- kinase (PI3K/ AKT) pathways are also activated by TGF-β in mesothelial cells and can also modulate MMT alone, through cross-talk with Smad signalling , or by converging onto Smad proteins to regulate their activity (Javelaud and Mauviel, 2005, Derynck et al., 2014).

MAP kinases are a family of serine/threonine kinases that mediate downstream transcriptional activity in response to extracellular signals through a cascade of phosphorylation events (Javelaud and Mauviel, 2005). There are four major groups of MAPKs that are associated with MMT (Javelaud and Mauviel, 2005, Derynck et al., 2014). These include the extracellular signal-regulated kinases 1/2 (ERK1/2 or p42/44

MAPK), ERK5 (big MAPK), p38 MAPKs and the c-Jun N-terminal kinases/stress-activated protein kinases (JNK/SAPKs) (Javelaud and Mauviel, 2005, Son et al., 2011). Each of these MAPK cascades involves at least three tiers of kinases phosphorylation events: MAP3K which activates MAP2K that in turn phosphorylates and activates MAPK to finally modulate target gene expression (Son et al., 2011, Gui et al., 2012).

The ERK1/2 signaling cascade is the major pathway involved in promoting mitogenesis, differentiation, cell survival and, if dysregulated, cell transformation (Son et al., 2011, Gui et al., 2012). Upon binding of the TGF-β ligand to its receptors, Shc/Grb2/Sos/Ras complexes are recruited and assembled on the TβRI platform (Son et al., 2011, Gui et al., 2012). The GTP-binding protein Ras subsequently activates and recruits Raf kinase which in turn activates and recruits MAPK/ERK kinase 1 (MEK1) and MEK2, which are the upstream activators of ERK1/2 respectively (Son et al., 2011, Gui et al., 2012).

The JNK and the P38 MAPK pathways are activated in response to stress signals (such as pro-inflammatory cytokines, ultraviolet radiation, and reactive oxygen species) and mediate apoptosis and in some cell systems proliferation and differentiation (Son et al., 2011, Gui et al., 2012). JNK members are activated by MKK4/MKK7 that in turn are substrates for TAK1. This kinase also activates MKK3/6 kinases that are upstream MAP2K activators p38 MAPK (Son et al., 2011, Gui et al., 2012). Finally TGF-β ligands have recently been shown to activate ERK5 through the phosphorylation of MKK2/3 that then activate MEK5 a specific MAP2K for ERK5, with downstream roles in stabilizing Snail1 expression and therefore enhancing EMT in hepatocytes (Gui et al., 2012, Marchetti et al., 2008, Browne et al., 2008).

Perhaps the best-characterized interactions between TGF-β and MAPK signalling in mesothelial cells are the JNK and p38 MAPK cascades (Liu et al., 2008). *In vitro* stimulation of rat, peritoneal mesothelial cells (RPMCs) with TGF-β activated both JNK and Smad2/3 proteins 5 and 10 minutes post-treatment respectively and induced MMT (Liu et al., 2008). The use of SP600125, a small molecule inhibitor of JNK, prevented TGF-β induced Smad3 activation and effectively suppressed the high expression of αSMA and collagen I, and prevented the downregulation in Cdh1 (Liu et al., 2008).

Conversely, the p38 MAPK was described as a gatekeeper of MMT in human omentum-derived mesothelial cells (Strippoli et al., 2010). The loss of p38 either through the use of pharmacological inhibitors (SB203580 and BIRB796) or shRNA, knockdowns resulted in upregulated TAK1-NFκB signaling that in turn resulted in the loss of Cdh1 and the upregulation in the mesenchymal marker Vim (Strippoli et al., 2010). Furthermore, p38 MAPK activation was shown to promote Snail1 expression and Twist1 repression (Strippoli et al., 2010).

ERK1/2 signaling has been shown to play an important role in driving the TGF-β response towards MMT (Strippoli et al., 2008, Jin et al., 2016). Pre-treatment of rodent and human mesothelial cells in U0126, an inhibitor of MEK1/2 prevented TGF-β IL-1β/IL-6 induced MMT, by decreasing NFκB translocation into the nucleus and Snail1 expression (Strippoli et al., 2008, Jin et al., 2016). Furthermore, the *ex vivo* culture of mesothelial cells isolated from the PD effluents in U0126 restored the epithelial phenotype of the mesothelial cells (Strippoli et al., 2008). Some studies

have indicated that ERK1/2 may be capable of regulating the Smad signaling pathway by activating Smad2 (Jin et al., 2016).

The role in ERK5 modulating the epithelial cells remodeling and transdifferentiation has only recently been shown (Drew et al., 2012). ERK5 was required for the expression of Snail2 in human keratinocytes, and its loss decreased the gap closure rate in a wound healing assay (Arnoux et al., 2008). TGF-β is thought to mediate ERK5 activation through the activation of Raf, as Raf overexpression increased MEK5 signaling (Drew et al., 2012). Hepatocytes treated with TGF-β showed Snail1 stabilization through ERK5 mediated inactivation of GSK3β signaling (Marchetti et al., 2008). Silencing ERK5 enhanced Akt/GSK3β signaling and Snail1 expression, in turn, promoting EMT (Chen et al., 2012). Finally collagen I synthesis by mesangial cells is regulated by ERK5 activation (Dorado et al., 2008). While the role ERK5 plays in modulating MMT has not been described it would, however, seem that ERK5 may antagonize ERK2 induced MMT signaling, which could have implications in mesothelial cell regulation of MMT (Derynck et al., 2014).

1.3.2 EGF-induced MMT

In many epithelial cells and mesothelial cells, EGF has been demonstrated to induce EMT/MMT through its receptor tyrosine kinases, by activating downstream MAPKs, with the Ras–Raf–MEK–ERK and the MEK5-ERK5 MAPK pathways being the most activated. *In vitro* culture of UtMCs cultured in EGF for 15d promoted MMT and gave rise to functioning vascular smooth muscle cells (Lachaud et al., 2013). Adipose tissue derived mesothelial cells (AtMCs) also showed MMT capacity in the presence of EGF for 15d, since EGF stimulation resulted in the phosphorylation of AKT, ERK1/2, and

Smad-2 (Lachaud et al., 2014). In a rodent model of peritoneal fibrosis induced by chlorhexidine gluconate treatment, the administration of Gefitinib, selective inhibitor of EGFR tyrosine kinase, post injury halted fibrosis development and progression; and in vitro quashed TGF-β induced MMT (Marchetti et al., 2008). Gefitinib mediated its anti-MMT effects by decreasing overall EGFR, Smad3 and NFκB phosphorylation (Marchetti et al., 2008). Taken together it seems that EGF can augment epithelial cell differentiation into myofibroblasts in the presence of TGF-β.

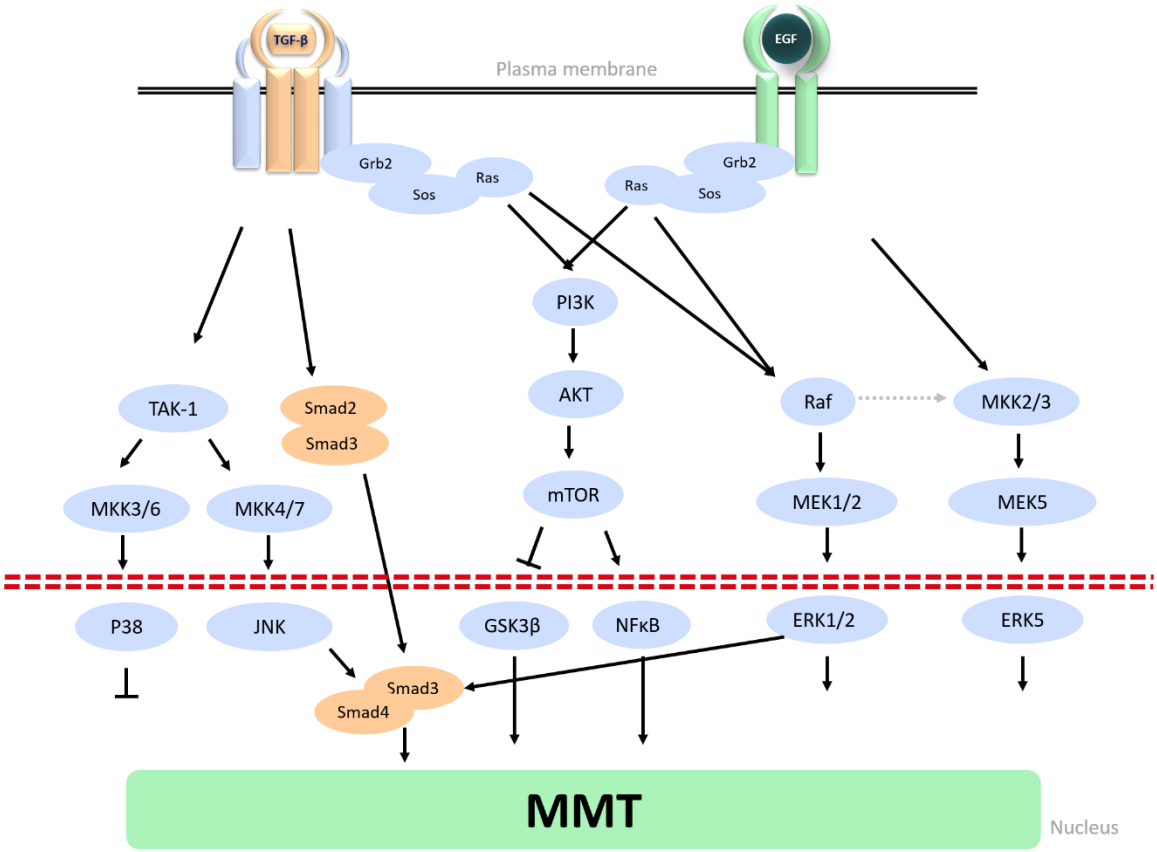

Figure 1.5: Intracellular cross-talk between TGF-β and EGF signaling pathways. The MAPK and PI3K/Akt pathways are linkers of TGF-β and EGF-mediated MMT. MAPKs and Akt modulate MMT either by directly modulating MMT associated genes or indirectly through R-Smad activity.

1.3.3 MMT transcription factors

Downstream of the signaling pathways, the process of MMT is tightly controlled by three transcription factor (MMT-TF) families; the Snails (Snail1 and Snail2), Zebs (Zeb1 and Zeb2) and basic helix-loop-helix (bHLH) transcription factors (Twist1) (Lamouille et al., 2014). These master regulators are activated early on in the MMT pathway, and therefore have central roles in the transdifferentiation of mesothelial cells (Lamouille et al., 2014). Specifically, these transcription factors are activated in a hierarchical manner, whereby the Snail TFs are the first to be induced, and they can cooperate with Twist to activate Zeb expression (Hugo et al., 2011, Garg, 2013). This is important for maintaining the mesenchymal phenotype as Snail proteins were shown to have relatively short half-lives (Lamouille et al., 2014, Hugo et al., 2011).

Snail transcription factors

The Snail superfamily of transcriptional repressors are essential for complete gastrulation during development, whereby the loss of these EMT modulators is embryonic lethal (Carver et al., 2001). In adult mesothelial cells, both Snail1 and Snail2 mediate MMT by transcriptionally repressing the expression of E-cadherin (Strippoli et al., 2008, Jang et al., 2013, Morishita et al., 2016). However, the forced expression of E-cadherin alone is not enough to reverse the mesenchymal phenotype back to an epithelial morphology, suggesting that these transcription factors also act on other epithelial gene targets. Both Snail1 and Snail2 were shown to also target cytokeratins (Strippoli et al., 2008) and occludins (Morishita et al., 2016) and in other cells, they have been demonstrated to upregulate the expression of vimentin (Vim) and fibronectin (Nieto, 2002, Garg, 2013).

Snail1 and Snail2 show differential expression patterns in cases of peritoneal dialysis and TGF-β induced MMT, suggesting that they play different roles in MMT which could be associated with the difference in the binding affinities of these MMT-TF to target genes (Loureiro et al., 2011, Villarejo et al., 2014).

Twist1 transcription factor

Twist 1 has been documented to be upregulated in the mesothelial cells isolated from the peritoneal effluents of patients undergoing PD (Li et al., 2012). Furthermore, the overexpression of Twist1 in mesothelial cells *in vitro*, induced full MMT (He et al., 2015). Twist1 can mediate EMT and MMT alone and in combination with other transcription factors (He et al., 2015, Zhang and Klymkowsky, 2009). Twist1 induces epithelial cells to transdifferentiate into myofibroblasts by binding of its bHLH domain to the E-cadherin E-box promoter (Garg, 2013). Twist1 and Snail2 were shown to be functionally linked both in development and metastasis, whereby the loss of *Snail2* to a decrease in *Twist1* mRNA level and vice versa (Zhang and Klymkowsky, 2009). Twist1 was also demonstrated to bind to Snail2 E-box promoter and activates its expression (Casas et al., 2011, Zhang and Klymkowsky, 2009). The loss of TWIST1 in human peritoneal mesothelial (HPMCs) treated in high glucose medium inhibited MMT and the overexpression promoted it (He et al., 2015).

Zeb transcription factors

The Zeb (zinc finger E-box-binding homeobox) transcription factors have been shown to mediate epithelial transdifferentiation by targeting and repressing E-cadherin expression at the E-box promoter (Garg, 2013). Several studies have identified that Zeb transcription factors are significantly upregulated in malignant pleural

mesotheliomas (MPM) that show hallmarks of MMT through the downregulation of epithelial genes and upregulation of vimentin and fibroblast-specific marker 1 (FSP1 or S100A4) (Fassina et al., 2012, Merikallio et al., 2013). Targeting the knockdown of just ZEB1 alone was not enough to suppress proliferation and reverse MMT (Horio et al., 2011). Rather studies that targeted and suppressed both ZEB1 and ZEB2 with miR-205 reversed the MMT phenotype back to an epithelial cell morphology and also inhibited migration and invasion (Fassina et al., 2012). These results suggested that both proteins need to be targeted for effective reversal of MMT (Reid, 2015, Horio et al., 2011).

The expression of these MMT-TF in mesothelial cells is context specific (Liu et al., 2008). Compared to Snail1, Snail2 is only weakly activated, while Twist1 is not induced following stimulation with TGF-β1 (Strippoli et al., 2016). The pharmacological inhibition of Smad3, MEK/ERK1/2, and NFκB signaling molecules downregulates Snail1 expression in rodent peritoneal mesothelial cells (Duan et al., 2014, Jin et al., 2016, Strippoli et al., 2010, Strippoli et al., 2008). Whereas the inhibition of p38 parallels Snail inhibition in MCs, where the induction of Twist is observed (Strippoli et al., 2010). A summary of the MMT-TF functions during MMT progression are collated in table 1.3.

Table 1.3: MMT is driven by Snail, Twist1, and Zeb transcription factors. The MMT-TF are activated through Smad-dependent and -independent pathways and act to repress epithelial genes and upregulate mesenchymal genes.

	Induction	Repression	Regulatory Signaling Pathways
Snail1/2	• Twist1 • Zeb1/2 • Cdh2 • Fibronectin • Collagen	• Cdh1 • Cytokeratins • Claudins • Occludins • Desmoplakins	• TGF-β-Smad3 • PI3K-AKT • EGF • NFκB • bFGF
Twist1	• Cdh2 • Fibronectin • SPARC	• Cdh1 • Claudins • Occludins • Desmoplakins	• MAPK
Zeb1/2	• Cdh2 • MMPs	• Cdh1 • ZO1	• TGF-β-Smad3 • Ras-MAPK

1.4 The role of MMT in disease

Mesothelial cells are a source of fibrogenic cells that arise as a result of aberrant pro-MMT signalling during serosal inflammation, pleural and peritoneal fibrosis and adhesion formation (Strippoli et al., 2016, Batra and Antony, 2015).

1.4.1 Peritoneal dialysis induced fibrosis

PD is a form of renal replacement therapy for patients with end-stage renal failure (Leypoldt, 2002). It takes advantage of the semi-permeable membrane function of the peritoneum which separates the fluid-filled cavities from the capillaries. PD fluids are introduced into the abdomen via a catheter and uremic toxins are replaced by electrolytes and small molecules (Leypoldt, 2002). The high glucose concentration present in the PD fluids drives osmotic pressure for ultrafiltration. Meanwhile, solutes are exchanged by diffusion and absorption (Leypoldt, 2002). At the end of the PD treatment, the fluids are drained and disposed (de Lima et al., 2013, López-Cabrera, 2014) However, long-term exposure to the bio-incompatible PD fluid agents (low pH, high glucose and lactate) results in peritoneal damage and subsequently dialysis induced fibrosis (Akira Onishi, 2011, Strippoli et al., 2016). Peritoneal fibrosis develops in most patients within 2 years of treatment and is associated with increased peritoneal membrane thickness, reduced mesothelial cell viability, the loss of the mesothelial monolayer and eventually the complete loss in the membrane ultrafiltration capacity (Akira Onishi, 2011, Strippoli et al., 2016). The histological examination of peritoneal tissue biopsies taken from patients and mice exposed to PD identified myofibroblastic cells in the fibrotic tissue (Strippoli et al., 2015, Margetts et al., 2005). Lineage tracing studies showed that mesothelial cells which were triggered to undergo MMT contributed to fibrosis following their invasion into

the sub-mesothelial stroma (Chen et al., 2014). A number of pro-MMT signalling factors are secreted as a result of peritoneal wounding that contributes to peritoneal fibrosis. As discussed earlier, TGF-β1 is a known master molecule in the induction of fibrosis in several tissues and organs and has also been shown to be upregulated in the effluents of patients diagnosed peritoneal fibrosis (Gangji et al., 2009). Further evidence to support the role of TGF-β in mediating peritoneal fibrosis comes from Margetts and colleagues who showed that transient overexpression of TGF-β gene in the intraperitoneal membrane significantly increased expression of MMT related genes including collagen type I, αSMA and Snail1, and induced fibrosis (Margetts et al., 2005). Furthermore, peritoneal fibrosis was inhibited through the delivery of TGF-β1-siRNA-nano particle complex or by TGF-β1 blocking peptides in mice that were receiving PD fluids (Yoshizawa et al., 2015, Loureiro et al., 2011). Recently the growth factor EGF that has already established roles in promoting EMT in other tissue types was also shown to promote MMT (refer to section 1.3.2 for more details) and as a result induce peritoneal fibrosis through cross-talk with TGF-β between Smad3 and NFκB signalling cascades (Wang et al., 2015).

1.4.2 Pleural fibrosis

Pleural fibrosis is progressive irreversible lung disorder that is characterized by the presence of localized lesions and diffuse thickening and fibrosis in the pleural membrane (Batra and Antony, 2015). The alterations in the pleural cavity are the result of increased deposition of ECM components and the increased presence of αSMA expressing myofibroblasts (Batra and Antony, 2015, Zolak et al., 2013). A number of agents including exposure to tuberculosis effusions, radiation, and

inhalation of inorganic particles such as talc and asbestosis fibres are known to induce pleural fibrosis (Batra and Antony, 2015, Zolak et al., 2013).

Human and mouse derived pleural mesothelial cells (PMCs) were demonstrated to transdifferentiate via MMT into myofibroblasts *in vitro* in response to TGF-β stimulation via Smad-dependent and independent pathways (Nasreen et al., 2009, Zolak et al., 2013, Batra and Antony, 2015). These mesenchymal mesothelial cells showed increased αSMA, NADPH oxidase 4 and fibroblast-specific protein-1 expression, higher contractility, haptotaxis, and increased production of ECM component, collagen I (Nasreen et al., 2009, Zolak et al., 2013, Batra and Antony, 2015). Furthermore, histological analysis of TGF-β induced pleural fibrosis revealed that GFP-labelled PMCs injected into the pleural space trafficked into the lungs following their transformation into αSMA expressing myofibroblasts (Zolak et al., 2013). Moreover, WT1 and mesothelin-expressing human PMCs were found in the fibrotic lesions of idiopathic pulmonary fibrosis lung explants (Mubarak et al., 2012, Zolak et al., 2013).

1.4.3 Liver fibrosis

The liver parenchyma is covered by a monolayer of squamous mesothelial cells that have active roles in liver development and fibrosis (Lua and Asahina, 2016). Liver fibrosis is defined by scarring following excessive fibrin deposition (Lua and Asahina, 2016). This is brought about by excessive alcohol consumption, hepatitis infections, cirrhosis and obesity (Lua and Asahina, 2016). Under basal conditions mouse liver mesothelial cells expressed high levels of mesothelin, Wt1, podocalyxin-like protein 1 (Podxl), uroplakin 1b and epithelial and mesenchymal genes Krt8, Krt19 and Vim

respectively (Li et al., 2013b, Lua et al., 2016). Furthermore, they showed poor Cdh1 and Snail1 expression (Li et al., 2013b). In a carbon tetrachloride (CCl_4) and bile duct ligation models of liver injury, GFP-tagged liver mesothelial cells transformed into αSMA expressing myofibroblasts and invaded the liver (Lua et al., 2016). *In vitro* treatment of liver-derived mouse mesothelial cells for 4 days with TGF-β, induced MMT and as a consequence upregulated collagen 1 synthesis, through phosphorylation of Smad3 (Li et al., 2013b). Targeting the TGF-β signalling pathway with pharmacological inhibitors against Smad3, TGF-β receptor II (TGF-βRII) or conditional knockouts for this receptor blocks MMT induction in mesothelial cells (Li et al., 2013b, Li et al., 2016, Lua et al., 2015).

1.4.4 Postoperative adhesions

Postoperative adhesions manifests as fibrous tissue bands that form between the opposing tissues and organs following insult from surgery, ischemia, and infections (Lua and Asahina, 2016, Jin et al., 2016). It is a common disorder that affects up to 93% of patients that have undergone abdominopelvic surgery and can cause small bowel obstruction in two-thirds of patients, chronic pelvic pain, infertility in women and repeat hospital admission (Lua and Asahina, 2016, Jin et al., 2016). The mesothelium synthesizes and secretes lubricants that mediate anti-adhesive functions between abdominal viscera (Lua and Asahina, 2016, Jin et al., 2016). Trauma to the mesothelium lining the liver was shown to provoke mesothelial cells denudation from the opposite intact liver lobe. That in turn induced fibrin deposition and adhesion formation between the liver lobes (Suzuki et al., 2015).

1.5 Plasticity and translational potential of mesothelial cells

Developmentally, mesothelial cells contribute to the vasculature of the forming heart, liver, intestine and lungs by transdifferentiating into vascular smooth muscle, possibly via MMT (Wilm et al., 2005, Que et al., 2008, Zhou et al., 2008, Asahina et al., 2011, Rinkevich et al., 2012). The potential to give rise to the mural part of the vasculature is maintained in adult mesothelial cells (Lachaud et al., 2013, Kawaguchi et al., 2007). *In vitro* UtMCs transdifferentiated into functional vascular smooth muscle-like cells that expressed the contractile cell marker smoothelin-B, following stimulation (Lachaud et al., 2013). Furthermore, both adult human and rodent mesothelial cells were capable of differentiating along the osteocyte, adipocyte and chondrocyte lineages following stimulation in inductive medium (Lansley et al., 2011, Lachaud et al., 2014, van Tuyn et al., 2007). *In vivo* lineage tracing also supported this, by showing Wt1 expressing adult mesothelium that lined the visceral fat depots were the progenitor source of adipocytes (Chau et al., 2014).

Due to this reported capacity, a number of studies have attempted to harness this regenerative potential *in vivo.* The transplantation of mesothelial cell sheets on to a fibrotic peritoneum contributed to the regeneration of the peritoneal surface within 3 days (Hekking et al., 2003). Furthermore, activated omentum that was wrapped around rat kidneys that had undergone 5/6 nephrectomy, slowed the rate of chronic kidney disease and Wt1-expressing cells were shown to contribute to repair (Garcia-Gomez et al., 2014). Moreover, transplantation of genetically modified mesothelial cells that over-expressed proteins critical for wound repair also contributed positively to the wound healing process (Nagy et al., 1995). However, recent studies have shown the contrary, where mesothelial cell transplantation actually aggravated the inflammatory response, further promoting tissue damage through the increased

secretion of pro-inflammatory factors TGF-β, VEGF and MMP-2 (Kanda et al., 2014). The MMT state of mesothelial cell influences therapeutic outcome (Kitamura et al., 2014). E-state and M-state cells were transplanted into the peritoneal cavity of previously injured mice (Kitamura et al., 2014). The E-state cells attenuated peritoneal membrane thickening and adhesion formation, contrary to the M-state cells (Kitamura et al., 2014).

Taken together mesothelial cell transplantation by direct injection or via a matrix grafting have therapeutic potential. Also, the availability of a number of mesothelial cell sources (including the omentum, mesenteric membranes and peritoneal effluents) and the advantages of autologous transplantation are what make mesothelial cells an ideal source of cells for transplantation therapies (Kanda et al., 2014, Kitamura et al., 2014, Mutsaers et al., 2015). Nevertheless, a clearer understanding of the mechanisms regulating MMT and a better understanding of mesothelial cell plasticity are necessary factors for the development of novel therapeutic strategies.

1.6 Thesis aims

Based on this we wanted to further explore the plasticity and MMT regulatory networks of mesothelial cells in culture. To do this we aimed to address the following points:

1) Assess the effect of repeated passaging on mesothelial cell characteristics, including MMT state and differentiation potential
2) Characterise mesothelial cell progenitor properties by studying stem cell gene expression and assessing clonogenic potential

3) Study the potential contribution of mesothelial cells to kidney development using an *ex vivo* embryonic kidney rudiment assay
4) Determine the role of EGF and TGF-β in controlling the E/M state of mesothelial cells

Chapter 2: Materials and methods

2.1 Dissection of embryos, tissues, and organs

2.1.1 Animal Husbandry

Animal handling and experimentation were conducted in accordance with the UK Home Office under the Animal (Scientific Procedures) Act, 1986. CD1 female mice at 6-12 weeks of age (Charles River, Margate, UK) were housed in ventilated environment chambers, with a 12 hour (h) light-dark schedule and free access to food and water. Animals were culled by asphyxiation with an automated CO_2 chamber, followed by cervical dislocation to confirm death.

2.1.2 Dissection of tissues and organs from adult mice

Animal coats were sprayed with 70% ethanol to reduce hair dispersion during subsequent steps. The abdominal cavity was exposed and the stomach and spleen complex were harvested into DMEM medium supplemented with 10% FCS and 1% penicillin and streptomycin (v/v). The omentum was carefully freed under a stereoscopic microscope (Leica MZFLIII) using Dumont fine scissors and fine forceps, size 5 (Dumont, Switzerland). Any residual blood vessels and fat droplets were removed. For the establishment of mesothelial cell lines, the tissue was compacted and cut into smaller fragments using disposable scalpels, size 11 (12387999, Fisher Scientific) and seeded into 35 mm dishes (D7804, Nunc) containing fresh standard full growth medium (FGM) (see section 2.15.1). Approximately 8 to 13 explants were routinely isolated from one omentum tissue and on average 90% of the explants attached from which mesothelial cells moved out within 48 h.

For RNA isolation the freshly cleaned omental tissue was placed into TRIzol® Reagent (see section 2.12.1). For RNA extraction from kidneys and gonadal white adipose

tissues, the organs were harvested using sterilized stainless steel fine forceps and scissors and processed as described (section 2.12.1).

2.1.3 Dissection of embryonic kidney rudiments

Kidney rudiments were isolated and dissociated from CD1 mouse embryos at embryonic day 13.5 (E13.5) based on the Unbekandt and Davies (2010) protocol. For this, adult time mated CD1 mice (8-12 weeks old) were sacrificed by asphyxiation and the uterine horns were transferred into ice-cold MEME (M5650, Sigma) supplemented with 1% FCS (v/v). Using fine forceps (Dumont) the embryos were cleaned from extra-embryonic membranes and decapitated. The caudal parts were transferred into fresh ice cold 1% FCS MEME medium. The rudiments were isolated by turning the caudal part onto its dorsal side and cutting down the sagittal plane under a stereoscopic microscope (MZFLIII, Leica). The rudiments dissected using this protocol were either cultured *in vitro* or re-aggregated with labeled MCs, following dissociation for the chimeric rudiment assay (see section 2.10.1) or samples were subjected to RNA extraction (section 2.12.1).

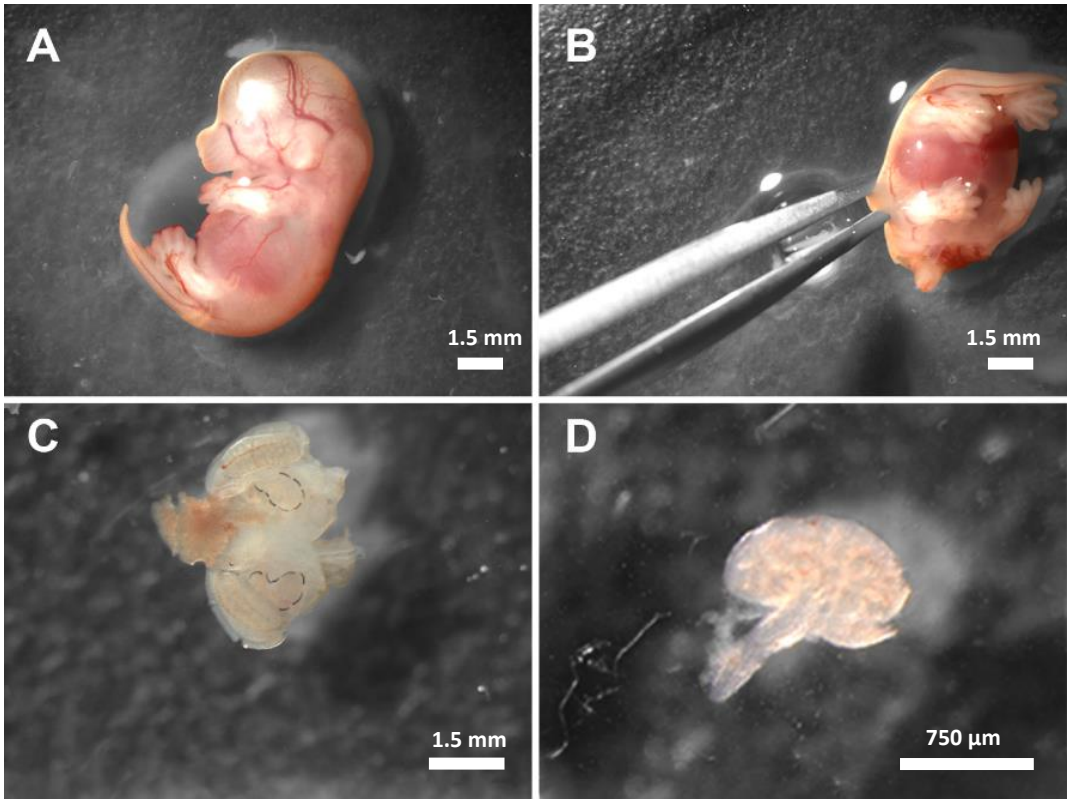

Figure 2.1: Kidney rudiment dissection from mouse embryos at embryonic day 13.5. A. E13.5 embryo isolated from the uterine horns of the CD1 mothers. B. Following decapitation, the embryos were turned over and the kidneys were isolated from the back of the caudal parts. C, D. The kidney rudiments (highlighted) were separated from the gonads

2.2 Primary cells and stem cell lines

2.2.1 Primary Mesothelial cells isolation and establishment

Following the attachment of the omentum explants to the tissue culture dish, the standard growth medium was carefully replaced, with fresh medium provided every 3-4 days. Radial outgrowths of mesothelial cells could be seen as early as 24 hours post seeding. Culturing the explants for a period greater than 14 days resulted generally in the loss of epithelial features and the appearance of a large, flattened, terminally differentiated fibroblastic phenotype. To generate stable primary mesothelial cell cultures, the explants and outgrowths were rinsed in $CaCl_2$ and $MgCl_2$ free Dulbecco's phosphate-buffered saline (DPBS, D8537, Sigma) and dissociated in 500 µl of trypsin (10x trypsin, T4174, Sigma) for 30 minutes, at 37°C with gentle agitation every 10 minutes (min). Once the cells had detached, the cell suspension in trypsin was added to 3.5 ml of fresh standard growth medium and equally distributed into 4 wells of a 12 well plate (BC011, Corning). The cells were left to attach overnight and the medium was changed the next day and subsequently replaced every 2-3 days with conditioned media (section 2.15.2). A homogeneous population of mesothelial cells with cobblestone appearance was usually achieved at passage 4 (P4) and at this point the cells could reach up to 80-90% confluence and be passaged into a larger dish (section 2.3.1). During the course of this project, twelve mesothelial cell lines were generated from independent biological samples with similar phenotypes. The data presented in this study were from 3 independent lines unless otherwise stated.

Established mesothelial cells were routinely subcultured every 3-4 days when they had reached 80-90% confluence.

2.2.2 Mesenchymal stem cells

The mouse mesenchymal stem cell (MSC) line D1 (ORL UVA [D1] (ATCC® CRL-12424)) was selected as a positive control for assessment of mesodermal lineage differentiation, due to their multipotential properties. The cells were maintained in standard growth medium (section 2.15.1) and were passaged at 70% confluence (section 2.3.1). The D1 cells were used between passages 19 and 32.

2.2.3 H6 clonal kidney stem cell line

The mouse kidney stem cell (KSC) line H6, is a clonally derived cell line from the kidneys of 2-6 day old neonate CD1 pups. This cell line was established by Dr. Cristina Mora (2009) and kindly gifted to us from the Murray lab. The cells were included as a positive control for stem cell gene profiling and comparison. The cells were also maintained in standard growth medium (section 2.15.1) and sub-cultured at 80% confluence. The H6 clonal lines were used between passages 21 and 24.

2.3 Routine tissue culture techniques

The cells used in this study were of mouse origin and were cultured in a humidified environment at 37°C with 5% CO_2.

2.3.1 Cell passaging

The same passaging protocol was used on all the adherent cells used in this study. The culture medium was aspirated off the cells and residual medium and debris were washed away in DPBS (D8537 Sigma). Next, the cells were incubated in an appropriate trypsin-EDTA (10x trypsin, T4174, Sigma) volume to cover the cells for 30 seconds (s) to 5 min at 37°C in a humidified environment. Gentle tapping of the tissue culture dishes was used at regular intervals to encourage cell detachment. To

neutralize the trypsin solution, 5 ml of pre-warmed standard culture medium was added to the dishes. The cell solution was transferred to a 15 ml centrifuge tube (188271, Greiner Bio-One) and cells were pelleted at 1000 rpm for 5 min. Following on from this, the supernatant was removed, the cell pellet was re-suspended in 1 ml of pre-warmed standard culture medium (section 2.15.1) and cells were counted twice in an automated cell counter (TC20™, BioRad) using the trypan blue (T8154, Sigma) exclusion assay. The H6 KSCs and MSCs were split at a 1:5 ratio, meanwhile the mesothelial cells were passaged at a higher ratio of 1:6 to 1:10 due to their fast-growing nature.

2.3.2 Cell freezing protocol

The cells in this study were frozen down using standard protocols. In short, the cell medium was aspirated and the cells were washed once with DPBS to remove debris. Following the described passaging protocol (see section 2.3.1) the cells were trypsinized, pelleted and counted. The cell medium solution was once again pelleted at 1000 rpm and the supernatant was discarded. For every $1x10^6$ cells, 1 ml of freezing solution (section 2.15.5) was added and transferred into 2 ml cryovials (BC163, Corning) and left to slowly freeze down overnight at -80°C in a freezing container (5100-0001, ThermoFisher Scientific). The cryovials were transferred into liquid nitrogen containers for long-term storage.

2.3.3 Cell thawing protocol

To limit cell death during the thawing procedure, the cryovials were quickly transferred from the liquid nitrogen tanks into a 37°C water bath, where they were continuously agitated to speed the process of cell thawing. For every 1 ml of cells in

freezing solution, 10 ml of pre-warmed cell growth medium was pipetted into a 100 mm dish (430167, Corning). The cells were pipetted in a drop by drop fashion into the culture medium and were left to adhere overnight in standard culture environments. The medium was replaced the following day to remove the traces of dimethyl sulfoxide (DMSO, D8418 Sigma).

2.4 Generation of Mesothelial Cell clones

Mesothelial cell clones (MC clones) were generated by standard dilution cloning assays. P5 mesothelial cells were pelleted and counted following the outlined protocols (section 2.3.1). The starting cell density was $2x10^3$ cells, which were serially distributed across the 96 well plate (4616-7008, Nunc) using a multichannel pipette (F14403, GILSON). The next morning, the wells which contained single cell colonies were scored and had their medium replaced with fresh pre-warmed conditioned media. The medium was changed every 3-4 days and the clonal cells were sub-cultured into a 48 well plate once they had reached 90% confluence. The clonal cells were maintained in conditioned medium for a further passage until they were transferred into a 100 mm dish (430167, Corning) where they were maintained in standard culture medium. Three clonally derived cell lines were generated from independent biological samples. The process was imaged using an inverted microscope (TS100-F, Nikon Eclipse).

2.5 Population doubling Studies

2.5.1 Trypan blue exclusion study

P4 mesothelial cells were the earliest passage assessed for the cell doubling time due to the heterogeneous nature of the cells at earlier passages. The cells for this study were trypsinized at 90% confluence, counted using the trypan blue (T8154, Sigma)

and seeded at a density of $6x10^5$ in a 100 mm dish (664160, Greiner Bio-One). The population doubling time (PDT) was calculated by dividing the time in culture (t) by the log of the cell number at the end of the experiment (N1) over the log of the cell number at the start of the incubation (N0): PDT = t*ln(2)/(ln(N1)-ln(N0)). The experiment was repeated three times (n=3).

2.5.2 Cytokinetics analysis by CCK-8

Mesothelial cells at P7 – P12 were seeded in triplicates, in 24 well plates at $2.5x10^2$, $5.0\ x10^3$, $1.0x10^4$, $2.0x10^4$, $5.0x10^4$, $7.5x10^4$ and $1.0x10^5$ cells per well in 100 µl of media, to generate a standard curve relating to cell and optical density values. The same cells were also seeded at $2.5\ x\ 10^2$ cells/ well density. The samples were assayed at 0, 24 and 48 h to test the effects of the pharmacological small molecule inhibitors on cell viability. In which the standard growth medium was removed and replaced with 100 µl of fresh medium containing 10% CCK-8 solution (96992, Sigma). The cells were incubated in the CCK-8 containing medium for 3 h at 37^oC. Next, the optical density values were measured by transferring 100 µl of the CCK-8 containing cell medium mix to a clean 96 well plate and measuring against a reagent blank at a test wavelength of 460 nm (FLUOSTAR Omega plate reader). From the standard curves, the cell number was extrapolated based on the OD readings. From which PDT was calculated using the same formula stated in section 2.5.1 and the percentage cell viability was derived through PCV = (treated PDT / untreated PDT) *100.

2.6 Mesodermal Differentiation assays

2.6.1 Mesothelial cells

The ability of mesothelial cells to differentiate along the mesodermal lineages was assessed over time by studying early (P5), mid-passage cells (P13) and late passage cells (P26). Due to the cells' highly proliferative nature, they were seeded at 1000 cells/well in a 12 well culture dish (3513, Corning) overnight and stimulated the next day. The adipogenic and osteogenic inductive media (section 2.15.4 and 2.15.5 respectively) were changed every 2-3 days and the cells were sub-cultured for 2 weeks, before either their RNA was harvested (section 2.12.1) or they were stained to identify calcium deposits (section 2.6.3) or fat droplets (section 2.6.4). Each treatment group had its own controls, which were cells sub-cultured in standard growth medium; and each condition for each passage was done as 3 independent biological replicas for both RNA collection and staining.

2.6.2 MSCs

The MSCs are an already established multipotential cell line and were incorporated as positive controls of differentiation. The cells were seeded at 1000 cells/well in a 12 well culture dish (3513, Corning) and left to reach 70% confluence in full growth medium. Next, the cells were treated in the inductive mediums for 7 days, with regular media changes every 2-3 days. The cells were stained for calcium mineral deposits (section 2.6.3) and fat droplets (section 2.6.4) and also had their RNA harvested (section 2.12.1) for mRNA quantification.

2.6.3 Visualization and quantification of mineral deposits through Alizarin red S staining:

At the end of the inductive period, the treated cells and their respective controls were fixed in 4% paraformaldehyde solution in PBS (PFA; P6148, Sigma) for 10 min and stained for 2 min in 2% Alizarin red S solution, pH4.5 (see section 2.16.7). Samples were washed 3 times with 2 ml of double distilled water per well, to remove the excess stain. Positive cultures stained orange-red and mineral deposits were visible with the naked eye. Samples were imaged on the inverted microscope (DM2500, Leica) connected to the DFC350FX camera.

2.6.4 Visualization and quantification of lipid formation through Oil red staining

Following the two-week treatment period in the adipogenic medium, the cells were fixed in 4% PFA and washed twice in 2ml of 60% isopropanol for 5 min at room temperature. The cells were incubated in 1ml of 0.3% oil red solution for 10 min. This was followed by 4 washes in double distilled water for 5 min, before being viewed on Leica DM2500 microscope and imaged DFC350FX camera.

2.7 EMT studies

2.7.1 Small molecule inhibitors and growth factor studies

Mesothelial cells were seeded at $5x10^5$ viable cells per well in a 24 well culture plates for mRNA, western blot, and immunolabelling studies. After the establishment of a cell monolayer at 24 h, the cells were serum starved for 24 h in 1% FCS DMEM medium and then exposed to the agents of interest diluted in the 1% FCS DMEM for a 48 h period (see table 2.1 and 2.2for the list of agents). Treatment conditions applied are denoted in the relevant chapters. In all experimental sets, controls were included of untreated cells cultured in full growth medium and in low serum medium.

Table 2.1: A list of the small molecule inhibitors used in this study.

Product name	Reference throughout the thesis as	Mode of action	Final concentrations	Product details
LY364947	TβRi	A selective, ATP-competitive inhibitor of TGFβ type I receptor kinase	5 – 20 µM	L629, Sigma
PD153035 hydrochloride	EGFRi	A potent and selective ATP-competitive inhibitor of the EGF receptor tyrosine kinase	5 – 20 µM	SML056, Sigma
PD184352	MEKi	A potent and selective non-competitive MEK inhibitor	5 µM	PZ0181, Sigma
Bix02189	MEK5i	Selective MEK5 and ERK5 inhibitor	1.25 – 5 µM	4842, Tocris
XMD8-92	ERK5i	Selective ERK5/BMK1 inhibitor	1.25 – 5 µM	4132, Tocris

Table 2.2: Growth factors used in this study

Product name	Mode of action	Final concentrations	Product details
TGFβ	Role in inducing EMT	50 ng/ml	100-21C, R&D
EGF	Role in augmenting EMT	50 ng/ml	236-EG, R&D

2.7.2 Transient siRNA knockdown of EMT effectors

Cells were seeded in 12 well plates at a density of 8×10^4 cells/well and reached 80% confluence 16 h later. They were transfected with siRNAs at a final concentration of 40 nM using Lipofectamine® 2000 transfection reagent (11668027, ThermoFisher Scientific) in Opti-MEM™ (31985070, ThermoFisher Scientific) according to the manufacturer's instructions. The cells were then cultured for 48 h to allow the knockdown to have full effect. Total RNA was harvested and the relative knockdown levels were calculated against control lipofectamine-treated cells. The siRNAs used were predesigned and purchased from Sigma Mission® siRNA (see table).

Table 2.3: a list of siRNA target sequences

Gene Name	Product Gene ID #	siRNA ID	Target sequences 5' – 3'
Snail2	NM_011415	SASI_Mm01_00143833	GGAUCACAGUGGUUCAGAA UUCUGAACCACUGUGAUCC
Zeb1	NM_011546	SASI_Mm02_00320896	CAUAGUGGUUGCUUCAGGA UCCUGAAGCAACCACUAUG
Zeb2	NM_015753	SASI_Mm01_00062546	GUAUGCAUGUGACUUAUGU ACAUAAGUCACAUGCAUAC

2.8 *In vitro* wound healing assay

2.8.1 Small molecule inhibitors and growth factors studies

Mesothelial cells between passages 13 to 23 were seeded at $4x10^5$ viable cells per well of a 24 well culture plate and serum starved in 1% FCS in DMEM medium for 24 h. To investigate the effect of inhibitors and growth factors on cell migration, cells were pre-treated for the next 24 h in low serum media containing the inhibitors/ growth factors listed in tables 2.1 and 2.2 respectively. Next, the cell layer was gently wounded using a 1 ml tip, and the wells were washed twice with DPBS to remove cell debris. Fresh medium containing the growth factors or inhibitors were added to the cells at 37° C for a further 24 h. Gap closure was imaged at 0, 4 and 12 h using the (DM2500, Leica) microscope and the DFC350FX camera.

2.8.2 *In vitro* wound healing assay in the presence of mitomycin C

To more accurately determine the contribution the growth factors and inhibitors had on cell migration, similar experiments in the presence of the mitomycin C were performed. In brief, $5x10^5$ mesothelial cells were seeded and serum starved as described in section X. The cells were treated with mitomycin C (10 µg/ml) for 4 h and washed 3 times to inhibit cell proliferation. The treatments were added and the cells were incubated for 24 h at 37° C, 5% CO_2. An artificial wound was created with a 1 ml pipette tip at 0 h and unattached MCs were removed by a DPBS wash. Images of the experimental groups were acquired at 0 h, 4 h, 12 h and 24 h, using an inverted light microscope (Leica DMIL).

2.8.3 Wound healing assay on siRNA transfected Cells

Mesothelial cells at 8×10^4 were plated in each well of a 12 well plate. Following overnight incubation, the cells were transfected with 40 nM siRNA for 6 h and then allowed to recover overnight. The cell monolayers were serum starved for 16 h in 1% FCS DMEM and wounded by scraping with a 1 ml tip. They were washed several times with DPBS to remove dislodged cells and placed back in low serum medium. Images were captured using a phase-contrast microscope immediately and at, 6 and 24 h after wounding.

2.8.4 Gap closure analysis

The TScratch software is an automated image analysis tool for the objective and reproducible quantification of open wound areas. The default threshold settings were able to detect the cell boundaries. However in the cases of the later time points, where the open areas were small, the areas were manually adjusted down to a single cell. The software computed out the percentage open area per time point. These values were transferred into Excel and the percentage wound closure was calculated as % WCR = (Original gap – gap at indicated time)/ (original gap) *100. Next the fold change in migration was calculated where FCM = (% WCR treated) / (% WCR untreated). Experiments were performed as at least 2 independent biological replicas.

2.9 Cell labelling

To be able to monitor the cells within the chimeric kidney rudiment assay, three labelling techniques were individually employed. These three techniques are as follows:

A) The carboxyfluorescein diacetate succinimidyl ester (CFDA SE) Cell Tracer Kit (C1157, ThermoFisher Scientific) utilises amine-reactive probes that covalently bind to cytosolic components of cells once they penetrate and are metabolized [REF].

B) The PKH67 (PKH67GL, Sigma) is a lipophilic dye that stains the plasma membrane of cells through lateral diffusion [REF].

C) Cells were transduced with a lentivirus vector expressing green fluorescent protein (GFP).

The dye labelling kits were applied to the mesothelial cells following the standard recommended manufacturer's instructions. Optimisation of dye loading concentrations was first identified, based on the brightest signal and limited impact on cell viability. The fluorescence intensity of all 3 labelling techniques was monitored over the course of 7 days via flow cytometry (BD Biosciences FACSCalibur, BD Biosciences), through the FL1 channel (530±30 nm). Meanwhile, cell death was determined by the trypan blue staining and cell counting using the automated cell counter.

2.9.1 PHK67

The mesothelial cells were washed twice in DPBS, before being detached, centrifuged at 1000 rpm in growth medium and counted. $1x10^6$ cells were transferred to fresh 15 ml centrifuge tubes, washed and pelleted. The supernatant was aspirated off leaving no more than 25 µl of residual fluid, and 500 µl of diluent C was added to evenly re-suspend the cells. Since cell membrane staining is nearly instantaneous, a 2x working stock solution of 2 µM was made by adding 1 µl of 1 mM PKH67 dye (PKH67GL, Sigma) to 500 µl of diluent C in a fresh 1.5ml tube and vortexed. This was immediately

transferred onto the cells in suspension and mixed by pipetting to ensure uniform labeling. The cells were incubated with the probe at room temperature for 3 min, after which 1 ml FBS was added to stop dye uptake into cell membranes, followed by a further 1 min incubation step. The cells were pelleted at 1000 rpm for 10 mins, the supernatant removed, and the cells were washed a further 2 times in full growth medium before they were either plated out into 6 well plates for dye fading experimental monitoring; or co-cultured in the ex vivo rudiment assay.

2.9.2 CFDA SE

A 10 mM stock solution of the CFDA SE (C1157, ThermoFisher Scientific) was prepared prior to use by dissolving component A of the kit in 90µL DMSO. Mesothelial cells at passages 5 to 10 were used in this study and labeled in suspension. Firstly, the mesothelial cells were washed, pelleted and the supernatant was removed. A final concentration of 5 µM probe was added to the cells in pre-warmed DPBS and the cells were incubated for 15 mins at 37°C, 5% CO_2 in a humidified environment. The cells were re-pelleted at 1000 rpm for 5 mins and re-suspended 1 ml of FCS/ $1x10^6$ cells and left to incubate for a further 30 min at 37°C, 5% CO_2 to ensure complete probe modification. Finally, the cells were re-pelleted at 1000 rpm for 5 min and were either seeded in a 6 well culture plate (10119831, Nunc) for probe monitoring via flow cytometry or co-cultured in the chimeric rudiment assay (see section 2.10.1).

2.9.3 GFP lentivirus-labelled MCs

Mesothelial cells had been previously transduced by Dr. Anne Herman and Kelly Ward (Wilm group, 2011). Briefly, this involved culturing the mesothelial cells to 60%

confluence for transduction. Culture medium was aspirated and replaced with OptiMEM® (11058021 ThermoFisher Scientific)-based lentiviral infecting medium containing polybrene (8 µg/ml) and lentivirus particles based on the pLNT-SFFV-GFP vector for overnight incubation. The medium was replaced 24 h after transduction and the cells were cultured for a further 72 h at 37°C in 5% CO_2. Finally, an 88% GFP positive stable mesothelial cell line was achieved through fluorescence-activated cell sorting (FACs) using the 488nm laser of the FACSAria II

2.10 Metanephric kidney culture

2.10.1 Kidney re-aggregation chimera assay

The embryonic kidney re-aggregation assay used in this study was based on the Unbekandt and Davies (2010) protocol (Unbekandt and Davies, 2010). As described in section 2.1.3, kidneys rudiments were harvested from E13.5 CD1 mouse embryos. The rudiments were held on ice throughout sample harvest and preparation. The rudiments were transferred into a 15 ml centrifuge tube and washed with 3 ml of DPBS for 3 times with gentle, pulse centrifugation, to remove any traces of blood. The DPBS was carefully aspirated and the rudiments were incubated in 3 ml 5 x trypsin/ DPBS (T4174, Sigma) for 10 min, with intermittent gentle agitation at 37°C in 5% CO_2. The trypsin was neutralized in 10 ml of full growth rudiment culture medium containing 10% FCS, for 5 min at 37°C. The dissociated embryonic kidney cells were collected by centrifugation at 3000 rpm for 2 min and re-suspended in 1 ml the fresh full growth rudiment medium. Both the embryonic kidney cells and the labeled mesothelial cells were counted using trypan blue – exclusion assay. The embryonic kidney cells were either co-cultured by mixing with labeled mesothelial cells at a 1:10 ratio; or were seeded alone to form pellets of $2x10^5$ cells. To achieve this, the cell

mixtures were spun down at 3000 rpm for 2 min in 1.5 ml centrifuge tubes (10509691, Eppendorf). The re-aggregated control rudiments (rControl), the chimeric rudiments (MC rudiments) or whole embryonic rudiments (eControl) which had not been dissociated, were transferred using a 200 µl pipette tip onto 1.5 µm membrane filters (RTTP02500, Millipore) placed on 0.4 mm holes metal grids (Inoxia Ltd) at a liquid-air-interface at 37°C, 5% CO_2. The samples were cultured in kidney rudiment medium containing 5 µM Rho kinase inhibitor (Y-27632, Millipore) for the first 24 h, and subsequently cultured in kidney rudiment medium without Rho kinase inhibitor. Samples were harvested at days 4 and 7 for confocal image analysis. GFP labeled mesothelial cells at passages 22-32 were used throughout the kidney rudiment study, and the assay was successfully repeated on 7 independent occasions. Labelling with the CFDA SE and PKH67 probes was performed on younger mesothelial cells between passages 7 and 10. Each dye labeling technique was assayed using 3 independent biological samples. Figure 2.2 shows a schematic representation of the kidney rudiment assay culture technique.

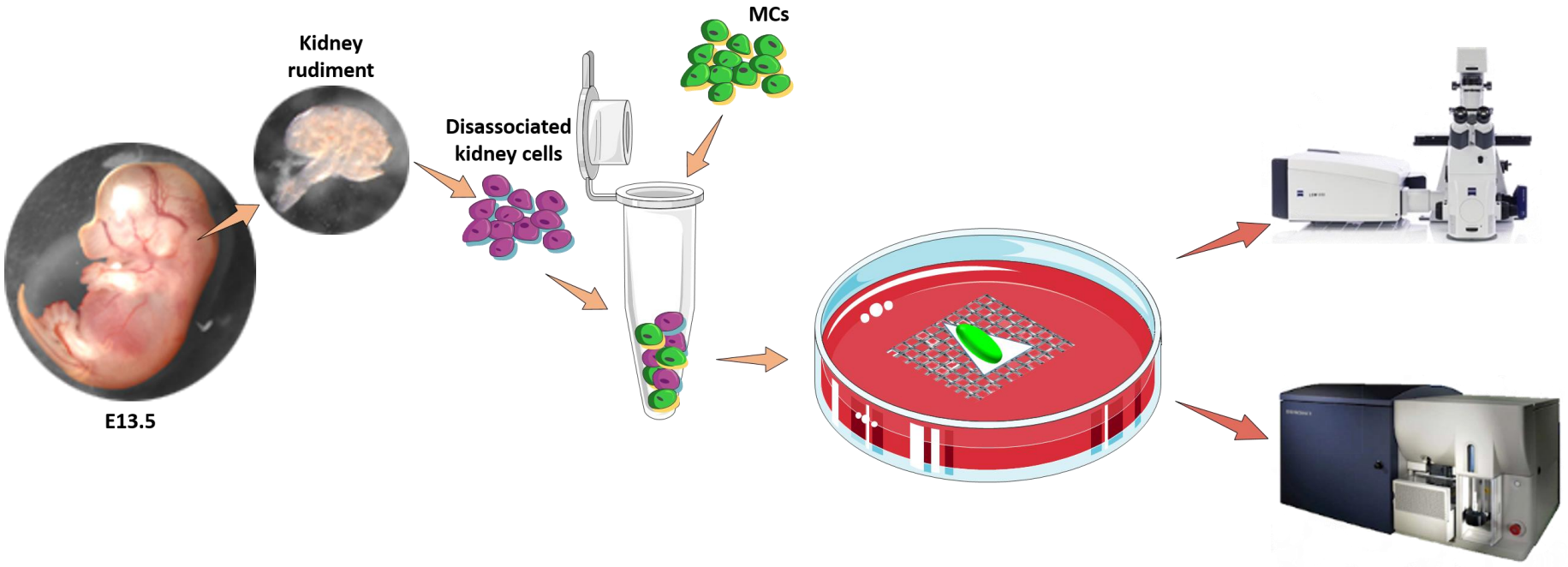

Figure 2.2 Kidney rudiment assay. The embryonic kidney rudiment assay was performed following the Unbekandt and Davies protocol (Unbekandt and Davies, 2010). Kidney rudiments were harvested from E13.5 mouse embryos and disassociated in x5 trypsin. The single rudiment cells were mixed with the labeled mesothelial cells at a 1:10 ratio and pelleted. The chimeric pellets were cultured on an air-media interface for a 4 and 7 day periods before mesothelial nephrogenic potential was analyzed by confocal microscopy or qPCR of FACS labeled mesothelial cells for nephrogenic genes.

2.10.2 Isolation of GFP+ MCs from the chimeric rudiment assay

GFP labeled mesothelial cells between passages 30 and 32 that had incorporated into the chimeric rudiments, were isolated for qPCR analysis as follows: The pellets were first collected in a 15 ml centrifuge tube to be disassociated in 5x trypsin/ DPBS for 10 min with intermittent and gentle agitation at 37°C. The cells were pelleted at 1000 rpm for 5 min and re-suspended in ice-cold 10% FBS/DPBS and held on ice. Using the BD FACS ARIA III, GFP+ mesothelial cells were harvested from the single cell mix of embryonic and adult cells through a number of gating parameters that were initially set up using non-aggregated GFP-labelled mesothelial cells. The dead cells and debris were gated out using side scatter (SSC-A) against forward scatter (FSC-A). The cell clusters were next gated out by plotting FSC-A vs FSC-H and SSC-W vs SSC-H. GFP+ cells were then selected by plotting the signal detected with the 488-nm laser (GFP FITC-A log) vs SSC-A. A histogram was finally plotted with count vs GFP FITC-A parameters to select cells with the brightest fluorescence cells.

2.11 Immunofluorescence techniques

2.11.1 Immunofluorescence staining of cultured cells

For the characterisation of protein distribution in cells, mesothelial cells, and the clones were seeded at $4x10^4$ cells/ well in 8 well chamber slides (Lab-Tek™ II, Nunc) and cultured to 80% confluence. Omentum explants were analyzed by seeding 2 explant pieces per chamber and left to culture for 14 d. Finally, cells that were either stimulated with growth factors, or were cultured in small molecule inhibitors for 48 h, were seeded into 24 well plates, plated at $5x10^4$, and by the end of the treatment had reached 90% confluence. Finally, the mesothelial cells that were involved in the

siRNA-mediated transcription factor knockdown were plated in 12 well plates at $6x10^4$ and for 72 h post treatment.

Subsequently, the medium was aspirated from the cell monolayer or explant pieces and the cells were quickly rinsed twice in DPBS. Following a 15 min fixation in 4% PFA (section 2.16.5), the cells were once again washed in DPBS for 5 min at RT. Next, the cells were permeabilized in 0.25% Triton-X/PBS (93426, Fluka) for 10 min. Following a 5 min DPBS wash, the cells were blocked with 2% bovine serum albumin (BSA) (BPE9701, ThermoFisher Scientific) for one hour at RT. This was followed by an overnight incubation with primary antibody solution in 2% BSA at 4°C in a humid chamber (see table 2.4). The following day the cells were washed 3 times for 15 min. Cells cultured in chamber slides were subsequently incubated with secondary antibody solution in 2% BSA for 1 h at RT in the dark. Samples were imaged using a Leica DMR-HC microscope with Leica DFC350FX camera and Leica application software. Meanwhile, cells cultured in the 24 - 12 well plates were incubated in the secondary antibody solution overnight at 4°C with gentle rocking. The cells were extensively washed for an hour in DPBS. Samples that were cultured on the glass chamber slides were mounted in anti-fade mounting medium Gelmount (1798510, Biomedia). Meanwhile, cells cultured in the 12 and 24 well plates were left hydrated in DPBS and documented using the Leica DM IRBE inverted microscope. Experiments were performed with 3 - 4 independent biological samples.

2.11.2 Immunofluorescence of intact kidney rudiments and kidney chimeras

In this study, both the rControl (re-aggregated kidneys), and the eControl (whole embryonic kidneys) as well as the chimeric rudiments, were transferred from the grids into a 48 well plate, while attached to the membrane filters. They were quickly and gently rinsed in PBS, before being fixed in 4% PFA for 30 min. After a 10 min wash in PBS, the samples were blocked in 10% goat serum/PBS containing 0.1% Triton X100/ PBS. Since the pellets were quite large, the samples were incubated in 300 µl of primary antibody containing the same 10% goat serum block, with 0.1% triton X100/PBS; overnight at 4°C with gentle rocking. The following morning, the samples were carefully washed 3 times in PBS for 15 min, as not to flush the pellets off the membranes. Next, 300 µl of secondary antibodies in the same blocking solution were added to the rudiments and incubated for 2 hours at RT in the dark. Finally, the rudiments were washed 3 more times in PBS, for 15 min, before being mounted onto glass slides with 80% glycerol (section 2.16.6). Rudiments were imaged using the Zeiss LSM 510 Multiphoton confocal microscope.

Table 2.4: Details of the primary antibodies used throughout this study.

Antibody	Type	Concentration	Supplier
Bmi1	Rabbit Ig, polyclonal	1:50	AP8756a, Abgent
GFP	Rabbit IgG, polyclonal	1:5000	ab290; Abcam
Laminin α1β	Rat IgG, monoclonal	1:200	MAB1905, Millipore
Megalin	Mouse IgG1, monoclonal	1:200	DM3613P, Acris
Pan-Cytokeratin	Rabbit IgG, polyclonal	1:200	Z0622, Dako
Pax2	Rabbit IgG, polyclonal	1:200	PRB-276P, Biolegend
PECAM	Rat IgG2a, monoclonal	1:100	550274, BD Pharmingen
Six2	rabbit IgG, polyclonal	1:200	11562-1-AP/Proteintech
Sox9	Rabbit IgG, polyclonal	1:100	SC-20095, Santa Cruz
Vimentin	Goat IgG, polyclonal	1:200	64740, ICN Biomedicals Inc.
Wt1	Mouse IgG1, monoclonal	1:100	05-753, Millipore
ZO1	Rabbit IgG polyclonal	1:200	40-2200, Life Technologies
α1 Sodium Potassium ATPase - Plasma Membrane Marker	Mouse IgG1, monoclonal	1:200	Ab7671, Abcam
α-smooth muscle actin	Mouse IgG2a, monoclonal	1:200	A2547, Sigma

Table 2.5: Details of the secondary antibodies and nuclear stain used throughout this study.

Antibody	Type	Concentration	Supplier
Anti-goat, AlexaFluor 546	Donkey IgG	1:1000	A11056, ThermoFisher Scientific
Anti-mouse AlexaFluor 488	goat IgG	1:1000	A11001, ThermoFisher Scientific
Anti-mouse AlexaFluor 594	goat IgG1	1:1000	A21125, ThermoFisher Scientific
Anti-mouse AlexaFluro 594	goat IgG	1:1000	A11032, ThermoFisher Scientific
Anti-rabbit AlexaFluro 488	goat IgG	1:1000	A11008, ThermoFisher Scientific
Anti-rabbit AlexaFluro 647	goat IgG	1:1000	A21245, ThermoFisher Scientific
Anti-rabbit, AlexaFluor 488	Donkey IgG	1:1000	A21206, ThermoFisher Scientific
Anti-rat AlexaFluro 594	goat IgG	1:1000	A11007, ThermoFisher Scientific
Nuclear counterstain DAPI	----	1:1000	D1306, ThermoFisher Scientific

2.12 Molecular biology techniques

2.12.1 TRIzol® based RNA extraction:

Total RNA was extracted from cells and tissue samples using TRIzol® reagent (15596018, ThermoFisher Scientific) according to the manufacturer's instructions. Samples were washed with DPBS to flush away debris and media, and then appropriate TRIzol® volumes and cell lysis techniques were employed according to sample type, as described in table 2.6.

Table 2.6: homogenization techniques

Sample type	Action
Tissues	Whole omentum tissue and adult and embryonic kidney organs were directly homogenized in 1, 4 and 2 ml of TRIzol®, respectively, using a power homogenizer (15-340-145, Fischer Scientific). The samples were then filtered using 0.45 µM pore-size filter units (F8273-50EA, Sigma).
Adherent Cells (monolayers)	Cells in a 10 cm dish were incubated in 1 ml of TRIzol® for 5 min, at RT; before being further lysed by pipetting.
Cells harvested from the FACS	1ml of TRIzol® was added to the pelleted FACS GFP^+ MC. The cells were mechanically lysed by pipetting, following a 5 min incubation period at RT.

The lysed samples were transferred into a 1.5 ml microcentrifuge tube and per 250 µl of TRIzol® reagent used, 50 µl of chloroform was added and the homogeneous mixtures were vigorously shaken for 15 s. Following a 15 min centrifugation at 13000 rpm, three phases could be distinguished. The RNA in the aqueous phase was pipetted into a clean 1.5 ml tube and an equal volume of isopropanol was added. The solution was inverted 6 times and left to stand at RT for 10 min before being centrifuged at 13000 rpm for 10 min to obtain an RNA pellet. The supernatant was discarded and the pellet was washed twice with 75% ethanol at a slower speed of 7500 rpm for 5 min. Before the pellets could be re-suspended in 11-50 µl of DNAse and RNase-free distilled water, the ethanol was removed and the pellets were left to air dry. The RNA concentration (ng/µl) and quality (260/280nm where the ratio value lies between1.8-2.0) were determined spectrophotometrically (ND1000, NanoDrop). Meanwhile, the RNA integrity was determined on a 1% agarose gel.

2.12.2 DNase treatment

An RQ1 DNase digestion (M6101, Promega) was performed to remove residual DNA from the RNA samples prior to qPCR applications, as it is vital to maintain RNA integrity when obtaining meaningful gene expression data. A single DNase digestion reaction was composed of 1.4 µg of RNA in 8 µl of DNase/ RNase-free water, 1 µl of 10X reaction buffer and RQ1 endonuclease. The samples were incubated at 37°C for 30 min, in a thermocycler (ABgene). The reaction was terminated by incubating the samples with 1 µl Stop buffer at 37°C for 15 min.

2.12.3 cDNA synthesis

The Superscript III kit (18080-044, ThermoFisher Scientific) was used for the first-strand complementary DNA (cDNA) synthesis of 200 ng/µl template RNA. To denature the secondary structures of the RNA and any hexamer duplexes, 4 µl of DNase-treated RNA was incubated with 2 µl random hexamers (100 ng/µl) and 1 µl 10 mM dNTP mix, for 5 min, 65°C and cooled on ice for 1 min. Next, 4 µl of the 5x buffer, 2 µl of DTT (0.1 M) and 1 µl Superscript III polymerase (200 U/µl) were also added and the samples were collected at the bottom of the tube by pulse centrifugation. To facilitate random primer annealing, the reaction tubes were heated for 5 min to 25°C. The reaction mixture was heated to 50°C, for 60 min, for the DNA polymerase to catalyze cDNA synthesis. Finally, the enzyme was inactivated at 70°C for 15 min.

2.12.4 Primers

The primers used in this study were designed in-house to detect sequences that are common across all the alternative splicing variants. The primers also spanned across

multiple exons (2 or more) to reduce the risk of false positives from contaminating genomic DNA amplification. The oligonucleotides were purchased from Sigma-Aldrich as a lyophilized product and reconstituted in nuclease-free water to a stock concentration of 100 µM. Primer specificity was validated in several ways. The optimal annealing temperature was determined via a thermal gradient qPCR assay using cDNA of a positive control sample know to express the target gene of interest. The temperature giving the lowest cycle threshold (Ct) without any amplicons was selected. Meanwhile, the presence of secondary nonspecific products and primer-dimers was determined via melt curve and 1% agarose gel analysis, and if detected, the respective primers were discarded from the study.

2.12.5 Quantitative polymerase chain reaction

Quantitative polymerase chain reactions (qPCR) were used to assess the relative changes in gene expression of samples after culture and in specific stimulation studies. Each reaction comprised of 7.5 µl of SYBR® Green Jumpstart™ Taq readymix™ (S4438, Sigma), 1.5 µl of the forward primer (250 nM final concentration), 1.5 µl of the reverse primer (250 nM final concentration) and the diluted cDNA (4.5 ng/ µl final concentration), and the volume was adjusted to 15 µl with nuclease free PCR grade water. The samples were vortexed to mix the cDNA with the SYBR green and were plated into hard shell white-coated 96 well plates (HSP-9645, BioRad). The qPCR was run on the CFX Connect Real-Time PCR (BioRad), using 2 step amplification settings. A melt curve was generated at the end of the amplification. The cycling programme used is shown in table 2.7. All samples were run as triplicates for each gene per reaction plate. Target experimental values were normalized to 2

housekeeping genes using the relative quantification method with 3 independent biological samples per condition.

Table 2.7: qPCR cycling conditions

qPCR conditions for the characterization studies		Wt1 isoform qPCR study	
Cycles	Description	Cycles	Description
1 cycle	95°C for 3 min	1 cycle	95°C for 3 min
50 cycles	Denaturation at 95°C for 10 sec Annealing and extension at 60/ 62°C for 30 sec	40 cycles	Denaturation at 95°C for 10 sec Annealing 58°C for 20 sec Extension 72°C for 1 min
1 cycle	Melt curve: 65°C to 95 °C, in 0.5 °C increments for 5 sec	1 cycle	Melt curve: 65°C to 95 °C, in 0.5 °C increments for 5 sec

Table 2.8: Details of primer sequences and product length are shown below

Gene	Forward primer	Reverse primer	Melting temperature	Product length
Housekeeping genes				
Gapdh	CATCTTCCAGGAGCGAGACC	GAAGGGGCGGAGATGATGAC	60°C/ 62°C	150
β-actin	GTACCCAGGCATTGCTGACA	CTGGAAGGTGGACAGTGAGG	60°C/ 62°C	145
EMT markers/ mediators				
TGF-β1	GCCTGAGTGGCTGTCTTTTG	CAGTGAGCGCTGAATCGAAA	60°C/ 62°C	93
TβRI	TCCAAACCACAGAGTAGGCAC	GTCAGCGCGTTTGAAGGATTC	60°C/ 62°C	97
TβRII	GTGAGACTGTCCACTTGCGA	TGTCGTTCTTCCTCCACACG	60°C/ 62°C	112
EGFR	CACATGCAAAGACACCTGCC	TCGTAGTAGTCAGGCCCACA	60°C/ 62°C	117
Cell-junctional markers				
Krt8	GATGAACCGCAACATCAACCG	GGTCTGGGCATCCTTAATGGC	60°C	127
Cdh1	GCTCTCATCATCGCCACAGA	GCAGTAAAGGGGGACGTGTT	60°C	197
ZO1	TGCCATTACACGGTCCTCTG	AGGGACTGGAGATGAGGCTT	60°C	175
Vcl	CCGCTGCTCGGATCTTACTG	CAATAGCCTCGTCCACCAGC	60°C	123
Msln	ATGTACTCCCACGGAGGTCT	GCCACAAATTTCCCAGGCAG	60°C	145
Mesenchymal markers				
Cdh2	CGCAAAGACCTTGTGGAGGG	AGGCGTTTCAAGTCTGCCAC	60°C	149
Vim	TCTGCCTCTGCCAACCTTTT	ACCTGTCCATCTCTGGTCTCA	60°C	126
S100A4	AGCTACTGACCAGGGAGCTG	ATCTGGGCAGCCCTCAAAGA	60°C	179
Acta2	AGAGGCACCACTGAACCCTA	CACCATCTCCAGAGTCCAGC	60°C	158
Stem cell genes				
Sox9	CAAGACTCTGGGCAAGCTCT	CCGGGGCTGGTACTTGTAATC	60°C	124
Bmi1	GCTCCAATGAAGACCGAGGA	ATTGCTGCTGGGCATCGTAA	60°C	178
Sox2	CACATGTGAGGGCTGGACTG	TCCTCTTTTTGCACCCCTCC	60°C	146
CD34	TCATCTTCTGCTCCGAGTGC	GCCTCAGCCTCCTCCTTTTC	60°C	176
Transcription factors				
Wt1	CCAAATGACCTCCCAGCTTGA	TGCTCTGCCCTTCTGTCCAT	58°C/ 60°C	116
Twist 1*	AGCGGGTCATGGCTAACG	GGACCTGGTACAGGAAGTCGA	60°C	162
Zeb1	GGGGAAACCGCAAGTTCAAG	AGCCAGAATGGGAAAACCGT	60°C	141

Zeb2	TCAAGTACCGCCACGAGAAG	CTTGCGGTTACCTGCTCCTT	60°C	155
Snail 1	AGCCCAACTATAGCGAGCTG	GTAGGGCTGCTGGAAGGTGA	60°C	112
Snail 2	CGAACCCACACATTGCCTTG	GTGAGGGCAAGAGAAAGGCT	60°C/62°C	117
Kidney markers				
Ret	TGAAGACAGGCCACAGGATG	CAGCAAACACTGGCCTCTTG	62°C	108
CD10	CAGCCTCAGCCGAAACTACA	CATAAAGCCTCCCCACAGCA	60°C	140
AqpI	CACCTGCTGGCGATTGACTA	CACCTTCATGCGGTCTGTGA	60°C	195
AqpII	CCCTGCTCTCTCCATTGGTT	AGGGGAACAGCAGGTAGTTG	60°C	200
Synaptopodin	TTCCTTCTCCACCCGGAATG	CTCCACGAGGGGGACATTG	62°C	207
Wnt4	CGAGGAGTGCCAATACCAGTT	CCTTGTGTCACCACCTTCCC	62°C	90
Wnt6	GATGTGGACTTCGGGGATGA	GTTGCACCAATGCACGGATA	62°C	88
Eya1	CAATAATCCCTCCCCTCCCC	CCGTATCTGTTGGCGTAGGA	62°C	117
Wt1	AATGCGCCCTACCTGCCCA	CCGTCGAAAGTGACCGTGCTGTAT	60°C/ 62°C	116
Notch2	TGTGACAGCCCTTATGTGCC	GGGCAGTCGTCGATATTCCG	62°C	143
Sdf1	GCTCTGCATCAGTGACGGTA	TCAGATGCTTGACGTTGGCT	62°C	98
Fgf7	AAGACTGTTCTGTCGCACCC	CAATTCCAACTGCCACGGTC	62°C	122
Igf11	ACCTCAGACAGGCATTGTGG	TCTTGGGCATGTCAGTGTGG	62°C	137
FoxC1	GAAGGACGCAGTGAAGGACAA	ACACGTACCGTTCTCCGTCTT	62°C	178
Pax2	TCCAGGCATCAGAGCACATC	GGCCGATGCAGATAGACTGG	62°C	104
Sal1	TTTCCAATCCGACCCCGAAG	CCACAGACATGGGCATCCTT	62°C	105
Bmp7	CTCGATACCACCATCGGGAG	CAGCAAGAAGAGGTCCGACT	62°C	188
Gdnf	CGCTGACCAGTGACTCCAAT	AAACGCACCCCCGATTTTTG	62°C	222
Adipocyte markers				
Fatp1	CAGTGCGTCATCTACGGGTT	AGGTAGCGGCAGATTTCACC	60°C	125
Fatp4	CAGCCTCAGCCGAAACTACA	CATAAAGCCTCCCCACAGCA	60°C	140
Glut4	CATTGTCGGCATGGGTTTCC	GGCAGCTGAGATCTGGTCAA	60°C	151
Pparγ	ATTGAGTGCCGAGTCTGTGG	GCAAGGCACTTCTGAAACCG	60°C	191
Osteoblast markers				
Igfbp3	CACAATGCTGGGAGTGTGGA	TGTCCTCCATTTCTCTGCGG	60°C	185

Fgf23	CCGCTGCTGCATTTCTACAC	CTCGCGAGAGCAGGATACAG	60°C	135
Dmp1	TCCTTGTGTTCCTTTGGGGG	CCAGATTCACTGCTGTCCGT	60°C	199
Sparc	TGTTGGCCCGAGACTTTGAG	CGTGTGGTGCAATGTTCCAT	60°C	160
Alpl	CCGGCTGGAGATGGACAAAT	CTCATTGCCCTGAGTGGTGT	60°C	184
Mesodermal markers				
Brachyury	TCCCCACCTGAAGACAGGAA	CAGGATGGGTCTGGATCACG	60°C	155
Fgf5	AAGTCAATGGCTCCCACGAA	TCCTCGTATTCCTACAATCCCCT	60°C	88
FoxF1	CCAAAACAGTCACAACGGGC	TCACACACGGCTTGATGTCT	60°C	191
FoxC2	GAAGAAGGATGTGCCCAAGGA	CCGCCTCGCTCTTAACCAC	60°C	146
Nodal	CAAGCCTGTTGGGCTCTACTC	CCGGTCACGTCCACATCTTG	60°C	179
Wnt3a	GCTCTGCCATGAACCGTCA	CACCAGCAGGTCTTCACTTCA	60°C	118
Wnt8a	GGGAACGGTGGAATTGTCCT	CAGCCGCAGTTTTCCAAGTC	60°C	163
Osr1	GCCCCCAAAAAGGAGAGAGT	AGCCACAGCTCATCCTTTACC	60°C	161

Table 2.9 Wt1 primer sequences for isoform studies

WT1 variant	Primer sequence		
EX5(-)fwd	GAGCCA CCTTAAAGGGCCA		
EX5(+)fwd	ATGGACAGAAGGGCAGAGCA		
KTS(-)-rvs	GCTGAAGGGCTTTTCACCTGTA		
KTS(+)-rvs	CTGAAGGGCTTTTCACTTGTTTTAC		
Wt1 isoforms detected	Primer sequence combination		Product length
Wt1 A	EX5(-)fwd	KTS(-)-rvs	455
Wt1 B	EX5(+)fwd	KTS(-)-rvs	460
Wt1 C	EX5(-)fwd	KTS(+)-rvs	463
Wt1 D	EX5(+)fwd	KTS(+)-rvs	468
(Kramarzova et al., 2012)			

2.12.6 qPCR data analysis

Following completion of the qPCR runs, each experimental study set had the baseline threshold adjusted consistently through the Biorad CFX manager software. All cycle threshold values (C_T) were then transferred into an excel spreadsheet for the calculation of fold change. The C_T corresponds to the cycle number at which the fluorescent signal crosses the threshold. In order to assess the difference in expression between treated and control samples, the following steps were performed:

Firstly, the average C_T of the target gene of interest (GOI) was normalized against the average combined C_T of each sample's internal housekeeping genes (HKG) to calculate the dC_T, using the following equation: $dC_T = C_{T\ (GOI)} - C_{T\ (HKG)}$. Since each experiment was performed on 3 independent biological replicas, the mean dC_T was ascertained. Following on, the ddCts were calculated relative to the control group with the following formula: $ddCt = dC_{T\ (Control\ group)} - dC_{T\ (Target\ group)}$. Finally, the relative fold change in gene expression was determined by the equation: $2^{-(ddCT)}$.

2.13 Biochemistry

2.13.1 Cell Lysis

The cells were washed in ice-cold PBS, supplemented with protease inhibitors and sonicated in 120 µl ice-cold cell extraction buffer (section 2.16.1). The lysates were transferred into a 1.5 ml centrifuge tube and centrifuged at 13,000 rpm for 10 min at 4°C. The clear lysates were aliquoted into fresh tubes for protein quantification.

2.13.2 Protein quantification

Protein concentrations were quantified using the Pierce™ BCA Protein Assay Kit (23225, ThermoFisher Scientific), following manufacturer's instructions. Briefly, a protein standard curve was generated by serially diluting a 1 mg/ml BSA stock solution in distilled water to values between 0 - 1000 µg/ml. These and the unknown protein samples were added to the preformed BCS solution which consists of a 50:1 mixture of Reagent A (Bicinchoninic acid solution) and Reagent B (copper sulfate solution). The samples were incubated at 37°C for 30 min and absorbance was read at 562 nm using the FLUOstar Omega spectrophotometer.

2.13.3 Resolving proteins with western blotting

Samples were denatured at 90°C for 5 min before 15 µg of total cell lysates were loaded onto a 4-12% Bis-Tris gel (NP0335BOX, NuPAGE®, ThermoFisher Scientific) for electrophoresis in MOPs running buffer (section 2.16.2) at 200 V constant for 50 min. Following protein separation, the contents were transferred onto an activated PVDF 0.2 µm pore blotting membrane (ISEQ00010, Merk Millipore) using wet transfer apparatus (XCell II™ Blot Module, EI9051, ThermoFisher Scientific) for 1 h at 3 V. The membranes were blocked for 1 h at RT in Western Blocker Solution (W0138, Sigma), before being incubated overnight with the primary antibody solutions on a rocker at 4°C. The membranes were washed for 30 min the following morning in Tris-buffered saline with Tween (section 2.16.4). The secondary antibodies were added to the membranes for 1 h on a rocker at RT. Following a 45 min TBST wash, the proteins were visualized using Pierce ECL (32109, ThermoFisher Scientific) or the more

sensitive Amersham ECL prime (GERPN2232, GE Healthcare) on Amersham Hyperfilm (28906835, GE Healthcare).

2.13.4 Quantification of the fold change in relative protein expression

Following film development, the samples were quantified using imageJ application software. The target protein values were normalized to their own loading control and the fold change in expression was compared against the untreated control samples. Meanwhile, the proportion of phosphorylated proteins was calculated as follows: [(phosphoprotein/β-actin)/total protein/β-actin]. Experiments were performed as 2 independent biological samples.

Table 2.9: western primary antibodies

Antibody	Type	1°Ab Concentration	2°Ab Concentration	Supplier
β-actin (8H10D10)	Mouse monoclonal	1:10000	1:20000	3700, CST
Slug (C19G7)	Rabbit monoclonal	1:1000	1:5000	9585, CST
α-smooth muscle actin	Rabbit polyclonal	1:500	1:5000	ab5694
ZO1	Rabbit IgG polyclonal	1:200	1:5000	40-2200, Life Technologies
Vimentin	Goat IgG, polyclonal	1:200	1:5000	64740, ICN Biomedicals Inc.
Phospho-Erk5 (Thr218/Tyr220)	Rabbit monoclonal	1:2000	1:5000	3371, CST
Erk5 (D23E9)	Rabbit monoclonal	1:1000	1:5000	3552, CST
Phospho-p44/42 MAPK (Erk1/2) (Thr202/Tyr204) (D13.14.4E) XP®	Rabbit monoclonal	1:2000	1:5000	4370, CST
p44/42 MAPK (Erk1/2) (3A7)	Mouse monoclonal	1:1000	1:5000	9107, CST

Table 2.10 western secondary antibodies

Antibody	Type	Supplier
Peroxidase-AffiniPure	Goat Anti-Rabbit IgG	111-035-144-JIR, Jackson ImmunoResearch
Peroxidase-AffiniPure	Goat Anti-Mouse IgG	115-035-003-JIR, Jackson ImmunoResearch
Peroxidase-AffiniPure	Donkey Anti-Goat IgG	705-035-003-JIR, Jackson ImmunoResearch

2.14 Statistical analysis

The data from each experiment were first averaged and presented as means with standard error bar (SEM). The statistical analysis was performed using either a student T test or a one-way ANOVA to determine statistical significance between groups. This was followed by a Sidak multiple-comparison test to determine significance between individual groups (unless otherwise stated). A p value of ≤ 0.05 was considered significant. All statistical data was analysed using GraphPad Prism version 6.00 for Windows.

2.15 Medium composition

2.15.1 Mesothelial cell standard growth medium

DMEM (D5796, Sigma) containing 10% (v/v) FBS (F6178, Sigma), and 1% (v/v) streptomycin - penicillin (P4333, Sigma)

2.15.2 Conditioned medium

The medium was aspirated off the cultured mesothelial cells and was pelleted to collect the debris. The conditioned medium was then transferred to a fresh tube and mixed with fresh standard full growth medium at a 1:1 ratio.

2.15.3 Kidney rudiment medium

MEME (M5650, Sigma) containing, 10% (v/v) FCS and 1% (v/v) 200mM L-glutamine (G7513, Sigma)

2.15.4 Adipogenic medium

Standard FGM supplemented with 100nM dexamethasone (D4902, Sigma), 500nM 3-isobutyl-1-methylxanthine (I7018, Sigma), 50µM indomethacin (I7378, Sigma) and 1µg/ml insulin (I6634, Sigma)

2.15.5 Osteogenic medium

MC FGM supplemented with 100nM dexamethasone, 10mM β-glycerophosphate (G9422, Sigma) and 25µg/ml of 2-Phospho-L-ascorbic (49752, Sigma).

2.15.6 Cell Freezing solution

The freezing solution was composed of 90% fetal bovine serum (FBS; (F6178, Sigma)) and 10% dimethyl sulphoxide (DMSO; D2438, Sigma).

2.16 Buffers, solutions, and dyes

2.16.1 Cell lysis buffer

- 4.733 ml Cell Extraction Buffer (FNN0011, ThermoFisher Scientific)
- 17 µl phenylmethanesulfonyl fluoride or phenylmethylsulfonyl fluoride (PMSF) (1 mM final concentration)
- 250 µl Protease inhibitor cocktail that is composed of AEBSF (2 mM), Aprotinin (0.3 µM), Bestatin (116 µM), E-64 (14 µM), Leupeptin (1 µM) and EDTA (1 mM) (P-2714, Sigma).

2.16.2 MOPS buffer

- 950 ml dH_2O
- 50 ml NuPAGE® MOPS SDS Running Buffer (20X) (NP0001, ThermoFisher Scientific)

2.16.3 Transfer buffer

- 849 ml dH_2O
- 50 ml NuPAGE® MOPS SDS Running Buffer (20X) (NP0001, ThermoFisher Scientific)
- 1 ml NuPAGE® antioxidant (NP0005, ThermoFisher Scientific)
- 100 ml analytical grade methanol

2.16.4 TBST

- 50 ml Pierce™ 20X TBS Tween™ 20 Buffer (28360, ThermoFisher Scientific)
- 1 ml Tween-20 (0.1% final concentration)
- 949 ml dH_2O

2.16.5 4% PFA

- 20 g PFA (Sigma)
- 500 ml PBS

PFA powder was dissolved on a heated magnetic stirrer at 60°C. The solution's pH was then adjusted to 7.4-7.6, filtered and stored long-term storage at -20°C.

2.16.6 Kidney rudiment mounting solution

- 80 ml glycerol (G5516, Sigma)
- 20 ml dH_2O
- Autoclaved before use

2.16.7 Alizarin S red dye

- 2 g Alizarin Red S (C.I. 58005)
- 100 ml distilled water

Adjust pH to 4.1~4.3 with 10% ammonium hydroxide.

2.16.8 Oil red dye

- 0.5 g oil red O (CI 26125, Sigma)
- 100.0 ml isopropanol

Chapter 3: Isolation and characterisation of mesothelial cells in long-term culture

3.0 Introduction and aims

There is accumulating evidence pointing towards the presence of a population of progenitor cells within the peritoneum that under certain cues become activated to drive regeneration processes through differentiation. Such properties may explain the healing potential of omentum transpositions, however, the mechanisms underpinning this remain elusive.

The overall goal of this chapter was to assess the phenotype of cultured mouse omentum-derived mesothelial cells *in vitro*.

Specifically, we aimed to characterize the cell morphology of the isolated mesothelial cells and assess the effect of repeated passaging and prolonged culturing on mesothelial cell characteristics. We aimed to investigate these effects by studying changes in gene expression signatures relative to the omentum cultures. We analyzed at a molecular level the regulatory mechanisms that resulted in any changes observed in the culture of mesothelial cells; furthermore, we wondered which implications these changes in cultured mesothelial cells had on regenerative therapeutic outputs.

Lastly, we also aimed to explore the plasticity of mesothelial cells by studying their potential clonogenic properties and the expression of stem cell markers.

3.1 Isolation and culture of mesothelial cells

The mouse omentum is a peritoneal - fold of tissue composed of two mesothelium layers which connect the stomach, spleen and the pancreas (Fig 3.1). The mesothelial cells are the predominant cell type in this fenestrated membrane-like structure, and due to the relative ease of access, the omentum it is an ideal source of mesothelial cells (Fedorko et al., 1971).

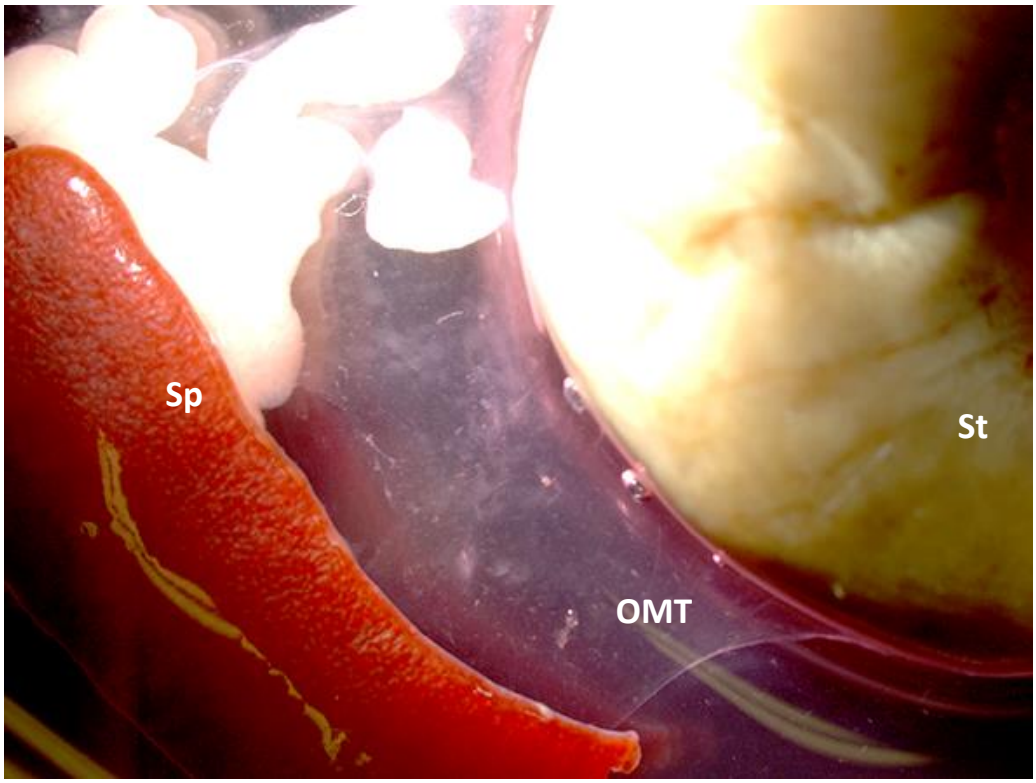

Figure 3.1: CD1 mouse omentum (OMT) is located between the stomach (st) and spleen (sp) complex.

Previously published work by our group demonstrated the culture of omentum explants for 5 d, with mesothelial cells emerging 2 d post seeding (Kawaguchi et al., 2007). In the current study, we were able to replicate this, showing epithelial sheets of mesothelial cells migrating radially from the explanted tissues within 4 d of seeding (Fig 3.2A). Prolonged omentum explant culture (OMC) for more than 14 d resulted in

the appearance of longer, spindle-shaped cells. These cells occurred initially at the leading edge of the epithelial sheet before spreading more widely (Fig 3.2B). In order to avoid that subsequent passaged mesothelial cultures contained the spindle-shaped cells, we treated the omentum cultures by 14 d to generate passage 1 (P1) mesothelial cell lines. The explant cultures were sensitive to physical detachment protocols such as scraping and vigorous pipetting, and as a result, we could not establish mesothelial cell lines through these techniques. Instead, we found that prolonged exposure to enzymatic treatment resulted in the complete dissociation of the omentum-derived cells and the eventual establishment of a mesothelial cell line. Cell density was not a limiting factor in the establishment of murine mesothelial cell cultures. However, typically it took up to 4 passages to achieve a homogeneous monolayer as the cells needed to be serially expanded. This is contrary to other primary cultures established from human and rat peritoneum (Książek, 2013, Jiang et al., 2010).

Following trypsin incubation, detachment and seeding as P1 cells, subconfluent mesothelial cells had a slightly elongated phenotype (Fig 3.2C), however, the cobblestone phenotype was restored upon confluence in P1 cells (Fig 3.2D). From passage 4 onwards, the mesothelial cells adopted a less cobblestone phenotype, which was largely maintained even at higher passages (Fig 3.2D-E). Throughout this research project, 12 biologically independent mesothelial cell cultures were successfully generated through this procedure and the cells were successfully sub-cultured to P40.

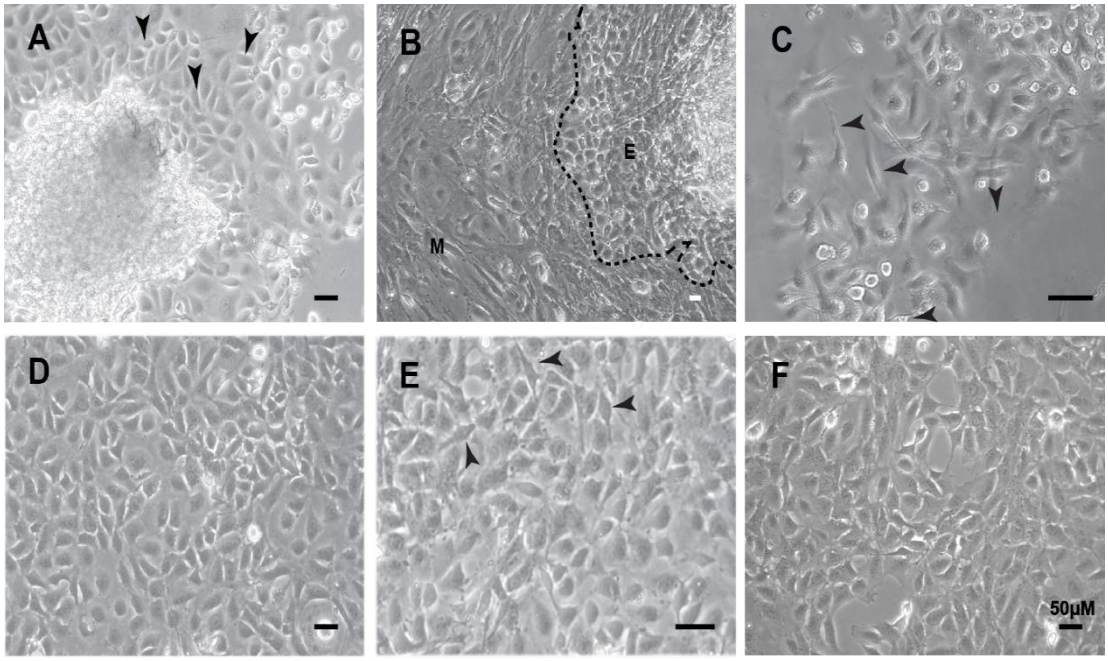

Figure 3.2: Generation of the mesothelial cell line. [A] The omentum culture explants (OMC) that were cultured for 4 d were surrounded by a sheet of epithelial-like mesothelial cells (arrowheads). [B] Prolonged cultured led to the appearance of fibroblastic mesothelial cells (M) that bordered (dashed line) the few remaining epithelial cells (E). [C] Following subculture, the sub-confluent P1 cells adopted an elongated morphology (arrowheads), however, the cobblestone appearance returned upon confluence [D]. With time in culture, the cells became slightly more elongated (arrows) but the general phenotype remained stable from P4 [E] to P24 MCs [F]. Images are representative of n≥3 independent biological replicates.

3.2 Long-term cultured mesothelial cells displayed a capacity to proliferate in even high passages

Since we were able to successfully culture mesothelial cells up to P40, we aimed to investigate the effects of repeated passaging had on the population doubling times (PDT). The trypan blue exclusion assay is a simple technique for calculating the rate of cell proliferation and the percentage of viable cells because the dye easily diffuses across cell membranes of dead or dying cells only (Berridge et al., 2005). The PDT of mesothelial cells was monitored between passages 5 through to 18. The cells were grown to 90% confluence before harvesting and staining with trypan blue to quantify cell death. We had chosen to start the assay at P5 which was the lowest homogeneous passage available following isolation from the omentum explants. Our analysis showed that the PDT of P5 to P18 cells ranged from 20 to 40 h, stabilizing at about 24 h between P8 and P16 (Fig 3.3). The mesothelial cells could be passaged to P40 and even at the higher passages, they did not show signs of senescence as they shared a similar cell morphology and maintained the capacity to proliferate.

Figure 3.3: Population doubling times of mesothelial cells throughout passages. The PDT

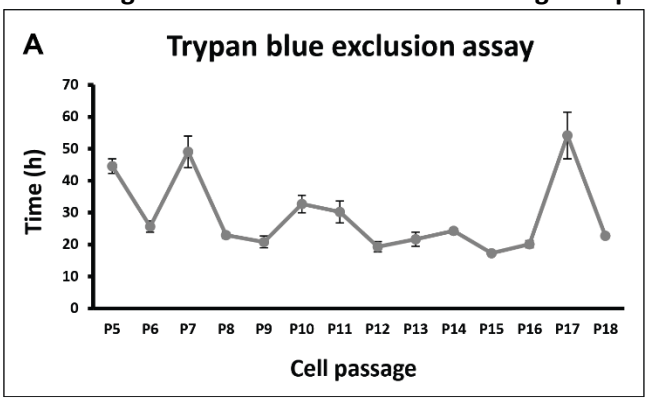

for mesothelial cells was performed using the trypan blue exclusion assay. The PDT ranged from 20 –40 h. Figure A is representative of 2 independent biological replicates.

3.3 Long-term cultured mesothelial cells expressed the mesothelial markers Wt1 and Msln

To assess whether the mesothelial cells maintained their characteristics throughout culture, OMC (P0 cells) through to P24 cells were studied for their expression of the classical mesothelial markers Wilms tumor protein 1 (Wt1) and mesothelin (Msln).

Immunolabeling studies revealed that Wt1 was expressed in the nuclei of OMC (Fig 3.4A-B), P4 (Fig 3.4D-E), P12 (Fig 3.3G-H) and P24 mesothelial cells (Fig 3.4J-K). Mesothelin, a cell surface glycoprotein (Lua et al., 2016), was localized on the cell membranes of the P4 (Fig 3.4F), P12 (Fig 3.3I) and P24 cells (Fig 3.4L). However, mesothelin staining in the OMC was diffuse and punctate (Fig 3.4C).

Next, we performed quantitative gene expression analysis to study the effects of mesothelial long-term culture on the levels of mRNA transcripts of these two mesothelial markers, relative to the OMC. Freshly isolated omentum tissue (OMT) was also included in the analysis to see if placing the tissue in culture had an effect on these key mesothelial markers. *Wt1* mRNA was detected in all samples, and more or less maintained between the OMT and the OMC. However, with cell passaging we saw a more than 4000 - fold drop in expression at passage 5 ($P<0.001$) relative to the OMC (Fig 3.5A). The expression level of *Wt1* was maintained in the P10 and P25 cells compared to the P5 mesothelial cells; suggesting that the *Wt1* transcript levels were stabilized once the cells were passaged. Of note, the delta Ct values for Wt1 expression in passaged cells were in the range between 17-19, while in the range between 3-6 in OMT and OMC, suggesting that very high levels of Wt1 expression was strongly attenuated in the cells from passage 5 onwards (table 3.1). Interestingly, with culturing the OMC downregulated *Msln* expression ~80 - fold relative to the

OMT. Then, with repeated passaging the mesothelial cells upregulated *Msln* mRNA levels 5 - fold by passages 5-10 ($P<0.001$), and a further 16 - fold increase was seen in the P25 cells ($p<0.01$) (Fig 3.5B) relative to the OMC. Overall, these results show that the process of isolating and establishing mesothelial cell cultures altered the expression levels of the two mesothelial cell markers analyzed.

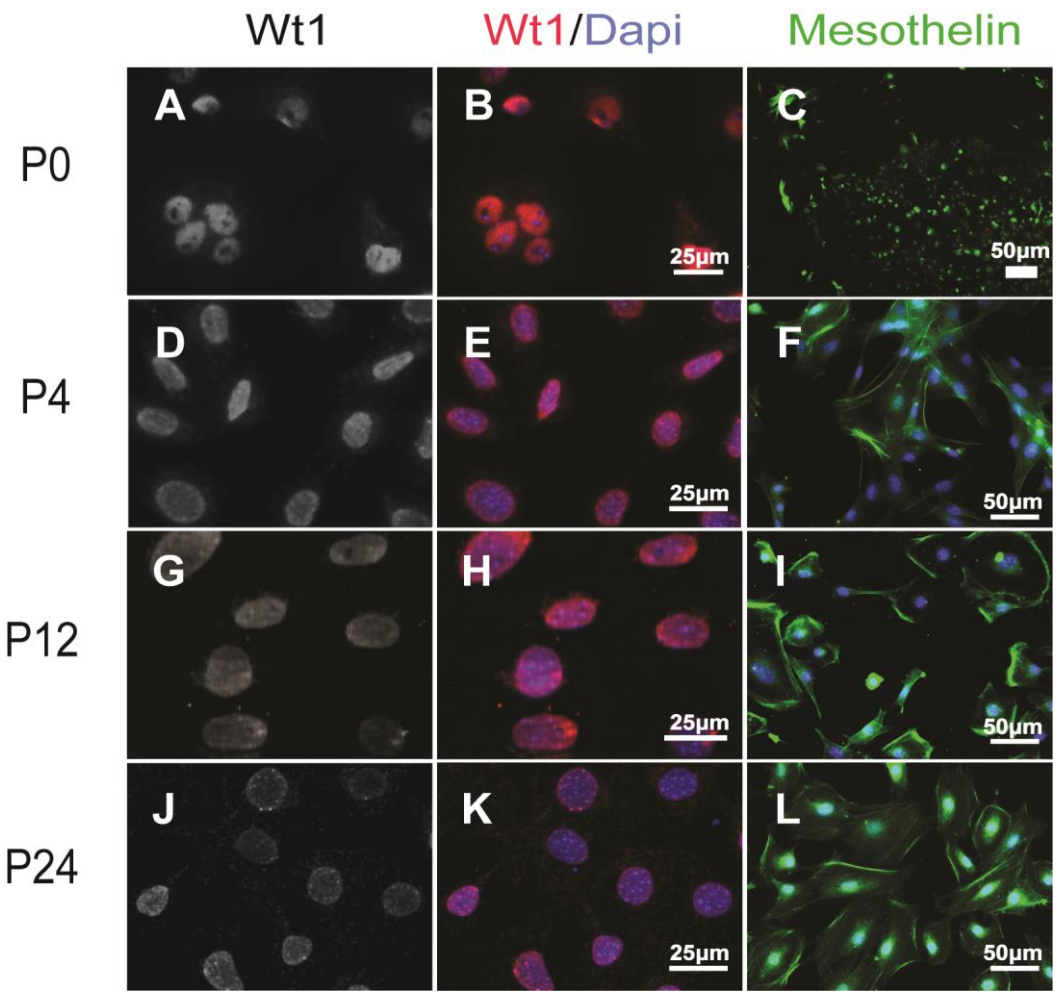

Figure 3.4: Mesothelial cells expressed Wt1 and Msln. Mesothelial cells at P4-P24 were seeded into 8 well glass chamber slides and left to reach 80% confluence, while 2-3 pieces of omentum explants were cultured for 14 d. Samples were fixed and stained for mesothelial markers Wt1 and Msln. Mesothelial cells consistently expressed Wt1 in the nuclei of cells [A-B, D-E, G-H and J-K]. Msln was localized to the membranes of P4-P24 cells [F, I and L]. The OMC cell (P0) staining was diffuse and punctate [C]. Representative images from 3 biologically independent samples, per passage, are shown.

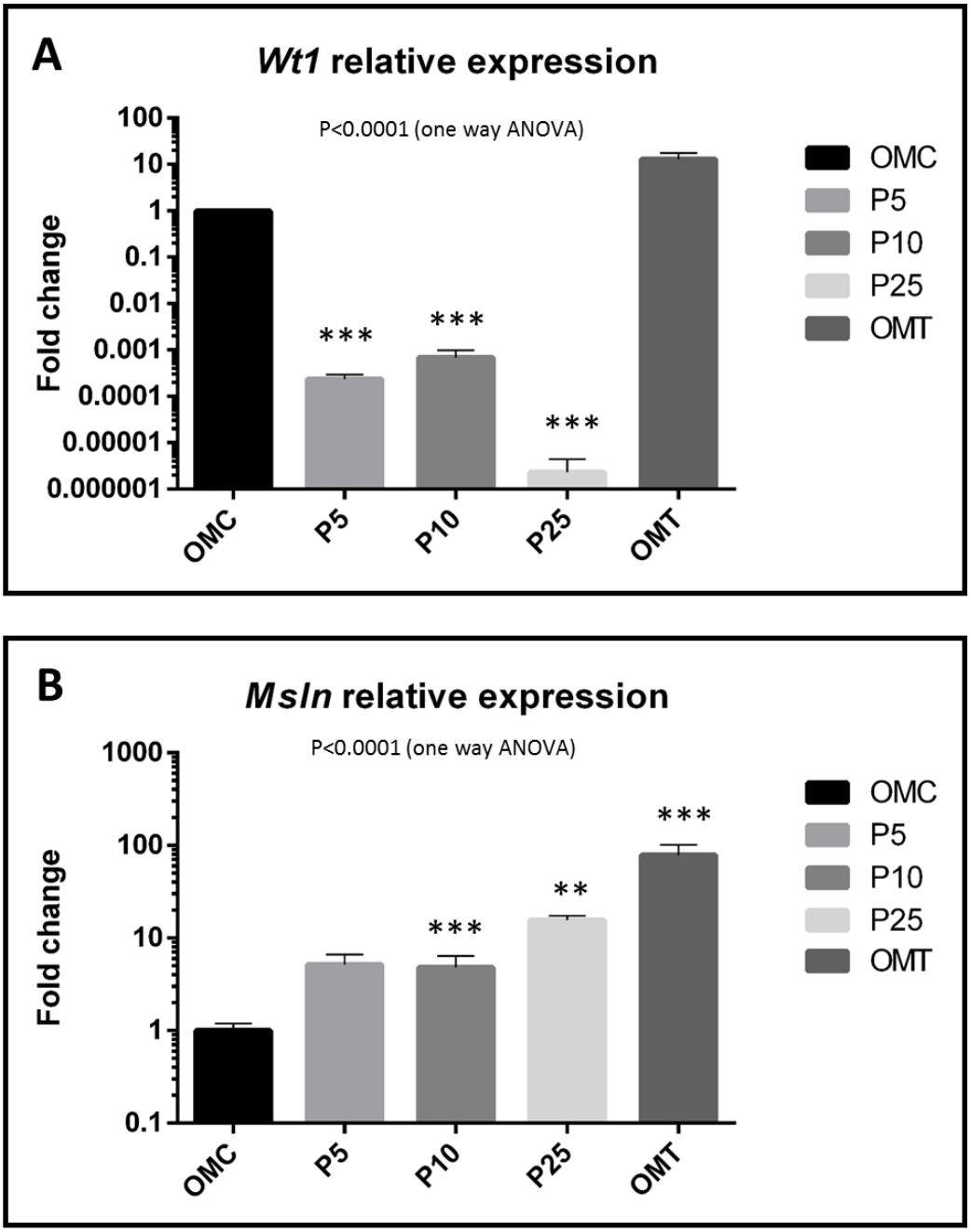

Figure 3.5: Relative expression of *Wt1* and *Msln* in omentum tissue, omentum cultures and MC of different passages. RNA from omentum tissue (OMT), omentum cultures (OMC) and P5, P10 and P25 mesothelial cells was harvested for relative - fold change in gene expression of *Wt1* [A] and *Msln* [B]. Data presented as 3 independent biological replicates per condition. Compared to the OMC, $^{***}p < 0.001$, $^{**}P<0.01$.

Table 3.1: dCt and - fold change values for *Wt1* and *Msln* gene expression analysis data

Sample	dCt	SEM	- fold Change	SEM
Wt1				
OMT	2.81	0.65	12.9	4.71
OMC	6.50	0.09	1.00	6.12×10^{-2}
P5	18.56	0.44	2.34×10^{-4}	6.18×10^{-5}
P10	17.01	0.80	6.88×10^{-4}	2.94×10^{-4}
P25	25.22	3.41	2.32×10^{-6}	2.10×10^{-6}
Msln				
OMT	5.08	0.49	78.71	22.61
OMC	11.38	0.29	1.00	0.18
P5	9.02	0.50	5.13	1.51
P10	9.11	0.58	4.82	1.59
P25	7.40	0.16	15.69	1.66

3.4 Mesothelial cells downregulate epithelial genes with prolonged culture

Since the MCs at P4-P24 displayed a slight but notable increase in more elongated cells, thus resulting in a moderate loss of the perfect characteristic cobblestone morphology in the OMC cultures, we wished to determine the molecular mechanisms that contributed towards this change. Therefore, we analyzed the protein expression patterns and mRNA profiles of epithelial and mesenchymal markers in mesothelial cells from OMC to P25.

Epithelial cells are classically identified by their cobblestone morphology which is the result of a network of cellular adhesion proteins maintaining cell-cell contacts and polarity (see Fig. 1.1) (Knights et al., 2012). Immunofluorescence analysis for the tight junctional marker zonula occludens 1 (ZO1) protein revealed that the OMC expressed ZO1 strongly as discrete bands at the circumference of the cells (Fig 3.6A). By contrast, in the P4-P24 cells, ZO1 was mostly localised in a punctate fashion around the cell perimeter and there was increased nuclear accumulation of the protein (Fig 3.6B-D). However, it is important to note that the punctate ZO1 pattern at the cell perimeter appeared very similar between P4 and P24 cells.

Cytokeratins (CK) are intermediate filament proteins that link to desmosomes and are associated with maintaining the epithelial cell morphology by establishing an intercellular adhesive framework (Knights et al., 2012). Pan-cytokeratin immunolabeling revealed that cells in the OMC cultures robustly expressed CK across the cytoplasm (Fig 3.6E). However, this cytokeratin distribution was retracted to the perinuclear region in a dot-like morphology in some of the P4 cells compared to the OMC (Fig 3.6F). This retraction was also seen in the P12 and P24 mesothelial cells, respectively (Fig 3.6G and H).

To further quantify the effects that prolonged cell passaging had on the epithelial characteristics of mesothelial cells, the expression levels of a panel of epithelial markers were studied through qPCR. E-cadherin-1 (*Cdh1*) is the major transmembrane protein of the adherens junctions and is required to maintain lateral cell-cell contacts and regulate the actin cytoskeleton (Knights et al., 2012). Vinculin (*Vcl*) is also a component of adherens junctions and a novel regulator of *Cdh1* function (Peng et al., 2010). Expression analysis of revealed that, while in OMT the levels were unchanged, the passaged mesothelial cells significantly downregulated the relative expression of *Cdh1* when compared to the OMC. This loss of expression was most pronounced at P10, where there was 3000 - fold reduction ($P<0.05$) in *Cdh1* relative expression (Fig 3.7A). Meanwhile, the P5 and P25 cells showed roughly a 300 - fold reduction in relative expression.

While we observed also a 3 - fold reduction in the expression of the *Vcl* gene, these changes were not significant between the assayed samples (Fig 3.7B).

Peritoneal mesothelial cells have been reported to express cytokeratin 8 (*Krt8*) as an epithelial marker (Li et al., 2013b, Lua et al., 2016). In our study, the passaged cells but not the OMT gradually downregulated relative expression of the *Krt8* gene with prolonged culture between 42 to 400 - fold between passages 5 to 25 ($P<0.001$), relative to the OMC (Fig 3.7C). The relative mRNA transcript levels of the tight junctional protein *ZO1* fluctuated considerably between the passages and compared to the OMC there was no statistical change in expression despite the roughly 400 - fold increase in relative expression at P5 (Fig 3.7D).

Taken together, while the immunolabeling studies showed that the mesothelial cells maintained epithelial characteristics following passaging, the qPCR studies revealed that passaging reduced the expression levels of some but not all of the key epithelial markers we analyzed. The mesothelial cells, however, maintained expression of these genes at relatively low levels with repeated passaging.

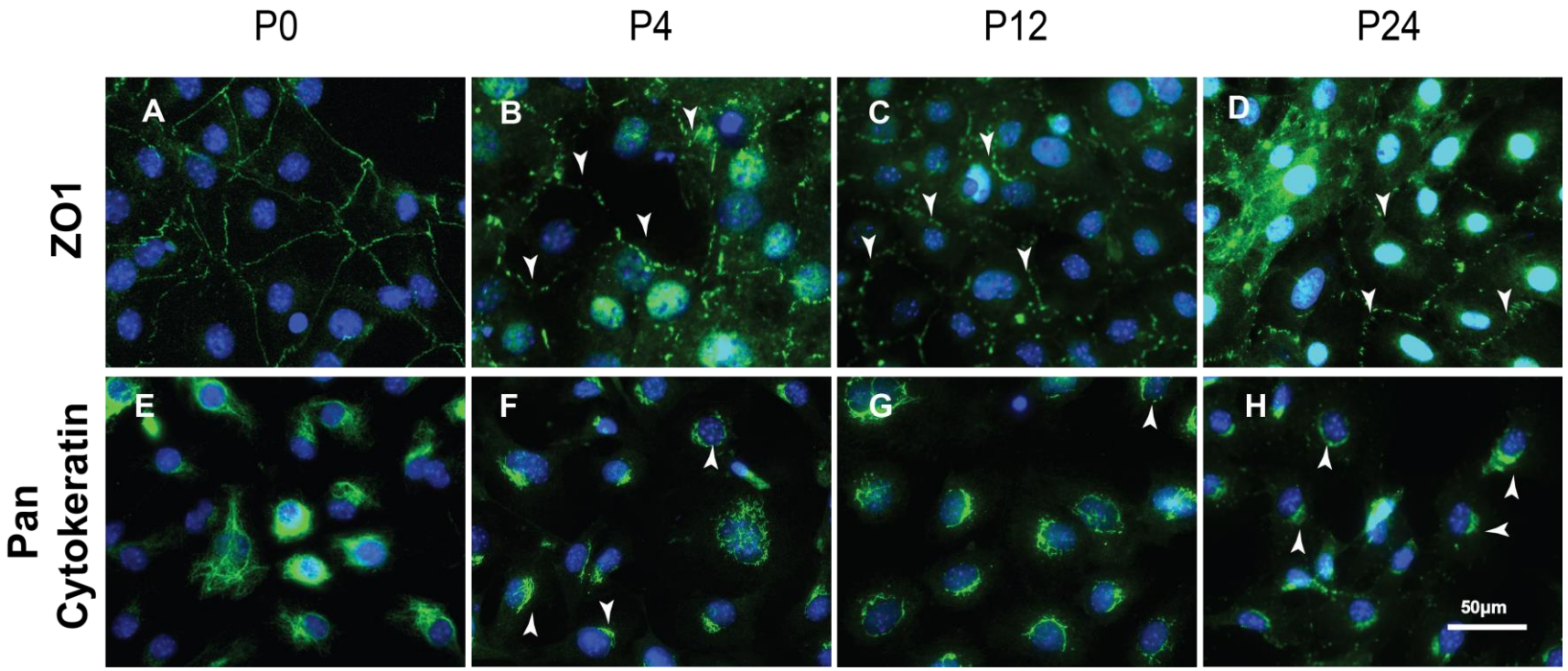

Figure 3.6: Cellular localisation of epithelial markers in mesothelial cells was slightly changed with increased passage. Mesothelial cells from passages 4, 12 and 24 at near confluence, and OMC (P0) 14 days after seeding were immunolabelled with ZO1 and pan-cytokeratin antibodies. The OMCs [A] showed strong ZO1 bands around the cell perimeter, while in the P4, P12 and P24 cells ZO1 appeared more punctate (arrowheads) and also localised to the nucleus [B-D]. Cytokeratin was expressed across the cytoplasm of the cells in the OMC [E]. This expression was reduced to the perinuclear region of the P4, P12 and P24 cells (arrowheads) [F-H]. Images are representative of at least 3 independent biological samples per condition.

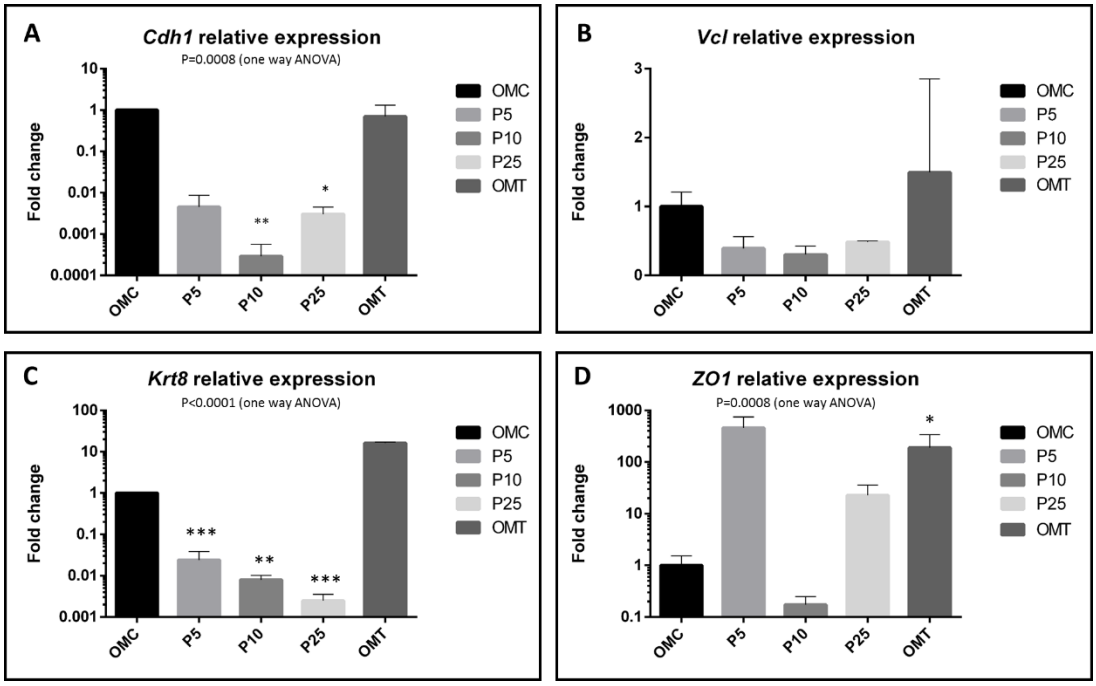

Figure 3.7: Relative expression analysis of epithelial markers in cultured MCs. MCs were cultured to 80-90% confluence for total RNA extraction and reverse transcription and subsequent qPCR analysis of epithelial gene expression. [A] *Cdh1* expression decreased nearly $2.3x10^4$ - fold at P5 relative to OMC, and this level was maintained thereafter. [B] *Vcl* expression was roughly 3 - fold downregulated in the passage 5-25 cells (relative to OMC), however, this was not statistically significant. [C] Culturing and passaging significantly reduced *Krt8* expression in the P5-P25 mesothelial cells 40-400 - fold relative to the OMC. [D] *ZO1* relative expression fluctuated considerably between passages. Data are presented as a mean of n=3 biologically independent samples and normalized to two housekeeping genes (GAPDH and ?actin). Error bars are presented as SEM. Compared against the OMC group, $^{***}p < 0.001$, $^{**}p < 0.01$ and $^{*}p < 0.05$.

3.5 Cultured mesothelial cells changed expression of key mesenchymal markers

In light of the fact that with repeated passaging the mesothelial cells downregulated epithelial markers, we assessed whether the cells became more mesenchymal throughout this process. We characterised the protein localisation and gene expression profiles of mesenchymal markers in OMC and in mesothelial cells at the three passage time points, early (P4), medium (P12) and late (P24). When immunolabelled with vimentin (Vim) and alpha smooth muscle actin (αSMA), OMC and the passaged cells (P4-P24) displayed for both markers a uniform expression pattern throughout the cytoplasm (Fig 3.8A-H). Interestingly the expression of αSMA consistently varied between cells across the populations (arrowheads Fig 3.8E-G).

We next assessed the mRNA levels in the passaged cells (P5-P25) relative to the OMC to detect any changes in expression of the three mesenchymal markers *Vim*, *αSMA,* and *Cdh2*. The intermediate filament gene *Vim* was statistically unchanged throughout the passaged mesothelial cells, but expressed at 7 - fold higher levels in the OMT ($P<0.01$) (Fig 3.9A). The expression of *αSMA* was 20 - fold downregulated in the P10-25 relative to the OMC, although this change was not statistically significant (Fig 3.9B). By contrast, in the OMT, *αSMA* transcript levels were 1000 - fold lower relative to the OMC ($P<0.001$). We were unable to detect any changes in relative expression of the transmembrane glycoprotein N-cadherin (*Cdh-2*) in the tested samples (P5-P25, OMT) compared to the OMC (Fig 3.9C).

Overall these data suggest that prolonged passaging failed to change the mesothelial cells into a complete myofibroblastic cell type, while the initial cell dissociation

procedure caused the adult mesothelial cells to respond by altering the expression of Vim and *αSMA* expression levels.

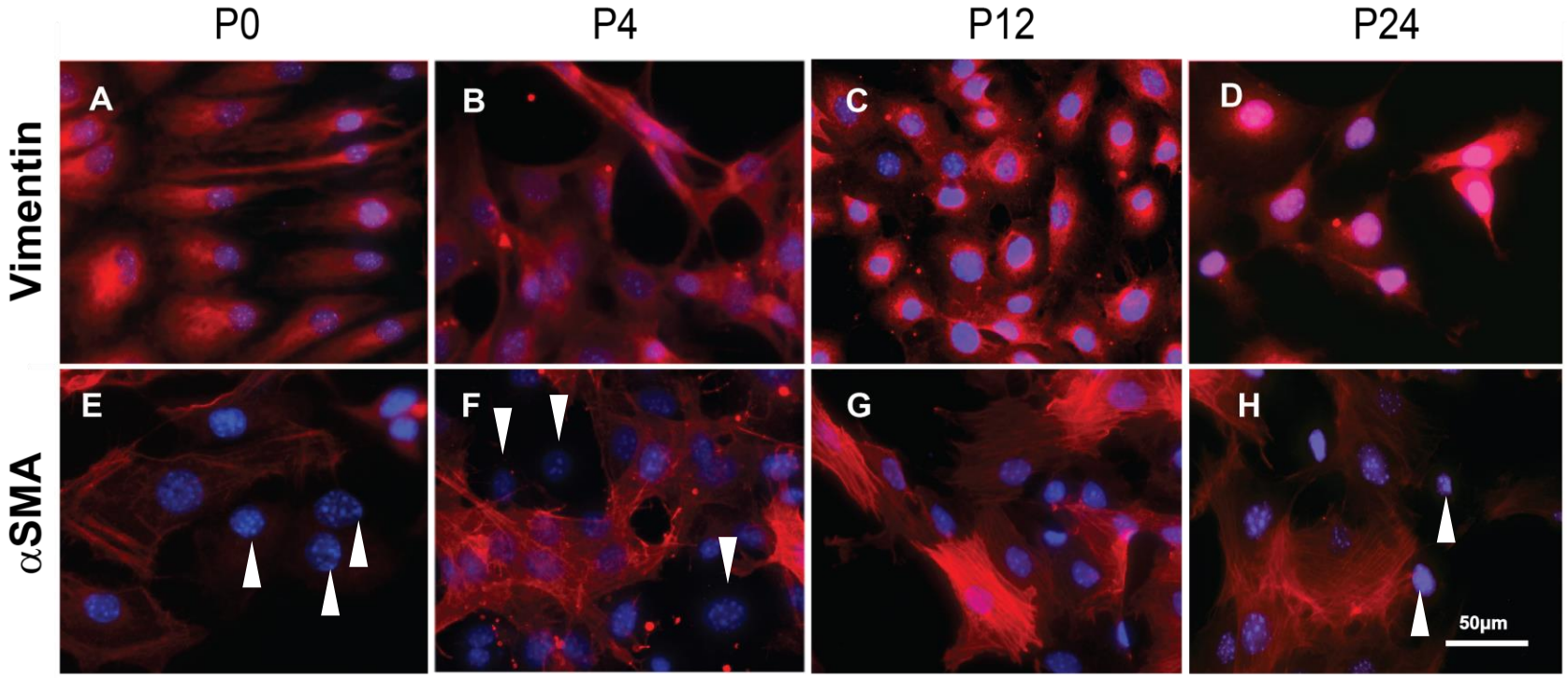

Figure 3.8: Mesothelial cells expressed mesenchymal markers. Confluent mesothelial cells of OMC (P0) and at P4-P24 were stained with Vim and αSMA antibodies. Throughout passages, the MCs showed strong filamentous staining for Vim in the cytoplasm [A-D]. The expression of αSMA was maintained throughout culture, with some cells expressing more of the protein than others (arrowheads) [E-H]. Representative images of n≥3 biological samples per passage.

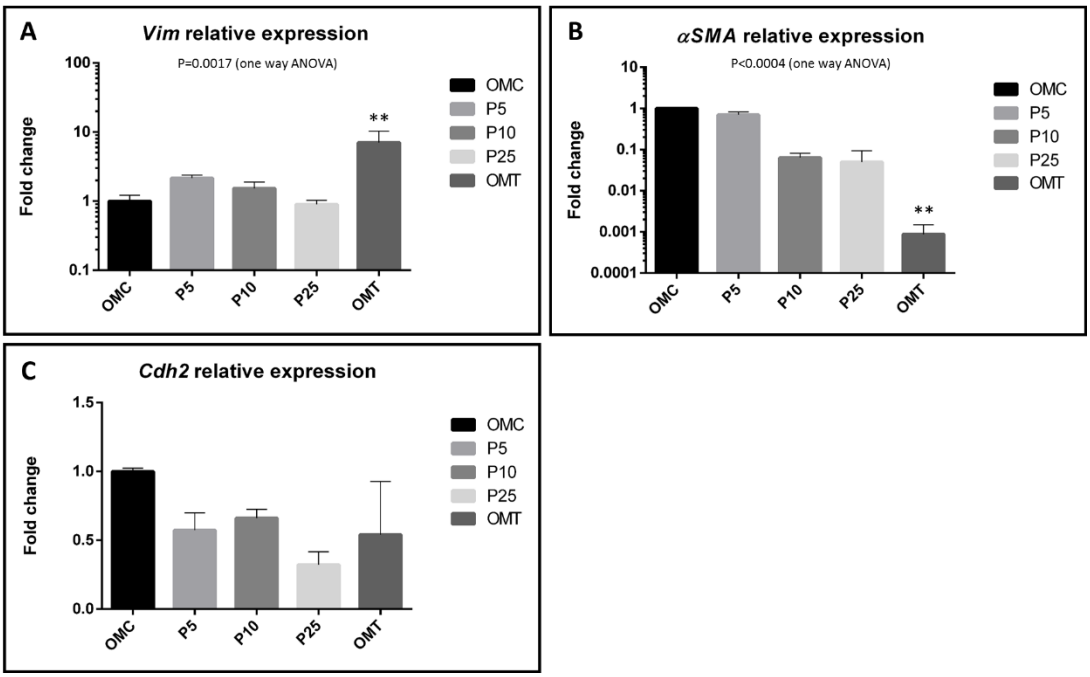

Figure 3.9: Relative expression analysis of mesenchymal markers in cultured MCs. Total RNA was harvested from confluent cells and used for gene expression analysis by qPCR. [A] Relative expression of *Vim* was maintained between the cultured cells (OMC – P25) and 2-fold downregulated between the OMT to OMC (P<0.01) [B] In OMCs, *αSMA* was upregulated 47 - fold relative to OMT (P<0.01); while statistically unchanged in the passaged cells [C] *Cdh2* mRNA expression was unchanged between cultured cells (OMC-P25). Data shown is representative of 3 biological replicates per passage or tissue that are normalized to *GAPDH* and *β-actin*housekeeping genes. Error bar are presented as SEM. Statistics presented are representative of a one-way ANOVA, where the cultured cells were compared against the OMC group, $^{***}p < 0.001$, $^{**}p < 0.01$ and $^{*}p < 0.05$.

3.6 The effect of mesothelial cell culture on the relative expression of EMT transcription factors

We have so far demonstrated that the mesothelial cells in the cultured samples (OMC-P25) have characteristics of a 'hybrid' cell, expressing genes that are markers of both epithelial and mesenchymal cell states. While mesothelial cells in the OMT/*in vivo* also expressed both epithelial and mesenchymal markers, their levels changed in response to culturing the cells. However, our data also showed that the process of repeated passaging seemed to contribute to the loss of epithelial characteristics.

Previously, the ability of mesothelial cells to transdifferentiate into myofibroblasts in response to stress or injury has been coined mesothelial-to-mesenchymal transition (MMT) (Liu et al., 2015, Strippoli et al., 2016). Physiologically, MMT provides mesothelial cells with the ability to contribute to repair of damaged peritoneum through a tightly orchestrated signaling network regulated by the transcription factors Snail1/2, Zeb1/2 and Twist1 (Li et al., 2013b, Hugo et al., 2011, Lamouille et al., 2014). However, the progression through MMT is not a fluid process, and the cells may reside in a spectrum of intermediate states where they gradually lose epithelial features while simultaneously gaining mesenchymal characteristics similar to the situation during EMT in other cell types (Tam and Weinberg, 2013). Therefore, our results suggested that the mesothelial cells during culture adopted an intermediate MMT (Lamouille et al., 2014, Li and Kang, 2016).

Therefore, we next wished to explore whether in cultured mesothelial cells the loss of cell adhesion was associated with the acquisition of an intermediate MMT phenotype. For this purpose we assessed the mRNA expression levels of the transcriptional factors (TFs) *Snail1*, *Snail2*, *Zeb1*, *Zeb2* and *Twist1*, which had

previously been shown to be involved in regulating the MMT transdifferentiation process (He et al., 2015, Horio et al., 2011, Morishita et al., 2016).

Since the mesothelial cells of OMCs had strong epithelial characteristics, we used these cells as the relative control. Our analysis showed that there was no statistical change in *Snail1* expression between the OMC and the passaged mesothelial cells, while it was significantly higher (30 - fold) expressed in the OMT, relative to the OMC ($P<0.0001$)(Fig 3.10A). By comparison, there was a 4-7 - fold upregulation in *Snail2* mRNA amounts in the passaged cells (P5-P25) relative to the OMC. However, this change was only statistically relevant in the P10 samples ($P<0.05$) (Fig 3.10B).

Both *Zeb1* and *Zeb2* relative mRNA expression levels were unaffected by the isolation and culturing procedures when compared to OMC, as there was an 11 - 20 fold reduction in expression between the OMC and the cultured cells (P5-P25), which was not statistically significant (Fig 3.10C-D).

Our analysis showed that prolonged culturing of the mesothelial cells did not significantly alter the relative mRNA amounts of *Twist1* in comparison to OMC (Fig 3.10E), while *Twist1* expression levels were 8000-- fold higher in the OMT ($P<0.001$).

Taken together, of the classical transcriptional regulators of EMT assessed here, only *Snail2* was significantly upregulated and *Twist1*, *Snail1,* and *Zeb1/2* were maintained in passaged mesothelial cells when compared to OMCs.

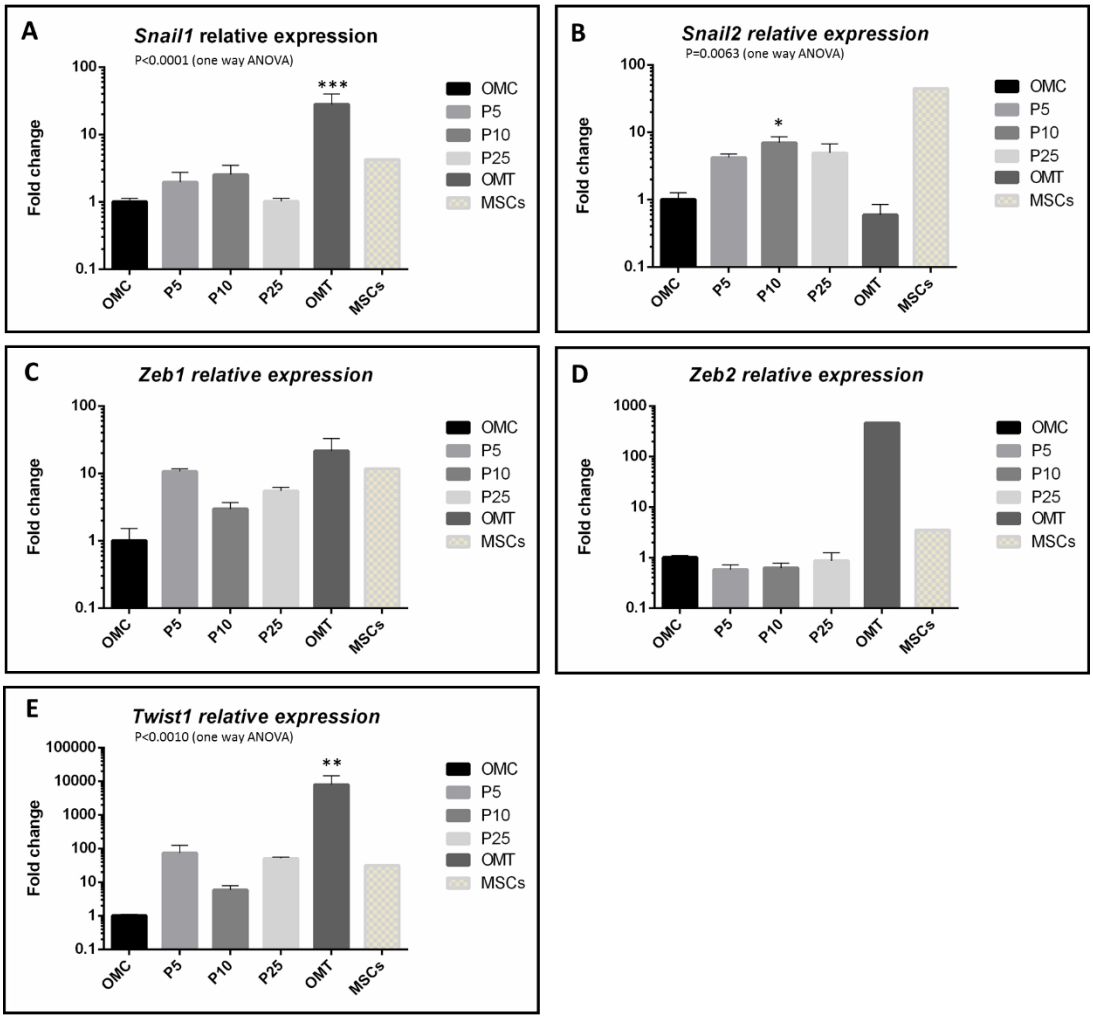

Figure 3.10: The expression of MMT-regulating TFs was altered in mesothelial cells throughout culture. The mRNA levels of the main MMT-inducing TFs in mesothelial cells were compared to the OMC by qPCR using biological triplicates. Samples were normalised to GAPDH and β-actin control genes. Relative [A] *Snail1* expression was between 40-80 - fold reduced in the cultured cells but statistically not significant [B] Relative *Snail2* expression was roughly 5-8 - fold increased P5-P25 cells.[C] *Zeb1* and [D] *Zeb2* relative expression was unchanged in the cultured cells. [E] *Twist1* was $5x10^3$ - fold significantly downregulated in the OMC ($P<0.01$). This relative decline was then maintained in the P5-P25 cells compared against the OMC group. MSCs were the positive control samples used to compare MMT-TF expression. A one-way ANOVA was used to calculate statistical significance, where $^{****}p < 0.0001$, $^{***}p < 0.001$, $^{**}p < 0.001$ and, $^{*}p<0.05$ relative to the OMC.

3.7 Passaged mesothelial cells changed expression of TGFβ and corresponding TGFβ receptors *in vitro*

The expression analysis of epithelial and mesenchymal markers, and MMT regulators in cultured omentum explants and passaged cells suggested that the cultured cells were passing through the MMT programme without fully differentiating into myofibroblasts. Therefore, we aimed to further characterize the underlying signaling mechanisms by assessing the expression levels of transforming growth factor-β (TGF-β) and epidermal growth factor (EGF) and their receptors. TGF-β and EGF are known potent mediators of MMT and EMT induction in a number of cell types including mesothelial cells (Strippoli et al., 2012, Lachaud et al., 2014, Xu et al., 2009). In order to address whether the observed changes in cultured mesothelial cells were associated with autocrine or paracrine mechanisms, we assessed the relative expression of *TGF-β, EGF* and their receptors in the same samples. Our results showed that repeated passaging led to a significant 7 - fold reduction in the relative *TGF-β* mRNA transcripts in the P5, ($P<0.001$) P10 and P25 cells when compared to OMC ($P<0.01$) (Fig 3.11A), while the expression levels of *TGF-β* were unchanged in OMTs relative to OMC. *TβRI* expression levels showed similar dynamics between the different passages as relative expression of *TβRI* was 5-9 - fold downregulated in the passaged cells (P5 $P<0.001$ and P10-P25 $P<0.01$) when compared to OMC, while in OMT it was expressed at similar levels (Fig 3.11B). While the expression of *TβRII* was reduced in all passaged cells, it was significantly reduced (5 - fold) only in the P10 cells ($P<0.05$) (Fig 3.11C), and expressed significantly higher in the OMT.

Our assessment of the expression levels by qPCR of the EGF ligand and its corresponding receptor in mesothelial cells throughout passages was only partially

conclusive as we were unable to detect mRNA expression of *EGF* and its receptor in the OMC and P5 cells. However, the transcripts for *EGFR* could be detected in P10 and P30 mesothelial cells, and for *EGF* in the P30 cells (Fig. 3.11D).

Collectively, these data indicate that placing omentum tissue explants into culture changes their expression profile and that the cultured mesothelial cells pass through MMT, possibly via the intermediate stages of MMT (M/E state). Our data further suggest that this complex process may be regulated by a number of growth factors and that TGF-β and EGF may potentially have a role in mediating these changes.

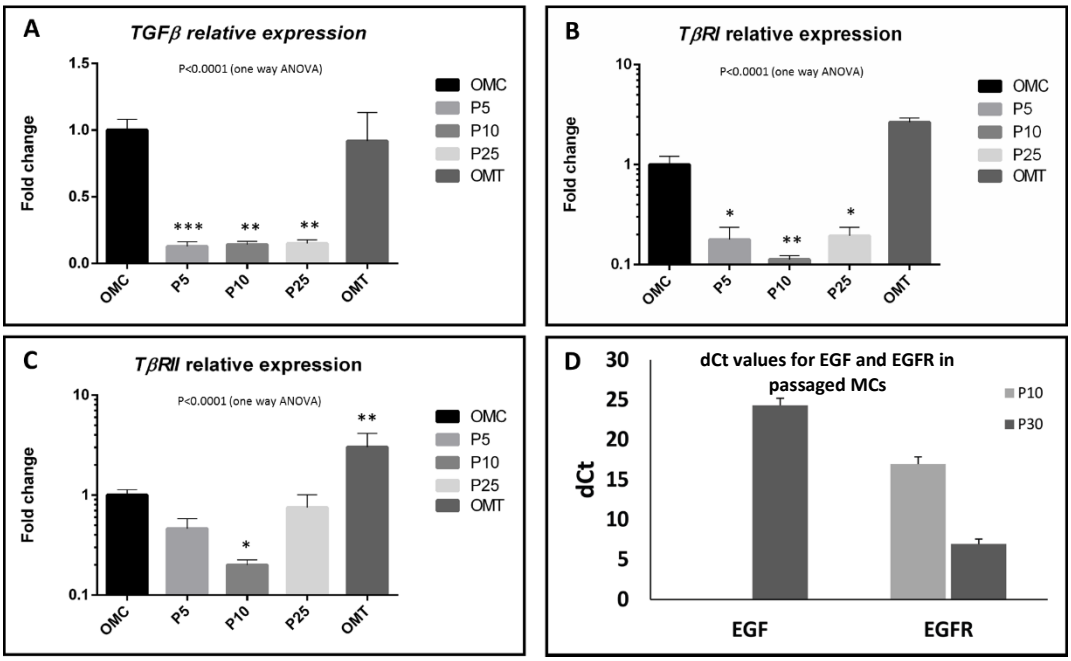

Figure 3.11: Expression analysis of *TGF-β*, EGF, and their receptors: *TβRI*, *TβRII, and EGFR* in passaged mesothelial cells. [A] *TGF-β* mRNA expression was 7 - fold reduced in P5 to P25 passaged mesothelial cells with respect to OMCs (P5 P<0.001 and P10-25 P<0.01). [B] Passaging also resulted in roughly a 5-9 - fold loss in expression of type I transforming growth factor receptor, in the passaged cells (P5 and P25 P<0.05 and P10 P<0.01). [C] The *TβRII* was also downregulated 5 - fold in the P10 cultured cells (P<0.05) relative to the OMC. [D] We were unable to detect the expression of *EGF* and its corresponding receptor in the OMC and P5 cells, however, we could amplify transcripts in P10 and P30 samples. Sample genes were normalized to *GAPDH and β-actin* housekeeping genes. Averages are presented with SEM for error. Statistical analysis was performed using a one-way ANOVA, where samples compared to the OMC had a significance of ***P<0.001, **P<0.01 and *P<0.05.

3.8 Mesothelial cells expressed stem cell markers

Even though we observed changes in mRNA expression for a range of EMT-associated genes, the overall phenotype of the mesothelial cells derived from adult omentum remained largely unchanged between the passages 5 to 25. Furthermore, the cultured MCs continued to divide into high passages (P40). Therefore, we aimed to determine whether these characteristics were related to the expression of stem cell markers.

Immunolabelling of OMC and mesothelial cells at P4, P12, and P24 for the polycomb repressive complex 1 (Bmi1) transcription factor revealed nuclear expression throughout passages (Fig 3.12A-D). Next, we performed qPCR analysis for *Bmi1* expression and observed that mRNA levels were roughly 500 - fold downregulated in the P5 – P10 passaged cells ($P<0.05$) and >1000 fold downregulated in the P25 cells ($P<0.01$) relative to the OMC (Fig 3.13A); in OMT the expression levels were also significantly lower than in OMT.

We could detect a 6 - fold drop in the expression levels of *Sox9* (*Sex Determining Region Y)-Box 9*) in the P5 ($P<0.05$) samples relative to the OMC, and a further 9 - fold downregulation in the P10 and P25 cells; however, changes in the latter samples were statistically not significant compared to OMC (Fig 3.13B). Expression levels of the hematopoietic stem cell marker *CD34* were maintained in the early passage P5 cells but significantly downregulated in P10 and P25 cells when compared to OMC ($P<0.01$) (Fig 3.12C), while in the OMT expression levels were also significantly lower ($P<0.05$). Finally, the mRNA expression levels of the self-renewal gene *Sox2* (*SYRBox2*) were unchanged amongst all the assayed samples (Fig 3.12D).

Of note, we were unable to detect the expression of the pluripotent stem cell markers *Oct4* and *Nanog* (data not shown), which are involved in maintaining the embryonic stem cell phenotype along with Sox2 (Luo et al., 2013).

Taken together, our data indicate that OMC cells and passaged mesothelial cells expressed stem cell markers, which was attenuated, but not lost, throughout the long-term culture. Interestingly, it appears that dissection of omentum tissue into explants for culture induced upregulation of *Bmi1* and *CD34* expression.

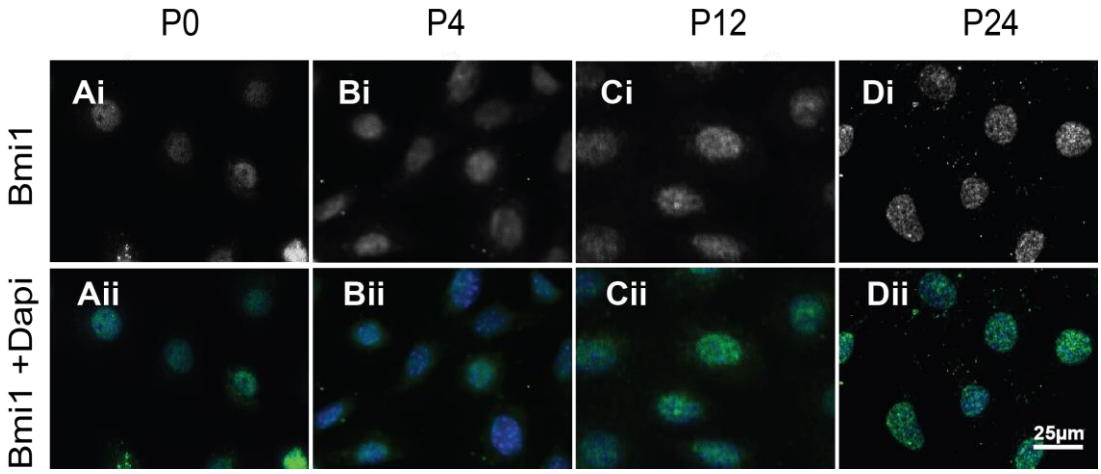

Figure 3.12: Mesothelial cells expressed stem cell markers. Bmi1 was detected in the nuclei of OMC (P0) [A], P4 [B], P12 [C], and P24 cells [D], respectively.

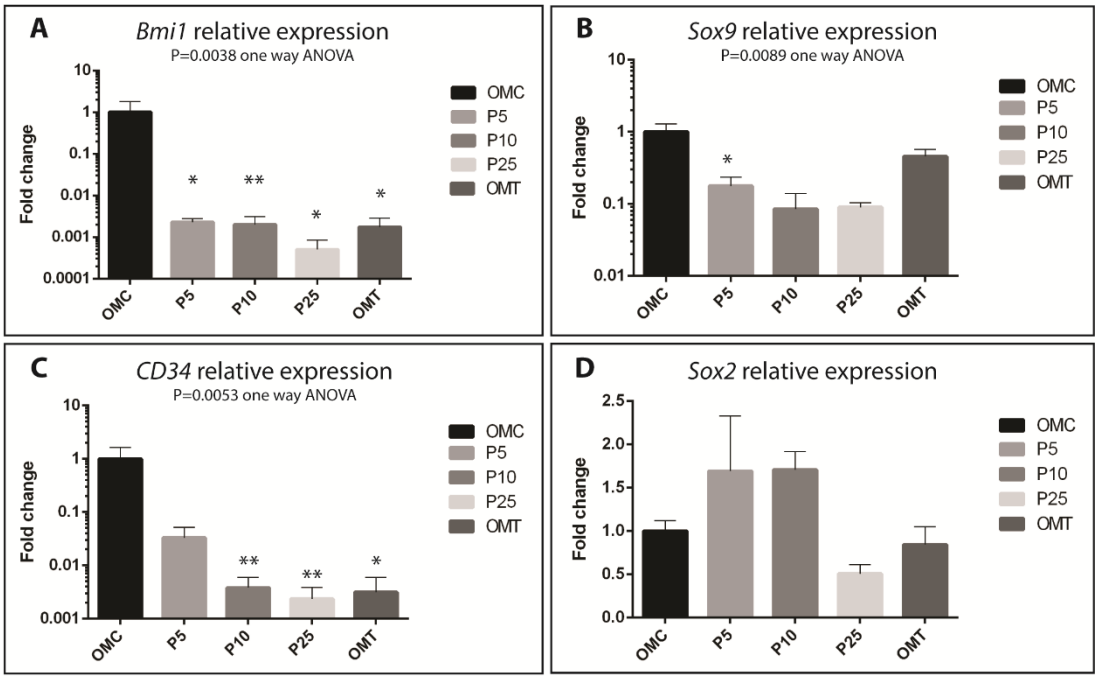

Figure 3.13 OMC upregulate *Sox9* and *Bmi1* expression. [A] The relative - fold change values for the stem cell gene *Bmi1* were roughly 500 - fold downregulated in both the passaged cells and OMT relative to the OMC. [B] *Sox9* expression was only significantly downregulated in the P5 cells, 6 - fold ($P<0.05$) relative to the OMC. [C] Meanwhile the expression of *CD34* was up to 400 - fold downregulated in the OMT and the older passaged cells (P10 and P25). [D] There was no change in expression in the self-renewal marker, *Sox2.* Data is representative of 3 biological replicates with SEM bars. One-way ANOVA statistics was performed, comparing the cultured cells and OMT to the OMC group, $^{*}p < 0.05$ and $^{**}p < 0.01$.

3.9 Mesothelial cells have clonogenic potential

A feature of stem or progenitor cells is their ability to form colonies from a self-renewing single cell. Based on the findings that the mesothelial cells maintained the expression of several self-renewal stem cell genes throughout the long-term culture, we tested the capacity of mesothelial cells to give rise to clones. Passage 5 mesothelial cells were serially diluted in 96 well plates and single cells were identified at 16 h post seeding. The limiting factor of this assay was the relatively low chance in successfully seeding a single cell in one well. However, we were able to generate 4 clonal cell lines from 3 biologically distinct tissue samples. The cells were cultured for more than 20 passages and shared the same slightly elongated morphology as the mesothelial cells pre-cloning (Fig. 3.14A-D).

The similarity of the cloned mesothelial cells to the appearance of passaged mesothelial cells was confirmed by immunofluorescence analysis of protein marker expression. Cytokeratin was localized in a punctate pattern in the perinuclear region of the cells (Fig 3.14E), while ZO1 appeared in a discontinuous band in the tight junctions (Fig 3.14F). The clonal cells also strongly expressed Vim and αSMA proteins (Fig 3.14G and H, respectively), and maintained nuclear expression of the transcription factor Wt1 (Fig 3.14I). We also detected the stem cell marker Bmi1 in the cloned mesothelial cells (Fig 3.14J).

Thus, the clonogenic assay revealed that the mesothelial cells have the ability to self-renew and give rise to colonies of daughter cells. The characterisation studies with immune-labelling showed that the cloned cells showed a similar distribution of epithelial and mesenchymal markers as the passaged cells pre-cloning. Therefore, we conclude that mesothelial cells in culture have unipotent progenitor characteristics.

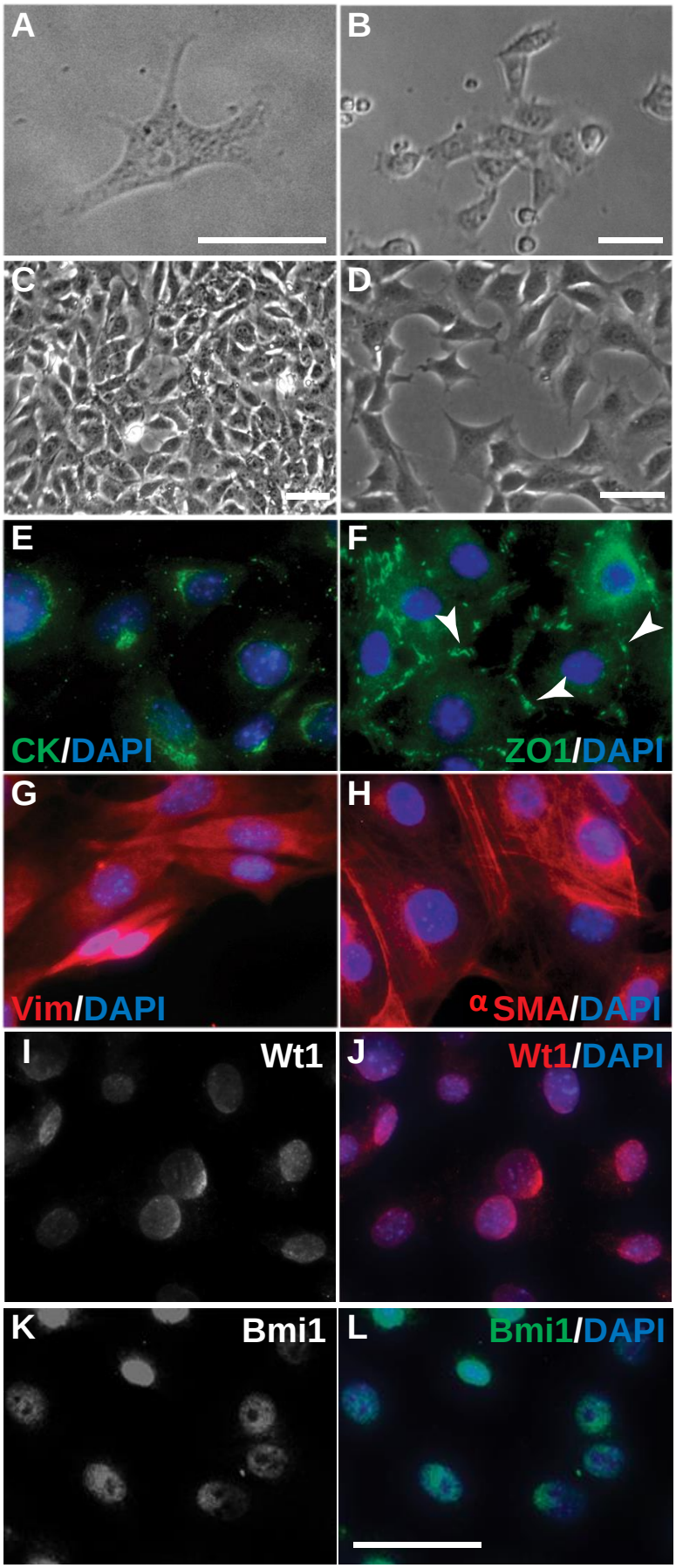
A
B
C
D
E
CK/DAPI
F
ZO1/DAPI
G
Vim/DAPI
H
αSMA/DAPI
I
Wt1
J
Wt1/DAPI
K
Bmi1
L
Bmi1/DAPI

Figure 3.14: The clonogenic potential of mesothelial cells. [A] Passage 5 mesothelial cells were serially diluted and single cells were identified 16 h post seeding. [B] The cells were left to grow for 7 d when distinct colonies could be seen. [C] Individual clones of mesothelial cell clones reached confluence by around 14 d of culture. [D] Mesothelial cell-derived clones were seeded into 8-well glass chamber slides and cultured to 80% confluence. Pan-cytokeratin was localized to the perinuclear region [E], while ZO1 was expressed in a punctate pattern at cell-cell contacts along the cell membranes [F] in a similar fashion as the passaged cells. Similarly, Vim [G] and αSMA [H] were strongly expressed throughout the cytoplasm. The mesothelial marker Wt1 was expressed in the nucleus [I]. The stem cell marker Bmi1 was also detected in the cloned cells [J]. Representative images are shown of experiments conducted on n=3 independent biological samples. Scale bar 50μm.

3.11 Discussion

In this chapter, we describe the successful long-term culture of mesothelial cells after isolation from omentum explants. These cultures were propagated to passage 40 and showed relatively stable population doubling times. Furthermore, they maintained a cobblestone-like phenotype even at the higher passages, expressed mesenchymal markers and maintained some epithelial and mesothelial characteristics that were confirmed by immunohistochemistry and qPCR. Moreover, they also expressed stem cell genes and displayed clonogenic potential.

3.11.1 Long-term culture of omentum-derived mesothelial cells

Peritoneal mesothelial cell cultures are an invaluable tool for studying the effects of PD solutions or various inflammatory molecules on proliferation and wound healing in the absence of systemic modulating factors (Lachaud et al., 2015, Yung and Chan, 2007). Thus, *in vitro* studies using peritoneal mesothelial cells in combination with complementary *in vivo* studies could pave the way for translation into the clinic (Lachaud et al., 2015, Yung and Chan, 2007).

A common problem faced with autologous cellular therapies is the identification of a reliable source of cells for harvesting at therapeutically relevant numbers and with minimal health impact (Lachaud et al., 2015, Yung and Chan, 2007, Asano et al., 2005). The mesothelium lines the serous cavities and the surfaces of internal organs, and shows similar morphological characteristics across different sites of the serosa (Lachaud et al., 2015, Yung and Chan, 2007), thus offering a number of accessible sources for cell harvest.

In this chapter, we have described the generation of several mesothelial cell cultures from mouse omentum explants. The cultures had PDTs that stabilized at around 24 h between passages 8 to 16 and could be propagated for over 30 passages without showing signs of senescence.

Several groups have published a number of diverse techniques for the isolation and culture of mesothelial cells from different tissues sites (Yung and Chan, 2007). Trypsinization is the most widely accepted protocol for harvesting mesothelial cells from whole omentum, tunica vaginalis, or general body cavity (Zhou and Yu, 2016, Asano et al., 2005, Hjelle et al., 1989). Other protocols included scraping the serous membrane off snap frozen organs and the isolation of cells from spent PD effluents (Jiang et al., 2010, Chen and Chen, 2012). However, contamination with other cell types, including fibroblasts (including myofibroblastic mesothelial cells), adipocytes, endothelial and inflammatory cells has been described as a major limiting factor that often required further sorting using mesothelial specific makers (Chen and Chen, 2012, Yung and Chan, 2007, Zhou and Yu, 2016).

Both human and rodent-derived mesothelial cells share similar phenotypic characteristics following isolation (Yung and Chan, 2007, Zhou and Yu, 2016). They often take 5 – 7 days post seeding of 3 – $5x10^3$ cells/ cm^2 for successful monolayer formation (Yung and Chan, 2007, Zhou and Yu, 2016, Chen and Chen, 2012). Similar to our findings, during the propagation of mesothelial cell cultures, the cells adopted an elongated multipolar morphology, and once confluent, the polygonal morphology was restored (Chen and Chen, 2012, Hjelle et al., 1989). However contrasting to our findings, the primary mesothelial cells showed a limited life span in culture based on

the observations that their polygonal phenotype was only maintained up to the third passage, and become senescent by the 6th passage (Yung and Chan, 2007, Zhou and Yu, 2016). Culturing on matrix components (collagen/ gelatin) or plastic alone did not attenuate premature senescence in mesothelial cells (Chen and Chen, 2012, Hjelle et al., 1989).

Here, we have not characterized the mechanisms that contributed to maintaining the mesothelial cell cultures for prolonged periods, *in vitro*. However, a study by Ksiazek and colleagues showed in human omentum-derived mesothelial cells, that early senescence was associated with oxidative stress-induced DNA damage in non-telomeric DNA regions (Ksiazek et al., 2007). Furthermore, exposing young mesothelial cell populations that did not contain senescent cells to conditioned medium from senescent mesothelial cells resulted in the reduced growth and the induction of senescence-associated beta-galactosidase expression (Ksiazek et al., 2008).

3.11.2 Mesothelial cells downregulate key mesothelial and epithelial characteristics with prolonged passage

The cobblestone morphology of the cultured mesothelial cells was present but less pronounced in the passaged cells relative to the mesothelial cells directly surrounding the omentum explants. Although we were able to detect key mesothelial, epithelial and mesenchymal markers within our passaged cell samples, the distribution and gene expression levels were altered in the passaged cells relative to the OMCs.

The mRNA amounts of the mesothelial makers *Wt1* and *Msln* showed opposing responses to repeated passaging. *Wt1* significantly decreased in the passaged cells while *Msln* increased in the higher passages. Wt1 deletion in the epicardium of developing hearts failed to affect Msln expression (von Gise et al., 2011), while Wt1 knockout in the mesothelium that lines the forming liver severely reduced the expression of Msln, hampering embryonic mesothelial cell differentiation (Onitsuka et al.). These results suggest that both Wt1 and Msln play different roles in regulating the mesothelial cell state depending on the tissue context.

Wt1 is a zinc finger transcription factor that in development regulates the maintenance of the mesothelial cell phenotype in a number of mesodermal tissues (Que et al., 2008, Chau and Hastie, 2012). In adult pleural mesothelial cells the loss of Wt1 induced a mesenchymal transition and increased migration and contractility through Smad2 signalling (Karki et al., 2014). Therefore, the downregulation in both *Krt8* and *Cdh1* that we observed in the passaged cells could be linked to the loss of *Wt1*.

Although we were able to detect the expression of ZO1 and pan-cytokeratin, their protein distribution was altered. ZO1 was detectable by IF in a punctate manner around the cell perimeter and also accumulated in the nucleus of the passaged cells. Furthermore, pan-cytokeratins showed perinuclear re-organisation in the passaged cells, while the mesenchymal markers were unchanged relative to the omentum explants.

ZO1 functions as an adaptor, linking the tight junctions to the actin cytoskeleton (Knights et al., 2012, Georgiadis et al., 2010). *In vitro* studies have shown that the

shuttling of ZO1 to the nucleus is inversely related to the extent of cell-cell contacts and degree of their maturity. Specifically, nuclear ZO1 translocation is increased under pro-migratory conditions (such as exposure to EMT-inducing growth factors) and during phases of proliferation (Benezra et al., 2007, Gottardi et al., 1996).

Intermediate filament organization is associated with migration and invasive capacity of a cell. In general, the loss of cytokeratins through phosphorylation and the gain of vimentins is associated with increased migration and is a characteristic of MMT/EMT (Kalluri and Weinberg, 2009, Kim et al., 2015). The phosphorylation of Krt8 and 18 in pancreatic and gastric cancer cells through MEK-ERK, JNK and p38 signalling cascades was shown to induce their perinuclear accumulation and consequently enhanced the migration capacity of these epithelial tumour cells (Busch et al., 2012, Beil et al., 2003, Kim et al., 2015).

Collectively, the passaged mesothelial cells show changes in key epithelial marker distribution that are associated with MMT, transdifferentiation.

3.11.3 Repeated passaging of mesothelial cells alters the MMT programme

Due to the changes in the overall epithelial organization and expression in the passaged cells, we sought to profile the overall expression patterns of key MMT mediators and downstream transcriptional regulators in the cultured cells. It is important to note that for the majority of markers analyzed the OMT and the OMC shared similar expression characteristics, and the changes seemed to occur between the explants and the passaged cells.

While we observed a decline in the expression of the *TGF-β* ligand and its corresponding adaptor signaling receptor (*TβRI*), we noted an upregulation in the

expression of *EGF* and *EGFR* and increased *Snail2* expression. This suggested that Snail2, and possibly also EGF and EGFR, induced a less epithelial state of the mesothelial cells.

Mesothelial cells derived from adult livers shared a number of characteristics seen in the mesothelial cells of this study. With culturing the liver-derived cells lost epithelial features and upregulated the mRNA expression of the *EGFR* (Li et al., 2013b).

Stimulation with EGF has been reported to induce MMT in uterine-derived mesothelial cells by upregulating Snail1/2 and Twist1 protein and mRNA expression (Lachaud et al., 2013). However, whether there is a link between the loss of *Wt1* and the gain in *Snail2* in mesothelial cells is still not known. A study by Takeichi and colleagues reported an increase in Snail2 expression following Wt1 deletion in the developing epicardium, which in turn promoted EMT (Takeichi et al., 2013).

The loss of *Wt1* and the gain in *EGF*, *EGFR* and *Snail2* mRNA transcripts; together with the reduced expression of epithelial genes in the passaged cells shows that the mesothelial cells have adopted a more mesenchymal intermediate MMT phenotype.

3.11.4 Mesothelial cells show clonogenic potential and express stem cell genes

The mesothelial cells in this study demonstrated an ability to proliferate over many passages, and seeding density was not a limiting factor in their propagation. We, therefore, wanted to test the clonogenic potential of the passaged mesothelial cells. The mesothelial cell clones generated shared similar morphological and phenotypical characteristics as the parent cells, which is similar to the behavior to MSCs clones (da Silva Meirelles et al., 2006). This was in contrast to clones generated from KSCs derived from mouse neonatal kidneys, and from human keratinocyte stem cells: KSCs gave rise to clonal lines with different renal phenotypes and characteristics, and the keratinocytes showed alteration in *Krt19* expression, organelle number, and cell cycle distribution (Dong et al., 2003, Fuente Mora et al., 2012).

Based on the observation that the mesothelial cells showed clonogenic potential we analyzed the expression of a number of stem cell genes over prolonged culture. While the OMC showed the highest expression of key stem cell genes *Sox9, CD34,* and *Bmi1*, we noted no changes in the self-renewal gene *Sox2*. However, the role that these stem cell genes have in the mesothelial cells requires further analysis.

3.12 Chapter conclusions

In summary, the data presented in this chapter show that the process of culturing and passaging mesothelial cells slowly induces a less epithelial-like state and that prolonged culturing promotes changes in the overall gene signature. Comparison with the gene expression profile of KSCs isolated from neonatal pup's and MSCs stem cell marker expression showed some similarity. However, we also observed characteristics of stem or progenitor cells due to their clonogenicity and expression of a range of stem cells markers. This led us to ask whether the presence of these stem cell genes was an indicator for multi-lineage differentiation capacity in the mesothelial cells and if age was a contributing factor. These aims are addressed in Chapter 4.

Furthermore, we aimed to understand the molecular mechanisms that regulate the mesenchymal-intermediate phenotype that we observed in the cultured cells. Therefore, we asked whether paracrine effects played a role in these processes; these studies are described in Chapter 5.

In conclusion, the mesothelial cells seemed to maintain some mesothelial associated characteristics following their isolation and repeated passaging relative to the OMC. The cells displayed clonogenic potential and expressed stem cell markers, even in the higher passages. However, they underwent changes that led them to a more mesenchymal- intermediate (M/E) phenotype.

Chapter 4: Analysis of the multi-lineage potential of mesothelial cells

4.0 Introduction and aims

The results from the previous chapter suggested that passaging affected the overall phenotype of the cells, whereby the mesothelial cells downregulated *Wt1* along with epithelial genes; however, the mesenchymal characteristics were largely unchanged even with prolonged culturing. In addition, we had observed that the stem cell genes *Sox9, Bmi1* and *CD34* were upregulated in the OMC relative to OMT, but then downregulated in the passaged cells, and that the mesothelial cells demonstrated clonogenic potential around passage 5. These findings led us to hypothesize that the cultured mesothelial cells may possess progenitor cell characteristics.

The mesothelium is derived from the embryonic mesoderm and the mesothelial cells are renowned for their ability to differentiate along the mesodermal lineages (Lansley et al., 2011). Specifically, mesothelial cells derived from rat omentum or human pericardial cavity were demonstrated to differentiate along the osteogenic and adipogenic lineages *in vitro* (Lansley et al., 2011). Furthermore, the mesothelial cells have also been demonstrated to contribute to the repair of injured peritoneum and liver tissues via the process of MMT (Li et al., 2013a). Recently, the omentum has been shown to ameliorate kidney associated pathologies (Garcia-Gomez et al., 2014). Specifically, in a 5/6 nephrectomy rat model of renal injury, the progression of chronic kidney disease (CKD) was slowed in the remnant kidney after attachment of omentum explants. The rats had reduced plasma creatinine and urea nitrogen levels and improved creatinine clearance compared to the renal ablation control group (Garcia-Gomez et al., 2014). However, the exact mechanisms behind this regeneration remain to be fully characterized.

The Unbekandt and Davies recombinant kidney *ex vivo* culture model is an invaluable tool for studying the nephrogenic potential of labeled cells in a controlled environment due to the easy recombination step (Unbekandt and Davies, 2010).

Nephrogenesis is a tightly orchestrated process characterized by the sequential appearance of three excretory organs; the pronephros, mesonephros and the metanephros (Uhlenhaut and Treier, 2008). The metanephros becomes the permanent kidney and its development starts at embryonic day (E) 10.5–11 when GDNF released from the metanephric mesenchyme (MM) binds Ret on the Wolffian duct and induces ureteric bud (UB) invasion into the MM (Krause et al., 2015, Rak-Raszewska et al., 2015, Uhlenhaut and Treier, 2008). At E11.5 the MM induces UB branching through bifurcation to give rise to the collecting duct system. Branching morphogenesis is induced by HGF, FGF, GDNF, and EGF signaling through Ret, while signaling mediators BMP4, Slit2 and Robo2 inhibit ectopic branching (Krause et al., 2015, Rak-Raszewska et al., 2015). The UB undergoes roughly 10 cycles of branching in mice to give rise to a collecting duct system that channels the urine to the bladder (Krause et al., 2015, Rak-Raszewska et al., 2015). During this process, the mesenchyme surrounding the UB undergoes mesenchymal to epithelial transition (MET) and differentiates into mature nephrons (Krause et al., 2015, Rak-Raszewska et al., 2015, Uhlenhaut and Treier, 2008). This differentiation process takes place in morphogenetic stages where renal vesicles mature into a comma- then S-shaped bodies until they finally connect to the collecting duct (Krause et al., 2015, Rak-Raszewska et al., 2015, Uhlenhaut and Treier, 2008). Figure 4.1 highlights the key events and signaling molecules involved in kidney development.

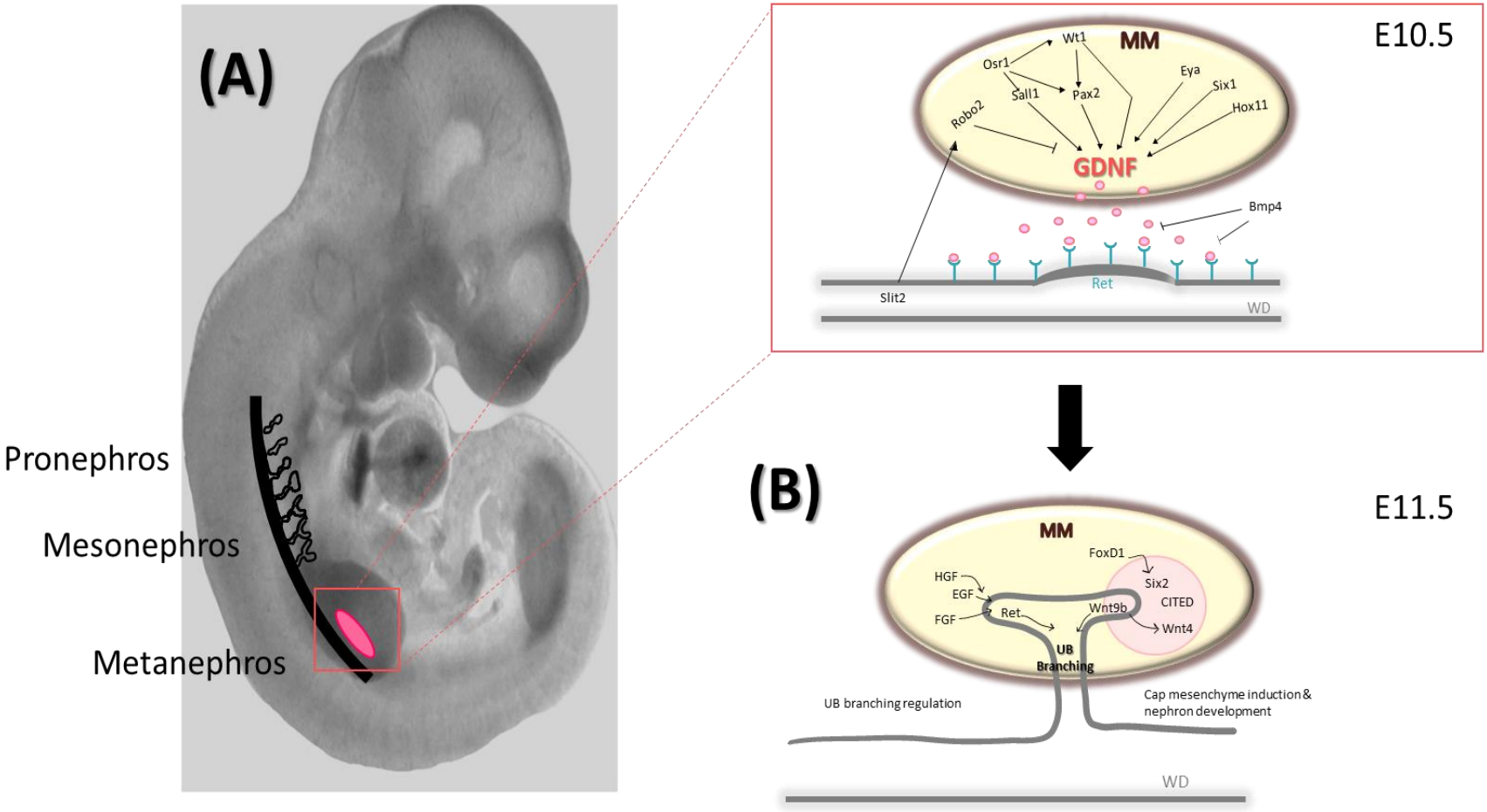
(A)
Pronephros
Mesonephros
Metanephros
E10.5
MM
Wt1
Osr1
Sall1
Pax2
Eya
Six1
Hox11
Robo2
GDNF
Bmp4
Ret
Slit2
WD
(B)
E11.5
MM
FoxD1
Six2
CITED
HGF
EGF
FGF
Ret
Wnt9b
Wnt4
UB
Branching
UB branching regulation
Cap mesenchyme induction &
nephron development
WD

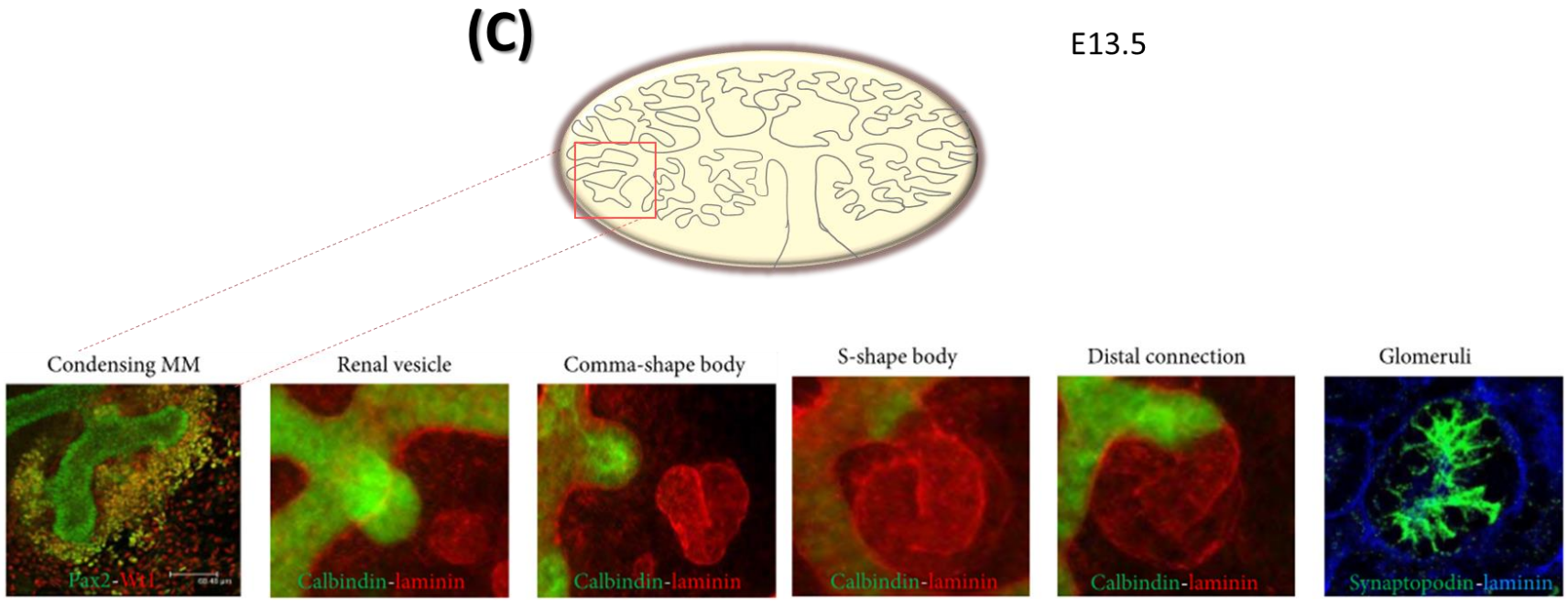

Figure 4.1. A schematic summarizing mammalian kidney development. A) Kidney development ensues over 3 stages, the pronephros, mesonephros and the metanephros. Metanephros is formed following the invasion of the UB through the release of GDNF from the MM. GDNF production and signalling is upregulated by Osr1, Wt1, Pax2 and Sall1 transcription factors. Meanwhile Slit2 and Robo2 attenuate UB budding by inhibiting GDNF production. B) UB branching is induced by a number of growth factors (EGF, FGF and HGF) that act on the Ret receptor. At the tips of the UBs the MM condenses and a heterogeneous pool of CITED1, Six2, Pax2, Wnt4 expressing stem cells aggregate. Signalling through Wnt9b induces the Wnt4 expressing cells to undergo MET and nephron formation occurs. C) The main stages of mouse nephron development stages are outlined. Micrographs were taken from (Rak-Raszewska et al., 2015).

While the mesothelial cells have demonstrated a plasticity; studies, however, have not verified if this multi-lineage capacity along mesodermal lineages is affected by cell passage where the mesothelial cells may lose their plasticity as they age in culture. In this chapter, we aimed to test this by exposing mesothelial cells from various passages to adipogenic, osteogenic inducing conditions and to an *ex vivo* forming nephron.

4.1 Mesothelial cells express mesodermal and metanephric mesenchyme markers.

The mesothelium is of mesodermal origin and arises from the lateral plate mesoderm in the peritoneal cavity, situated close to the intermediate mesoderm, which contributes to the kidneys. Initially, we were interested in screening OMC and passaged mesothelial cells for a number of mesoderm lineage genes to determine if prolonged culturing affected their mesodermal signature. Analysis of mRNA transcript levels of passaged cells revealed that the cells stably expressed the early mesoderm marker *brachyury* (*Bra*) relative to the OMC (P=0.9317) (Fig. 4.2A). Meanwhile, no considerable change in expression was observed for the paraxial and intermediate mesoderm marker *forkhead box protein C2* (*FoxC2*) (P=0.9694), or the intermediate mesoderm marker *odd-skipped related transcription factor 1* (*Osr1*) (P=0.1234) (Fig. 4.2A). However, we could not detect the expression of the *Wnt3a* or *Wnt8a* (data not shown), which are associated with primitive streak development of the early mesoderm and direct cells towards a hematopoietic fate (Fehling et al., 2003, Waghray et al., 2015). Among the mesodermal genes analyzed, only expression levels of *forkhead box F1* (*Foxf1*), which is expressed in the lateral plate/extraembryonic mesoderm, were altered with passaging (Fig 4.2B). Specifically, we could see a substantial increase in relative expression between the OMC and the P5-P25 cells ($P<0.05$ for the P5 and P10 cells and $P<0.01$ for the P25 cells). Overall, the cultured mesothelial cells expressed *Bra, Osr1,* and *Foxf1*, markers of the lateral plate mesoderm, suggesting they maintained some early mesoderm characteristics.

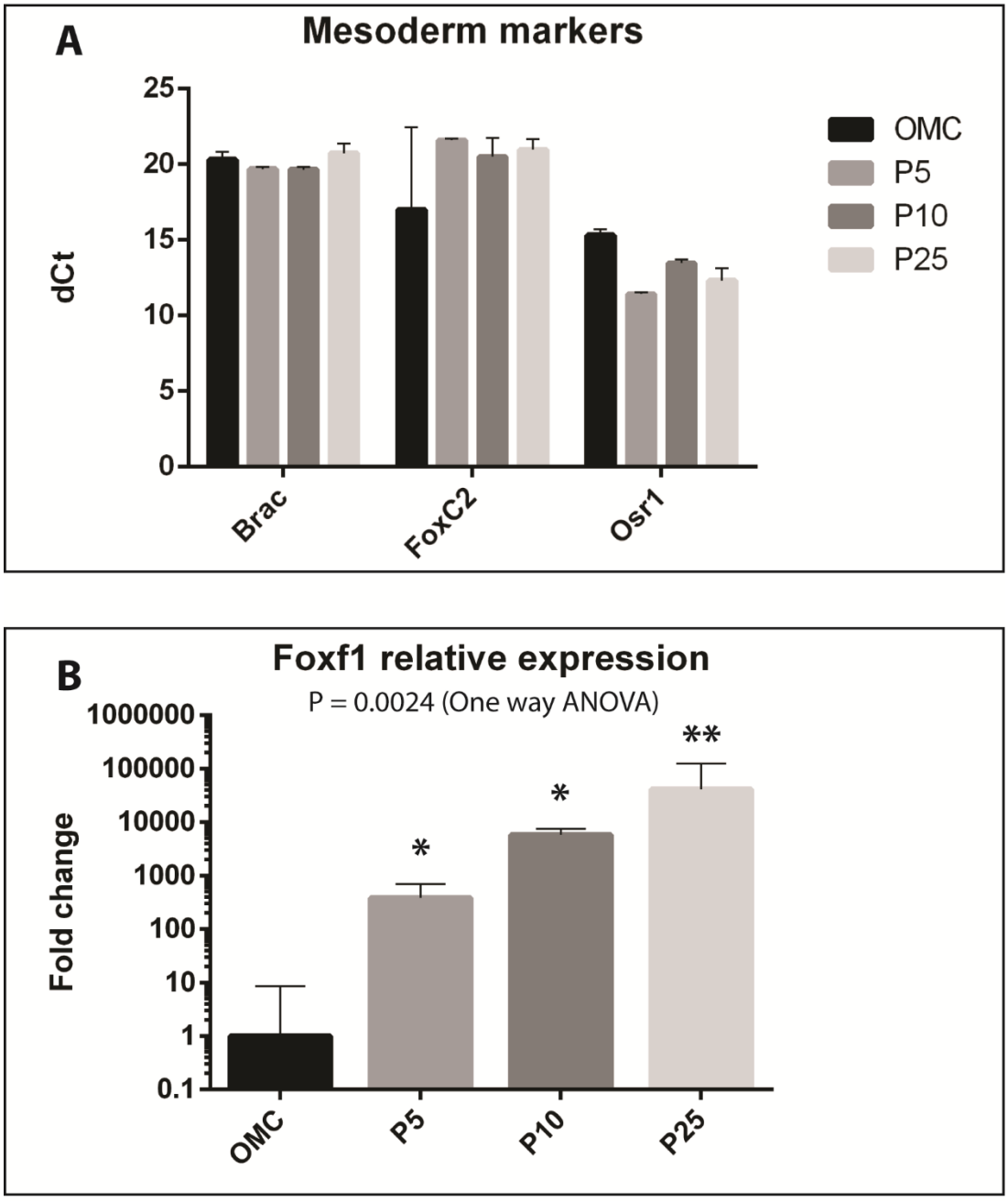

Figure 4.2: Cultured mesothelial cells express markers of the early mesoderm. [A] Mesothelial cells maintained the expression of early (Bra), paraxial/intermediate (Foxc2) and intermediate mesoderm (Osr1) genes. [B] Foxf1 expression that is found in the lateral plate showed between 400 – 40,000 fold upregulation in the cultured cells relative to the OMC. Data are presented as a mean ± SEM for 3 independent biological replicates. A one-way ANOVA with Sidak post hoc analysis was used to determine statistical significance between the group means.

4.2 Mesothelial cells demonstrate multi-lineage potential *in vitro.*

Since the mesothelial cells expressed early mesodermal markers, our next aim was to assess their differentiation capacity along the mesodermal lineage across different passages *in vitro.* Initially, the mesothelial cells were seeded at a high density for the differentiation assays; however, the cells reached confluence within 3 d post seeding and by 5 d formed a tightly-packed sheet which detached from the plate. Therefore, the mesothelial cells were seeded at 1000 cells/cm^2 (d 0), treatment for differentiation started the following day (d 1), and lasted until 14 d. We included murine MSCs as a positive indicator of differentiation for osteogenesis and adipogenesis.

In the presence of osteogenic inducing media (MCs growth medium supplemented with β-glycerophosphate, dexamethasone, and ascorbic acid), the P5-P26 mesothelial cells (Fig. 4.3D-E) and the MSCs (Fig. 4.3F) responded robustly by generating calcium deposits. To further confirm differentiation, we analyzed the gene expression of the osteoprogenitor marker *alkaline phosphatase* (*Alpl*), the osteoblast marker *osteonectin* (*Sparc*), and odontogenic differentiation marker *dentin matrix protein I* (*Dmp1*) in treated cells relative to untreated passage matched cells. *Sparc* has been shown to promote mineralization during bone formation , while *Dmp1* has a crucial role in the mineralization of bone and dentin (Teti et al., 2015). In response to osteogenic stimuli, the mesothelial cells at P5 and P13 expressed higher levels of *Sparc* transcripts when compared to untreated cells; at P13, this increase was significant (P=0.0115) (Fig. 4.3G). By contrast, expression levels for *Sparc* were unchanged in P26 cells between treated and untreated cells. We also observed a step-wise increase until P13 in the relative expression of *Dmp1*, although not

statistically significant. Moreover, the expression was unchanged in treated cells at P26 when compared to the controls (Fig. 4.3H). Analysis of *Alpl* showed that the transcript could not be detected in treated and non-treated mesothelial samples, while it could be amplified in the differentiated MSCs (data not shown).

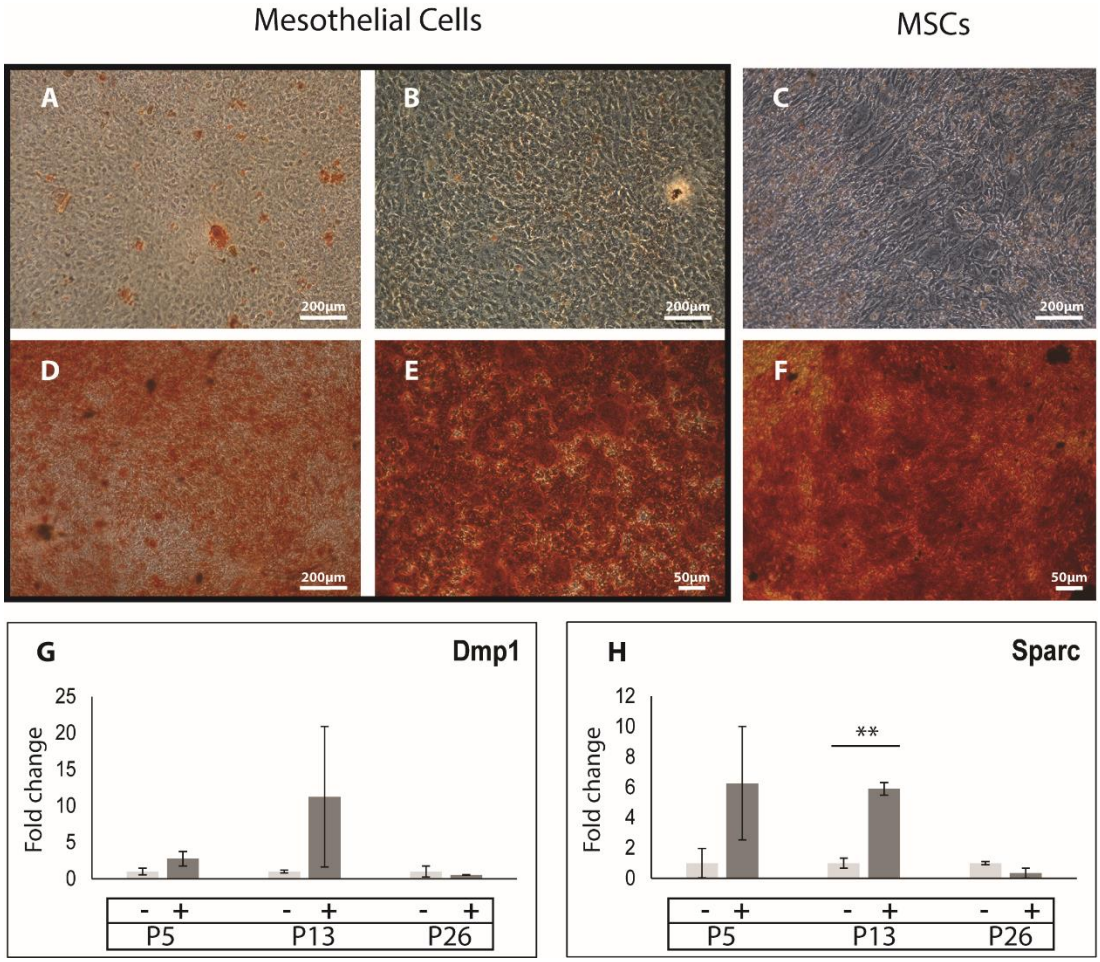

Figure 4.3 Mesothelial cells demonstrate osteogenic potential. Mesothelial cells passages 5, 13 and 26 were seeded into 6-well plates and either treated with osteogenic inducing medium or in full growth medium for 14 d. The samples were stained with the alizarin red S dye to detect calcium mineralisation. In P5 and P13 mesothelial cells [A-B] and MSCs [C] not treated in osteogenic medium, the strong orange dye failed to develop. Calcium deposits were detected in P5 and P13 mesothelial cells [D and E] and P21 MSCs [F] that were cultured in osteogenic medium. Analysis of relative gene expression for *Dmp1* [G] and *Sparc* [H] revealed that they were mostly up-regulated in the lower passages, with a 6-fold change for *Sparc* expression at P13 (P=0.0115). Data is representative of 3 biological replicates for each condition.

Following adipogenic culture conditions, we could detect lipid droplet formation using Oil Red O dye staining in the stimulated P5, P13, and P26 mesothelial cells and in the MSCs, but not in the untreated cells (Fig. 4.4A-C and not shown). Visual inspection indicated that more lipid droplets accumulated in the P5 cells than in P13 cells (Fig. 4.4D-E), but in both MC passages the cells were more dispersed when compared to the MSCs (Fig 3F). We, therefore, characterized this apparent adipogenic differentiation process further by quantifying relative transcript levels of markers for adipogenesis in the cells. We assayed the samples for the expression of *peroxisome proliferator-activated receptor gamm*a (*PPARγ*), a master regulator of adipogenesis (Siersbaek et al., 2010), and found it significantly upregulated in stimulated P5 (P=0.0064), but not in P13 and P26 cells (Fig. 4.4G). We also detected *fatty acid transport protein 1* (*Fatp1*) expression in the stimulated mesothelial cells. This gene product is involved in regulating fatty acid uptake in adipocytes (Lobo et al., 2007). Overall, while we observed an increase in expression following stimulation at P5, there were large variations between the biological samples; however, this increase was lost in stimulated MCs at P13 and P26, with levels dropping below those in control MCs (Fig. 3H). The *glucose transporter type 4* (*Glut4*), is an insulin-regulated glucose transporter that is primarily located in adipose tissues (Huang and Czech, 2007). We were unable to detect expression of this gene in the mesothelial cells but could amplify the mRNA in the stimulated MSCs (data not shown).

Taken together, these data indicate that mesothelial cells cultured up to P13 generally maintained the ability to respond to osteogenic inducing cues, while the potential to respond to adipogenic cues was attenuated past passage 5.

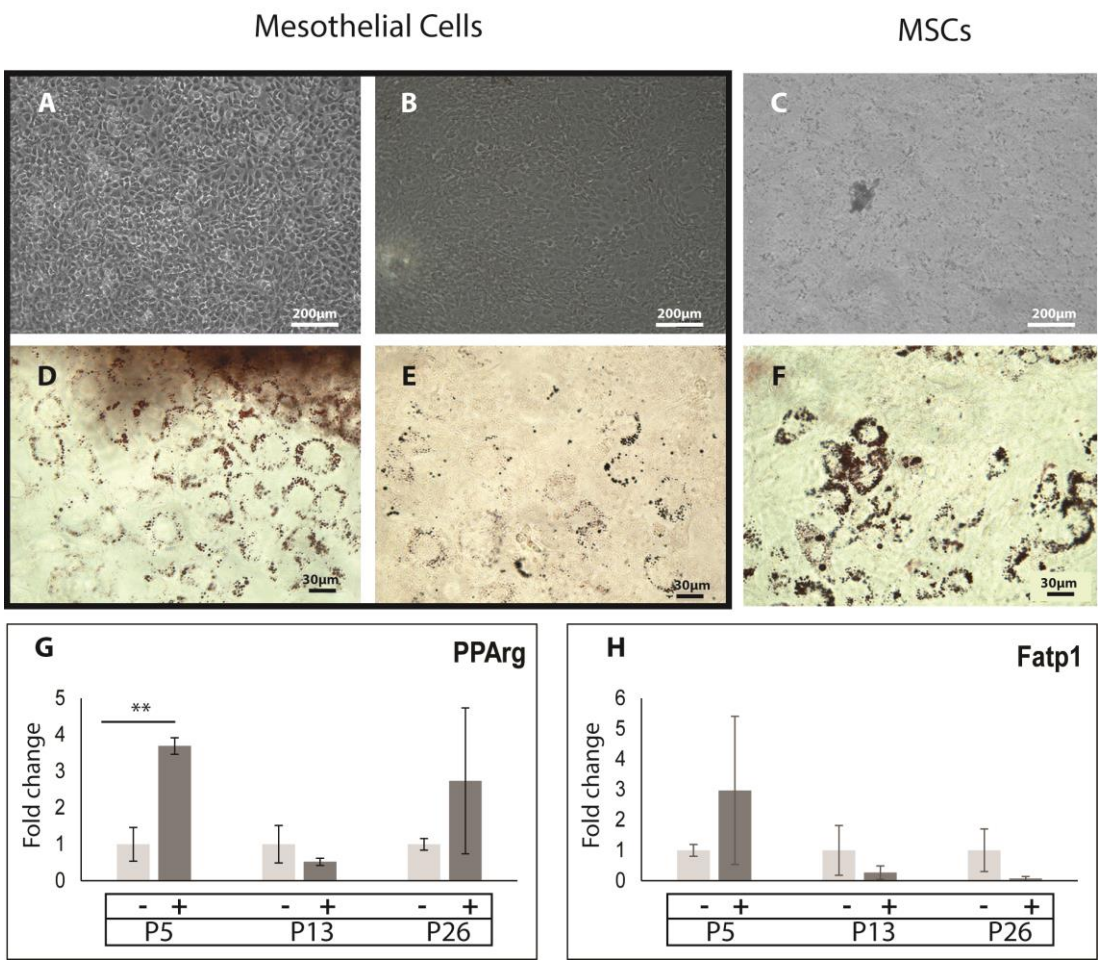

Figure 4.4. Mesothelial cells demonstrate adipogenic potential. Mesothelial cells from various passages and MSCs were seeded and stimulated in adipogenic inducing medium for 14 d. Lipid vacuole accumulation was detected using Oil Red O staining and could be seen in passage 5 and 13 [D-E] mesothelial cells, and in P21 MSCs [F]. Mesothelial cells [A-B] and MSCs [C] cultured in control medium failed to stain for fat droplets. A 3.7-fold increase in *PPARγ* expression was detected at passage 5 (P=0.0064) [G], while a non-significant increase in relative *Fatp1* expression was observed [H]. In MCs of P13 or P26, levels were either reduced or not significantly increased. Images are representative of 3 independent biological replicates for the mesothelial cells and averages for fold change in expression for qPCR analysis.

4.3. Assessing the potential of mesothelial cells to integrate into kidney structures using an *ex vivo* embryonic chimeric kidney rudiment assay.

As shown earlier, the mesothelial cells maintained the expression of early mesoderm markers during culturing. However, their differentiation capacity along the osteoblast and adipocyte lineages was limited by passage. Based on their mesodermal lineage and the fact that the omentum could alleviate CKD, we wondered if they mesothelial cells could contribute to nephrogenesis and if this plasticity was passage limited. To do this we decided to use an *ex vivo* kidney rudiment assay which ,under appropriate culture conditions, takes advantage of the ability of the stem and progenitor cells present in the kidney rudiment to re-organize themselves into early collecting duct systems, nephrons, and stroma. This technique gives rise to structures that resemble whole kidney rudiments, however, they lack a single collecting duct tree (Davies, 2015).

The experimental design comprises the aggregation of dissociated labeled exogenous cells with dissociated metanephric cells through gentle centrifugation. The chimeric pellets were then cultured on an air-media interface throughout the experiment, however, for (Batchelder et al., 2015)the first 24 h the pellets were treated with Rho-associated protein kinase (ROCK) inhibitor to protect them from apoptosis related to anoikis (Davies, 2015). Finally, the samples were collected at 4 d and 7 d to assess overall renal structural development and integration of exogenous cells.

4.3.1 Optimising conditions for mesothelial cell labeling

In order to assess the potential of mesothelial cells to integrate into kidney structures *ex vivo*, we first needed to establish a suitable labeling technique that imparted the strongest fluorescence signal and had limited impact on cell viability. A lentivirus-based GFP labeling method had been previously established in our lab, which was followed by FACs sorting to yield cells with continuously stable uniform fluorescent protein expression (Ranghini et al., 2013). By contrast, cytoplasmic and membrane dyes carry several advantages over other labeling techniques for single cell monitoring in *in vivo* and *ex vivo* studies (Progatzky et al., 2013). These labeling procedures usually consist of a simple, robust method for uniform cell staining. However these probes used for the labeling of cells can have cytotoxic effects or exert unintended modification in cell function if not properly optimized (Progatzky et al., 2013).

Therefore, we compared the lentivirus approach with two transient labeling dyes (CFDA SE and PKH67) in order to identify the cell dye that would stably label the mesothelial cells without signs of cytotoxicity or signal fading over several population doublings, while ideally allowing early, medium and late passage MCs to be assessed.

CFDA SE is a colorless, non-fluorescent cytoplasmic dye that upon entry into the cell through passive diffusion is deacetylated by esterases into the fluorescent CFSE (carboxy-fluorescein succinimidyl ester). The fluorescent dye–protein complexes that form in cells are retained for up to 8 cell divisions and are equally passed onto the daughter cells (Progatzky et al., 2013, Thayer and Wong, 2016). PKH67 is a carbocyanine fluorescent dye that adducts to the lipid bilayer of cell membranes

through its aliphatic carbon tail. It has an estimated *in vivo* fluorescence half-life of up to 100 days (Progatzky et al., 2013, Nagyova et al., 2014).

We were able to successfully label mesothelial cells between passages 5-10 using 5 µM CFDA SE (Fig. 4.5A) and 1 µM PKH67 (Fig. 4.5B). GFP-lentivirus transduction of mesothelial cells was performed by another member in the lab and kindly gifted. Passage 6 mesothelial cells were used at the start of the labelling protocol, however, an 88% GFP-labelled population of cells was only achieved at passage 20 after several rounds of FAC sorting (Fig. 4.5C).

To monitor the fluorescence stability of the two dyes over time and its dilution with increasing cell population doubling, labelled mesothelial cells were monitored over a course of 7 days. The labelled cells were also compared against GFP-transduced cells and unlabelled cells. The fluorescent signals emitted from the probes and GFP-protein were quantified through FACS (Fig. 4.6A-C). The intensity of the CFDA SE was the brightest at day 0, however, the fluorescent signals released by both PKH67 and CFDA SE dyes declined at a relatively similar rate (Fig. 4.6D). Both probes were brighter and more uniform throughout the 7 day period than the autofluorescence emitted by unlabelled cells. In contrast to this, the GFP-transduced cells had a stable signal intensity, throughout.

Taken together the CFDA SE and PHK67 probe kits carry the advantage over GFP transduction due the ease of uniformly labelling the mesothelial cells in a short space of time, which is convenient for using lower passage cells.

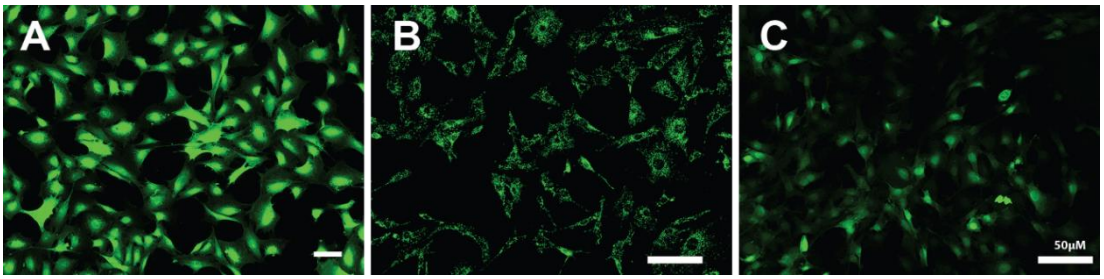

Figure 4.5 Mesothelial cells were labelled with either dye-probes or transduced with GFP. Adherent mesothelial cells were labelled with CFDA SE 5 µM [A] or PKH67 1 µM [B] or transduced with GFP-lentivirus [C]. While both the CFDA SE and the GFP had cytoplasmic and nuclear localization, PKH67 displayed a punctate staining pattern. Images were taken at 1 s exposure for the 488 nm channel of live cells, 1 h post labelling. Scale bar 50 µM.

4.3.2 Embryonic kidney *ex vivo* culture

Before we co-culture the labelled mesothelial cells into the re-aggregated metanephros, we first wanted to demonstrate that the process of disaggregation and reaggregation of the rudiment cells allowed for the development and reorganisation of embryonic kidney structures. We were able to detect Wt1 and sine oculis homeobox homolog 2 (Six2) expression in the whole embryonic rudiments (eControl) following 7 d of culture; both proteins have important roles in the condensing mesenchyme that give rise to the nephrons, while Wt1 continues to be expressed in the developing nephrons (Fig. 4.7A-E). Pax2 positive regions represented induced MM, but it is also found in the UB (Fig. 4.7J-l). Megalin^{+} proximal tubules were also detected in the whole organoids (Fig. 4.7M-O), and laminin/ PNA (peanut agglutinin) positive staining was found localised to the basement membranes surrounding the forming nephrons and UBs (Fig. 4.7J - Q).

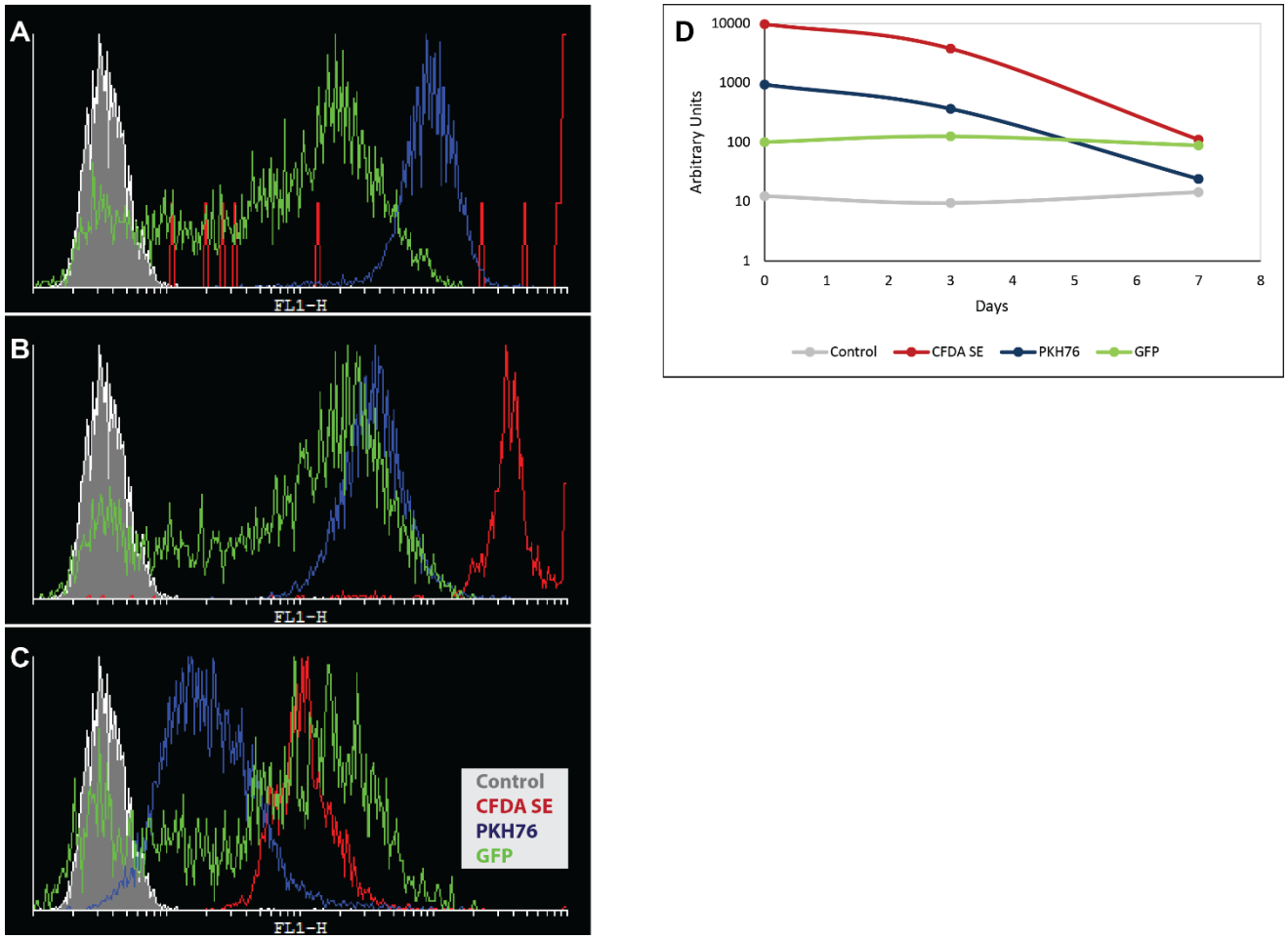

Figure 4.5 Analysis of the fluorescence signal intensity of CFDA SE-, PKH67- and GFP- labelled cells. Low passage mesothelial cell were incubated in suspension in either 5 µM CFDA SE for 30 mins or in 1 µM PKH67 for 3 mins. The fluorescence intensities of the labelled cells were measured on day 0 [A], day 3 [B] and day 7 post labelling [C], using the FL1-H channel. Unlabelled Control cells were also included. [D] Over the course of 7 days the intensity of the fluorescence signals imparted by both linker-kits declines, while the GFP signal is stably expressed although less brightly.

The process of dissociation followed by reformation as tightly compressed pellets of E13.5 rudiments (rControls) did not impart any negative consequences on structural development of the metanephric mesenchyme and nephrons (Fig. 4.8). We were able to detect megalin expressing proximal tubules (Fig. 4.8A-F) and Wt1 expressing MM across the pellets by 7 d in culture (Fig. 4.8G-L). Staining with PNA (Peanut agglutinin) also labelled the outer surfaces of tubules (Fig 4.8M).

Since the culture conditions and the dissociation process did not hinder the formation of early nephron structures, we moved on to co-culturing the labelled mesothelial cells with the metanephric cells in chimeric kidney rudiments.

4.3.3 GFP-labelled cells maintained the signal most consistently in chimeras throughout culture

Preliminary studies using the GFP-labelled mesothelial cells had shown that the optimal seeding ratio of mesothelial cells to kidney rudiment cells was 1:10. This allowed for an even distribution of mesothelial cells throughout the pellet by the end of the experiment without their overgrowth (not shown). We were interested in analysing the integrative potential of low and high-passaged cells; of which the two dyes could achieve this. We also the P20 GFP-labelled MCs for comparison.

Passage 5 – 10 cells were labelled with either the CFDA SE or the PKH67 and subsequently added to the single metanephric cell suspension. While P22 – 32 GFP labelled cells were used to test the effects of high passage. Mesothelial cell distribution in the re-aggregated rudiments was intermittently monitored at days 1, 4 and 7 (Fig. 4.9). We could easily detect the cells 24 h post seeding in all 3 conditions (CFDA SE-, PKH67- and GFP-labelled MC-containing re-aggregated chimeric

rudiments). We observed a clear reduction in signal intensity by day 4 in rudiments containing PKH67-labelled cells (Fig. 4.9A-C), and by day 7 in those containing CFDA SE-labelled cells (Fig. 4.9D-F). These results confirm the findings from the FACS analysis on signal intensity of the differently labelled cells over time. All 3 labelling techniques shared similar ring-like structures that were most prominent at day 4. Interestingly, the chimeric rudiments containing GFP-mesothelial cells had a more compacted morphology (Fig. 4.9G-I) as opposed to the rudiments containing dye-labelled cells (Fig. 4.9A-F).

The incorporation of GFP-labelled mesothelial cells into the re-aggregated rudiments was performed on 12 separate occasions with a total of 108 GFP chimeric rudiments successfully cultured. In all those accounted instances there was an even distribution of GFP mesothelial cells with prominent ring-like structures across the pellets. In the cases of the CFDA-SE and PKH67 probe kits, each of the labelling and incorporation procedures was performed on 3 independent occasions with roughly 12 pellets each. While all labelling techniques did show similar pellet formation, using the GFP^+ mesothelial cells was the only condition in which the signal was maintained throughout the culture period. Since the signal from the probes was still detectable at 4 d, we preceded to use this technique to monitor the effects of early passage on mesothelial cells integration potential and metanephric development.

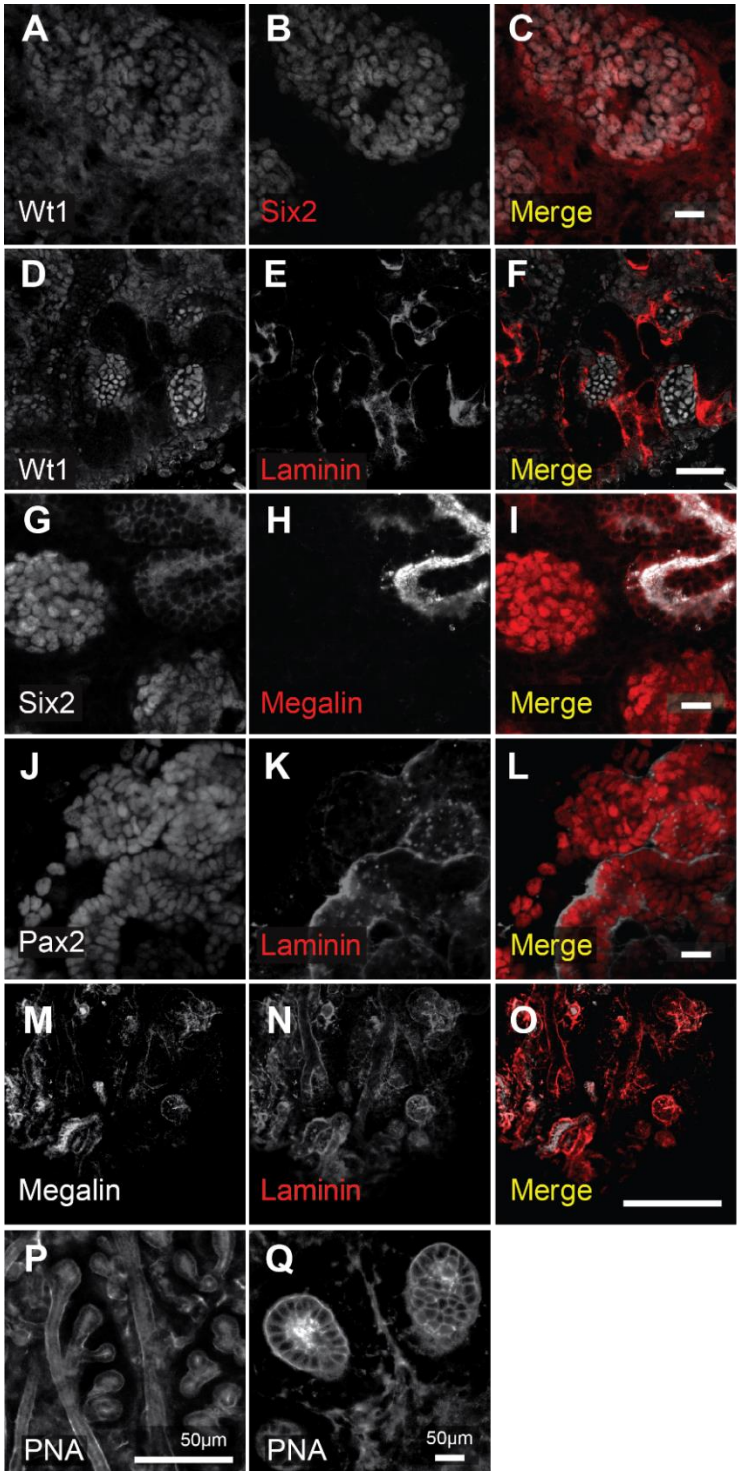

Figure. 4.7 Whole embryonic rudiment show expression of key kidney markers. Whole embryonic kidney rudiments (eControl) were harvested from E13.5 embryos and cultured for 7 days, on a media-air interface. The samples were immunostained for a range of functional and structural markers, including markers for condensed mesenchyme Wt1 and Six2. Early podocyte precursors were also detectable through Pax2 and Wt1 labelling. Megalin staining detected proximal tubule structures, while laminin and PNA were found surrounding the basement membrane of the developing nephrons and UBs. Representative images of n≥3 independent biological samples. Scale bar 50 µM.

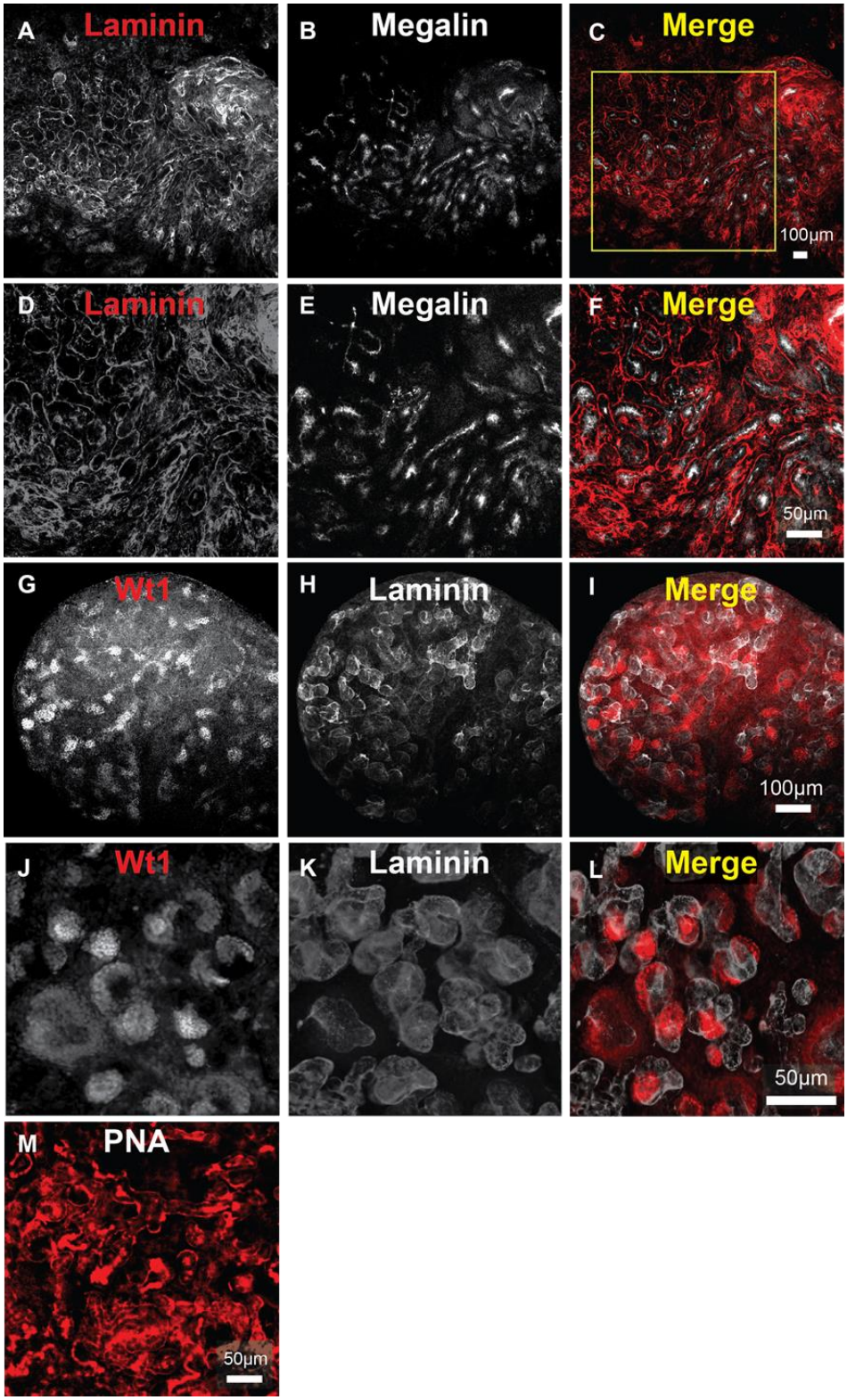

Figure 4.8. E13.5 re-aggregated rudiments form renal structures. Murine kidney rudiments (rControl) were isolated from E13.5 mice and dissociated in trypsin for 10 mins, before being re-aggregated and cultured as $2x10^5$ cells/ pellet for 7 d. The rControl samples displayed characteristic kidney development features during the *ex vivo* culture period, such as megalin expressing proximal tubule structures [A-F], and condensing mesenchyme and developing nephrons depicted through Wt1 staining [G-L]. PNA staining also detected the outer surfaces of forming tubules [M].

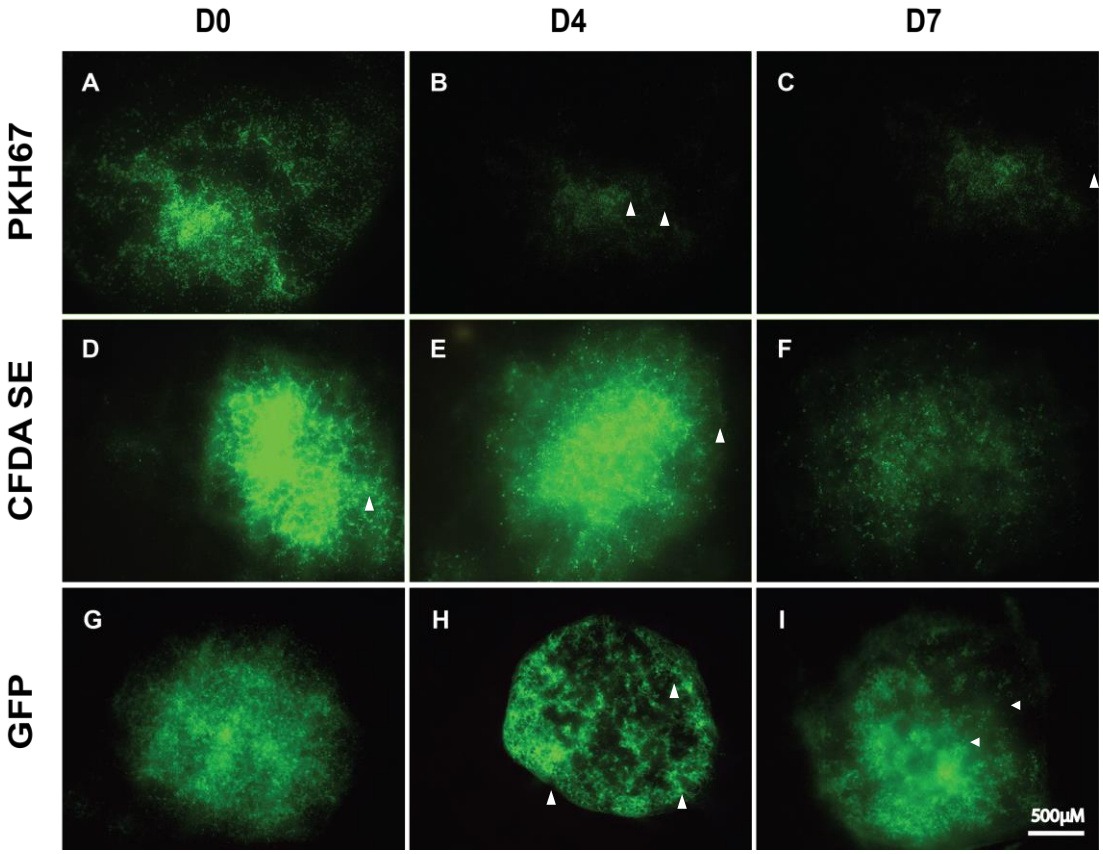

Figure 4.9. Labelled mesothelial cells can be identified in the chimeric rudiments. Re-aggregated kidney rudiments containing mesothelial cells labelled with PKH67 [A-C], CFDA SE [D-F], and GFP [G-I], were imaged at 1, 4 and 7 d post seeding. Distinct loop-like structures of mesothelial cells (white arrows) were most prominent at day 4, however, as fluorescence progressively declines in the dye-labelled cells, becoming less visible. In GFP-labelled rudiments, the population and arrangements of the cells remained comparatively more pronounced. All chimeric rudiments were captured at 488nm wavelength following a 500 ms exposure time.

4.3.4 PKH67 and CFDA SE dyes transferred to neighbouring embryonic kidney cells

As shown in the previous section, the labelled mesothelial cells distributed throughout the re-aggregated chimeric rudiments and were still detectable by the end of the experiment. Accordingly, we wanted to address if these cells could integrate into the developing nephron structures. Therefore, samples were harvested at days 4 and 7 in order to assess the potential contribution of the cells as the chimeric rudiments increased in size and matured over time.

After 4 days of co-culture, the rudiments appeared to have developed structures similar to control rudiments. This indicated that mesothelial cells did not exert an inhibitory effect on the rudiment development. Furthermore, laminin staining revealed that the chimeric rudiments contained the different stages of nephron development, including renal vesicle (Fig. 4.10B), S-shaped (Fig. 4.10F-G) and tubule elongation of the S-shaped bodies (Fig. 4.10B). Pax2 expression was seen in UB epithelium surrounded by a laminin-positive basement membrane (Fig. 4.10A-C). PECAM is a marker of endothelial cells and was located in close proximity to an S-shaped body (Fig. 4.10E-H). However, we were unable to identify the PKH67 labelled mesothelial cells, as the dye seemed to have leaked from the mesothelial cells and appeared to have been taken up by the neighbouring metanephric cells.

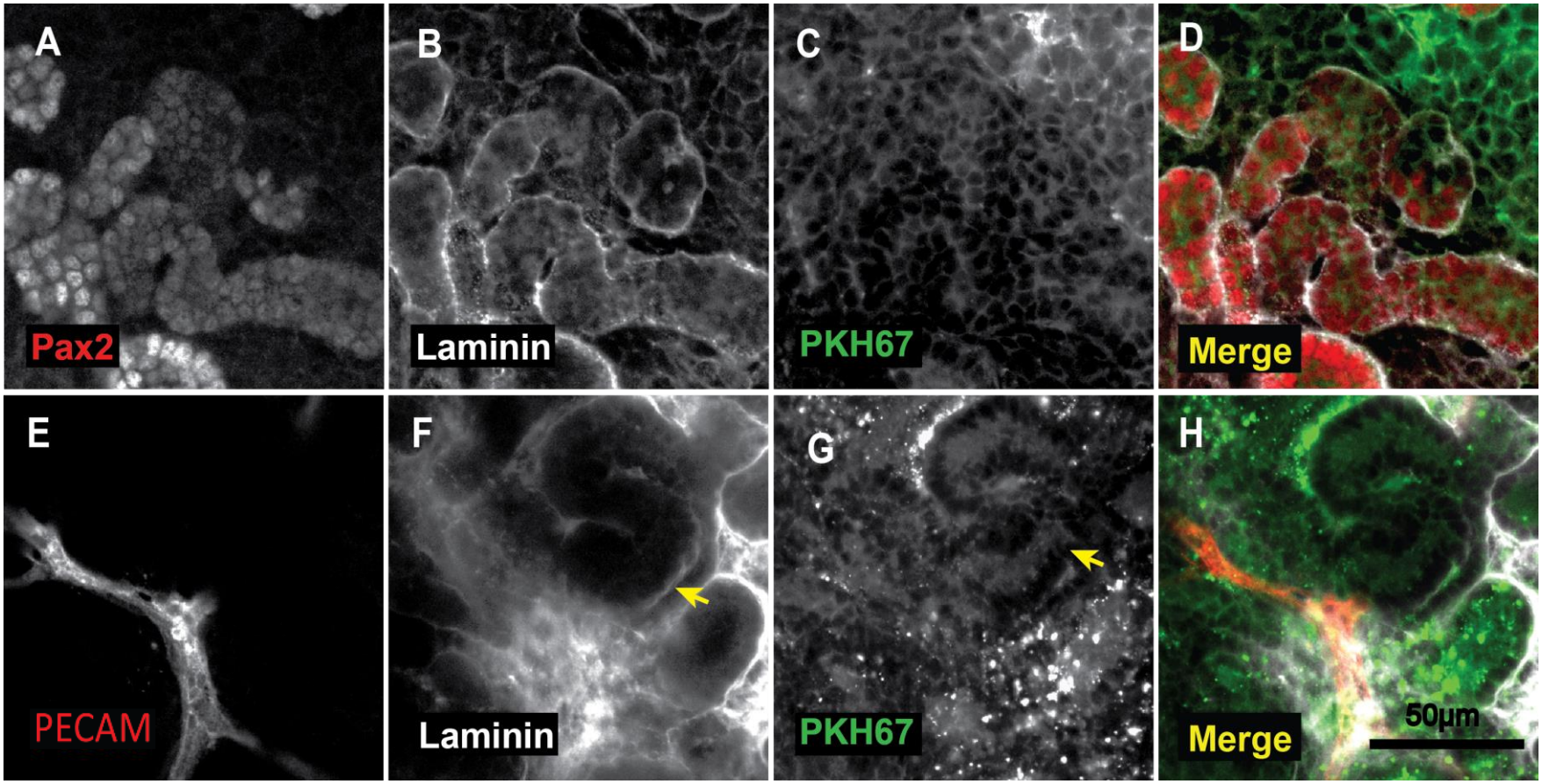

Figure 4.10: PKH67-labelled mesothelial cells in chimeric rudiments after 4 days *ex vivo* culture. The chimeric rudiments show features characteristic of nephron development, as shown by immunofluorescence for Pax2/ laminin staining of forming nephrons and UB branches. The presence of the renal vesicle [blue arrows], S-shaped [yellow arrows] and tubule elongation [pink arrows] are revealed through PKH dye uptake by embryonic cells [D, H]. Endothelial networks were detected in the chimeric rudiments by immunolabelling for PECAM [E-H]. PKH67-labelled mesothelial cells were not clearly identifiable as the dye appeared to have dissociated from the cells [C, G].

Although PKH67 had leaked from the mesothelial cells, this did not seem to affect the development of the nephron structures over time, as we could see numerous comma-shaped and renal vesicle structures, populated with Pax2 positive cells, after 7 days of culture (Fig. 4.11A-D). Similarly, a population of Six2 and Wt1 expressing cells were maintained in the induced metanephric mesenchyme, suggesting cap mesenchyme structures (Fig. 4.11E-H).

Similarly to PKH67, the CFDA SE-labelled MCs that were cultured for 7 days in the chimeric rudiments were also not identifiable since the dye appeared to have dissociated from the cells (Fig. 4.11). Importantly, we observed that the CFDA SE dye had consistently negatively impacted chimeric rudiment nephrogenesis in all the independent experiments performed. This was because the number of observed kidney structures appeared reduced and Wt1 positive structures were undetectable (data not shown). However, we still were able to detect Pax2 expressing cells (Fig. 10I-L) and endothelial network development (Fig. 4.11M-O).

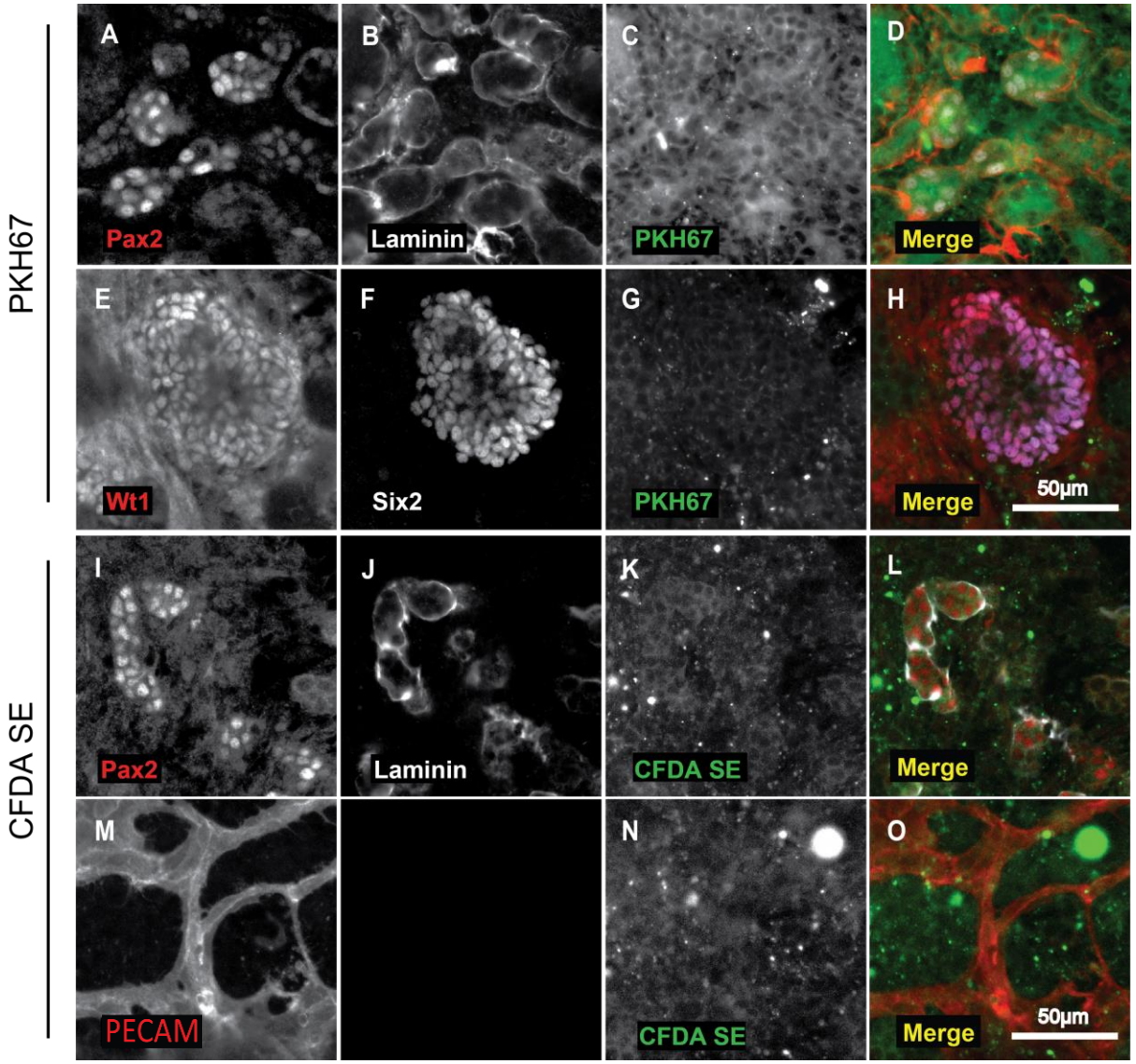

Figure 4.11 PKH67 and CFDA SE-labelled mesothelial cells in chimeric kidney rudiments after 7 days of *ex vivo* culture. Mesothelial cells P5-10 were labelled with the two dyes and co-cultured in the chimeric rudiments for 7 days. Both dyes disappeared from the mesothelial cells and the PKH seemed to spread throughout the rudiments. Nevertheless, the formation of nephron structures was maintained [A-D, I-J] and Six2 progenitors were unaffected [E-H], as shown by immunofluorescence. Endothelial networks could be detected using PECAM immunofluorescence [M-O].

4.3.5 Mesothelial cells integrated into embryonic kidney rudiments, *ex vivo*

Our results have so far demonstrated that the inclusion of mesothelial cells in the chimeric rudiments allowed the formation of normal nephron structures including cap mesenchyme, proximal tubules, and comma-shaped bodies. However, it still remained unclear whether the mesothelial cells had a supporting role in nephron development. Since the two cell dyes had proven to be of little use as markers of mesothelial cells in the rudiment assay, we turned to the GFP-labelled mesothelial cells that had been transduced with the lentivirus. MC-containing re-aggregated chimeric rudiments were cultured for 4 and 7 days and analysed by confocal microscopy for marker expression and GFP+ MC localisation. As mentioned before, due to the approach followed to generate the GFP-labelled mesothelial cells, they were at P22-32. We never observed any differences in rudiment development with the use of either P22 cells or P32 cells (Fig. 4.9G-I).

After 4 days of culture within the embryonic rudiments, the GFP-labelled mesothelial cells were well dispersed within the rudiment and found localised mostly around developing structures. This was in contrast to the previously observed inhibitory behaviour of other cell types tested in chimeric rudiments in our group, where the cells formed a cap at the top of the rudiment (unpublished results of Santeramo et al and Kuzma-Kuzniarska et al., 2012).

By confocal microscopy, it became clear that the ring-like GFP+ structures noted earlier (Fig. 4.9H-I) were the result of the mesothelial cells arranged around the developing nephroi (Fig. 4.12). Immunofluorescence showed that the MC-GFP labelled cells were localised in the proximity of Pax2 (Fig. 4.12A-D), Wt1 (Fig. 4.12E-G), Six2 (Fig. 4.12G-I) and megalin expressing structures (Fig. 4.12J-L).

Given that the mesothelial cells were found throughout the day 4 chimeric rudiments close to developing renal structures, we wanted to further explore this interaction at a later stage. We observed that the prolonged culture of the GFP-MCs in the chimeric kidney rudiments for 7 days did not impart any negative consequences on the development of nephron structures (Fig. 4.13). Immuno-detection revealed expression of Pax2 in the UB and in early MM condensates, Six2 in the induced MM and of Wt1 in pre-tubular aggregates, proximal parts of the renal vesicle and the forming glomerulus which confirmed that the developing nephrons could mature in the presence of the mesothelial cells (Fig. 4.13A-I). However, we could not locate any GFP-mesothelial cells inside either comma- or S-shaped bodies or in the UB tips (Fig. 4.13D-F).

The proximal tubules were identified through Megalin, a multi-ligand receptor that is found expressed in the proximal domains of the nephron. PNA was also used to identify the basement membranes of developing nephrons and UBs. The GFP-labelled cells were found in the zones of the proximodistal axis of the forming nephrons; arranging around the tubular structures and directly abutting the basement membranes (Fig. 4.13J-O).

Overall, GFP-labelled mesothelial cells demonstrated integrative potential in the chimeric nephrons and allowed for the formation of embryonic kidney structures. However, we could not see evidence of dedifferentiation.

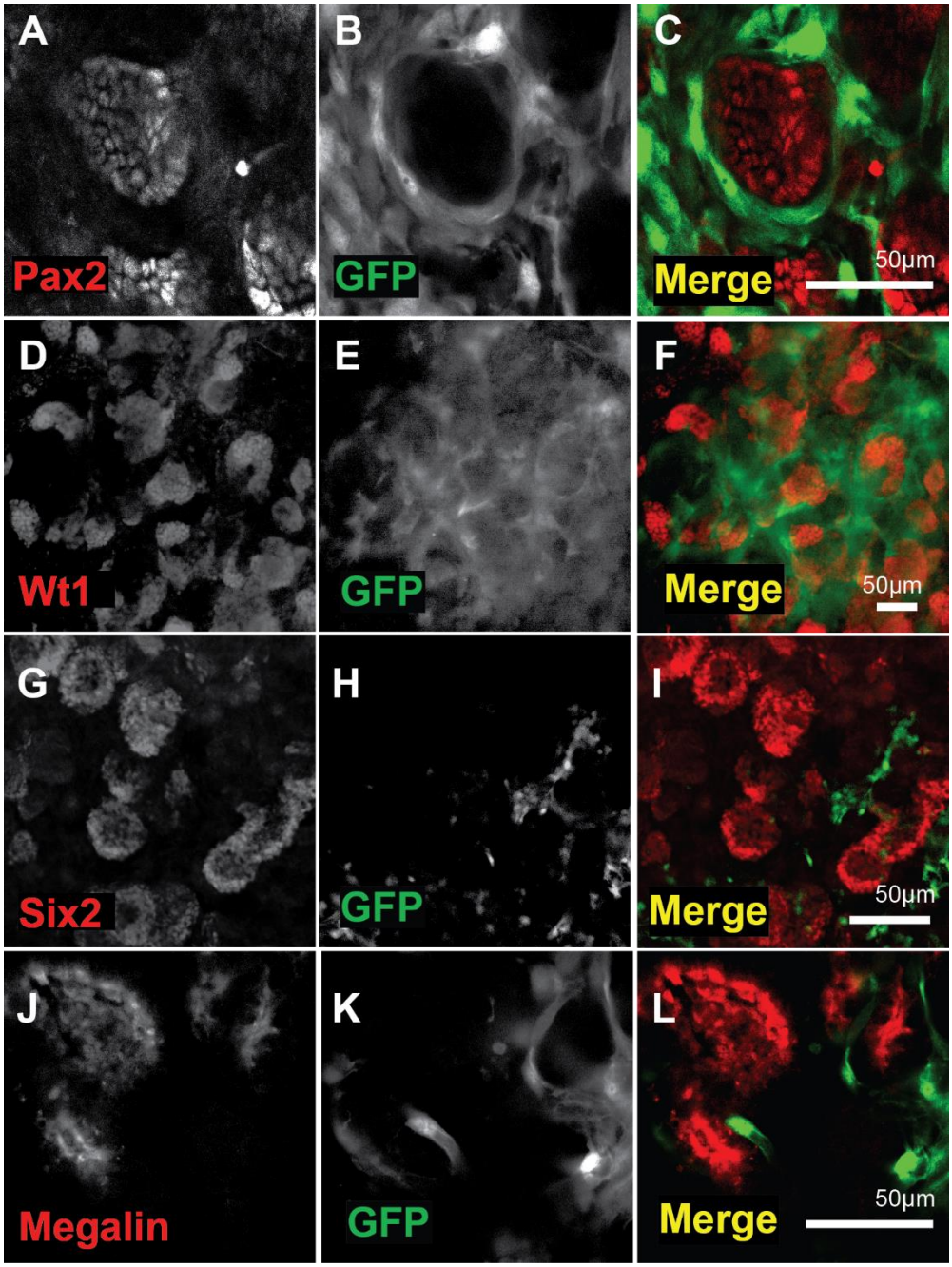

Figure 4.12 GFP-labelled mesothelial cells in chimeric kidney rudiments after 4 days *ex vivo* culture. The mesothelial cells were found located around the forming cap-mesenchyme [A-I] and the proximal tubules [J-L].

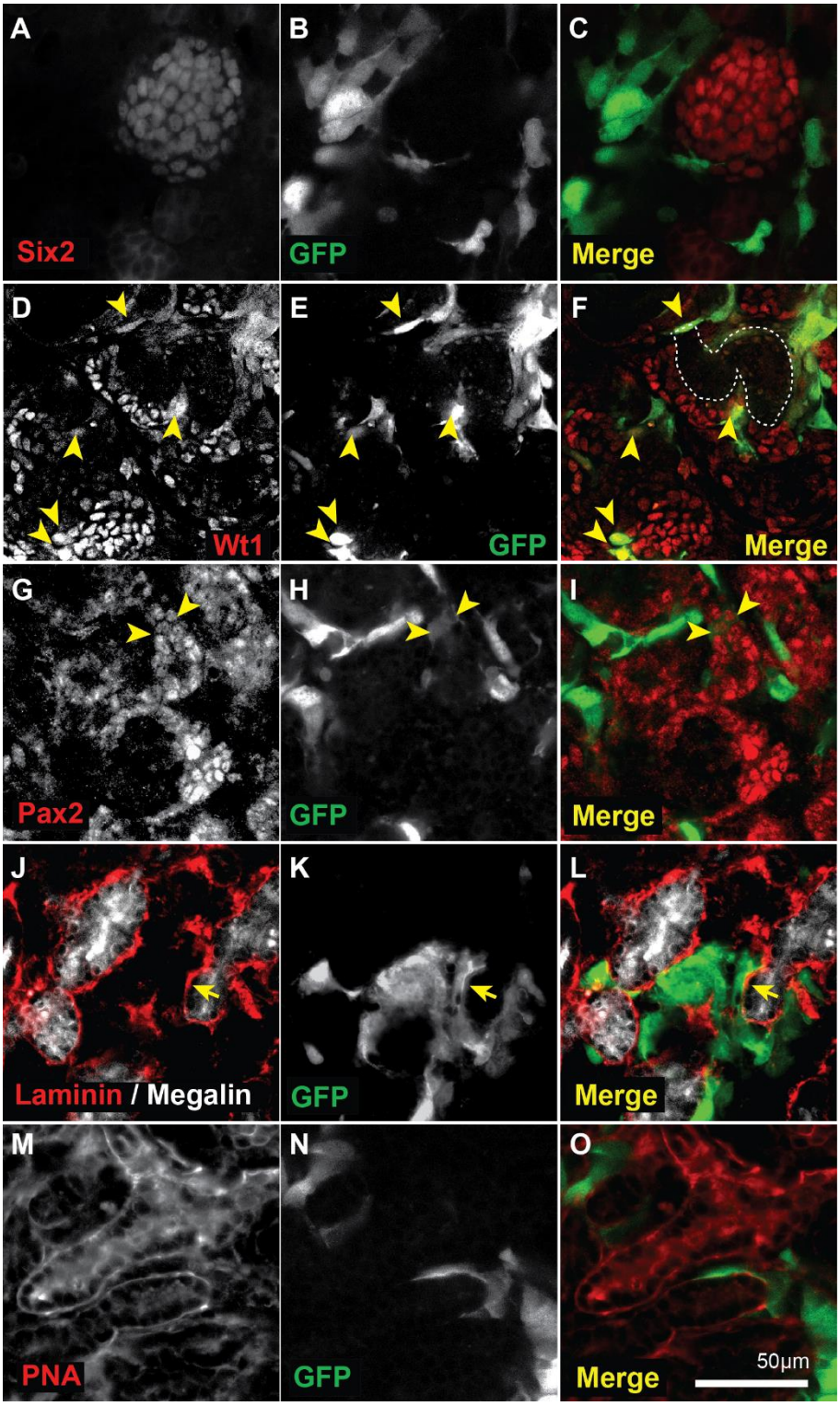

Figure 4.13 Mesothelial cells are found throughout the developing kidney rudiment, 7 days post culture. GFP-positive mesothelial cells were found arranged around the UB like Six2 expressing structures [A-C]. They were also found located around Wt1 expressing s-shaped bodies of forming nephrons [D-F] and around Pax2 positive condensing mesenchyme [G-H]. [D-L], (arrowheads denote co-localisation). The mesothelial cells appeared to be attached to the basement membrane of the megalin-labelled proximal tubules [arrows, G-I] and PNA-positive structures [M-O].

4.3.6 Mesothelial cells showed alignment to forming endothelial networks in chimeric rudiments.

PECAM as a marker of endothelial cells is an adhesion molecule. It has been shown that endothelial progenitors are recruited through the secretion of VEGF to the forming S-shaped bodies during nephrogenesis (Vaughan and Quaggin, 2008). We were able to visualise complex capillary-like networks throughout the developing embryonic kidneys that were cultured for 4 (Fig. 4.14A) and 7 days (Fig. 4.14B) *ex vivo*. Interestingly, the re-aggregation process maintained the pool of endothelial progenitor cells, and complex capillary like-networks were formed across the entire rudiment plane (Fig. 4.14C). However, these PECAM-positive endothelial networks were located only in the top two-thirds of the re-aggregated rudiments. We found that the presence of the GFP-positive mesothelial cells did not have any negative consequences on the orchestration of the endothelial tube networks (Fig. 4.14D, E). Interestingly, the mesothelial cells showed alignment to the endothelial tubes (Fig. 4.14E-F), and higher magnification clearly demonstrated that the mesothelial cells had aligned directly with the endothelial tubes (Fig. 4.14G-I).

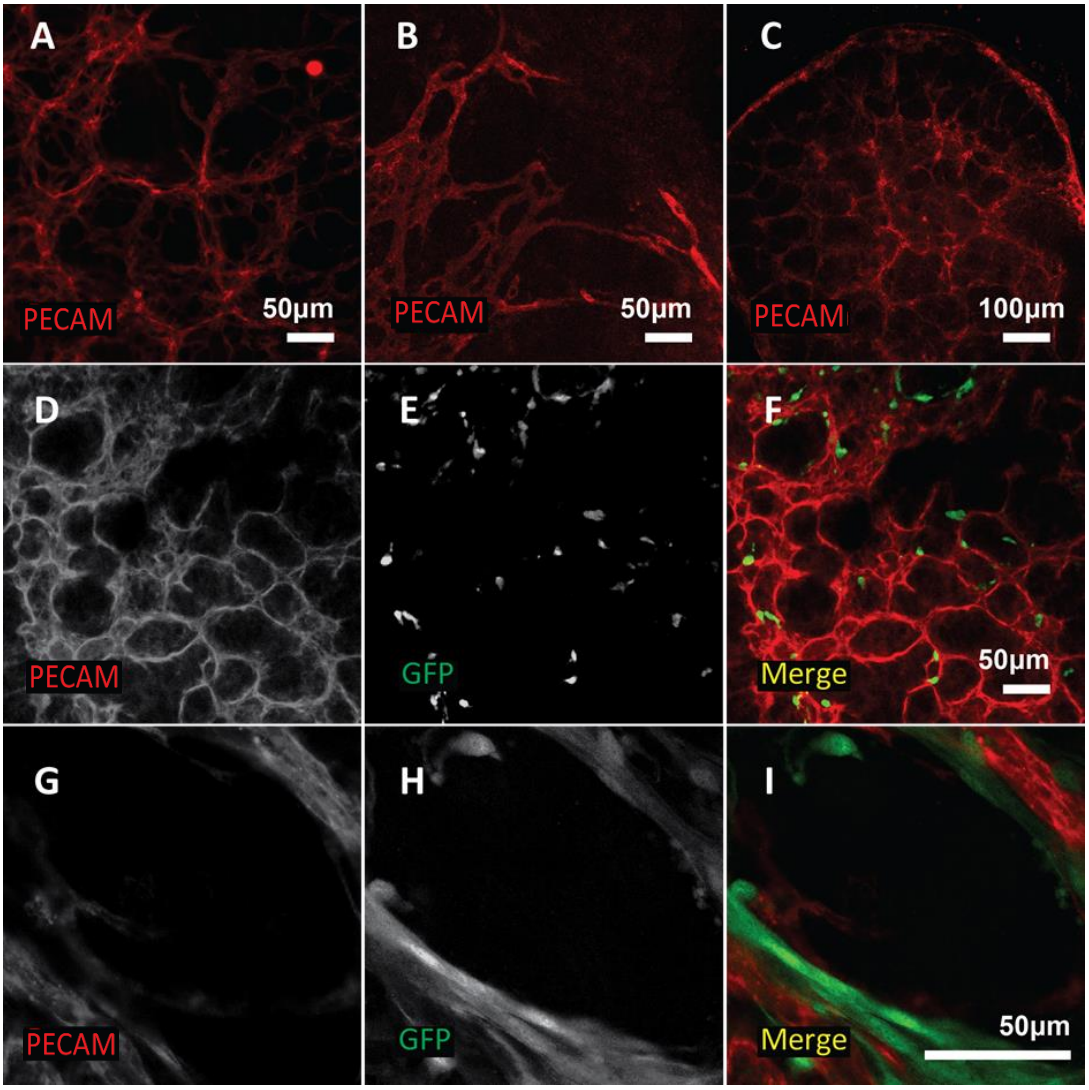

Figure 13: GFP-mesothelial cells showed alignment to PECAM-positive endothelial networks in the chimeric rudiments. Developing endothelial networks were detected in eControl rudiments that were cultured for 4 days [A] and 7 days [B] *ex vivo*. PECAM positive networks were also detected in the rControl samples that were cultured for 7 days [C]. GFP-labelled mesothelial cells showed alignment to endothelial networks following 7 days culturing [D-F]. The mesothelial cells aligned directly with the PECAM positive endothelial tubes [G-I].

4.3.7 Gene expression profiling of GFP-mesothelial cells isolated from the chimeric rudiments after 7 days of *ex vivo* culture.

Since we could not observe MCs that had integrated into developing nephron structures, or robustly expressed nephron markers, we aimed to determine whether we could detect changes to the gene expression profile of the cells after 7 days of exposure to a nephrogenic environment. Therefore, we isolated the GFP-positive mesothelial cells 7 days post-culture through FACS and analysed the gene expression profile for key kidney markers against passage matched un-challenged GFP-mesothelial cells. From among the list of assayed kidney markers (table 4.1), we could detect the expression of *Wt1, Wnt6, Wnt4, FGF7, Notch2* and *Sdf1* genes (Fig. 14A) in the mesothelial cells although the relative change in gene expression was not statistically significant following exposure to the nephrogenic environment.

The metanephric organoid system is a rich source of growth factors and so we aimed to determine the effect of the chimeric rudiment on mesothelial cell morphology, in particular, MMT signature. Our data showed that the mesothelial cells cultured in the chimeric rudiments were triggered to undergo MMT through the up-regulation of MMT transcription factors *Snail1* (7 fold), *Zeb1* (>1000 fold) and *Twist1* (100 fold). *Vim* a marker of mesenchymal cells was also 500 fold upregulated in the stimulated GFP mesothelial cells (Fig. 14B).

Kidney Structure	Marker
General epithelial	Krt8 ZO1 Cdh1 Vcl Msln
Ureteric Bud	Wnt6 Ret Pax2 AqpII
Metanephric Mesenchyme	Wt1 Gdnf Pax2 Sall1 Eya1 Bmp7 Vim
Distal tubule	Wnt4
Proximal Convoluted Tubule	Notch2 Pax2
Podocytes	Wt1 Cxcl12/ CD10
Stromal cells	Cxcl12/ CD10

Table 4.1: List of genes involved in embryonic kidney development that were studied for their expression in mesothelial cells, post chimeric rudiment stimulation.

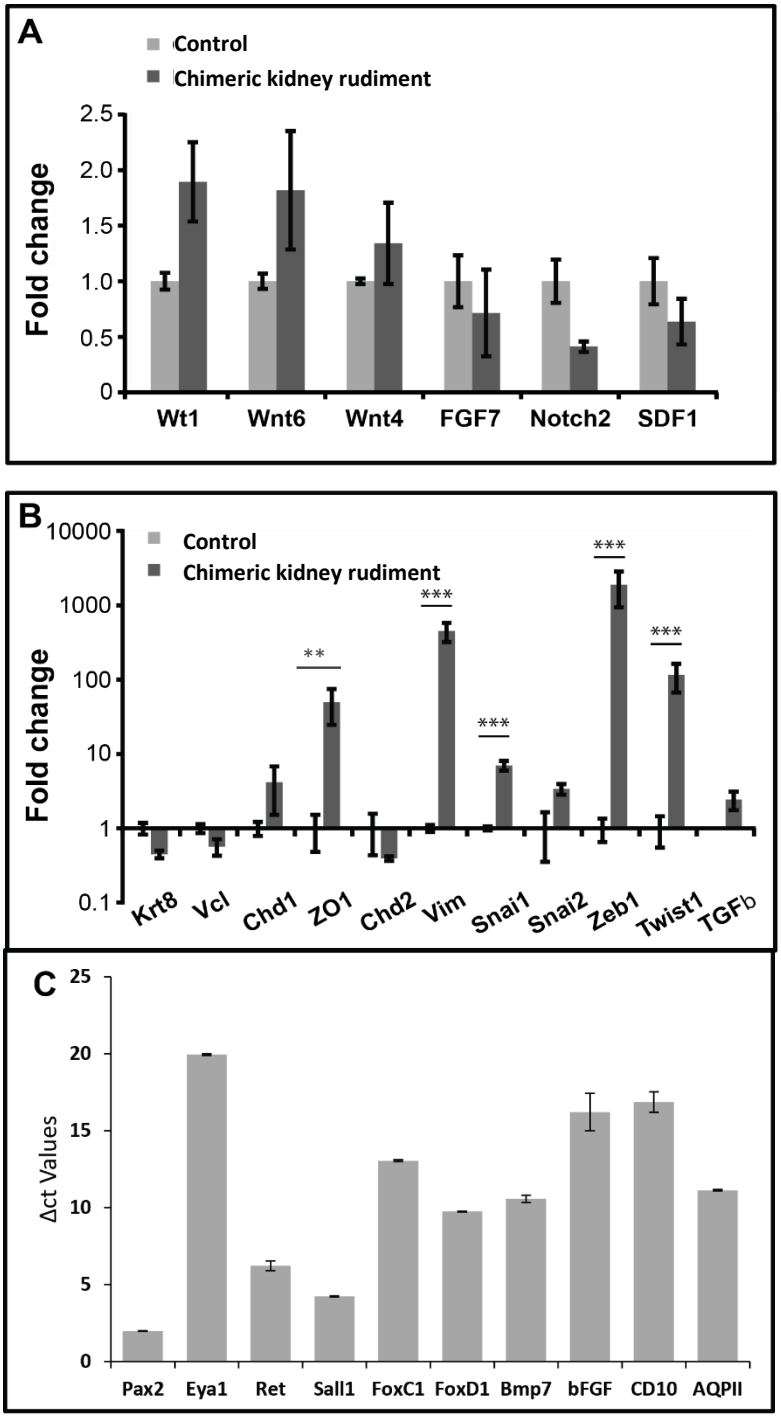

Figure 14: Mesothelial cells respond to the nephrogenic environment. GFP-labelled mesothelial cells were isolated by FACS following 7 day *ex vivo* culture in chimeric rudiments, and analysed for relative expression of embryonic kidney [A] and EMT genes [B] by qPCR. *Wt1*, *Wnt6*, and *Wnt4* were increased following stimulation, while the markers of the stromal compartment, *FGF7*, *Notch2* and *SDF1* were decreased. [B] The mesothelial cells isolated from the chimeric kidney rudiment (KRA) stimulated to undergo both EMT and MET as epithelial genes *ZO1*, the mesenchymal marker *Vim* and the EMT-TF *Snail1*, *Zeb1* and *Twist1* were significantly up-regulated relative to the unstimulated GFP-mesothelial cells from the same passage. [C] Key regulators of embryonic kidney development were only found expressed in the eControls and not in the stimulated or un-stimulated mesothelial cell populations. Data is presented as means ± SEM for 3

4.4 Discussion

In this chapter, we evaluated the effects of repeated passaging on the capacity of mesothelial cells to differentiate along the adipogenic, osteogenic mesodermal lineages, and their ability to contribute to nephrogenesis using the metanephric organoid system. While mesothelial cells expressed a number of early mesoderm markers consistently throughout culture, their differentiation capacity into osteoblasts and adipocytes was limited by cell passage. In the chimeric kidney rudiment, the mesothelial cells did not impart negative effects on metanephric development. Rather they aligned around the laminin/ megalin positive developing proximal tubules and PECAM expressing endothelial networks. Although we did see GFP-mesothelial cells wrapped around $Wt1^{+}$ forming S-shaped bodies, $Six2^{+}$ induced mesenchyme and mesenchymal Pax2 expressing domains around the UBs, the mesothelial cells were never found within these forming structures. Ultimately, the presence of mesothelial cells within this organoid environment did not stimulate the cells to differentiate into embryonic kidney cells, while it promoted the cells to undergo MMT.

4.4.1 Multilineage potential of mesothelial cells

An important parameter of stemness is potency, in other words, the stem/ progenitor cells can produce multiple differentiated cells. The multilineage capacity of mesothelial cells has previously been reported in rat and human pleural mesothelial cells. Lansley and colleagues showed that stimulated mesothelial cells underwent MMT during differentiation into osteoblast and adipocyte cells (Lansley et al., 2011). In this chapter, we were able to confirm the multilineage differentiation of mouse omentum-derived mesothelial cells into osteoblast-like and adipocyte-like cells following appropriate stimulation. Induction with the osteogenic medium resulted in the accumulation of calcium deposits that reacted with the alizarin red S dye. However, quantification of mRNA amounts for key osteoblast markers revealed that the

osteogenesis differentiation potential was only retained up to passage 13 as the higher passage cells failed to significantly respond. Moreover, stimulation with adipogenic inducing medium resulted in lipid vacuole accumulation, however, significant upregulation of the key adipogenic marker PPARγ was limited to the passage 5 cells only.

The effects of increased time in culture and reduced differentiation potential has been reported in MSCs and haematopoietic stem cells. MSCs from both animal and human sources showed reduced osteogenic, adipogenic and the chondrogenic potential with increased donor age or/ and cell passage (Kretlow et al., 2008, Elkhenany et al., 2016, Alves et al., 2010, Rossi et al., 2007, Chambers et al., 2007). However, osteogenesis and chondrogenesis were more affected by ageing than adipogenesis, regardless of source (Kretlow et al., 2008, Elkhenany et al., 2016, Alves et al., 2010). Accumulation of DNA double-stranded breaks and the respective reduced ability to activate the non-homologous end joining repair pathway with successive passaging was associated with reduced MSCs multi-lineage potency (Hare et al., 2016, Alves et al., 2010, Elkhenany et al., 2016). Haematopoietic stem cells also demonstrated reduced function that was associated with increased DNA damage and epigenetic modification (Chambers et al., 2007, Rossi et al., 2007).

In conclusion, the mesothelial cells in this study demonstrated multilineage differentiation potential, however, this was limited by mesothelial cell passage. Further investigations are however required to see if there are an accumulation of DSB with passaging, and whether this reduces the plasticty of the mesothelial cells in our culture system. . In light of this, mesothelial cells for regenerative medicine purposes should only be expanded and used for a limited number of passages.

4.4.2 Cell labelling techniques for monitoring the renogenic potential of mesothelial cells *ex vivo*

As another means of testing the relative plasticity of mesothelial cells along mesodermal lineages, we extended our work to co-culturing the cells in an embryonic kidney organoid culture system. This ex vivo approach to kidney development has been used to assess the renogenic potential of a number of progenitor and stem cell types (Kuzma-Kuzniarska et al., 2012, Ranghini et al., 2013, Rak-Raszewska et al., 2012, Little and Takasato, 2015, Takasato et al., 2014).

However, first, we needed to select a labelling method suitable for long-term detection with limited side effects on both the exogenous mesothelial cells and host embryonic kidney cells. For this we employed 3 labelling techniques; the CFDA SE, PKH67 and GFP lentiviral transduction.

According to our adipogenesis and osteogenesis results, mesothelial cells showed passage related changes in their differentiation capacity. The low transduction efficiency of the GFP-lentivirus in mesothelial cells meant several rounds of FAC sorting and expansion were required to achieve an 88% GFP-positive population of cells by P20. On the contrary, the CFDA SE and the PKH67 dye labelling techniques rapidly and uniformly labelled P5-10 mesothelial cells to which they were directly incorporated in the chimeric kidney development model.

The initial fluorescence monitoring studies in mesothelial cell monolayers revealed that the CFDA SE gave the brightest initial fluorescent intensity and throughout the 7 d culture period the signal dropped to an intensity that matched the GFP^+ mesothelial cells. While the PKH67 gave a brighter signal that the GFP labelled cells, its fluorescence signal was lost by 7 d culture. To counteract this problem we decided to stop the chimeric co-culture study at 4 d, where the signals for PKH67 was still above cellular autofluorescence.

Detailed analysis of the chimeric rudiments showed that while we were able to visualize embryonic kidney structures in the rudiments when cells were labelled with PKH67 or GFP lentivirus, the chimeric pellets that contained the CFDA SE labelled mesothelial cells seemed to show a perturbed development of renal structures. There appeared to be less Pax2- and laminin-containing structures and Wt1- compartments were not detectable in the CFDA SE harbouring chimeric pellets. Furthermore, we were unable to detect the labelled mesothelial cells. Our previous analysis of the PDT of mesothelial cells showed an average doubling time of 32 h in P5-10 cells. Since the CFDA SE dye has been reported to be visualized for up to 8 consecutive cell divisions, by 7 d the mesothelial cells should still be traceable (Wang et al., 2005). During this study, we labelled the mesothelial cells directly before incorporating them in the chimeric rudiment. The CFDA SE is known to passively enter cells and form random covalent links with free amines found on cellular proteins (Wallace et al., 2008). However, during the first 24 – 48 h the unbound dye can still escape from the cell (Wang et al., 2005, Wallace et al., 2008). Therefore it is possible that the unbound CFDA SE dye escaped from the mesothelial cells and was taken up by neighbouring metanephric cells or remained in the intercellular spaces. It is known that the CFDA SE is toxic at high doses (Wang et al., 2005, Wallace et al., 2008). Which could explain why there was the poor and disrupted development of kidney structures. It is, however, important to note that the relative toxicity varies between cells as it is dependent on cell size and esterase content (Wang et al., 2005, Wallace et al., 2008).

While the PKH67 containing pellets showed embryonic structural development that resembled the rControls and eControls, also with this dye we failed to detect the mesothelial cells. Instead, it appeared that the dye had transferred across to neighbouring embryonic cells, as we could visualize S-Shaped renal structures. The PKH dye transfer to neighbouring cells

has been previously reported in *in vitro* co-cultures, were unlabelled GP293T fibroblasts acquired red fluorescence from the HL-60 cells labelled with PKH26 (Lassailly et al., 2010). Studies have suggested that dye transfer can occur through the exchange of lipid components, uptake of PKH-labelled exosomes and if the labelled cells are dead (Li et al., 2013a, Christianson et al., 2013, Franzen et al., 2014).

Labelling mesothelial cells with GFP did not result in signal deterioration over the course of the 7 d culture period. Furthermore, metanephric structural development could also occur in the presence of the GFP^+ mesothelial cells, indicating that GFP transduction was the better method to enable long-term *ex vivo* tracking of mesothelial cells. There are numerous reports describing the use of labelling cells with GFP lentivirus for long-term monitoring of migration and distribution *in vivo.* Tao and colleagues showed that the potency capacity of human umbilical cord-derived mesenchymal stem cells to differentiate into osteoblasts and adipocytes following stimulation was unaffected by labelling with either PKH26 or GFP-lentivirus (Tao et al., 2014). Similar to our findings, the PKH26 fluorescence intensity was lost after a few passages, while the GFP^+ cells maintained their signal (Tao et al., 2014).

In conclusion, GFP-lentiviral transduction was shown to be the better labelling method for long-term detection of mesothelial cells in the *ex vivo* chimeric rudiment. This is albeit the fact that this technique had the lowest efficiency for labelling the cells, which in turn meant we could not assess the possible nephrogenic potential of the lower passage mesothelial cells.

4.4.3 Analysis of mesothelial cell renogenic potential

(Kuzma-Kuzniarska et al., 2012, Ranghini et al., 2013, Rak-Raszewska et al., 2012)Using the chimeric kidney rudiment assay, we were able to co-culture P22-32 GFP^+ mesothelial cells in the chimeric rudiments at a ratio of 1:10, using a total of 200,000 cells. Over the course of the

7 d culture period and in the presence of the mesothelial cells we could see the adaptive self-organization of key embryonic structures, namely UBs, MM, forming nephrons and PECAM expressing endothelial tubules. The mesothelial cells in both 4 d and 7 d cultures could be seen enfolded around the Wt1-, Six2- and Pax2- expressing condensed mesenchyme, in a loop-like formation. The GFP-cells could also be found outside the laminin/ megalin and PNA proximal tubule compartments. However, the GFP-cells did not engraft into the forming nephrons, the condensing MM or the UBs. Analysis of FAC sorted GFP-cells that had been co-cultured in the chimeric rudiments for 7 d, confirmed this as the cells had failed to express or upregulate key metanephric markers. Rather, in response to cues from developing chimeric rudiments, the GFP-cells showed hallmarks of MMT through the expression of the *Twist1, Zeb1, Snail1* transcription factors and *Vim.*

Contrary to our findings, the co-culture of human and mouse MSCs in the chimeric organoid system was detrimental to nephrogenesis despite the fact that these cells expressed the renal markers *Osr1*, *Sall1*, *Lim1* and *Gdnf* prior to incorporation (Kuzma-Kuzniarska et al., 2012). In some regions of rudiments which contained quantum dot labelled cells, there was a complete absence in Wt1-expressing MM (Kuzma-Kuzniarska et al., 2012). By contrast, mouse ESC that were directed to differentiate and express mesodermal marker Bra, showed integration into UBs, proximal tubules and forming glomeruli (Rak-Raszewska et al., 2012). Furthermore, those labelled cells that had integrated into proximal tubules were functional, as they could transport labelled anionic molecules from the interstitium into the proximal tubules (Rak-Raszewska et al., 2012). An alternative cell type to ESCs for kidney regeneration are amniotic fluid stem cells (AFSCs) (Perin et al., 2007). Human AFSC were demonstrated to integrate into renal vesicles and comma- and S-shape bodies following co-culture in the chimeric rudiments for 10 d (Perin et al., 2007, Siegel et al., 2010). Furthermore the AFSCs showed hallmarks of

differentiation as they expressed ZO1, claudin, and GDNF (Perin et al., 2007). Overall, our data suggest that the older passage mesothelial cells have a rather low renogenic potential in the chimeric kidney rudiments.

Another pertinent finding was the presence of PECAM positive endothelial networks in the eControl, rControl and chimeric rudiments. In addition, the GFP-cells could be seen aligning to the forming endothelial networks.

Ex vivo metanephric development is halted at the stage of glomerular development, due to the lack of a blood supply (Rak-Raszewska et al., 2015). Contained within the *in vivo* forming kidneys is a pool of endothelial progenitor cells, and by E13.5 most of the vascular branches are perfused while at E15.5 the smaller-calibre peripheral vessels become also show blood flow (Rymer et al., 2014). However, it seems for the renal vasculature to form *ex vivo,* the chimeric rudiments need to be exposed to the correct environment (Xinaris et al., 2012, Rak-Raszewska et al., 2015). Xinaris and colleagues used a novel technique where E11.5 rudiments were re-aggregated, cultured for 5 d *ex vivo,* following which they rudiments were treated with VEGF for 4 h before being transplantation under the kidney capsule of athymic rats (Xinaris et al., 2012). This promoted the vascularization from donors which in turn aided glomerular maturation and function (Xinaris et al., 2012).

We cannot comment on whether the endothelial networks observed in the re-aggregation and chimeric rudiments were functional or if the glomeruli would have developed further, as no further exploratory tests were conducted. Furthermore, while the mesothelial cells aligned to the endothelial networks, they did not seem to increase vascularization nor inhibit it. It has been previously demonstrated that uterine-derived mesothelial cells had the capacity to transdifferentiate via MMT into functional vascular smooth muscle-like cells following

stimulation with EGF, *in vitro*. It remains to be certified whether or not the chimeric rudiment stimulated mesothelial cells did in fact display this plasticity.

4.5 Conclusion

Overall we were able to show that the mesothelial cells possess a multi-lineage capacity along the osteogenic and adipogenic lineages; however this was limited to the early passages. Furthermore, GFP lentiviral transduction was the optimal technique for the long term monitoring of cells. Moreover, in the chimeric rudiments, the mesothelial cells did not disrupt metanephric structural development. Despite this, we only saw hallmarks of MMT and not signs of differentiation into embryonic kidney cells in the mesothelial cells after co-culture. There is a possibility that this may be attributed to the fact that we were only able to track the older passaged cells which we had previously asserted as being less potent. While we failed to observe quantifiable differences in re-aggregated and chimeric kidney rudiments, the mesothelial cells could possibly have a role in supporting the development of the rudiments, as they are known to secrete an array of growth factors and ECM proteins which could contribute to nephrogenesis (Herrick and Mutsaers, 2004).

The results from this chapter and the previous one led us to ask whether EGF and or TGF-β were the growth factors that modulated the changes observed in the passaged mesothelial cells and through want signalling pathway. Furthermore, we aimed to address the roles of Zebs and Snail2 transcription factors involvement in modulating the cells MMT status.

Chapter 5: TβRI and EGFR antagonists block mesothelial migration through ERK5-dependent mechanisms.

Introduction and aims

In the previous chapters, we have shown that adult omentum-derived mesothelial cells in culture represented a 'hybrid' cell type, expressing both epithelial and mesenchymal features. During long-term culture, the adult mesothelial cells down-regulated the expression of epithelial markers and maintained mesenchymal characteristics when compared to cultured omentum explants. Further analysis of key MMT regulators and recognised inducers showed that with increasing time in culture, *Snail2* and *EGF* and its corresponding receptor were up-regulated. These results suggested that mesothelial cells in culture adopted a more intermediate phenotype within the MMT spectrum. However, the cells never fully transdifferentiated into myofibroblasts.

Physiologically, MMT is activated in response to injury in the adult (Li et al., 2013b). Mesothelial cells lose their basolateral polarity and gain a more migratory capacity, for example, to aid in wound repair; of note, this process is usually reversible (Li et al., 2013b). However, the prolonged exposure to PD fluids that contain glucose degradation products (GDP) as a result of exposing the fluids to heat, generates advanced glycation end-products (AGE), together these degradation products induce a proinflammatory response and cause the cells of the mesothelium to undergo complete transdifferentiation resulting in debilitating fibrosis or sclerosis (Abelardo Aguilera, 2013).

Free floating mesothelial cells have been demonstrated to contribute to the recovery of peritoneal membranes in rat testis through implantation and proliferation (Foley-Comer et al., 2002a), however approaches to utilise this technique to aid peritoneal repair have not been successful as the mechanisms that regulate MMT are not fully understood (Strippoli et al., 2016).

MMT is regulated by a number of growth factors and cytokines secreted in an autocrine and paracrine manner (Strippoli et al., 2016). While TGF-β is regarded as a master molecule of MMT both *in vitro* and *in vivo*, mediating this process through Smad-dependent and -independent mechanisms (Fig. 1.4) (Decologne et al., 2007, Li et al., 2016, Li et al., 2013b), EGF has been recently attributed as an inducer of MMT in human and rodent mesothelial cell (Lachaud et al., 2014, Lachaud et al., 2013). TGF-β-induced MMT has been linked with the activation of the Smad, PI3K, Akt/mTOR, JNK and MAPK signalling pathways (Javelaud and Mauviel, 2005, Liu et al., 2008, Strippoli et al., 2015), suggesting that the downstream signalling effectors of MMT are activated in a context specific manner and potentially through a synergistic convergence of multiple growth factors or cytokines (Li et al., 2016, Strippoli et al., 2016). Western blot analysis of downstream signalling effectors in P7 mesothelial cells identified potential candidates involved in regulating the MMT transdifferentiation process. Specifically, we could detect the expression of EGFR, phosphorylated serine/threonine kinase ERK1/2, ERK5 and pSmad 2/3 (Fig. 5.1). These results suggest that EKR1/2, EKR5, and Smad2/3 were activated as part of signalling through TGF-β and EGF. The expression of EGFR protein in the P7 mesothelial cells (Fig. 5.1), which corresponded with the observation of transcript expression from Chapter 3, further supported this hypothesis.

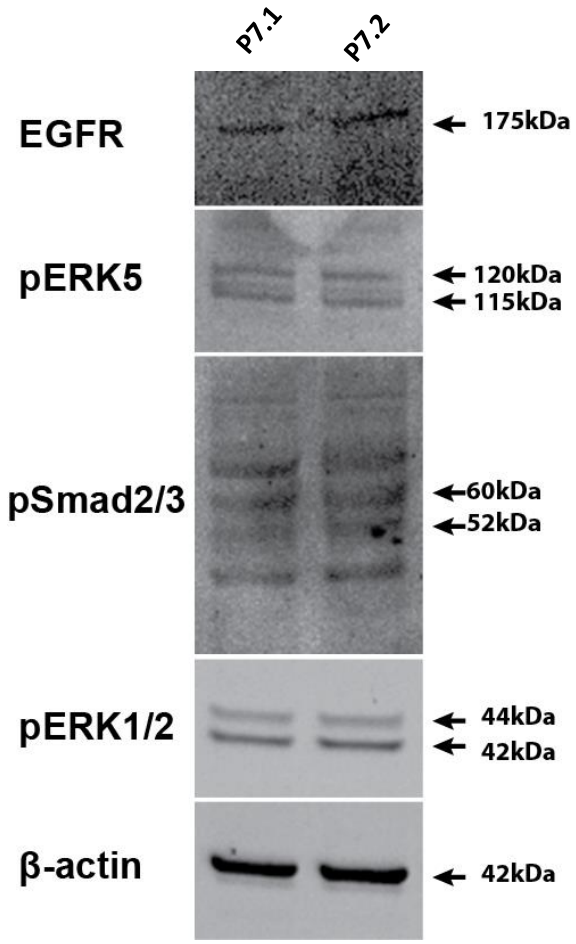

Figure 5.1: Mesothelial cells expressed intracellular proteins downstream of TGF-β and EGF signalling. Whole-cell lysates were isolated from P7 mesothelial cells that were cultured in standard growth medium. The lysates were resolved on a 4-12% Bis-Tris gel. We were able to detect the EGFR, pERK5, pSmad2/3 and pERK1/2 within the cells. Arrows indicate the expected band size for the proteins of interest.

Based on these results, we aimed to further analyse the potential convergence of the EGF and TGF-β signalling pathways in regulating MMT in the mesothelial cells, as EGF is a known mediator or MEK5 and MEK1/2. To address this question, we tested the role of these growth factors and their respective receptor inhibitors in regulating the migratory behaviour of mesothelial cells in an *in vitro* wound healing assay (tables 2.2 and 2.1 respectively). Furthermore, we studied any changes in the localization of MMT associated markers and the expression patterns at gene and protein levels in the mesothelial cells that were challenged in the wound healing assay. We also attempted to dissect the downstream signalling cascades and transcription factors involved in regulating the migratory behaviour of the MCs in the wound healing assay, in order to determine at which level there was a convergence of these two signalling cascades. Finally, we analysed the receptiveness of the various mesothelial cell 'states' (OMC – deemed more epithelial and the passaged mesothelial cells, intermediate mesenchymal) to undergo MMT in response to the growth factors and inhibitors.

5.1 TGF-β and EGF growth factors influence the phenotype of OMC mesothelial cells with a variable potency

5.1.1 The TGF-β receptor I (TβR-I) inhibitor LY364947 preserved the epithelial-like phenotype in OMC mesothelial cells

To explore whether cultured mesothelial cells maintained the intermediate MMT phenotype through TGF-β autocrine or paracrine-induced signalling loops, we first turned to OMC culture to analyse the response of either TGF-β cytokine or the small molecule TβRI inhibitor (LY364947, here called TβRi) (Hong et al., 2014) for 48 h. The samples were then immunolabeled with the tight junctional complex marker ZO1 and the myofibroblast marker αSMA in order to detect any changes in the MMT state mediated by these inhibitors and growth factors.

The OMCs were initially cultured in 10% FCS containing a medium for 5 d, before being serum starved for 24 h to be treated with the experimental conditions. Previous efforts in culturing the explants directly in low serum medium post dissection yielded poor long-term outcomes as explant attachment was reduced, and mesothelial cells failed to sufficiently grow out from the few attached explants (data not shown).

In the low serum control group, we could confirm a mixed population of mesothelial cell morphologies in the OMC cultures, which is not surprising since after 5 d in full growth medium both mesenchymal, αSMA+ and epithelial cells have been previously described (Kawaguchi et al., 2007). Within the small sub-confluent islands of mesothelial cells, we could detect discrete bands of ZO1 at points of cell-cell contact. However, some of these cells also co-expressed αSMA (Fig 5.2A-D). In addition, some mesothelial cells adopted a larger flatter morphology expressing brighter αSMA staining and nuclear accumulation of ZO1, which is indicative of a more mesenchymal-like phenotype. By comparison, TGF-β stimulation of OMCs

induced the mesothelial cells to transdifferentiate into larger, flatly shaped cells uniformly expressing αSMA stress fibres throughout the cytoplasm and nuclear accumulation of ZO1 (Fig 5.2E-H). The TβRI inhibitor re-established the epithelial-like phenotype of the mesothelial cells with strong ZO1 accumulation at the cell-cell contacts (Fig 5.2I-L).

Taken together, the data revealed that TGF-β could induce the transdifferentiation of the mesothelial cells into more myofibroblastic cells. This was supported by the observation that treatment of OMCs with the TβRI inhibitor resulted in the re-establishment of an epithelial phenotype in the outgrowing mesothelial cells.

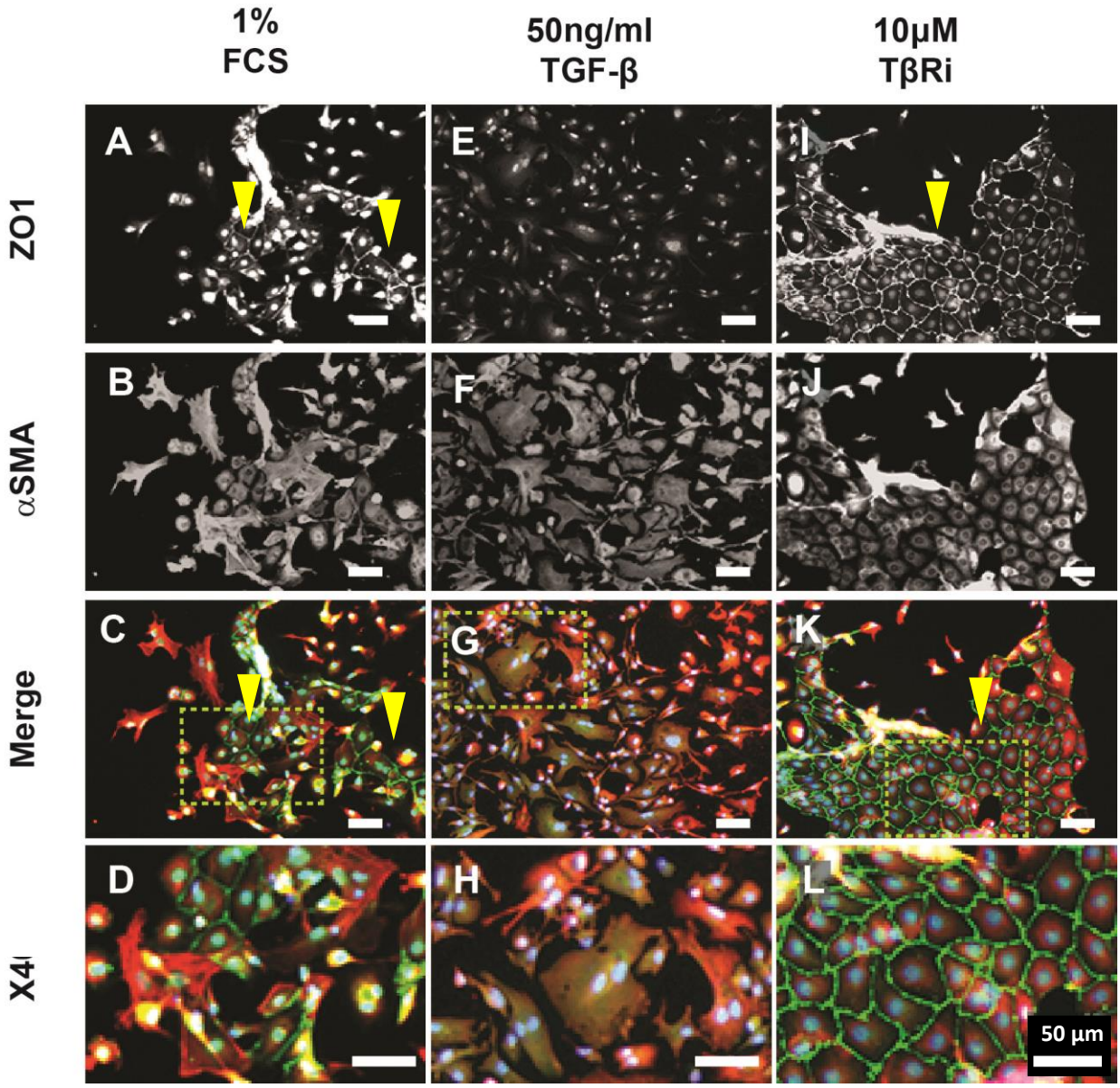

Figure 5.2: TGF-β induced mesothelial to mesenchymal transition in OMCs. Established OMC explants were incubated for 48 h with TGF-β or inhibitors respectively, and immunolabeled for MMT markers. [A-D] The control OMC (1% serum) cultures showed a mixed population of mesothelial cells with epithelial-like, ZO1 expressing islands (arrowheads) and αSMA-only, mesenchymal-like characteristics. [E-H] The OMC stimulated with TGF-β adopted a mesenchymal-like phenotype, with a flatter, longer fibroblastic shape, and strong αSMA expression. [I-L] The treatment with the TβRI inhibitor caused mesothelial cells to strongly express ZO1 tight junctional bands associated with epithelial characteristics. Images are representative of n=2. Images D,H and L were digitally enlarged.

5.1.2 EGFR inhibitor maintained hybrid cell phenotype in OMC mesothelial cells

As with the previous set of omentum explants, the cultures were left to attach for 5 d to allow the mesothelial cells to migrate out as an epithelial sheet. Next, the samples were serum-starved before being either stimulated with EGF or inhibited for 48 h with a selective EGFR tyrosine kinase inhibitor (PD153035, from now on called EGFRi) (Guan et al., 2016), a highly potent and selective non-competitive MEK inhibitor (PD184352, MEKi) (Wang et al., 2014) and a selective MEK5 and ERK5 inhibitor (BIX02189, MEK5i) (Amano et al., 2015) . Subsequently, the samples were immunolabelled with the epithelial and mesenchymal markers ZO1 and aSMA.

In the presence of EGF, some of the mesothelial cells growing out of the explants differentiated into elongated αSMA-expressing myofibroblasts. However, this process was not uniform as pools of epithelial-like cells expressing ZO1 at tight junctional bands were also present (Fig 5.3E-H). The presence of the EGFRi also resulted in epithelial, ZO1-expressing islands that were surrounded by αSMA-expressing myofibroblasts (Fig 5.3I-L). Both the MEK1/2 and the MEK5 inhibitors impacted OMC survival, therefore we could not analyse the cells for ZO1 or αSMA expression (data not shown).

Taken together the data suggests that EGF was a less potent mediator of MMT in the OMCs compared to TGF-β.

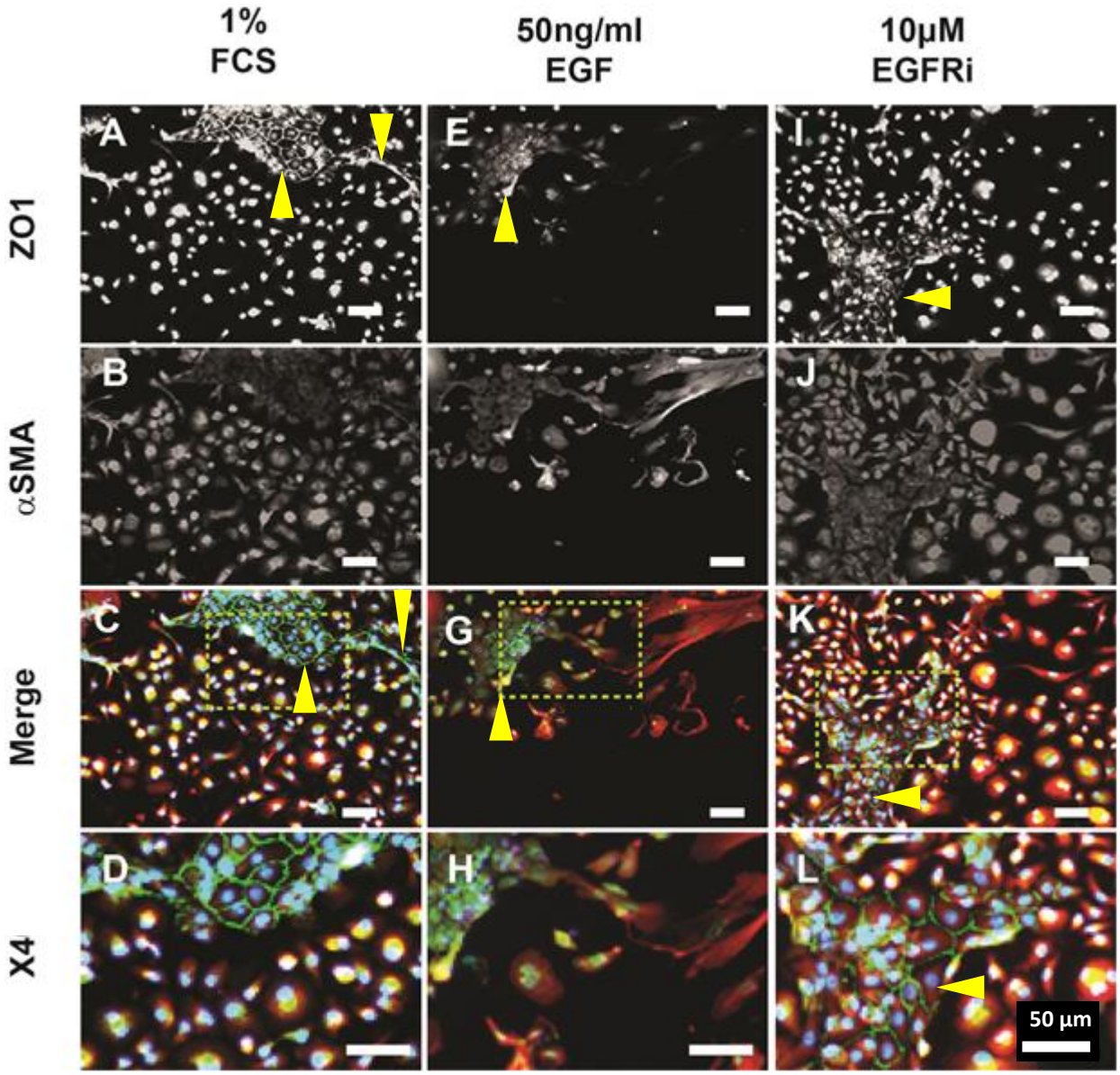

Figure 5.3: EGF induces MMT changes in some explant derived mesothelial cells. Established OMC explants were stimulated or inhibited with EGF growth factor or inhibitors, respectively, for 48 h. The samples were then immunolabelled for ZO1 and αSMA. [A-D] The control treatment group had a mixed population of mesothelial cells expressing either tight ZO1 junction complexes (arrowheads) or αSMA-expressing fibroblastic cells. [E-H] Some of the mesothelial cells that had been stimulated with EGF adopted a flatter longer fibroblast shape, with strong αSMA staining. [I-L] The treatment with EGFR inhibitor maintained the mixed pool of epithelial and mesenchymal cell morphologies. Images are representative of n=2 biological independent samples.

5.2 Stimulation in TGF-β and EGF for 48 h does not induce complete MMT in passaged mesothelial cells

5.2.1 Protein expression analysis in response to TGF-β and EGF in passaged mesothelial cells

In the previous experiments, we showed that TGF-β, and possibly EGF, had an effect on the transdifferentiation of mesothelial cells from OMC, therefore we wanted to determine whether TGF-β and EGF also induced the passaged mesothelial cells (P10-P25) to undergo full MMT by acquiring complete mesenchymal characteristics and losing epithelial features. To address this question, we assessed the effect of these growth factors on the localisation of key epithelial and mesenchymal protein markers.

Serum-starved mesothelial cells (P10-P25) were stimulated in 1% FCS growth medium containing either 50ng/ml EGF or TGF-β for 48 h, followed by immunolabelling with ZO1 and αSMA, respectively. The images for all the samples were captured at the same exposure time to gain a qualitative and semi-quantitative assessment of protein expression.

The tight junctional marker ZO1 was difficult to detect at the cell-cell contacts in the 1% FCS control group (Fig 5.4B-C), which is contrary to the mesothelial cells sub-cultured in full growth medium (Fig 3.6B-D). Meanwhile, the mesenchymal marker αSMA was unaffected by the low serum conditions (Fig 5.4A-C). Cells that had been stimulated with either EGF or TGF-β showed brighter αSMA staining (Fig 5.4D and G) relative to the low serum control group. Furthermore, stimulated cells, particularly those treated with EGF, expressed little to no ZO1 at the cell-cell junctional contacts (Fig 5.4E and H). Taken together, mesothelial cells cultured in low serum show some but very little ZO1 expression and stimulation in either EGF or TGF-β reduces this further. Therefore suggesting MMT progression.

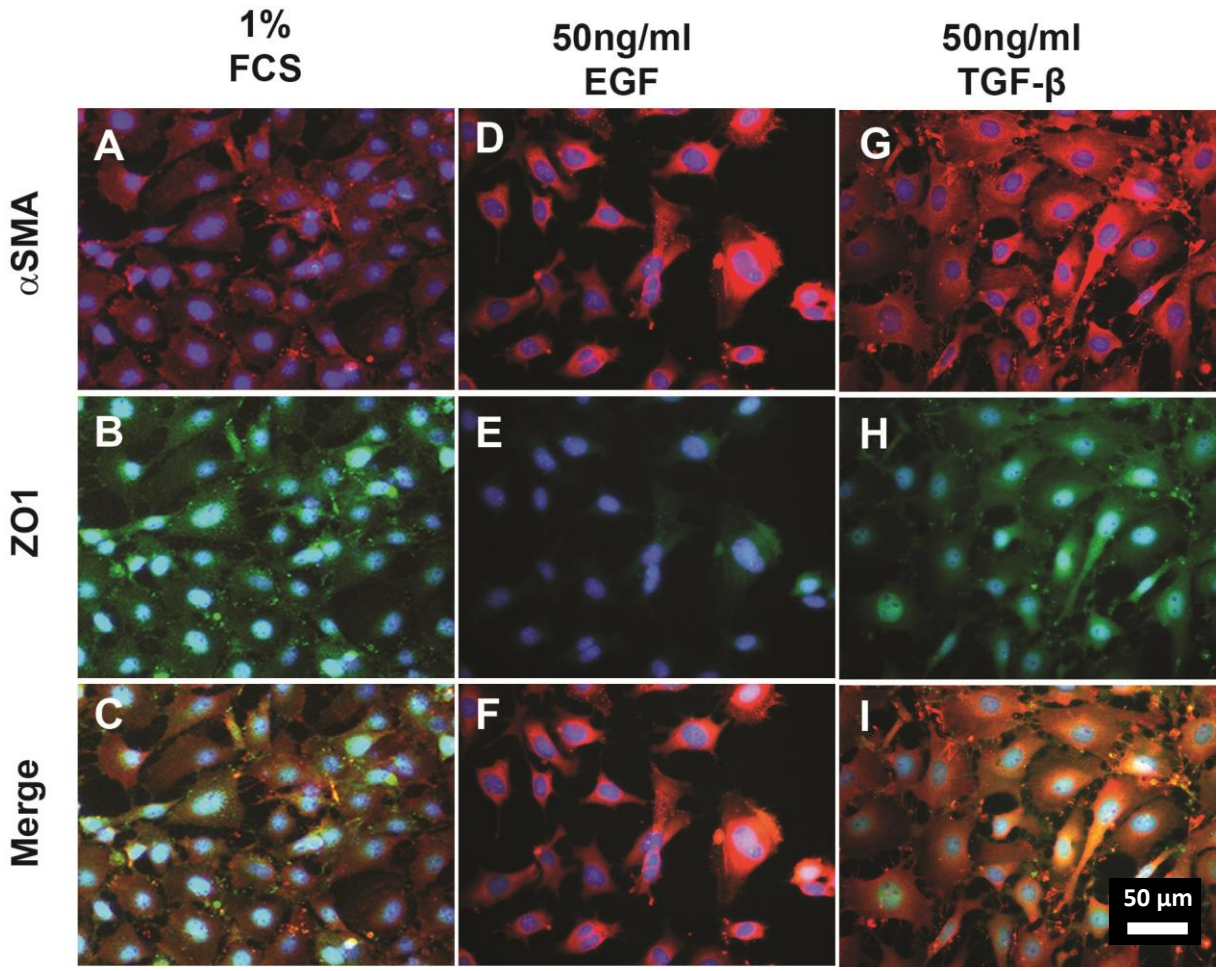

Figure 5.4: EGF and TGF-β induce some MMT changes in passaged mesothelial cells. Passaged mesothelial cells were stimulated for 48 h in EGF or TGF-β and immunolabeled for ZO1 and αSMA. [A - C] Cells in the 1% serum group expressed αSMA weakly, however, ZO1 was absent from the cell-cell contacts. [D - F] EGF-treated cells expressed αSMA uniformly in the cytoplasm, while ZO1 was not localised to the cell borders. [G - I] The passaged cells that were stimulated in TGF-β showed no ZO1 localisation at the cell-cell junctions and strong αSMA staining. Images were taken at 846.6 ms exposure for 594 channel and 2 s exposure for the 488 channel. Images shown are representative of n=2

Through western blot analysis, we could show that the stimulation with TGF-β and EGF did not significantly alter the expression of the MMT associated markers αSMA (Fig 5.5B), ZO1 (Fig 5.5C), and Snail2 (Fig 5.5D). Moreover, western analysis of the Ras/MAPK signalling pathway showed that EGF and TGF-β increased the expression of ERK1/2 and ERK5 levels in mesothelial cells, without changing the overall phosphorylation (Fig 5.5). This suggests that these growth factors stimulate the activation of these MAP kinases in mesothelial cells. Whether ERK1/2 and ERK5 have a role in mediating MMT in mesothelial cells needs further clarification.

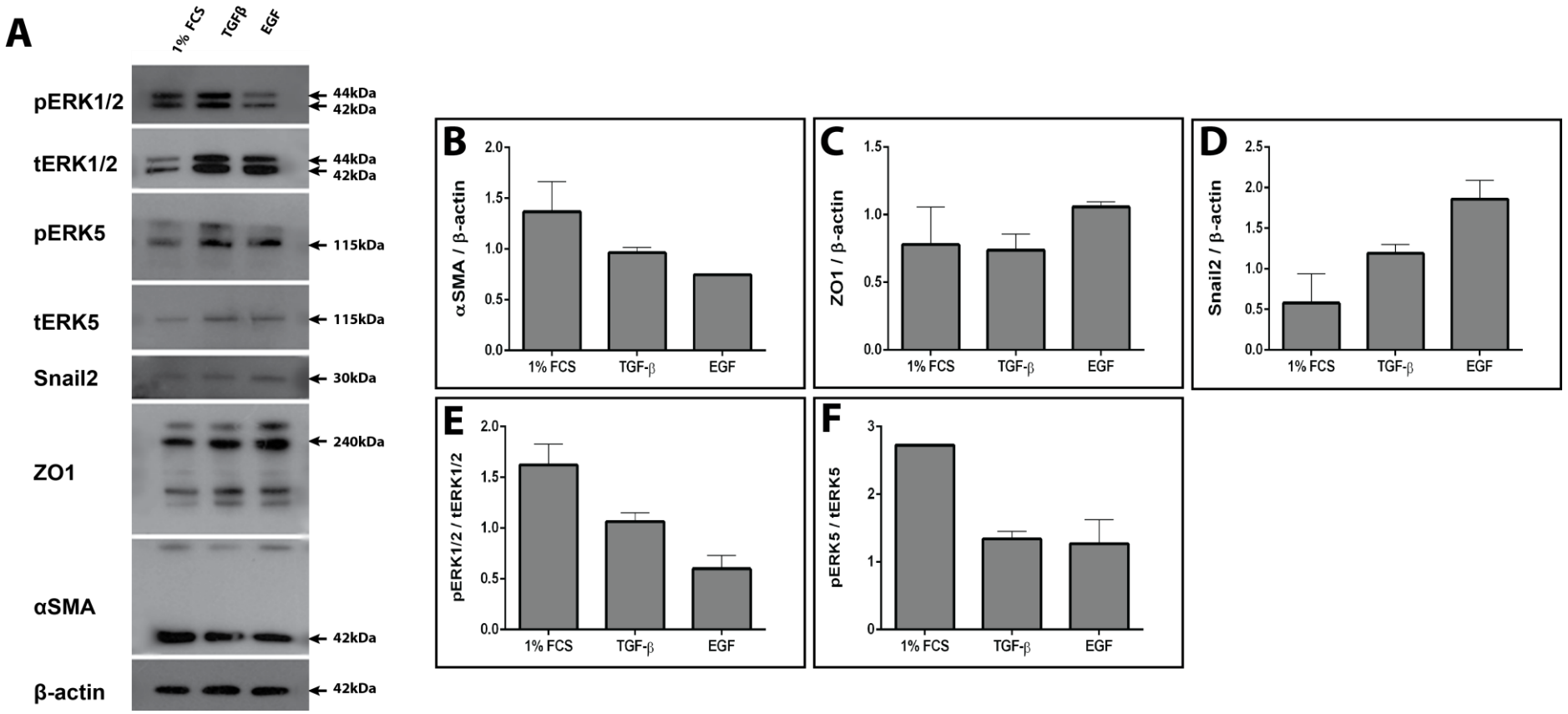

Figure 5.5: MAPK signalling in mesothelial cells treated with EGF and TGF-β [A] Mesothelial cells were treated for 48 h in TGF-β or EGF (50ng/ml) following which the cells were lysed and protein extract. Samples were resolved on a 4-12% Bis-TRIS membrane. Signal intensities of the bands were quantified and phosphorylation revealed no significant changes for αSMA [B], ZO1 [C], and Snail2 [D] expression, or for [E] ERK1/2 and [F] ERK5 phosphorylation. However, stimulation increased overall total protein expression of these signalling molecules. All samples were normalized against β-actin loading control and ERK phosphorylation was calculated as [(pERK/ β-actin) / (tERK/ β-actin)]. Data representative of n= 2 biologically distinct replicas.

5.2.2 Response in migratory behaviour of mesothelial cells after TGF-β or EGF stimulation

During insult induced by bio-incompatible agents or injury to the serosa, mesothelial cells can undergo MMT to gain migratory features of mesenchymal cells in order to assist with wound healing (Lee and Ha, 2007). Therefore, the ability of cytokines to regulate MMT could affect cell infiltration and cell aggregation at the site of the injury. Therefore, we next assessed the effects of TGF-β or EGF stimulation on the migration capacity of cultured mesothelial cells in an *in vitro* scratch assay.

Passaged mesothelial cells (between passages 10 and 16) were serum deprived for 24 h in 1% FCS medium. The cells were then stimulated with TGF-β or EGF for 48 h. Their ability to close the scratched area was analysed over a 24 h period in the presence or the absence of mitomycin C (10 μg/ml). Mitomycin C (MMC) is a potent DNA cross-linker and was used in order to assess the gap closure rate in the absence of cell proliferation (Liu et al., 2009) (Fig 5.7).

By 12 h, the percentage gap closure had reached 80% in the TGF-β stimulated conditions, and roughly 70% in cells stimulated with EGF (Fig 5.6), and full gap closure was seen by 24 h in all conditions that lacked MMC (Fig 5.6). In comparison to the control low serum group, the TGF-β stimulated cells showed a 1.8 fold faster rate of gap closure at the 4 h point, however by 12 h the rate of gap closure had attenuated to 1.4 fold compared to control cells (Fig 5.6A). On the other hand, stimulation with EGF slowed the rate of gap closure by 2.3 fold at the 4 h point, relative to the control cells (Fig 5.6A). Statistical significance was noted between the EGF and TGF-β growth factors at the 4 h point, where TGF-β induced a faster rate of migration by 4 fold when compared to EGF stimulation ($P<0.05$) (Fig 5.6A).

In the presence of MMC, we could not detect any significant changes in the percentage gap closure rate between the samples (Fig 5.6B).

Overall, stimulation with TGF-β for 48 h in the absence of MMC, showed the fastest rate of gap closure at 4 h and 12 h. Significance, however, was only noted at 4 h where the TGF-β induced faster migration relative to EGF stimulation. In the absence of cell proliferation, the migration rates between the treated and untreated groups were unaffected. Taken together, we showed that TGF-β and EGF-induced some changes in ZO1 localization and increased expression of ERK1/2 and ERK5, yet complete transdifferentiation into myofibroblasts was not achieved. This could due to the fact that the cells needed longer exposure to the growth factors for full MMT progression.

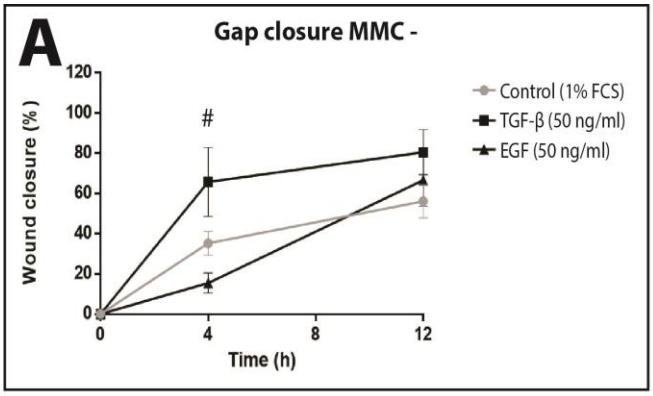

Treatment	% wound closure post scratch					
	4 h			12 h		
	Mean	SEM	Fold change	Mean	SEM	Fold change
Control (1% FCS)	35.28	5.92	1	56.15	8.29	1
EGF (50 ng/ml)	15.4	5.81	0.436508	66.6	13.07	1.186109
TGF-β (50 ng/ml)	65.72	17.19	1.862812	80.59	11.25	1.435263

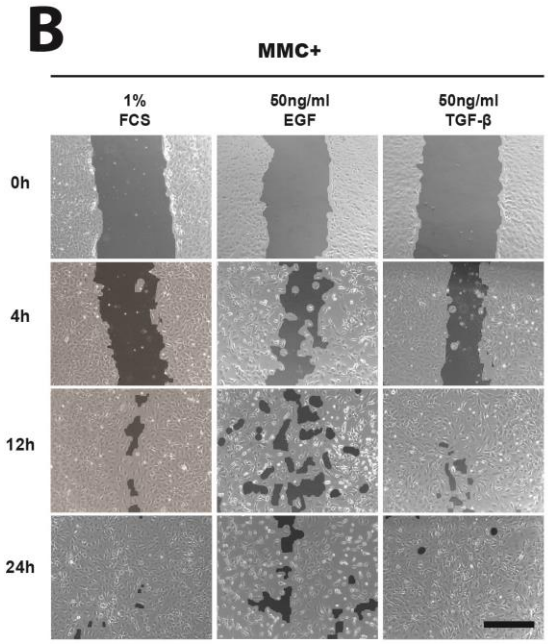

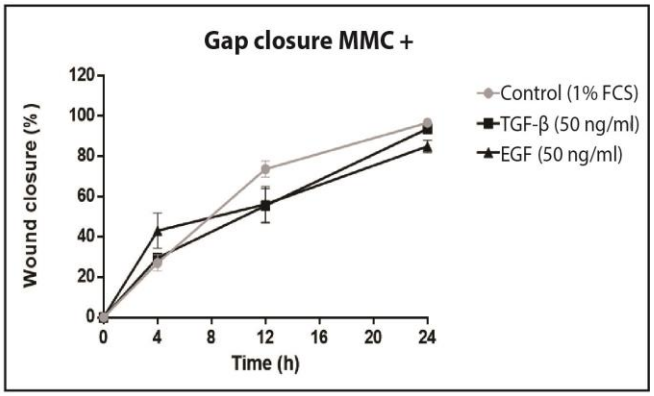

Treatment	% wound closure post scratch								
	4 h			12 h			24 h		
	Mean	SEM	Fold change	Mean	SEM	Fold change	Mean	SEM	Fold change
Control (1% FCS)	27.85	4.08	1	73.66	3.97	1	96.63	0.94	1
EGF (50 ng/ml)	43.33	0.63	1.56	56.2	8.88	0.76	84.90	3.07	0.88
TGF-β (50 ng/ml)	29.58	3.88	1.06	55.48	8.53	0.75	93.63	0.081	0.97

Figure 5.6 Stimulation with EGF or TGF-β growth factors for 48 h fails to change the rate of gap closure. Mesothelial cells (P10 -25) at 80% confluence were serum deprived for 24 h, before being stimulated for 24 h with either EGF or TGF-β in the presence or absence of mitomycin C (MMC+/-). They were then scratched and the medium was replaced. The cell wounds were imaged at 0, 4, 12 and 24 h post wounding. [A] In the absence of MMC, the cells showed a 4 fold faster rate of migration at 4 h post-scratch induction after stimulation with TGF-β when compared to the EGF stimulation ($P<0.05$). However, by 12 h the percentage wound closure was similar between all the groups. [B] In the presence of MMC the mesothelial cells showed a similar rate of wound closure between all groups. Data is representative of 2 biological replicas. A one-way ANOVA followed by a Sidak post hoc was performed to determine significance between the groups where $^{\#}$ = $P<0.05$ compared to the EGF treatment group. Scale bar 200 μm.

5.3 TGF-βRI and EGFR inhibitors rescued the expression of ZO1 in the mesothelial cells and slowed the rate of mesothelial cell migration in an *in vitro* wound healing assay

The previous sections had shown that stimulation with TGF-β or EGF caused the mesothelial cells to show reduced expression of ZO1 at cell contacts and increased overall ERK1/2 and ERK5 expression. We next sought to determine the effects of long-term inhibition of the TGF-β and EGF signalling pathways on the expression and localization of epithelial and mesenchymal-related markers. Following a 48 h culture period in 5-20 µM of either LY364947 (TβRi) or PD153035 (EGFRi), the mesothelial cells were fixed and immunolabeled with ZO1 and αSMA. Sample images were captured at the same exposure time to more accurately examine the effect of the inhibitors on protein localization.

The cells exposed to low serum only showed strong αSMA stress fibre expression and weak ZO1 expression (Fig 5.7A-C). In comparison, mesothelial cells treated with an escalating range of doses between 5-20 µM of TβRi showed brighter levels of αSMA and more restored ZO1 expression, especially in the higher doses, relative to the 1% FCS only group (Fig 5.7D-L). Treatment with EGFRi seemed to also increase the localisation the tight junctional protein ZO1 at the cell-cell contacts in a punctate manner (Fig 5.7M-U). However, the restoration of ZO1 in response to EGFRi seemed less pronounced when compared to the TβRi treatment group.

Overall, inhibiting signalling through TβRI and EGFR seemed to restore ZO1 expression at the cell contacts while simultaneously increasing the expression of αSMA. Suggesting that the cells had adopted an intermediate E/M state within the MMT spectrum.

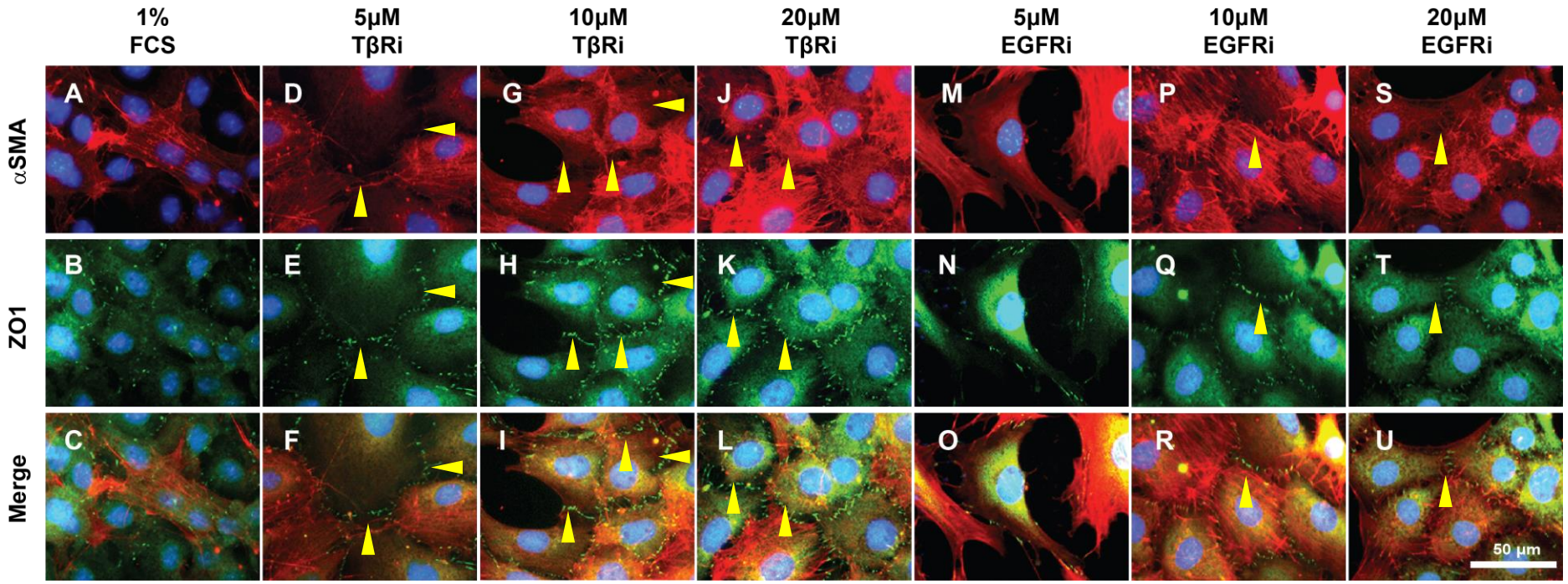

Figure 5.7: Blocking TGFb and EGF signalling with TβRi (LY364947) and EGFRi (PD153035) rescued ZO1 expression and increased αSMA in mesothelial cells. P10-25 mesothelial cells were inhibited for 48 h in TβRi and EGFRi, respectively, and immunolabelled for ZO1 and αSMA. [A-C] Cells of the low serum control group expressed αSMA, while ZO1 expression was absent from cell contacts. [D-L] After incubation with doses of between 5-20 μM TβRi, mesothelial cells upregulated the expression of αSMA and ZO1 in a dose-dependent manner. ZO1 was found localised to the cell borders in a punctate pattern (arrowheads). [M-U] Incubation with EGFRi resulted in faint punctate ZO1 localisation at the cell-cell junctions (arrowheads) and bright αSMA staining. Images were taken at 846.6 ms exposure for 594 channel and 2 s exposure for the 488 channel; a representative of n=2.

Since we have shown that the inhibition of TGF-β and EGF signalling resulted in the upregulation of both epithelial and mesenchymal markers, it was important to assess whether the inhibitors had an effect on the rate of mesothelial cell migration in the scratch assay. The passaged mesothelial cells were seeded at $4x10^5$ density/ well and left to attach overnight. They were serum deprived for 24 h following which they were inhibited for a period of 24 h in 5-20 μM TβRi (LY364947) (Fig 5.8) or EGFRi (PD153035) (Fig 5.9). The monolayers were subsequently scratched and fresh medium supplemented with inhibitors was re-added. The migration rates were assayed in the presence or absence of MMC over a course of 24 h.

Mesothelial cells treated with TβRi in the absence of MMC showed a dose-dependent response in migration into the wound area. At 4 h post wound generation, the mesothelial cells treated with TβRi had a 1.5-1.9 fold reduced rate of migration relative to the control cells. However by 12 h the TβRi-treated cells had closed the wound space 1.3-1.5 fold faster relative to the control cells ($P<0.01$ for the 20 μM treatment) (Fig 5.8A).

During the time course of the wound closure in the presence of MMC, the highest inhibitor concentration led to a significant reduction in the closure rate throughout the study. Overall, the wound closure rates were reduced in a dose-dependent manner over control conditions (Fig 5.8B).

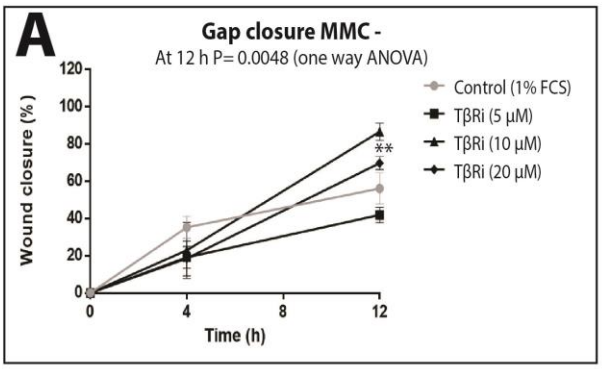

Treatment	% wound closure post scratch					
	4 h			12 h		
	Mean	SEM	Fold change	Mean	SEM	Fold change
Control (1% FCS)	35.28	5.92	1	56.15	8.29	1
TβRi (5 μM)	15.4	5.83	0.44	41.91	4.18	0.75
TβRi (10 μM)	22.93	15.16	0.65	86.62	4.631	1.54
TβRi (20 μM)	18.51	9.33	0.52	69.72	3.51	1.24

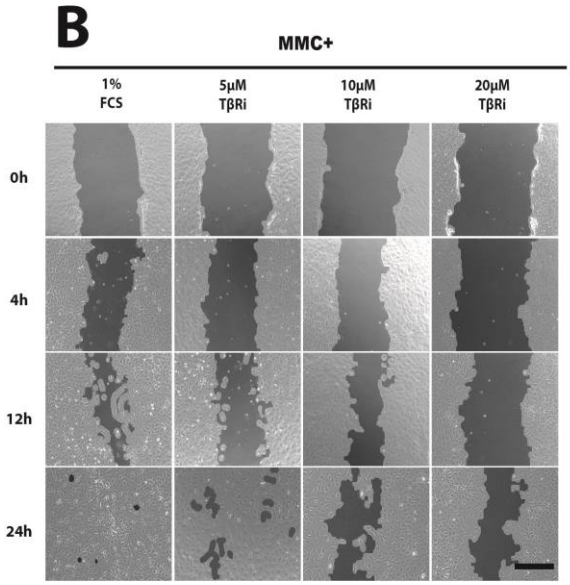

One way ANOVA: 12 h P= 0.0008 and 24 h P= 0.0244

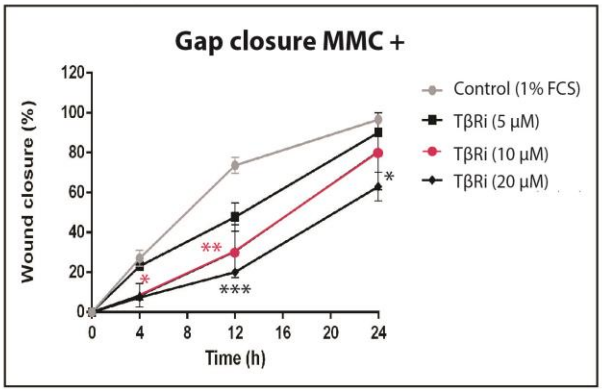

Treatment	% wound closure post scratch								
	4 h			12 h			24 h		
	Mean	SEM	Fold change	Mean	SEM	Fold change	Mean	SEM	Fold change
Control (1% FCS)	27.84	4.08	1	73.66	3.97	1	96.63	0.94	1
TβRi (5 μM)	15.4	5.83	0.83	41.91	4.18	0.65	90.19	0.48	0.93
TβRi (10 μM)	22.93	15.16	0.3	86.62	4.63	0.42	80.67	19.33	0.83
TβRi (20 μM)	18.51	9.33	0.27	69.72	3.51	0.27	63.02	7.27	0.65

Figure 5.8 Inhibition of TβRI for 48 h attenuates the rate of gap closure. Mesothelial cells between P10 -25 were serum deprived for 24 h, before being treated with TβRi for 24 h in the presence or absence of mitomycin C (MMC+/-). Following which the monolayer was scratched and the wounds were imaged at 0, 4, 12 and 24 h. [A] Under MMC- conditions, the mesothelial cells had attenuated the rate of gap closure at 4 h between 1.5 to 1.9 fold relative to the low serum group. Paradoxically, the percentage wound closure by 12 h was 1.2-1.5 fold faster ($P<0.01$ in the 20 µM treatment). [B] Under MMC+ conditions, the mesothelial cells attenuated the rate of gap closure in a dose-dependent fashion. At 4 h the rate of wound closure was roughly 4 fold slower in the 10 and 20 µM treatments ($P<0.01$). By 24 h the rate was 1.5 fold lower ($P<0.05$) at the 20 µM dose. Data is representative of 2 biological replicas. A one-way ANOVA was used to determine statistical significance between the groups where ** = $P<0.01$, and *** =$P<0.001$ when compared to the 1% FCS only group. Scale bar 200 µm.

Next, we examined the rate of gap closure of mesothelial cells in the presence of the EGFRi (Fig 5.4.2A). In the absence of the MMC, the rate of wound closure was attenuated over time relative to the low serum control cells, as the percentage of wound closure was roughly the same between the EGFRi-treated and untreated cells. By 12 h the rate of cell migration had dropped by 1.7 and 2.1 fold in the 10 and 20 μM dose treatments, respectively, however, this difference was not statistically significant (Fig 5.9A). In the presence of MMC, the rate of cell migration into the open wound in response to EGFRi stimulation was also slower relative to the control. Initially, the rate of migration across all doses of EGFRi was similar at both 4 h and 12 h since migration was attenuated 3 fold ($P<0.01$ at 12 h). However, by 24 h the gap closure rate showed a dose-dependent response since EGFRi at 10 μM attenuated gap closure by 1.33 fold, and at 20 μM the gap closure rate was 1.9 fold reduced ($P<0.01$) (Fig 5.9B).

In summary, the temporary inhibition of signalling through TβRI and EGFR in the absence of cell proliferation attenuated mesothelial cell motility in a dose-dependent manner.

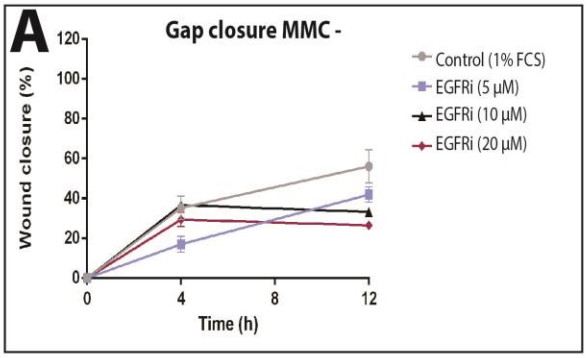

Treatment	% wound closure post scratch					
	4 h			12 h		
	Mean	SEM	Fold change	Mean	SEM	Fold change
Control (1% FCS)	35.28	5.92	1	56.14503	8.29	1
EGFRi (5 µM)	17.05782	4.021165	0.483454	41.91071	3.791736	0.746472
EGFRi (10 µM)	36.77403	2.180056	1.042253	33.2543	0.832412	0.592293
EGFRi (20 µM)	29.47688	3.499358	0.835436	26.50065	0.144286	0.472003

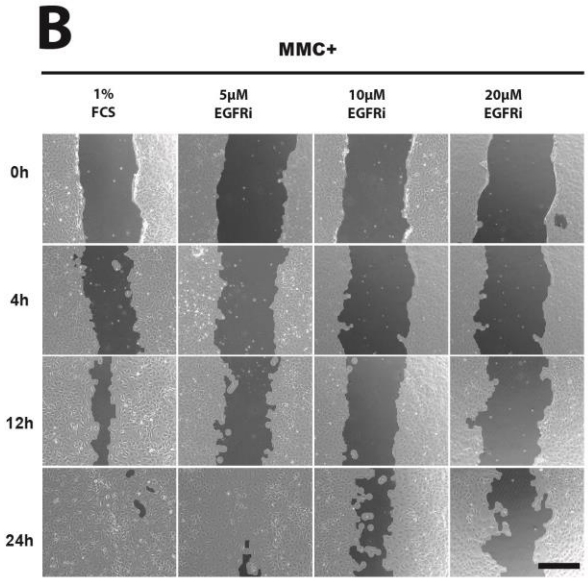

One way ANOVA:
4 h = 0.00067, 12 h P= 0.0008 and 24 h P= 0.0244

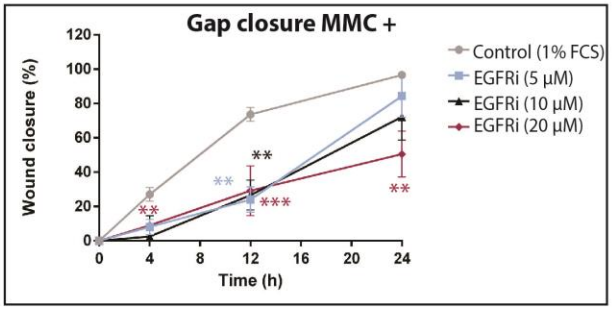

Treatment	% wound closure post scratch								
	4 h			12 h			24 h		
	Mean	SEM	Fold change	Mean	SEM	Fold change	Mean	SEM	Fold change
Control (1% FCS)	27.84	4.08	1	73.66	3.97	1	96.63	0.94	1
EGFRi (5 µM)	8.16	4.44	0.29	24.05	7.41	0.33	84.36	0.48	12.30
EGFRi (10 µM)	2.54	12.17	0.09	26.64833	8.69	0.36	72.20	19.33	13.63
EGFRi (20 µM)	9.06	0.48	0.33	29.27	14.53	0.4	50.54	7.27	13.34

Figure 5.9 Inhibition of EGFR for 48 h attenuates the rate of gap closure. Mesothelial cells were serum starved for 24 h in 1% FCS medium. This was followed by a 24 h period of treatment in the EGFR inhibitor (PD153035). A scratch was formed in the centre of the monolayer and medium was replaced. Samples were imaged at 0, 4, 12 and 24 h. [A] The mesothelial cells 12 h post wounding in the MMC- conditions showed a dose-dependent attenuated wound closure of 1.7 fold at the 10 µM dose and 2.11 fold slower closure at the 20 µM dose relative to the control group. [B] In the MMC+ condition the rate of mesothelial cells migration into the gap was most attenuated at 4 and 12 h post wounding, showing a 3 fold reduced migration relative to the control cells ($P<0.01$). By 24 h the percentage gap closure was 1.9 fold slower in the 20 µM PD153035 treated cells ($P<0.01$). The data presented is representative of 2 biological replicas, and a one-way ANOVA test was used to determine statistical significance where $P<0.01$, *** =$P<0.001$ and ****=$P<0.0001$ compared to the 1% controls. Scale bar 200 µm.

5.4 Inhibition of MEK5 and ERK5 gave rise to two distinct groups of cells that corresponded to the different MMT states.

So far we showed that stimulation by especially by TGF-β led to an increase of phosphorylated ERK1/2 and ERK5 in mesothelial cells, while both EGF and TGFb inhibition resulted in upregulation of ZO1 and decrease in migratory behaviour. Next, we aimed to determine if ERK5 and ERK1/2 played a role in mediating MMT. While ERK1/2 has been previously documented to induce MMT in mesothelial cells, the role of ERK5 signalling in mediating epithelial cell migration and transdifferentiation remains largely disputed and not well characterised, especially in mesothelial cells (Jin et al., 2016, Strippoli et al., 2015, Liang et al., 2015, Komaravolu et al., 2015, Badshah et al., 2014). Recent work on keratinocytes demonstrated that EGF-induced EMT was mediated through the ERK5 – Snail2 signalling cascade (Arnoux et al., 2008).

Our previous efforts to analyse the MMT status in the OMC explants following the inhibition of MEK1/2 and MEK5 for 48 h were not successful as the small molecule inhibitors induced cell death. In fact, treatment with PD184354 (a small molecule inhibitor of MEK, MEKi) induced cell death in the OMC-derived mesothelial cells just 2 h post treatment (data not shown). With this in mind, we decided to assess the impact of MEKi, BIX02189 (MEK5 inhibitor, MEK5i), and XMD8-92 (ERK5 inhibitor, ERK5i) on MMT and migration in mesothelial cell cultures using a range of doses.

Our preliminary tests using the inhibitors showed that even at a low dose (5 µM) MEKi negatively impacted on mesothelial cell proliferation and survival with most cells dying by 24 h ($P<0.0001$) (Fig 5.10). Treatment with 5 µM ERK5i resulted in a 55% loss in cell viability by 24 h, while by 48 h the cell viability was reduced to 62% relative to the 1% FCS controls ($P<0.001$ and $P<0.01$), respectively. Finally, 5 µM MEK5/ERK5i showed a delayed onset of

cytotoxicity in the mesothelial cells, as we noted a 35% drop in relative cell viability by 48 h (P<0.05).

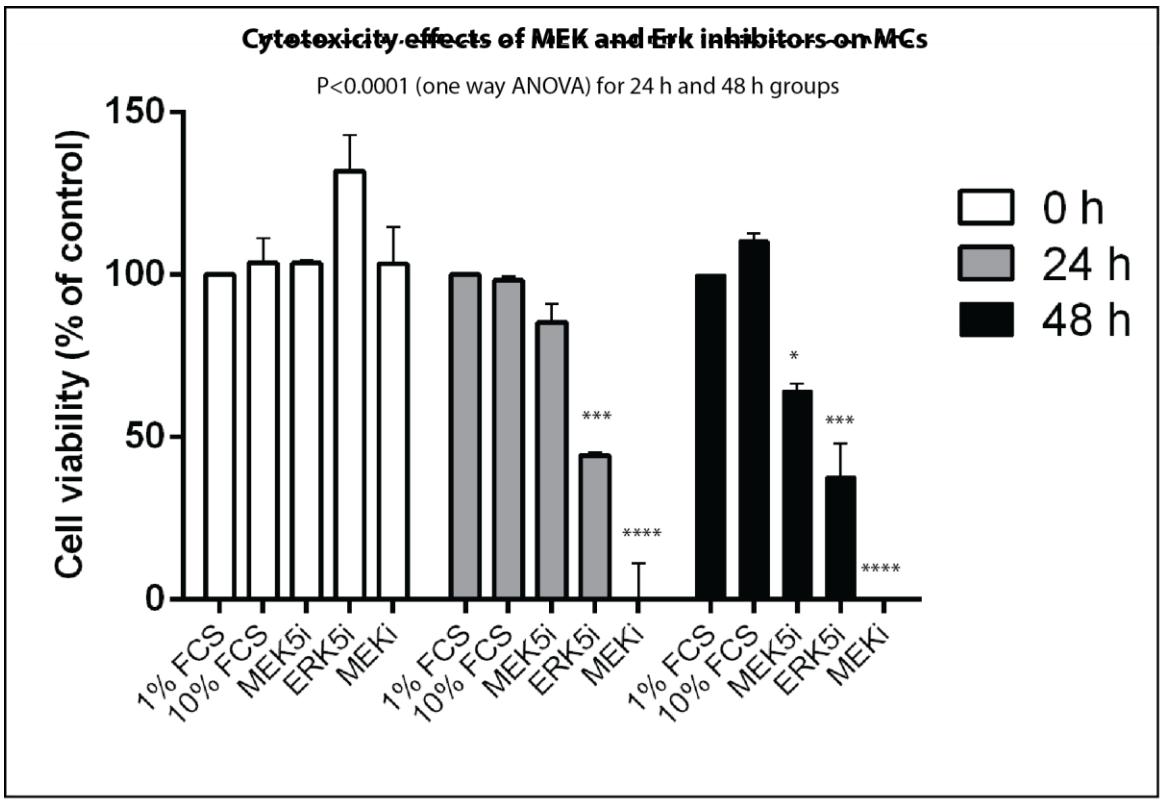

Figure 5.10: Inhibition of MEK5 and ERKs 1/2 and 5 are essential for mesothelial cell survival. Serum-starved mesothelial cells were treated with 5 µM of MEK5/ERK5i, ERK5i or MEKi. Cell cytotoxicity was assayed using the CCK-8 kit at 0 h, 24 and 48 h post treatments. MEK5/ERK5i showed a delayed onset of cytotoxicity in mesothelial cells since a significant difference was only detectable at 48 h. ERK5i reduced cell viability by 55% at 24 h and 62% by 48 h, while MEKi was most potent and induced complete cytotoxicity by 48 h. Data is representative of n=2 biologically independent samples. A One-way ANOVA determined statistical significance, where *=P<0.05, **=P<0.01, ***=P<0.001 and ****=P<0.0001.

Since MEKi showed a high degree of cytotoxicity, we decided to concentrate on MEK5i and ERK5i in order to determine the role of ERK5 and MEK5 on MMT using ZO1 and αSMA immuno-detection. We also aimed to test the effects of lower doses of these small molecule inhibitors to circumvent the cytotoxic effects seen in the 5 μM dose.

With immunolabeling, we were able to detect a spectrum of coexisting cells passing through the MMT programme since these cell populations would have otherwise been masked by whole cell lysis techniques that generate population average data.

In the absence of inhibitors, cells of the control group expressed αSMA and very little ZO1, as shown before (Fig 5.11A-C). When the mesothelial cells were exposed to a range of MEK5/ERK5i doses between 1.25 and 5 μM, they exhibited an increase in ZO1 abundance overall relative to the low serum group (Fig 5.11D–L). However, there was a mixed population of cells that expressed either $ZO1^{medium}$ / αSMA^{low} (white arrow) or $ZO1^{medium}$ / αSMA^{high} (yellow arrow), consistent with the MMT spectrum where the cells seem to exist in the intermediate state.

Treatment with ERK5i for 48 h also increased the expression of ZO1 at the cell-cell contacts; furthermore, we were able to see a similar spectrum of cells going through MMT. However, the mesothelial cells seemed to express less ZO1 at the cell borders even in the higher doses when compared to MEK5/ERK5i (Fig 5.11M-U).

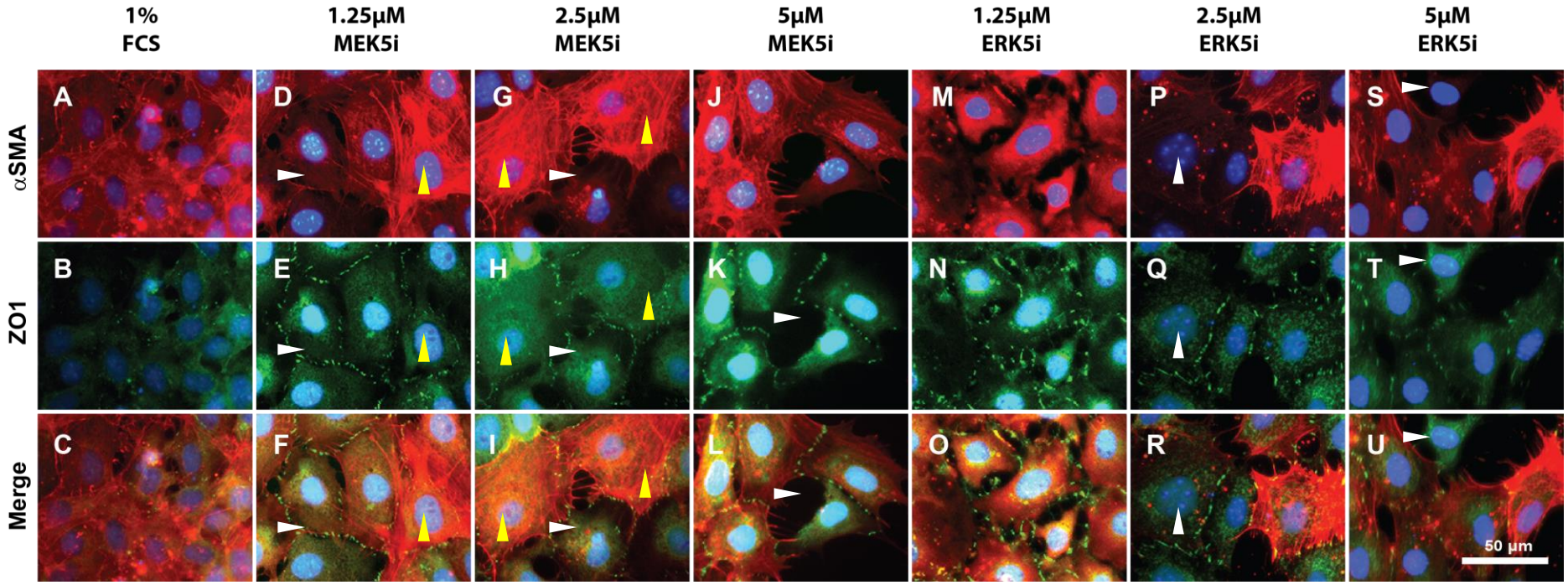

Figure 5.11: Treatment in MEK5/ERK5i and ERK5i gave rise to a spectrum of MMT cell states. Mesothelial cells between P10 and P25 were inhibited for 48 h in MEK5/ERK5i and ERK5i, respectively, and immunolabeled for ZO1 and αSMA. [A-C] Low serum controls expressed high αSMA and weak ZO1. [D-L] Inhibition with doses between 1.25 - 5 µM MEK5/ERK5i yielded a mixed population of cells that expressed αSMA^{low} /$ZO1^{medium}$ (white arrowheads) or αSMA^{high} /$ZO1^{medium}$ (yellow arrowheads). [G-I] Inhibition using ERK5i resulted in a similar but less pronounced population of cells with mixed expression of MMT state markers. Images were captured at 846.6 ms and 2s exposure times for 594 and the 488 channels for n=2.

5.5 Inhibition of MEK5 attenuates that percentage gap closure rate of passaged mesothelial cells in an *in vitro* wound healing assay.

Encouraged by the findings that MEK5 and ERK5 inhibitors led to an upregulation of the epithelial marker ZO1 in a spectrum of MMT cells, we aimed to explore whether MEK5 played a role in mesothelial cell migration in a scratch assay. Mesothelial cells treated with MEK5i and without MMC for 48 h showed a decreased gap closure rate over the first 12 h when compared to control cells (Fig. 5.12A). Specifically, by 4 h the migration rate was 1.6 fold slower in the 1.25 μM and 2.5 μM MEK5i treated cells relative to the control group. The migration rate of was slightly more attenuated by 12 h, falling to 1.8 fold in 1.25 – 5 μM dose treatment (Fig 5.12A). However, these findings were not statistically significant. In the absence of cell proliferation, mesothelial cells treated with MEK5i showed a reduced rate of cell migration at 12 h. Specifically, at this time point, the rate of wound closure depended on the dose of MEK5i as wound closure was reduced by 1.7 fold in the 2.5 μM condition, and by 2.5 fold in the 5 μM dose ($P<0.01$ and $P<0.001$ respectively) (Fig 5.12B).

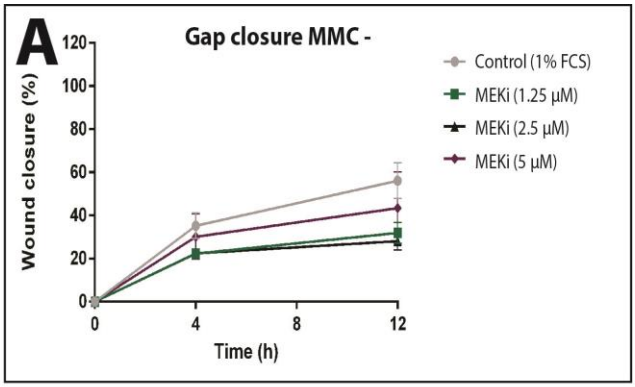

Treatment	% wound closure post scratch					
	4 h			12 h		
	Mean	SEM	Fold change	Mean	SEM	Fold change
Control (1% FCS)	35.28	5.92	1	56.15	8.29	1
MEKi (1.25 µM)	22.31	1.59	0.63	31.90	4.85	0.57
MEKi (2.5 µM)	22.50	1.69	0.64	28.16	4.16	0.50
MEKi (5 µM)	30.14	10.50	0.85	43.43	16.72	0.77

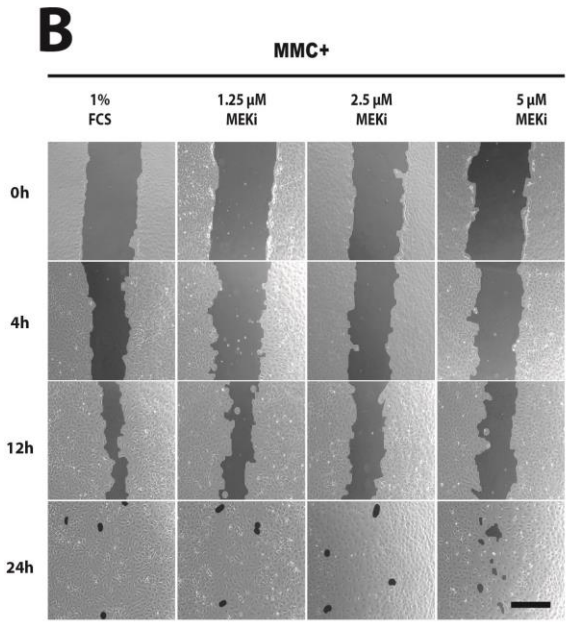

One way ANOVA: 12 h P= 0.022

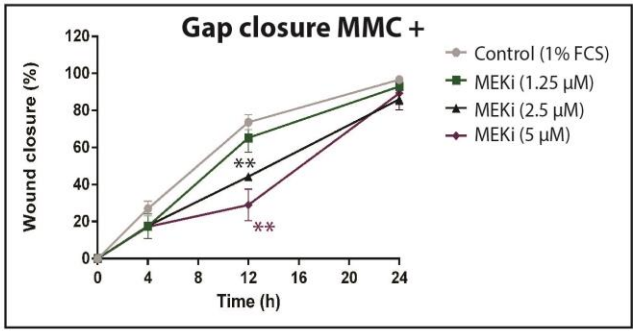

Treatment	% wound closure post scratch								
	4 h			12 h			24 h		
	Mean	SEM	Fold change	Mean	SEM	Fold change	Mean	SEM	Fold change
Control (1% FCS)	27.84	4.08	1.00	73.66	3.97	1.00	96.63	0.94	1.00
MEKi (1.25 µM)	17.58	6.65	0.63	65.26	7.83	0.89	92.92	0.02	0.96
MEKi (2.5 µM)	17.79	1.34	0.64	44.31	2.24	0.60	86.77	5.89	0.90
MEKi (5 µM)	17.24	0.72	0.62	29.77	8.56	0.40	89.35	6.10	0.92

Figure 5.12 Treatment with MEK5i for 48 h attenuated the percentage gap closure in the passaged mesothelial cells MEK5 signalling was inhibited for 48 h in mesothelial cells with and without MMC, and gap closure was imaged at 0, 4, 12 and 24 h post wounding. [B] Mesothelial cells 4 h post wounding in the MMC- conditions showed on average a 1.6 fold decreased the rate of percentage gap closure in MEK5/ERK5i-treated cells when compared to the control group. The rate of gap closure was slightly more attenuated by 12 h at 1.8 fold. [C] When cell proliferation was removed following MMC treatment, the rate of gap closure was most attenuated at 12 h in a dose-dependent fashion. Treatment with 2.5 µM MEK5/ERK5i slowed the wound closure by 1.7 fold and treatment with 5 µM of the inhibitor attenuated gap closure 2.5 fold, ($P<0.01$ and $P<0.001$ respectively). Means were calculated from 2 biologically distinct samples. A one-way ANOVA determined statistical significance where ** = $P<0.01$ and *** =$P<0.001$ relative to 1% FCS group. Scale bar 200 µm.

5.6 Long-term inhibition of TβR1 and EGFR decreases ERK5 activation

In the previous sections, we demonstrated that the inhibition of TβRI, EGFR signaling , and MEK5 reduced wound closure rate and increased accumulation of ZO1 at cell-cell contacts. We, therefore, wanted to see if ERK5 phosphorylation was affected by diminishing signalling through EGFR and TβRI. Whole cell lysates of mesothelial cells treated with various inhibitors were isolated and resolved on an SDS-Page gel (Fig 5.7.1A). Analysis of the band intensity in comparison to control cells showed that treatment with the inhibitors did not significantly alter the expression levels of the MMT markers, αSMA, and ZO1, even though we noted an increase in ZO1 expression (Fig 5.7.1B-D). ERK5 phosphorylation was 6 fold down-regulated following TβRi treatment, 17 fold downregulated in the EGFRi-treated cells, and 2.3 fold down-regulated in the ERK5i-treated cells ($P<0.05$) (Fig 5.21F).

While we could not demonstrate that the following stimulation with either EGF or TGF-β MMT transdifferentiation. We did, however, show that the inhibition of TGF-β and EGF signalling slowed the rate of mesothelial cell migration, increased ZO1 localization at cell contacts and reduces ERK5 activation in the passaged mesothelial cells. Which suggests that these factors do have a role in mediating MMT in a paracrine fashion. Table 5.1 summarizes the key findings.

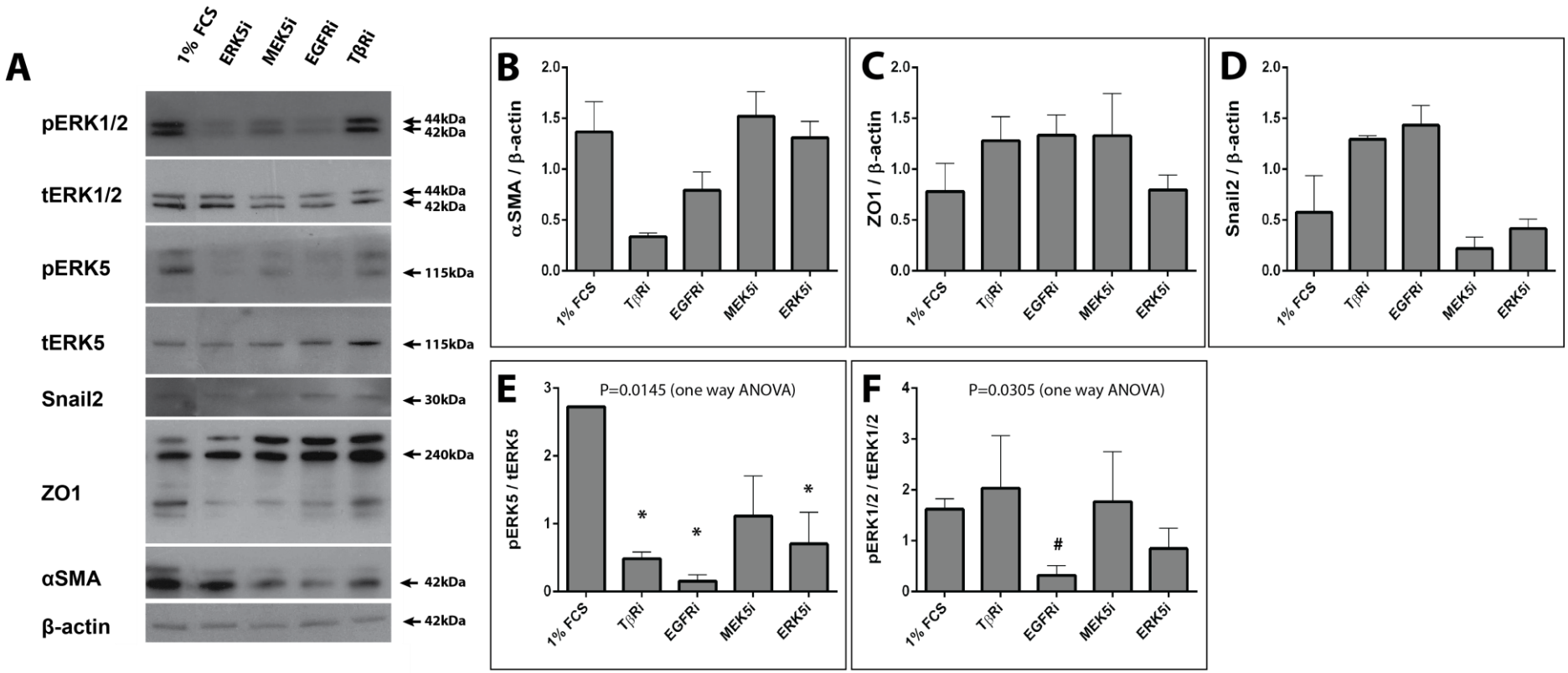

Figure 5.13 TGF-β and EGF show convergence at the level of ERK5. [A] Mesothelial cells treated for 48 h in the various inhibitors were lysed and the proteins were resolved on a 4-12% Bix-TRIS membrane. We could not detect statistically significant changes in [B] αSMA, [C] ZO1, [D] Snail2 expression following treatment with inhibitors relative to 1% FCS controls. [E] Inhibition of ERGR, TβRI MEK5 and ERK5, down regulated ERK5 phosphorylation between 5 -45 fold in mesothelial cells. [F] ERK1/2 phosphorylation was 6 fold down regulated between the TβRi and EGFRi treatment. All samples were normalized to β-actin loading control and ERK phosphorylation was calculated as [(pERK/ β-actin) / (tERK/ β-actin)]. Data presented as means of 2 biologically distinct replicas. Statistical analysis was calculated using a one way ANOVA followed by post hoc Sidak multiple comparisons test, where *=P<0.05, relative to the 1% FCS; $^{\#}$=P<0.05 was relative to TβRi.

TABLE 5.1: SUMMARY OF OBSERVED CHANGES IN PASSAGED MESOTHELIAL CELLS FOLLOWING EXPOSURE TO THE SMALL MOLECULE INHIBITORS, RELATIVE TO 1% FCS

Treatment	ZO1 at cell-cell contacts	αSMA expression	Migration rate	ERK5 phosphorylation
TBRi (LY364947)	++++	stronger	Dose-dependent attenuation	↓
EGFRi (PD153035)	+	stronger	Dose-dependent attenuation	↓↓
MEK5i (Bix02189)	+++	$\alpha SMA^{high/low}$ expressing cells	Dose-dependent attenuation	No change
ERK5i (XMD8-92)	++	$\alpha SMA^{high/low}$ expressing cells	N/A	↓

5.7 Transient Zeb1 and Zeb2 knockdown decrease mesothelial cell migration and increases ZO1 accumulation at cell edges.

A number of transcription factors have been implicated in modulating mesothelial cell transdifferentiation, and our analysis showed upregulation in *Snail2* and *Zeb1* mRNA expression levels with repeated passaging and following stimulation in the kidney rudiments, respectively. Thus, we aimed to further explore the role of these transcription factors in mesothelial cell migration capacity and expression of key MMT markers, by targeting them with siRNA. We achieved a transient knockdown range of between 60 – 75% in our cells, relative to the mock-treated samples (Fig 5.8.1). Through immunolabeling, we could detect increased ZO1 expression at the plasma membrane cell edges, following knockdown of Zeb1, Zeb2 or both, when compared to the mock controls (Fig 5.8.2A-L). However, transient Snail2 silencing failed to increase the tight junctional localization of ZO1 (Fig 5.8.2M-O). Meanwhile, there was a uniform distribution of the mesenchymal marker vimentin in the transfected cells compared to the mock samples (Fig 5.8.2A-O).

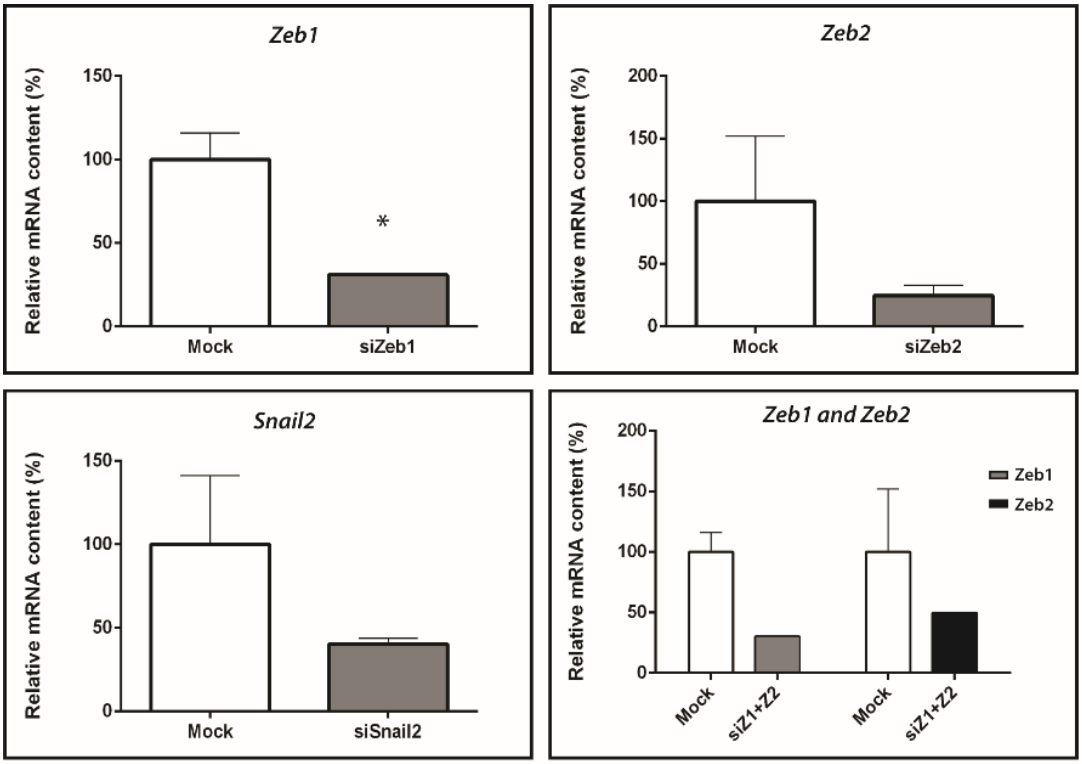

Figure 5.14 Relative Knockdown levels following siRNA transfections. Mesothelial cells were seeded and left to reach 80% confluence before transfection with siRNA or mock for 6 h. Following the 48 h knockdown period, the RNA was harvested and gene knockdown levels were calculated relative to the mock. We could achieve on an average a 70% knock-down in target genes. Data representative of N=2 biological independent samples.

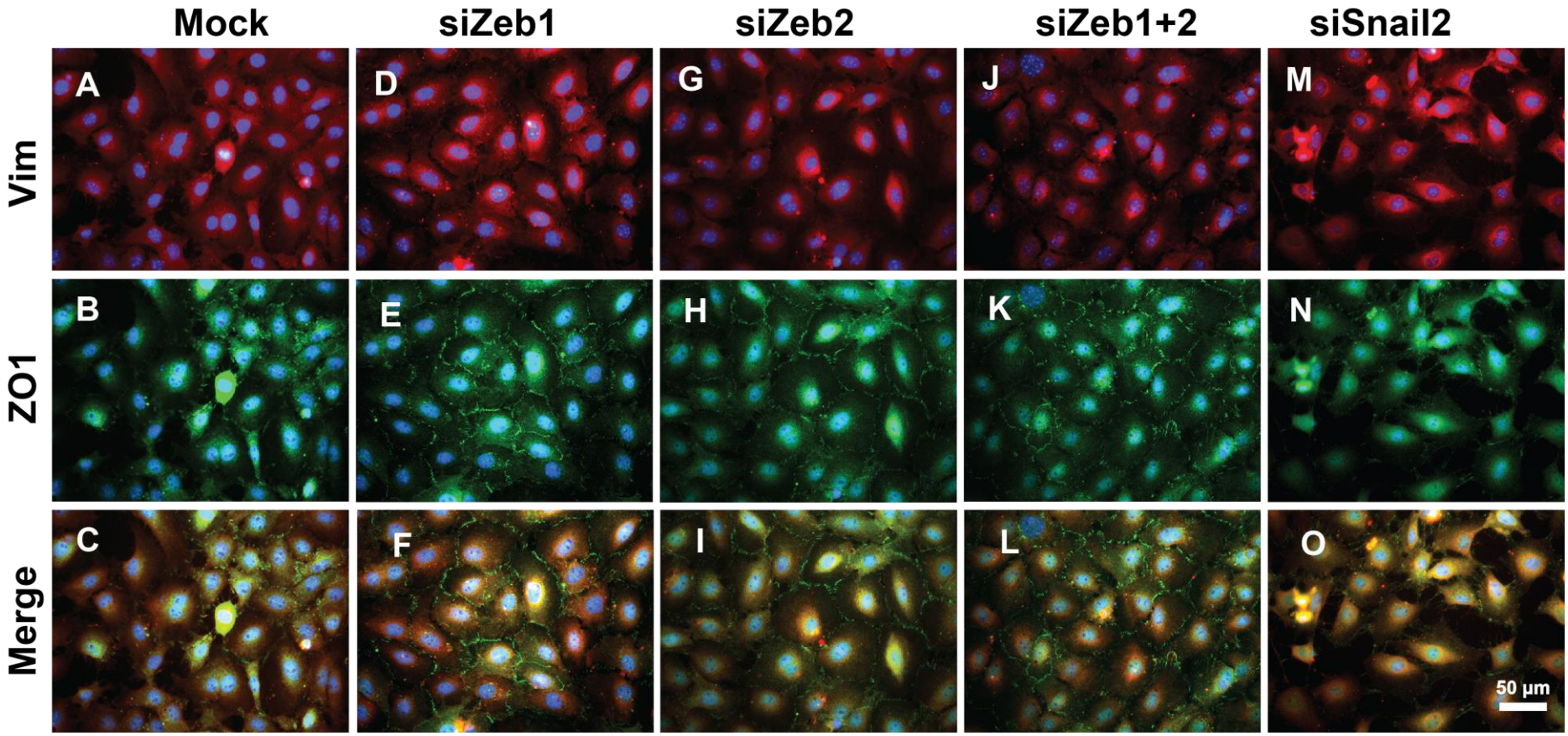

Figure 5.15 Silencing Zeb1 and Zeb2 increased the ZO1 expression at cell junctions. Seeded mesothelial cells were left to reach 80% confluence before being transfected with siRNA against Zeb1, Zeb2, Zeb1+2, Snail2 or mock. Following a 48 h knockdown period, the cells were immunolabeled with ZO1 and Vim, markers of MMT. [A-C] Mock-treated cells expressed Vim strongly throughout the cell cytoplasm, and ZO1 weakly at cell-cell junctions. Mesothelial cells transfected with siZeb1 [D-F], siZeb2 [G-I] or both [J-L] showed increased accumulation of ZO1 at cell-cell contacts. [M-O] siSnail2-treatment failed to increase ZO1 distribution. Vim expression was consistent between samples. Images were captured using consistent exposure times of 846.6 ms for the 594 and 2 s for the 488 channels for n=2.

It is well recognized that a feature of MMT is the gain of a migratory capacity. To this end, we performed a wound-healing assay in cells treated with siZeb1, siZeb2 or both. Our results showed that cell migration was markedly reduced over a 24 h period in siZeb1-, siZeb2- or siZeb1-siZeb2- transfected cells when compared with cells transfected with mock vectors. By 6 h, the migration rate of the siZeb1 transfected cells was 4 fold slower (P=0.0253) compared to the mock group. Moreover, the rate of cell migration further dropped to 7 fold by 24 h (P=0.0466) (Fig 5.8.3D-F, P). Transient Zeb2 silencing slowed the rate of cell migration 2 fold by 6 h (P= 0.0405) and 3 fold by 24 h (P<0.0001) (Fig 5.8.3G-I, P). Dual silencing of the Zeb transcription factors decreased the overall migration rate, however, there was no additive effect (Fig 5.8.3J-L, P). At 6h, there was a 3 fold reduced migration rate (P=0.0288) following Zeb1+2 silencing and at 24 h the migration rate was 2 fold slower than the mock treated cells (P=0.0009). On the other hand, the transient knockdown of Snail2 did not significantly alter the rate of mesothelial cell migration into the wound (Fig 5.8.3M-O, P). These results show that Zeb1 and Zeb2 are more potent at inducing MMT in the cultured mesothelial cells.

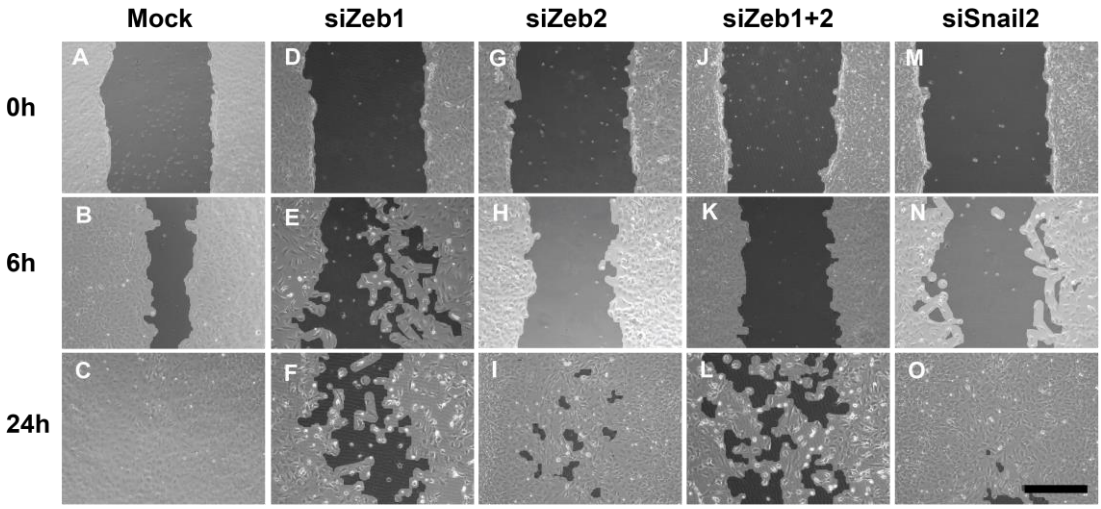

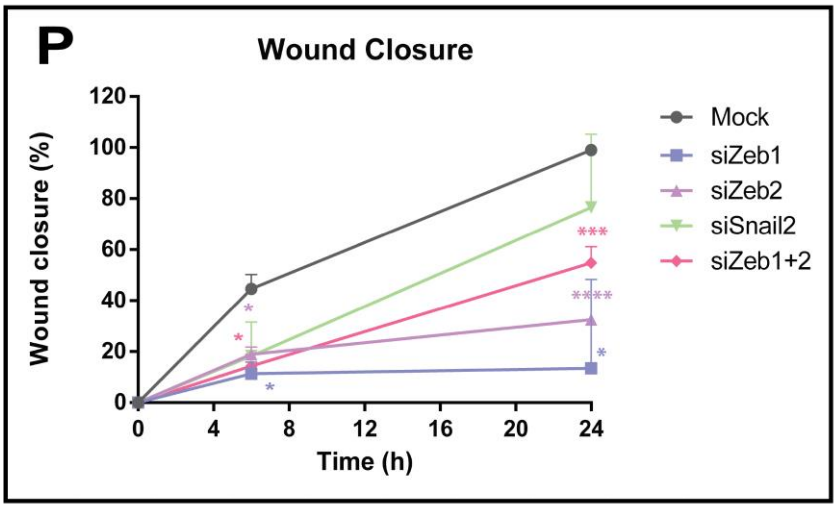

Treatment	% wound closure post scratch							
	6 h				24 h			
	Mean	SEM	Fold change	P Value	Mean	SEM	Fold change	P Value
Mock	44.60	5.61	1		99.01	0.04	1	
siZeb1	11.39	4.53	0.26	0.03	49.56	35.04	0.14	0.05
siZeb2	18.98	1.99	0.43	0.04	32.53	1.65	0.33	<0.0001
siZeb1+Zeb2	37.32	20.99	0.32	0.03	98.64	0.52	0.55	0.0009
siSnail2	18.25	9.42	0.41	n/s	76.54	20.31	0.77	n/s

Figure 5.16 Mesothelial cells transfected with siZeb1, siZeb2 or both showed a reduced gap closure rate. Mesothelial cells at 80% confluence were transfected with siRNA or treated with mock for 6 h. The cells were left for 48 h for effective gene knockdown, before being serum deprived and scratched. Images were taken at 0, 6 and 24 h. Representative images of [A-C] Mock, [D-F] siZeb1, [G-I] siZeb2 ls, [J-L] Zeb1 and Zeb2, and [M-O] siSnail2 treated mesothelial cells. [P] The wound closure rate was attenuated in the siZeb treated samples compared to the mock. Gap closure means were generated from n=2. Scale bar 200 µm.

5.8 Discussion

In this chapter, we demonstrated in the omentum explants that TGF-β and EGF signalling mediated MMT progression. Moreover, blocking signalling in the passaged mesothelial cells through TβRI, EGFR, and MEK5 small molecule inhibitors, inhibited cell migration in a dose-dependent fashion. Through western blotting, we could show diminished ERK5 phosphorylation following treated with TβRi and EGFRi; suggesting that TGF-β and EGF activate ERK5. While we could not detect significant changes in protein and mRNA ZO1 expression, there was increased accumulation at the cell-cell contacts in the inhibitor-treated groups. Finally, the transient knockdown of Zeb1 and Zeb2 transcription factors, but not of Snail2, perturbed cell migration and increased ZO1 accumulation at cell junctions. Overall, we failed to detect complete differentiation through the MMT programme after stimulation with TGF-β and EGF in our passaged cells, however, our results showed that mesothelial cell migration capacity could be mediated through ERK5 signalling.

5.8.1 EGF, TGF-β, and MMT

MMT is a complex stepwise process regulated by a web of signalling pathways that are context specific. In the adult, MMT is associated with repair, and if disrupted, gives rise to fibrosis and cancer. Understanding the underlying mechanisms is key to uncovering therapeutic targets.

Over the course of this study, we demonstrated that with repeated passaging the mesothelial cells lost some epithelial features, but failed to differentiate into fully myofibroblastic cells. We associated these alterations with progression through the MMT process and aimed to determine if these changes were regulated in cultured mesothelial cells through the paracrine effects of the known MMT mediators, EGF,

and TGF-β signalling. The mesothelial sheets that surrounded the omentum explants showed characteristics indicative of MMT, through the increased expression of αSMA and decreased the presence of ZO1 epithelial cell clusters following stimulation with 50 ng/ml of either EGF or TGF-β for 48 h. The contrary was seen in the cultures treated with the small molecule TβRI inhibitor and to a lesser extent with the EGFR tyrosine kinase inhibitor.

Interestingly, stimulation of passaged mesothelial cells with either of these factors for the same length of time did not alter the expression of ZO1/ αSMA at protein or mRNA levels compared to the low serum group (mRNA data not shown); this was consistent with the migration studies. Although we did observe a slight reduction in ZO1 localization at cell contacts by IF. Yet, to some extent, we could reverse MMT in the passaged cells by inhibiting receptor mediated signalling , which resulted in attenuated mesothelial cell migration in a dose-dependent manner, and increased ZO1 expression at cell-cell contacts. These results suggested that EGF and TGF-β also regulate MMT in the passaged cells, but it may be possible that the mesothelial cells required longer periods of stimulation for full MMT progression and myofibroblast differentiation.

TGF-β is a known inducer of MMT. Nasreen and colleagues demonstrated myofibroblastic conversion of pleural mesothelial cells following 96 h exposure to TGF-β and increased haptotactic migration to a concentration gradient of TGF-β exposure (Nasreen et al., 2009). However, a number of other studies have determined that TGF-β by itself is not enough to elicit full MMT *in vitro* (Yáñez-Mó et al., 2003, Strippoli et al., 2008, Strippoli et al., 2012). Co-stimulation of omentum-

derived mesothelial cells with TGF-β and IL-β for 48 h was shown to mediate robust myofibroblast conversion, compared to TGF-β only (Yáñez-Mó et al., 2003, Strippoli et al., 2008, Strippoli et al., 2012).

Instead of stimulating with a defined subset of growth factors and cytokines, other studies have instead resorted to supplementing the mesothelial cell full growth medium that contained 5-10% FCS with the stimulant of interest (TGF-β or EGF), to induce MMT (Kawaguchi et al., 2007, Lachaud et al., 2014, Lachaud et al., 2013, Li et al., 2013b).

Similar to the behavioural characteristics of omentum-derived mesothelial cells following culturing, adult liver derived mesothelial cells have been reported to undergo MMT differentiation by losing basolateral polarity and *Krt8* mRNA expression upon culturing and passaging (Li et al., 2013b). Through qPCR, the cells were shown to express both TGF-β and increasing amounts of EGFR with culturing, the authors stimulated these cells for 4 d in either of these factors in 10% FCS containing medium to determine their impact on the MMT state (Li et al., 2013b). Their results revealed that TGF-β was more potent than EGF in mediating myofibroblastic conversion in culture, through the increased expression of *Vim, αSMA* and *collagen 1* and decreased *ZO1* genes (Li et al., 2013b). The use of the small molecule inhibitor specific for TβRI (SB431542) reversed these changes (Li et al., 2013b). These findings were consistent with their *in vivo* work where the conditional deletion of TβRII in mesothelial cells decreased MMT transdifferentiation in CCL_4 liver injury model (Li et al., 2016).

The stimulation of omentum explants with EGF has been previously documented. Kawaguchi and colleagues reported that the integrity of the epithelial-like mesothelial sheet was maintained in serum-free medium following 5 d of culture; but lost in 10% FCS-containing medium (Kawaguchi et al., 2007). Stimulation in serum-free medium supplemented with 40 ng/ml of EGF was not enough to promote significant myofibroblastic conversion (Kawaguchi et al., 2007). Moreover, Lachaud and colleagues demonstrated the full MMT spectrum and complete transdifferentiation into vascular smooth muscle cells in both mouse uterine and adipose tissue derived mesothelial cells, over the course of 15 d stimulation (Lachaud et al., 2013, Lachaud et al., 2014). The authors reported that the full MMT process was only achieved in high glucose medium containing 20-50 ng/ml EGF, 10% FCS medium and 1 ng/ml hydrocortisone (Lachaud et al., 2013, Lachaud et al., 2014).

Overall, TGF-β and EGF are modulators of myofibroblastic differentiation of mesothelial cells in culture. However, for complete MMT progression *in vitro,* there must be a synergistic convergence of multiple ligands which in the majority of cases remain unidentified in the serum used as a supplement (Chen and Chen, 2012). Therefore, the alterations in the epithelial and mesothelial characteristics seen in our own system are likely due to the presence of serum. We had previously attempted to subculture both the omentum explants and the passaged cells in low serum (1% FCS) growth medium, however, both the explant cells and the passaged cells could not be sustained for longer than 6 d. Furthermore, substituting 1% FCS with Advanced™ medium slowed the growth characteristics of the passaged cells, whereby they needed >6 d to reach confluence. This finding suggested that serum contains some factors that are key for the survival of mesothelial cells in culture.

5.8.2 The role of ERK5 in MMT

The MMT process can be promoted through Smad and Smad-independent signalling cascades in mesothelial cells. Several groups have published the involvement of Smad2/3, ILK/ERK1/2 P38 MAPK, Akt/PI3K, JNK signalling in MMT after stimulation with TGF-β and EGF (Jin et al., 2016, Lachaud et al., 2014, Li et al., 2016, Li et al., 2013b, Strippoli et al., 2010, Strippoli et al., 2015).

In this chapter, we aimed to better characterize the intracellular signalling cascades involved in MMT modulation following EGF and TGF-β stimulation. Treatment of passaged mesothelial cells with either TGF-β or EGF for 48 h elevated the expression of the phosphorylated forms of ERK1/2 and ERK5 and the total levels of these proteins. Moreover, targeting TGF-β and EGF signalling with small molecule inhibitors showed the opposite effect. While we could not detect changes in overall ERK1/2 phosphorylation, we could observe a decline in the relative phosphorylation of ERK5 following treatment with TβRi (LY364947), EGFRi (PD153035) and ERK5i (XMD8-92). Furthermore, inhibition of MEK5/ERK5 in the passaged cells also attenuated relative mesothelial migration in the scratch assay and increased ZO1 accumulation at cell contacts. This suggests that TGF-β and EGF signalling regulates migration and ZO1 localization through ERK5.

TGF-β and EGF have been reported to mediate the loss of epithelial phenotype and gain in migratory capacity through ERK5; *in vitro* and *in vivo*. Indirect inhibition of ERK5 via the MEKi (BIX02189) in lung epithelial cells and fibroblasts perturbed TGF-β induced ECM production and Smad3 acetylation *in vitro* and impeded bleomycin-induced lung fibrosis in vivo (Kim et al., 2013). TGF-β also stimulated the

phosphorylation of ERK5 in podocytes, increasing the expression of P-cadherin and αSMA, while simultaneously reducing barrier function (Badshah et al., 2014). Not only did BIX02189 reverse these changes, it also attenuated the wound closure rate (Badshah et al., 2014).

EGF is an established activator of ERK5 (Arnoux et al., 2008). Human keratinocytes treated with EGF showed increased phosphorylated ERK5 that coincided with increased levels of *Snail2* mRNA. Stable knockdown of ERK5 using shRNA decreased motility, and *Snail2* mRNA expression in HaCaTs and keratinocytes (Arnoux et al., 2008). Furthermore, the loss of ERK5 resulted in disrupted desmosome organisation along with a gain in a compact epithelial-like morphology (Arnoux et al., 2008).

Although the data presented in this chapter is preliminary, the work suggests that ERK5 plays a role in regulating ZO1 organisation and motility of mesothelial cells, which has not been previously reported.

5.8.3 The role of Zeb1/2 in MMT

The Zeb family of transcription factors are essential players in the modulation of myofibroblastic differentiation in a number of epithelial cells. In our *ex vivo* kidney rudiment, the GFP-labelled mesothelial cells had significantly elevated *Zeb1* mRNA expression following the 7 d co-culture period. However, both Snail2 and Zeb1/2 as modulators of myofibroblast conversion in mesothelial cells are not widely characterised. In this chapter, we showed for the first time that the transient knockdown of Zeb1/2 attenuated mesothelial cell migration for longer periods of time in comparison to Snail2 knockdown. Furthermore, treatment with siZeb1/2

increased ZO1 accretion at cell contacts, implying that Zeb proteins also play a role in MMT progression.

Previously, it has been shown that the complete reversal of the TGF-β induced EMT programme in mouse mammary gland cells required the inhibition of both TβRI (SB431542) and RhoA Kinases (Y27632). In turn, this inhibition blocked Zeb1/2 induced mesenchymal gene expression and stabilized epithelial structures, respectively (Das et al., 2009). Furthermore, shRNA-mediated knockdown of Zeb1/2 in TGF-β stimulated cells restored Cdh1 expression, even though inhibition by ROCK was required to stabilize cortical actin (Das et al., 2009).

Furthermore, in response to treatment with TGF-β, Zeb1 was upregulated and was able to promote EMT in MDCK cells by downregulating the expression of its antagonizing miRNA, miR-200, while the removal of TGF-β stimulation restored the epithelial state (Gregory et al., 2011). Therefore suggesting, that these factors regulate each other in a negative feedback loop that ultimately acts as a molecular switch to modulate the existence of the E, M and E/M states (Fukuda et al., 2016, Gregory et al., 2011).

However, a number of reports have indicated the existence of a further layer of control for Zeb function via a Snail/miR-34 loop (Fig 5.17) (Jolly et al., 2015a, Zhang et al., 2014). In these computational modules it was suggested that the Snail/miR-34 switch acts as a buffer, preventing the activation of EMT from transient signals but itself not inducing complete EMT (Jolly et al., 2015a). This, in turn, regulates the Zeb/miR-200 loop that is associated with the existence of the 3 EMT states (Jolly et al., 2015a). In other words, the Snail loop instigates Cdh1 repression while Zeb is

needed for its complete inhibition (Jolly et al., 2015a, Zhang et al., 2014). This is further supported by work, which described that a complete EMT reversal was achieved only when both the EMT-inducing signal and Zeb are suppressed (Das et al., 2009, Zhang et al., 2014).

Overall, the data suggests that Zeb transcription factors play an integral role in mesothelial MMT plasticity; however, its exact role in maintaining the intermediate MMT state requires further investigation.

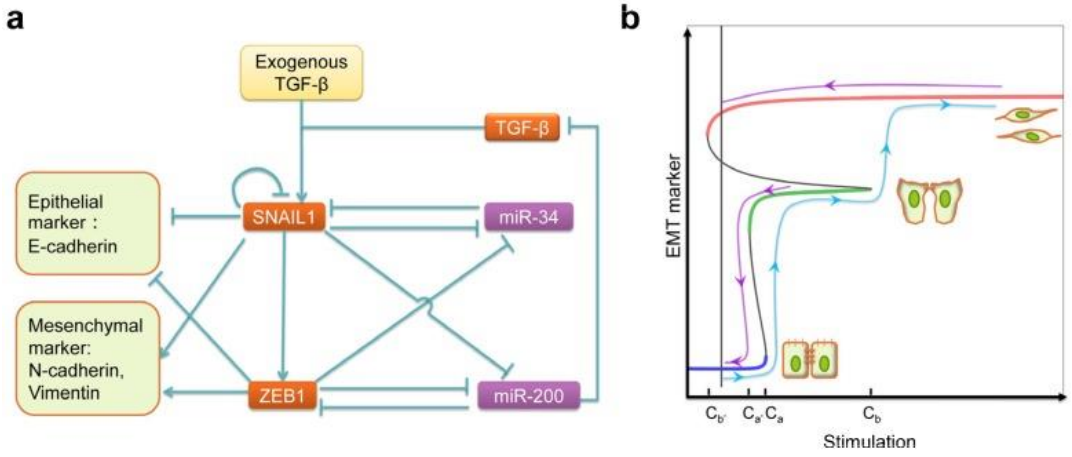

Figure 5.17 Computational models showing the bistable dynamics of TGF-β induced EMT. [A] The Snail1-miR-34 loop is postulated to regulate Zeb function in EMT. The arrows signify activation, and blunted lines denote inhibition. [B] Computational dose-response EMT curves show the different response of cells starting with different EMT phenotypes that are treated with increasing (blue line) and decreasing (purple line) concentrations of exogenous TGF-β. Overall the figures illustrate bistable dynamics of EMT that have also been confirmed in MCF10A cells. Adapted from (Jolly et al., 2015a, Zhang et al., 2014).

5.9 Chapter conclusions

In this chapter, we attempted to address on multiple levels the regulatory mechanisms that control the altered morphology we have observed in cultured mesothelial cells over passages. Our results indicate that paracrine TGF-β and EGF signalling , through MEK5/ERK5 signalling , had a role in regulating mesothelial cell migration and ZO1 distribution Not only so, but we also demonstrated a role of Zeb1/2 in MMT. However, in our experimental models, we were unable to manipulate the signalling pathways such that a fully induced MMT or complete reversal could be achieved. We postulate that for full MMT transdifferentiation to occur, the mesothelial cells should be exposed to a more sustained signal from multiple growth factors/ cytokines that act in a synergy to mediate myofibroblastic conversion. Whereas silencing the autocrine/ paracrine signalling cues and Zeb mediate transcriptional regulation should induce the cells to transition back into a more epithelial phenotype. This chapter certainly set up the basis for more experimental work into uncovering the regulatory networks involved in inducing and maintaining the intermediate state of mesothelial cells in the MMT process.

Chapter 6: General discussion and future directions

6.0 Final discussion

Regenerative medicine therapies aim to revolutionize the therapeutic approaches for the alleviation of diseases that result from failing organs, by replacing the damaged or aged cells with healthy functioning ones (Liu et al., 2016, Herrick and Mutsaers, 2007). Currently, adult stem cells show the greatest promise as a primary source of cells for regenerative applications as they do not carry the risk of teratoma formation, they are free from ethical concerns and confer low immunogenicity (Liu et al., 2016).

Mesothelial cells carry regenerative capacity through their ability to be recruited into the wounded area, transdifferentiate and secrete of a plethora of signalling molecules that mediate inflammation, fibrosis and angiogenesis (Kanda et al., 2014, Kitamura et al., 2014, Mutsaers et al., 2015). Together with the availability of a number of practical autologous sources, mesothelial cells are ideal candidates for the regeneration and preservation of the mesothelium. Current promising strategies for the alleviation of fibrosis and adhesions are carried out through direct mesothelial cell transplantation or cell sheet engineering (Bertram et al., 1999, Kanda et al., 2014, Kitamura et al., 2014, Lachaud et al., 2015). This treatment option requires the transplantation of a large cell volume and sometimes, multiple rounds are required for an effective therapeutic outcome (Kanai et al., 2014). As a result, the harvested mesothelial cells have to be expanded for prolonged periods of time, of which the effects are ill-defined. Mesothelial cell morphology is also a limiting factor associated with autologous transplantation since the transplantation of more fibroblast-like mesothelial cells was shown not alleviate peritoneal adhesions or thickening (Kitamura et al., 2014). Therefore, we aimed to address the effects of long-term culture on mesothelial cell characteristics, MMT status, and progenitor properties.

In this thesis, we established mesothelial cell cultures derived from the adult murine omentum for over 30 passages and showed relatively stable PDTs. However, repeated passaging caused the mesothelial cells to downregulate some epithelial features (table 6.1). The cultured mesothelial cells displayed progenitor characteristics through the expression of stem cell markers, their clonogenicity and differentiation capacity, however, the latter was confined to cells up to P5-P13. Using a chimeric kidney rudiment assay, we demonstrated that the presence of mesothelial cells allowed embryonic structures to form. Finally, we showed that mesothelial cell migration, a facet of the MMT process, was regulated through via MEK5/ERK5 through EGF and TGF-β signalling.

Table 6.1: A summary of the changes in genes expression and protein localization seen with repeated passaging. In this thesis we showed alterations in the expression of a number of mesothelial and epithelial markers, suggested that the mesothelial cells resided in the intermediate phase of the MMT spectrum.

		Expression	Expression	Distribution	Expression	Distribution
	Genes	**OMT**	**OMC**		**Passaged Cells**	
Mesothelial	*Msln*	+++	+	Poor/ non-specific	++	Membranous
	Wt1	+++	+++	Nuclear	+/-	Nuclear
Epithelial	*Cdh1*	+	+	--	+/-	--
	Krt8	++	+	Diffuse cytoplasmic staining	+/-	Perinuclear
	ZO1	+	+	Strong bands at cell contacts	+/-	Disrupted at cell membranes and nuclear accumulation
Mesenchymal	*αSMA*	+	+++	Prominent stress fibres	+++	Prominent stress fibres. Difference between intra-mesothelial populations
	Vim	+++	+++	Diffuse cytoplasmic staining	+++	Diffuse cytoplasmic staining

6.1 Mesothelial cell morphology and phenotype are dependent on length of culture

The use of simple epithelial-like mesothelial sheets seems a promising therapeutic avenue for the alleviation and treatment of debilitating adhesions and fibrosis induced by surgery and peritoneal dialysis respectively (Kawanishi et al., 2013, Kanai et al., 2014, Inagaki et al., 2015). The techniques can be categorized into (i) harvestable cell sheets generated on thermoresponsive cell culture dishes that in response to lower culture temperatures, forces the release of intact cell monolayers along with underlying ECM for cell sheet engineering purposes. (ii) Classical static cell-seeding approaches (Lachaud et al., 2015). In rodent models, these techniques often require the use of a large volume of cells over a small area (~$5x10^5$ cell/ cm^2) (Inagaki et al., 2015, Asano et al., 2005). Previous reports describing the establishment of mesothelial cell cultures from rodent and human sources reported morphological changes associated with senescence by passage 6 (Yung and Chan, 2007, Zhou and Yu, 2016). Contrary to these reports, in this study, we showed that the isolated mesothelial cells from murine omentum could be propagated long term, with PDTs ranging between 20 – 40 h. Therefore our method for isolating autologous mesothelial cells offers an option for the long-term culture of cells, which is a prerequisite for the expansion of the appropriate cell number for transplantation.

6.2 Mesothelial plasticity is affected by passage

It remains unclear whether the 'perfect' epithelial cobblestone phenotype is associated with plasticity and if it is necessary for the repair and regeneration of the serosa. Therefore, we next attempted to address the effects of time in culture on mesothelial plasticity. We could report clonogenic potential in P5 cells (although older P25 were not examined), a reduction in the expression of a number stem cell

genes in the passaged cells (P5-P25) compared to the OMC, and the ability to differentiate along the adipocyte and osteoblast lineages up to P5 and P13, respectively. The capacity of mesothelial cells and indeed the mesothelium to differentiate along the mesodermal lineages and to contribute to the repair of damaged tissue has been previously documented (Chau and Hastie, 2012, Lachaud et al., 2014, Lachaud et al., 2013, Lansley et al., 2011, van Tuyn et al., 2007). In light of this, we exposed the mesothelial cells to a developing chimeric kidney organoid system. While we struggled to effectively trace the lower passage cells, we could report that in higher passage cells, the mesothelial cells maintained the ability to undergo MMT in response to the nephrogenic challenge and key embryonic structures could develop in the presence of the GFP-labelled cells. This suggested that the grafting of the higher passage cells indeed does not exhibit damaging effects on neighbouring cells.

6.3 TGF-β and EGF signalling, potential targets for reversing passage induced changes

Within our culturing system, we observed changes that correlated with the progression of the mesothelial cells through the MMT programme. We wondered if these changes were mediated by paracrine mechanisms based on the presence of certain growth factors in the culture medium. Our initial qPCR analysis showed upregulation in *EGFR* expression with culture, a known mediator of MMT (Lachaud et al., 2014, Wang et al., 2015). Furthermore, we also decided to study TGF-β related signalling, as it is a well-established master molecule of MMT (Zolak et al., 2013, Karki et al., 2014, Strippoli et al., 2015). By targeting the both the EGF and TGF-β signalling pathways at the level of the tyrosine kinases, we noted attenuated migration

capacity and improved ZO1 distribution at the cell-cell contacts in a dose-dependent fashion. However, it remains to be clarified if sustained use of the pharmacological inhibitors to preserve the epithelial characteristics in higher passage cells would indeed result in maintenance of the associated plasticity seen in the lower passage cells. Studies that characterised the effects associated with age/ passage on MSC potency, demonstrated that the differentiation capacity of MSCs and haematopoietic stem cells was dependent on the accumulation of DNA damage (Alves et al., 2010, Chambers et al., 2007, Elkhenany et al., 2016, Kretlow et al., 2008). Which suggests that MMT transdifferentiation and differentiation along adipocyte and osteoblast lineages may be regulated and affected by different mechanisms.

6.4 Future directions

In this thesis, we attempted to address the effects of long-term culture on the characteristics of mesothelial cells, specifically their stem/progenitor status and transdifferentiation potential. We could show that the omentum explant-derived cells could be sustained in culture long term, yet a prominent and not addressed observation was the reduced *Wt1* mRNA expression seen in the passaged cells.

Wt1 is a multifunctional zinc finger transcription factor that has been reported to regulate apoptosis, proliferation, differentiation and mRNA processing (table 6.2) (Shandilya and Roberts, 2015). These distinct functions are thought to be brought about by the various Wt1 isoforms (Shandilya and Roberts, 2015). Of the 36 identified isoforms, 4 are abundantly expressed and arise from two independent splicing events at the exon 5 with 17 amino acids and the KTS site found between exons 9 and 10 (Shandilya and Roberts, 2015, Kramarzova et al., 2012).

Table 6.2: A summary of the functions that the various Wt1 isoforms have been shown mediate in adult cells.

Wt1 variants	Splicing events	Function
Wt1A	Exon 5- / KTS-	• Increases tumour size, dissemination, VEGF expression and decreases survival rates in a mouse ovarian cancer model (Yamanouchi et al., 2014). • Promotes ovarian cancer cell migration and invasion, *in vitro* (Jomgeow et al., 2006). • In mammary epithelial cells it acts as a tumour suppressor by regulating p21 expression (Burwell et al., 2006).
Wt1B	Exon 5+ / KTS-	• Induced apoptosis through the transcriptional repression of the EGFR in osteosarcoma cells (Haber et al., 1996)
Wt1C	Exon 5- / KTS +	• Inhibits apoptosis induced by anticancer antibiotic by promoting homologous recombination mediated DNA repair (Oji et al., 2015).
Wt1D	Exon 5+ / KTS -	• Induces EMT in mammary epithelial cells (Burwell et al., 2006).

In our preliminary data, we could also see a passage dependent loss of expression in the various *Wt1* isoforms (Fig. S1). In an attempt to address the role of the different *Wt1* isoforms had in maintaining the epithelial cell state, we transfected the cells with linearized GFP containing plasmids for the 4 main isoforms and initiated selection for stable transfection with blasticidin (Fig. S2). Unfortunately, we were unable to establish the mesothelial Wt1 expressing lines, due to the transfection protocol needing further optimisation. Addressing the function of these isoforms during the MMT process in mesothelial cells could further our understanding of the role Wt1 has on the physiology of mesothelial cells.

Another observation made was the dependence of mesothelial cell potency on passage. However, in the chimeric kidney rudiment, we could not assert if lower passage cells could contribute to nephrogenesis. Since the original transfections

were performed in our lab, a new more efficient technique has been established that results in >90% GFP+ expression within 1 sorting event. This technique would mean the lower passage mesothelial cells labelled with GFP could be co-cultured in these re-aggregated rudiments, and analysed for their potential to transdifferentiate into kidney cells

It also remains to be established if the passaged mesothelial cells in this study that showed reduced epithelial features could contribute to the regeneration of the damaged peritoneum, *in vivo.* One way to address this question would be through the use of cell sheet engineering

One way of addressing this could be to culture the passaged mesothelial cells in the presence or absence of EGFR and TβRI inhibitors in order to induce their epithelial state, although the length of culture prior to coating on matrices would still require further optimising.

6.5 Conclusion

The use of mesothelial cells in regenerative medicine applications is expanding rapidly. However, there still exists a number of unsolved issues that require addressing for such therapies to reach the clinic. In our hands, it appears that mesothelial cells that are expanded for shorter lengths of time are potentially a more useful source of cells for regenerative applications. Although, the effects of long-term culture on human omentum-derived mesothelial cells still needs to be addressed. Specifically, the molecular mechanisms that mediate these culture-induced changes, which could be targeted for pharmacological intervention to reverse, correct, or prevent these changes.

Supplements

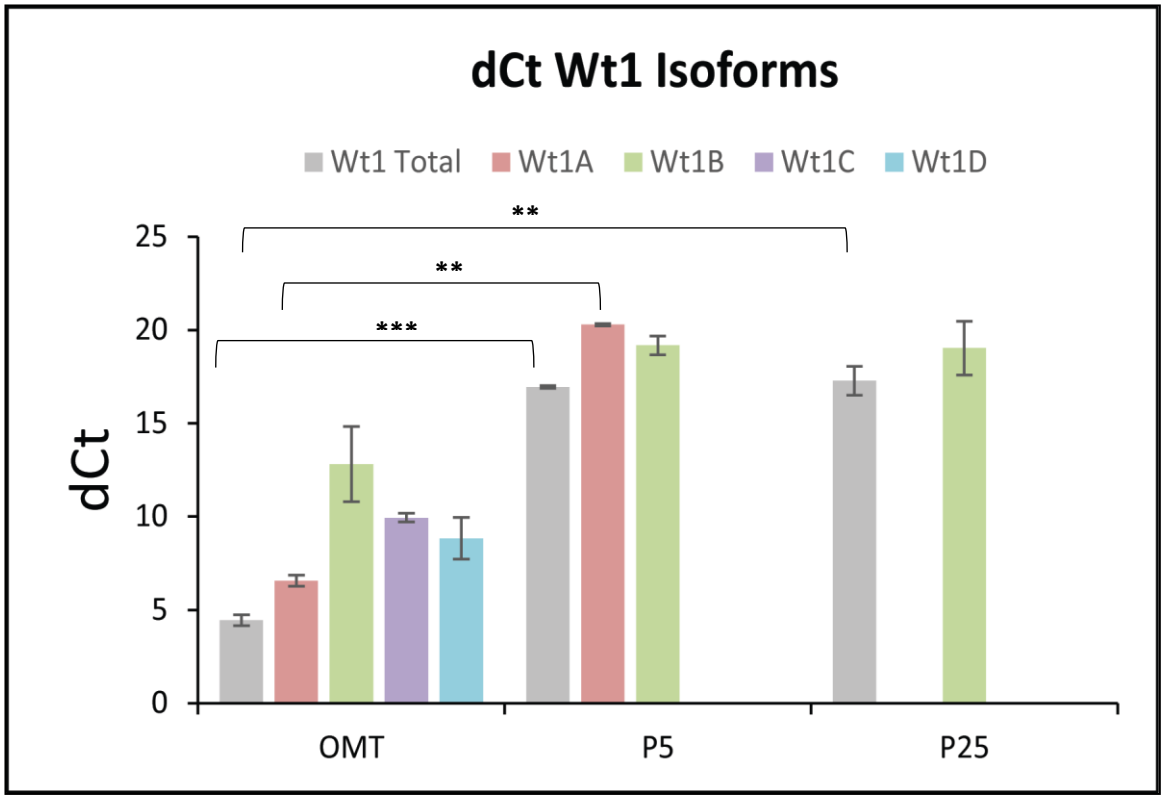

Figure S1: Repeated passaging results in the loss of Wt1 isoforms. OMT and P5 and P25 mesothelial cells RNA was harvested and reverse transcribed for qPCR analysis of *Wt1* isoform expression. With prolonged culturing, the mesothelial cells show reduced overall *Wt1* expression relative to the OMT (P=0.0006, P5, and P=0.0042, P25). *Wt1A* was >1X10^4 fold downregulated at P5 (P=0.0013) and was not detectable at P25. Isoforms *Wt1C* and *Wt1D* were not detectable by qPCR in the P5 and P25 samples. Meanwhile, there was not change in relative expression of *Wt1B* between the passaged cells and the OMT. Samples were normalised to *Gapdh* and *β-actin* housekeeping genes. Data shown is averages from 2 biologically independent samples.

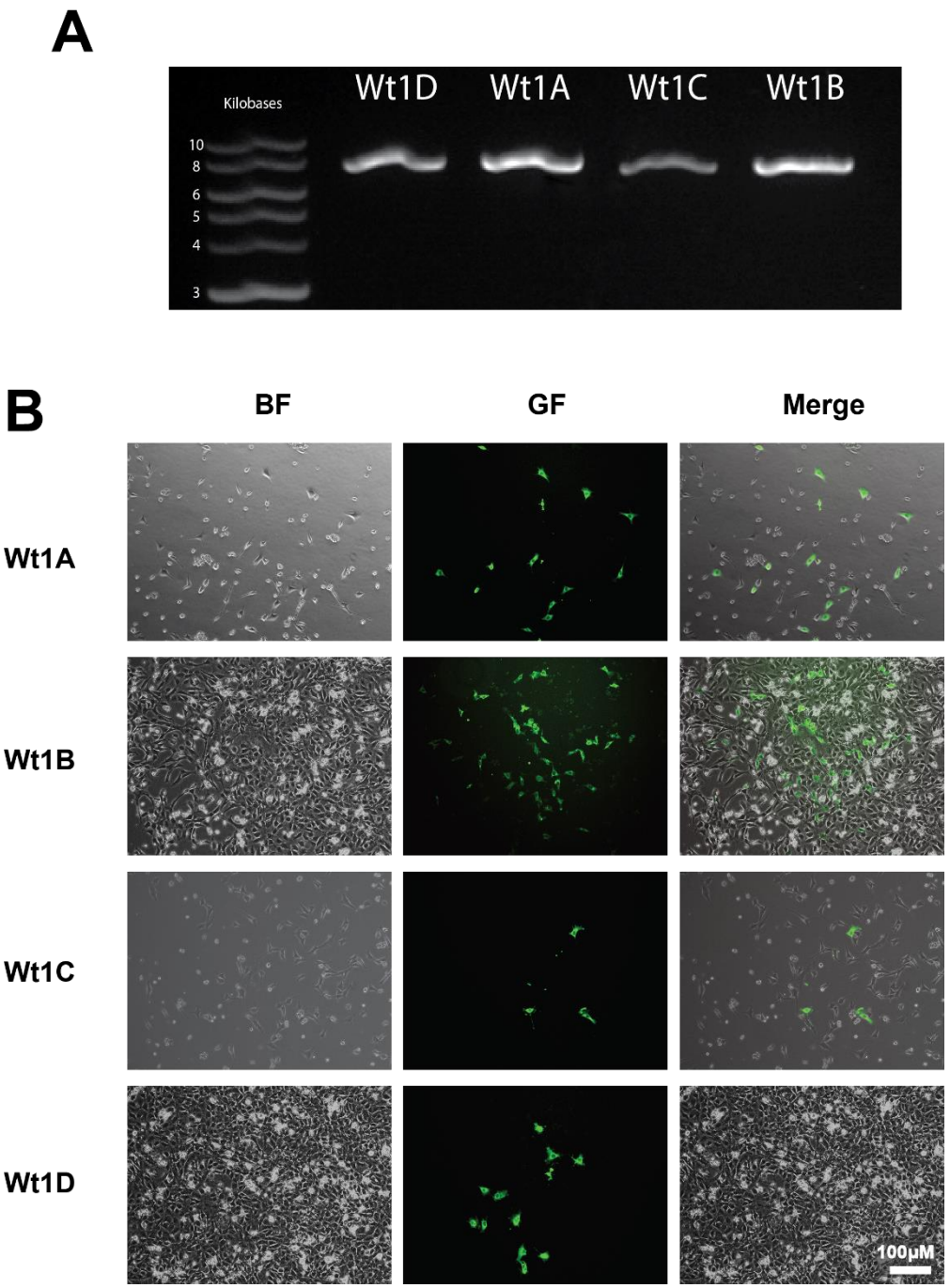

Figure S2: Mesothelial cell transfection with Wt1 isoform plasmids. Wt1 plasmids for the various isoforms were kindly gifted by Dr. Peter Hohenstein. [A] The plasmids were linearized AhdI restriction enzyme. [B] Passage 10 mesothelial cells were seeded $8x10^4$ cells/ well in a 12 well dish and left to attach overnight. The mesothelial cells were transfected with 2 µg of DNA per well for 6 h in OptiMEM medium containing 2 µl of lipofectamine 2000. The cells were left to recover overnight before being split 1:10. Once the cells had attached selection was initiated by culturing the transfected cells in growth medium containing 2 µg/ml blasticidin. Images were taken 1-week post transfection.

Bibliography

ABELARDO AGUILERA, J. L., GUADALUPE GÓNZALEZ-MATEO, RAFAEL SELGAS AND MANUEL LÓPEZ-CABRERA 2013. The Mesothelial to Mesenchymal Transition a Pathogenic and Therapeutic Key for Peritoneal Membrane Failure, The Latest in Peritoneal Dialysis, . *InTech*.

AKIRA ONISHI, Y. M., SHIGEAKI MUTO AND EIJI KUSANO 2011. The Mechanism of Peritoneal Fibrosis in Peritoneal Dialysis. *Journal of Nephrology and Theraputics* S3-002.

ALVES, H., MUNOZ-NAJAR, U., DE WIT, J., RENARD, A. J. S., HOEIJMAKERS, J. H. J., SEDIVY, J. M., VAN BLITTERSWIJK, C. & DE BOER, J. 2010. A link between the accumulation of DNA damage and loss of multi-potency of human mesenchymal stromal cells. *Journal of Cellular and Molecular Medicine,* 14**,** 2729-2738.

AMANO, S., CHANG, Y. T. & FUKUI, Y. 2015. ERK5 activation is essential for osteoclast differentiation. *PLoS One,* 10**,** e0125054.

ARNOUX, V., NASSOUR, M., L'HELGOUALC'H, A., HIPSKIND, R. A. & SAVAGNER, P. 2008. Erk5 Controls Slug Expression and Keratinocyte Activation during Wound Healing. *Molecular Biology of the Cell,* 19**,** 4738-4749.

ASAHINA, K., ZHOU, B., PU, W. T. & TSUKAMOTO, H. 2011. Septum transversum-derived mesothelium gives rise to hepatic stellate cells and perivascular mesenchymal cells in developing mouse liver. *Hepatology,* 53**,** 983-95.

ASANO, T., TAKAZAWA, R., YAMATO, M., KAGEYAMA, Y., KIHARA, K. & OKANO, T. 2005. Novel and simple method for isolating autologous mesothelial cells from the tunica vaginalis. *BJU International,* 96**,** 1409-1413.

BADSHAH, I. I., BAINES, D. L. & DOCKRELL, M. E. 2014. Erk5 Mediates TGFβ1-induced Loss of Phenotype and Function in Human Podocytes. *Frontiers in Pharmacology,* 5.

BATCHELDER, C. A., MARTINEZ, M. L. & TARANTAL, A. F. 2015. Natural Scaffolds for Renal Differentiation of Human Embryonic Stem Cells for Kidney Tissue Engineering. *PLoS ONE,* 10**,** e0143849.

BATRA, H. & ANTONY, V. B. 2015. Pleural mesothelial cells in pleural and lung diseases. *Journal of Thoracic Disease,* 7**,** 964-980.

BEIL, M., MICOULET, A., VON WICHERT, G., PASCHKE, S., WALTHER, P., OMARY, M. B., VAN VELDHOVEN, P. P., GERN, U., WOLFF-HIEBER, E., EGGERMANN, J., WALTENBERGER, J., ADLER, G., SPATZ, J. & SEUFFERLEIN, T. 2003. Sphingosylphosphorylcholine regulates keratin network architecture and visco-elastic properties of human cancer cells. *Nat Cell Biol,* 5**,** 803-811.

BENEZRA, M., GREENBERG, R. S. & MASUR, S. K. 2007. Localization of ZO-1 in the nucleolus of corneal fibroblasts. *Invest Ophthalmol Vis Sci,* 48**,** 2043-9.

BERTRAM, P., TIETZE, L., HOOPMANN, M., TREUTNER, K. H., MITTERMAYER, C. & SCHUMPELICK, V. 1999. Intraperitoneal transplantation of isologous mesothelial cells for prevention of adhesions. *Eur J Surg,* 165**,** 705-9.

BROWNE, J. A., PEARSON, A. L., ZAHR, R. A., NICULESCU-DUVAZ, I., BAINES, D. L. & DOCKRELL, M. E. 2008. TGF-beta activates ERK5 in human renal epithelial cells. *Biochem Biophys Res Commun,* 373**,** 440-4.

BURWELL, E. A., MCCARTY, G. P., SIMPSON, L. A., THOMPSON, K. A. & LOEB, D. M. 2006. Isoforms of Wilms/' tumor suppressor gene (WT1) have distinct effects on mammary epithelial cells. *Oncogene,* 26**,** 3423-3430.

BUSCH, T., ARMACKI, M., EISELER, T., JOODI, G., TEMME, C., JANSEN, J., VON WICHERT, G., OMARY, M. B., SPATZ, J. & SEUFFERLEIN, T. 2012. Keratin 8 phosphorylation regulates keratin reorganization and migration of epithelial tumor cells. *J Cell Sci,* 125**,** 2148-59.

CARVER, E. A., JIANG, R., LAN, Y., ORAM, K. F. & GRIDLEY, T. 2001. The mouse snail gene encodes a key regulator of the epithelial-mesenchymal transition. *Mol Cell Biol,* 21**,** 8184-8.

CASAS, E., KIM, J., BENDESKY, A., OHNO-MACHADO, L., WOLFE, C. J. & YANG, J. 2011. Snail2 is an essential mediator of Twist1-induced epithelial mesenchymal transition and metastasis. *Cancer Res,* 71**,** 245-54.

CHAMBERS, S. M., SHAW, C. A., GATZA, C., FISK, C. J., DONEHOWER, L. A. & GOODELL, M. A. 2007. Aging Hematopoietic Stem Cells Decline in Function and Exhibit Epigenetic Dysregulation. *PLoS Biology,* 5**,** e201.

CHAU, Y. Y., BANDIERA, R., SERRELS, A., MARTINEZ-ESTRADA, O. M., QING, W., LEE, M., SLIGHT, J., THORNBURN, A., BERRY, R., MCHAFFIE, S., STIMSON, R. H., WALKER, B. R., CHAPULI, R. M., SCHEDL, A. & HASTIE, N. 2014. Visceral and subcutaneous fat have different origins and evidence supports a mesothelial source. *Nat Cell Biol,* 16**,** 367-75.

CHAU, Y. Y. & HASTIE, N. D. 2012. The role of Wt1 in regulating mesenchyme in cancer, development, and tissue homeostasis. *Trends Genet,* 28**,** 515-24.

CHEN, K. S. & CHEN, W. S. 2012. Experience in primary culture of human peritoneal mesothelial cell. *Chin J Physiol,* 55**,** 274-83.

CHEN, R., YANG, Q. & LEE, J. D. 2012. BMK1 kinase suppresses epithelial-mesenchymal transition through the Akt/GSK3beta signaling pathway. *Cancer Res,* 72**,** 1579-87.

CHEN, Y. T., CHANG, Y. T., PAN, S. Y., CHOU, Y. H., CHANG, F. C., YEH, P. Y., LIU, Y. H., CHIANG, W. C., CHEN, Y. M., WU, K. D., TSAI, T. J., DUFFIELD, J. S. & LIN, S. L. 2014. Lineage tracing reveals distinctive fates for mesothelial cells and submesothelial fibroblasts during peritoneal injury. *J Am Soc Nephrol,* 25**,** 2847-58.

CHO, Y., HAWLEY, C. M. & JOHNSON, D. W. 2014. Clinical Causes of Inflammation in Peritoneal Dialysis Patients. *International Journal of Nephrology,* 2014**,** 9.

CHRISTIANSON, H. C., SVENSSON, K. J., VAN KUPPEVELT, T. H., LI, J.-P. & BELTING, M. 2013. Cancer cell exosomes depend on cell-surface heparan sulfate proteoglycans for their internalization and functional activity. *Proceedings of the National Academy of Sciences of the United States of America,* 110**,** 17380-17385.

CRONAUER, M. V., STADLMANN, S., KLOCKER, H., ABENDSTEIN, B., EDER, I. E., ROGATSCH, H., ZEIMET, A. G., MARTH, C. & OFFNER, F. A. 1999. Basic fibroblast growth factor synthesis by human peritoneal mesothelial cells: induction by interleukin-1. *Am J Pathol,* 155**,** 1977-84.

DA SILVA MEIRELLES, L., CHAGASTELLES, P. C. & NARDI, N. B. 2006. Mesenchymal stem cells reside in virtually all post-natal organs and tissues. *J Cell Sci,* 119**,** 2204-13.

DAS, S., BECKER, B. N., HOFFMANN, F. M. & MERTZ, J. E. 2009. Complete reversal of epithelial to mesenchymal transition requires inhibition of both ZEB expression and the Rho pathway. *BMC Cell Biology,* 10**,** 1-18.

DAVIES, J. A. 2015. Self-organized Kidney Rudiments: Prospects for Better in vitro Nephrotoxicity Assays. *Biomarker Insights,* 10**,** 117-123.

DE LIMA, S. M., OTONI, A., SABINO ADE, P., DUSSE, L. M., GOMES, K. B., PINTO, S. W., MARINHO, M. A. & RIOS, D. R. 2013. Inflammation, neoangiogenesis and fibrosis in peritoneal dialysis. *Clin Chim Acta,* 421**,** 46-50.

DECOLOGNE, N., KOLB, M., MARGETTS, P. J., MENETRIER, F., ARTUR, Y., GARRIDO, C., GAULDIE, J., CAMUS, P. & BONNIAUD, P. 2007. TGF-beta1 induces progressive pleural scarring and subpleural fibrosis. *J Immunol,* 179**,** 6043-51.

DERYNCK, R., MUTHUSAMY, B. P. & SAETEURN, K. Y. 2014. Signaling pathway cooperation in TGF-β-induced epithelial-mesenchymal transition. *Current opinion in cell biology,* 31**,** 56-66.

DONG, R., JIN, Y. & LIU, Y. 2003. [Selection and identification of human keratinocyte stem cells in vitro]. *Zhongguo Xiu Fu Chong Jian Wai Ke Za Zhi,* 17**,** 351-4.

DORADO, F., VELASCO, S., ESPARIS-OGANDO, A., PERICACHO, M., PANDIELLA, A., SILVA, J., LOPEZ-NOVOA, J. M. & RODRIGUEZ-BARBERO, A. 2008. The mitogen-activated protein kinase Erk5 mediates human mesangial cell activation. *Nephrol Dial Transplant,* 23**,** 3403-11.

DOUVDEVANI, A., RAPOPORT, J., KONFORTY, A., ARGOV, S., OVNAT, A. & CHAIMOVITZ, C. 1994. Human peritoneal mesothelial cells synthesize IL-1 alpha and beta. *Kidney Int,* 46**,** 993-1001.

DREW, B. A., BUROW, M. E. & BECKMAN, B. S. 2012. MEK5/ERK5 pathway: the first fifteen years. *Biochim Biophys Acta,* 1825**,** 37-48.

DUAN, W.-J., YU, X., HUANG, X.-R., YU, J.-W. & LAN, H. Y. 2014. Opposing Roles for Smad2 and Smad3 in Peritoneal Fibrosis in Vivo and in Vitro. *The American Journal of Pathology,* 184**,** 2275-2284.

EIGENBROD, T., PARK, J.-H., HARDER, J., IWAKURA, Y. & NÚÑEZ, G. 2008a. Cutting Edge: Critical Role for Mesothelial Cells in Necrosis-Induced Inflammation through the Recognition of IL-1α Released from Dying Cells. *The Journal of Immunology,* 181**,** 8194-8198.

EIGENBROD, T., PARK, J. H., HARDER, J., IWAKURA, Y. & NUNEZ, G. 2008b. Cutting edge: critical role for mesothelial cells in necrosis-induced inflammation through the recognition of IL-1 alpha released from dying cells. *J Immunol,* 181**,** 8194-8.

ELKHENANY, H., AMELSE, L., CALDWELL, M., ABDELWAHED, R. & DHAR, M. 2016. Impact of the source and serial passaging of goat mesenchymal stem cells on osteogenic differentiation potential: implications for bone tissue engineering. *Journal of Animal Science and Biotechnology,* 7**,** 16.

FALK, P., MA, C., CHEGINI, N. & HOLMDAHL, L. 2000. Differential regulation of mesothelial cell fibrinolysis by transforming growth factor beta 1. *Scand J Clin Lab Invest,* 60**,** 439-47.

FASSINA, A., CAPPELLESSO, R., GUZZARDO, V., DALLA VIA, L., PICCOLO, S., VENTURA, L. & FASSAN, M. 2012. Epithelial-mesenchymal transition in malignant mesothelioma. *Mod Pathol,* 25**,** 86-99.

FAULL, R. J., STANLEY, J. M., FRASER, S., POWER, D. A. & LEAVESLEY, D. I. 2001. HB-EGF is produced in the peritoneal cavity and enhances mesothelial cell adhesion and migration. *Kidney Int,* 59**,** 614-24.

FEDORKO, M. E., HIRSCH, J. G. & FRIED, B. 1971. Studies on transport of macromolecules and small particles across mesothelial cells of the mouse omentum. II. Kinetic features and metabolic requirements. *Exp Cell Res,* 69**,** 313-23.

FEHLING, H. J., LACAUD, G., KUBO, A., KENNEDY, M., ROBERTSON, S., KELLER, G. & KOUSKOFF, V. 2003. Tracking mesoderm induction and its specification to the hemangioblast during embryonic stem cell differentiation. *Development,* 130**,** 4217-4227.

FOLEY-COMER, A. J., HERRICK, S. E., AL-MISHLAB, T., PRELE, C. M., LAURENT, G. J. & MUTSAERS, S. E. 2002a. Evidence for incorporation of free-floating mesothelial cells as a mechanism of serosal healing. *J Cell Sci,* 115**,** 1383-9.

FOLEY-COMER, A. J., HERRICK, S. E., AL-MISHLAB, T., PRÊLE, C. M., LAURENT, G. J. & MUTSAERS, S. E. 2002b. Evidence for incorporation of free-floating mesothelial cells as a mechanism of serosal healing. *Journal of Cell Science,* 115**,** 1383-1389.

FRANZEN, C. A., SIMMS, P. E., VAN HUIS, A. F., FOREMAN, K. E., KUO, P. C. & GUPTA, G. N. 2014. Characterization of Uptake and Internalization of Exosomes by Bladder Cancer Cells. *BioMed Research International,* 2014**,** 11.

FUENTE MORA, C., RANGHINI, E., BRUNO, S., BUSSOLATI, B., CAMUSSI, G., WILM, B., EDGAR, D., KENNY, S. E. & MURRAY, P. 2012. Differentiation of podocyte and proximal tubule-like cells from a mouse kidney-derived stem cell line. *Stem Cells Dev,* 21**,** 296-307.

FUKUDA, S., NISHIDA-FUKUDA, H., NANBA, D., NAKASHIRO, K.-I., NAKAYAMA, H., KUBOTA, H. & HIGASHIYAMA, S. 2016. Reversible interconversion and maintenance of mammary epithelial cell characteristics by the ligand-regulated EGFR system. *Scientific Reports,* 6**,** 20209.

GANGJI, A. S., BRIMBLE, K. S. & MARGETTS, P. J. 2009. Association between markers of inflammation, fibrosis and hypervolemia in peritoneal dialysis patients. *Blood Purif,* 28**,** 354-8.

GARCIA-GOMEZ, I., PANCHOLI, N., PATEL, J., GUDEHITHLU, K. P., SETHUPATHI, P., HART, P., DUNEA, G., ARRUDA, J. A. & SINGH, A. K. 2014. Activated omentum slows progression of CKD. *J Am Soc Nephrol,* 25**,** 1270-81.

GARG, M. 2013. Epithelial-mesenchymal transition - activating transcription factors - multifunctional regulators in cancer. *World J Stem Cells,* 5**,** 188-95.

GEORGIADIS, A., TSCHERNUTTER, M., BAINBRIDGE, J. W., BALAGGAN, K. S., MOWAT, F., WEST, E. L., MUNRO, P. M., THRASHER, A. J., MATTER, K., BALDA, M. S. & ALI, R. R. 2010. The tight junction associated signalling proteins ZO-1 and ZONAB regulate retinal pigment epithelium homeostasis in mice. *PLoS One,* 5**,** e15730.

GOTTARDI, C. J., ARPIN, M., FANNING, A. S. & LOUVARD, D. 1996. The junction-associated protein, zonula occludens-1, localizes to the nucleus before the maturation and during the remodeling of cell-cell contacts. *Proc Natl Acad Sci U S A,* 93**,** 10779-84.

GREGORY, P. A., BRACKEN, C. P., SMITH, E., BERT, A. G., WRIGHT, J. A., ROSLAN, S., MORRIS, M., WYATT, L., FARSHID, G., LIM, Y.-Y., LINDEMAN, G. J., SHANNON, M. F., DREW, P. A., KHEW-GOODALL, Y. & GOODALL, G. J. 2011. An autocrine TGF-β/ZEB/miR-200 signaling network regulates establishment and maintenance of epithelial-mesenchymal transition. *Molecular Biology of the Cell,* 22**,** 1686-1698.

GUAN, H., ZHAO, P., DAI, Z., LIU, X. & WANG, X. 2016. SH3GL1 inhibition reverses multidrug resistance in colorectal cancer cells by downregulation of MDR1/P-glycoprotein via EGFR/ERK/AP-1 pathway. *Tumour Biol*.

GUI, T., SUN, Y., SHIMOKADO, A. & MURAGAKI, Y. 2012. The Roles of Mitogen-Activated Protein Kinase Pathways in TGF-β-Induced Epithelial-Mesenchymal Transition. *Journal of Signal Transduction,* 2012.

HABER, D. A., ENGLERT, C. & MAHESWARAN, S. 1996. Functional properties of WT1. *Med Pediatr Oncol,* 27**,** 453-5.

HARE, I., GENCHEVA, M., EVANS, R., FORTNEY, J., PIKTEL, D., VOS, J. A., HOWELL, D. & GIBSON, L. F. 2016. In Vitro Expansion of Bone Marrow Derived Mesenchymal Stem Cells Alters DNA Double Strand Break Repair of Etoposide Induced DNA Damage. *Stem Cells International,* 2016**,** 8270464.

HAUSMANN, M. J., ROGACHEV, B., WEILER, M., CHAIMOVITZ, C. & DOUVDEVANI, A. 2000. Accessory role of human peritoneal mesothelial cells in antigen presentation and T-cell growth. *Kidney Int,* 57**,** 476-86.

HE, L., CHE, M., HU, J., LI, S., JIA, Z., LOU, W., LI, C., YANG, J., SUN, S., WANG, H. & CHEN, X. 2015. Twist contributes to proliferation and epithelial-to-mesenchymal transition-

induced fibrosis by regulating YB-1 in human peritoneal mesothelial cells. *Am J Pathol,* 185**,** 2181-93.

HEKKING, L. H., HARVEY, V. S., HAVENITH, C. E., VAN DEN BORN, J., BEELEN, R. H., JACKMAN, R. W. & NAGY, J. A. 2003. Mesothelial cell transplantation in models of acute inflammation and chronic peritoneal dialysis. *Perit Dial Int,* 23**,** 323-30.

HELDIN, C.-H., VANLANDEWIJCK, M. & MOUSTAKAS, A. 2012. Regulation of EMT by TGFβ in cancer. *FEBS Letters,* 586**,** 1959-1970.

HERRICK, S. E. & MUTSAERS, S. E. 2004. Mesothelial progenitor cells and their potential in tissue engineering. *Int J Biochem Cell Biol,* 36**,** 621-42.

HERRICK, S. E. & MUTSAERS, S. E. 2007. The potential of mesothelial cells in tissue engineering and regenerative medicine applications. *Int J Artif Organs,* 30**,** 527-40.

HJELLE, J. T., GOLINSKA, B. T., WATERS, D. C., STEIDLEY, K. R., MCCARROLL, D. R. & DOBBIE, J. W. 1989. Isolation and propagation in vitro of peritoneal mesothelial cells. *Perit Dial Int,* 9**,** 341-7.

HONG, S., NOH, H., TENG, Y., SHAO, J., REHMANI, H., DING, H. F., DONG, Z., SU, S. B., SHI, H., KIM, J. & HUANG, S. 2014. SHOX2 is a direct miR-375 target and a novel epithelial-to-mesenchymal transition inducer in breast cancer cells. *Neoplasia,* 16**,** 279-90.e1-5.

HORIO, M., SATO, M., TAKEYAMA, Y., ELSHAZLEY, M., YAMASHITA, R., HASE, T., YOSHIDA, K., USAMI, N., YOKOI, K., SEKIDO, Y., KONDO, M., TOYOKUNI, S., GAZDAR, A. F., MINNA, J. D. & HASEGAWA, Y. 2011. Transient but Not Stable ZEB1 Knockdown Dramatically Inhibits Growth of Malignant Pleural Mesothelioma Cells. *Annals of Surgical Oncology,* 19**,** 634-645.

HUANG, S. & CZECH, M. P. 2007. The GLUT4 Glucose Transporter. *Cell Metabolism,* 5**,** 237-252.

HUGO, H. J., KOKKINOS, M. I., BLICK, T., ACKLAND, M. L., THOMPSON, E. W. & NEWGREEN, D. F. 2011. Defining the E-cadherin repressor interactome in epithelial-mesenchymal transition: the PMC42 model as a case study. *Cells Tissues Organs,* 193**,** 23-40.

INAGAKI, N. F., INAGAKI, F. F., KOKUDO, N. & MIYAJIMA, A. 2015. Use of mouse liver mesothelial cells to prevent postoperative adhesion and promote liver regeneration after hepatectomy. *Journal of Hepatology,* 62**,** 1141-1147.

JANG, Y. H., SHIN, H. S., SUN CHOI, H., RYU, E. S., JIN KIM, M., KI MIN, S., LEE, J. H., KOOK LEE, H., KIM, K. H. & KANG, D. H. 2013. Effects of dexamethasone on the TGF-beta1-induced epithelial-to-mesenchymal transition in human peritoneal mesothelial cells. *Lab Invest,* 93**,** 194-206.

JAVELAUD, D. & MAUVIEL, A. 2005. Crosstalk mechanisms between the mitogen-activated protein kinase pathways and Smad signaling downstream of TGF-[beta]: implications for carcinogenesis. *Oncogene,* 24**,** 5742-5750.

JIA, M. & SOUCHELNYTSTKYI, S. 2011. Comments on the cross-talk of TGFbeta and EGF in cancer. *Exp Oncol,* 33**,** 170-3.

JIANG, L., YAMASHITA, Y. & TOYOKUNI, S. 2010. A novel method for efficient collection of normal mesothelial cells in vivo. *J Clin Biochem Nutr,* 46**,** 265-8.

JIN, X., REN, S., MACARAK, E. & ROSENBLOOM, J. 2016. Pathobiological mechanisms of peritoneal adhesions: The mesenchymal transition of rat peritoneal mesothelial cells induced by TGF-beta1 and IL-6 requires activation of Erk1/2 and Smad2 linker region phosphorylation. *Matrix Biol,* 51**,** 55-64.

JOLLY, M. K., BOARETO, M., HUANG, B., JIA, D., LU, M., ONUCHIC, J. N., LEVINE, H. & BEN-JACOB, E. 2015a. Implications of the hybrid epithelial/mesenchymal phenotype in metastasis. *Frontiers in Oncology,* 5.

JOLLY, M. K., JIA, D., BOARETO, M., MANI, S. A., PIENTA, K. J., BEN-JACOB, E. & LEVINE, H. 2015b. Coupling the modules of EMT and stemness: A tunable 'stemness window' model. *Oncotarget,* 6**,** 25161-74.

JOMGEOW, T., OJI, Y., TSUJI, N., IKEDA, Y., ITO, K., TSUDA, A., NAKAZAWA, T., TATSUMI, N., SAKAGUCHI, N., TAKASHIMA, S., SHIRAKATA, T., NISHIDA, S., HOSEN, N., KAWAKAMI, M., TSUBOI, A., OKA, Y., ITOH, K. & SUGIYAMA, H. 2006. Wilms' tumor gene WT1 17AA(-)/KTS(-) isoform induces morphological changes and promotes cell migration and invasion in vitro. *Cancer Sci,* 97**,** 259-70.

KALLURI, R. & WEINBERG, R. A. 2009. The basics of epithelial-mesenchymal transition. *J Clin Invest,* 119**,** 1420-8.

KANAI, N., YAMATO, M. & OKANO, T. 2014. Chapter 5 - Principles of Cell Sheet Technology A2 - Orlando, Giuseppe. *In:* LERUT, J., SOKER, S. & STRATTA, R. J. (eds.) *Regenerative Medicine Applications in Organ Transplantation.* Boston: Academic Press.

KANDA, R., HAMADA, C., KANEKO, K., NAKANO, T., WAKABAYASHI, K., HARA, K., IO, H., HORIKOSHI, S. & TOMINO, Y. 2014. Paracrine effects of transplanted mesothelial cells isolated from temperature-sensitive SV40 large T-antigen gene transgenic rats during peritoneal repair. *Nephrology Dialysis Transplantation,* 29**,** 289-300.

KARKI, S., SUROLIA, R., HOCK, T. D., GUROJI, P., ZOLAK, J. S., DUGGAL, R., YE, T., THANNICKAL, V. J. & ANTONY, V. B. 2014. Wilms' tumor 1 (Wt1) regulates pleural mesothelial cell plasticity and transition into myofibroblasts in idiopathic pulmonary fibrosis. *The FASEB Journal,* 28**,** 1122-1131.

KAWAGUCHI, M., BADER, D. M. & WILM, B. 2007. Serosal mesothelium retains vasculogenic potential. *Dev Dyn,* 236**,** 2973-2979.

KAWANISHI, K., YAMATO, M., SAKIYAMA, R., OKANO, T. & NITTA, K. 2013. Peritoneal cell sheets composed of mesothelial cells and fibroblasts prevent intra-abdominal adhesion formation in a rat model. *J Tissue Eng Regen Med*.

KIM, H. J., CHOI, W. J. & LEE, C. H. 2015. Phosphorylation and Reorganization of Keratin Networks: Implications for Carcinogenesis and Epithelial Mesenchymal Transition. *Biomol Ther (Seoul),* 23**,** 301-12.

KIM, S., LIM, J. H. & WOO, C. H. 2013. ERK5 inhibition ameliorates pulmonary fibrosis via regulating Smad3 acetylation. *Am J Pathol,* 183**,** 1758-68.

KITAMURA, S., HORIMOTO, N., TSUJI, K., INOUE, A., TAKIUE, K., SUGIYAMA, H. & MAKINO, H. 2014. The Selection of Peritoneal Mesothelial Cells Is Important for Cell Therapy to Prevent Peritoneal Fibrosis. *Tissue Engineering. Part A,* 20**,** 529-539.

KITAYAMA, J., EMOTO, S., YAMAGUCHI, H., ISHIGAMI, H., YAMASHITA, H., SETO, Y., MATSUZAKI, K. & WATANABE, T. 2014. CD90(+)CD45(-) intraperitoneal mesothelial-like cells inhibit T cell activation by production of arginase I. *Cell Immunol,* 288**,** 8-14.

KNIGHTS, A. J., FUNNELL, A. P. W., CROSSLEY, M. & PEARSON, R. C. M. 2012. Holding Tight: Cell Junctions and Cancer Spread. *Trends in cancer research,* 8**,** 61-69.

KOMARAVOLU, R. K., ADAM, C., MOONEN, J. R., HARMSEN, M. C., GOEBELER, M. & SCHMIDT, M. 2015. Erk5 inhibits endothelial migration via KLF2-dependent down-regulation of PAK1. *Cardiovasc Res,* 105**,** 86-95.

KRAMARZOVA, K., STUCHLY, J., WILLASCH, A., GRUHN, B., SCHWARZ, J., CERMAK, J., MACHOVA-POLAKOVA, K., FUCHS, O., STARY, J., TRKA, J. & BOUBLIKOVA, L. 2012. Real-time PCR quantification of major Wilms' tumor gene 1 (WT1) isoforms in acute myeloid leukemia, their characteristic expression patterns and possible functional consequences. *Leukemia,* 26**,** 2086-95.

KRAUSE, M., RAK-RASZEWSKA, A., PIETILÄ, I., QUAGGIN, S. & VAINIO, S. 2015. Signaling during Kidney Development. *Cells,* 4**,** 112.

KRETLOW, J. D., JIN, Y.-Q., LIU, W., ZHANG, W. J., HONG, T.-H., ZHOU, G., BAGGETT, L. S., MIKOS, A. G. & CAO, Y. 2008. Donor age and cell passage affects differentiation potential of murine bone marrow-derived stem cells. *BMC Cell Biology,* 9**,** 60-60.

KSIĄŻEK, K. 2013. Mesothelial cell: A multifaceted model of aging. *Ageing Research Reviews,* 12**,** 595-604.

KSIAZEK, K., MIKULA-PIETRASIK, J., JORRES, A. & WITOWSKI, J. 2008. Oxidative stress-mediated early senescence contributes to the short replicative life span of human peritoneal mesothelial cells. *Free Radic Biol Med,* 45**,** 460-7.

KSIAZEK, K., PASSOS, J. F., OLIJSLAGERS, S., SARETZKI, G., MARTIN-RUIZ, C. & VON ZGLINICKI, T. 2007. Premature senescence of mesothelial cells is associated with non-telomeric DNA damage. *Biochem Biophys Res Commun,* 362**,** 707-11.

KUZMA-KUZNIARSKA, M., RAK-RASZEWSKA, A., KENNY, S., EDGAR, D., WILM, B., FUENTE MORA, C., DAVIES, J. A. & MURRAY, P. 2012. Integration potential of mouse and human bone marrow-derived mesenchymal stem cells. *Differentiation,* 83**,** 128-137.

LACHAUD, C. C., LÓPEZ-BEAS, J., SORIA, B. & HMADCHA, A. 2014. EGF-induced adipose tissue mesothelial cells undergo functional vascular smooth muscle differentiation. *Cell Death & Disease,* 5**,** e1304.

LACHAUD, C. C., PEZZOLLA, D., DOMÍNGUEZ-RODRÍGUEZ, A., SMANI, T., SORIA, B. & HMADCHA, A. 2013. Functional Vascular Smooth Muscle-like Cells Derived from Adult Mouse Uterine Mesothelial Cells. *PLoS ONE,* 8**,** e55181.

LACHAUD, C. C., RODRIGUEZ-CAMPINS, B., HMADCHA, A. & SORIA, B. 2015. Use of Mesothelial Cells and Biological Matrices for Tissue Engineering of Simple Epithelium Surrogates. *Frontiers in Bioengineering and Biotechnology,* 3**,** 117.

LAMOUILLE, S., XU, J. & DERYNCK, R. 2014. Molecular mechanisms of epithelial–mesenchymal transition. *Nat Rev Mol Cell Biol,* 15**,** 178-196.

LANSLEY, S. M., SEARLES, R. G., HOI, A., THOMAS, C., MONETA, H., HERRICK, S. E., THOMPSON, P. J., MARK, N., STERRETT, G. F., PRÊLE, C. M. & MUTSAERS, S. E. 2011. Mesothelial cell differentiation into osteoblast- and adipocyte-like cells. *Journal of Cellular and Molecular Medicine,* 15**,** 2095-2105.

LASSAILLY, F., GRIESSINGER, E. & BONNET, D. 2010. "Microenvironmental contaminations" induced by fluorescent lipophilic dyes used for noninvasive in vitro and in vivo cell tracking. *Blood,* 115**,** 5347-5354.

LEE, H. B. & HA, H. 2007. Mechanisms of epithelial-mesenchymal transition of peritoneal mesothelial cells during peritoneal dialysis. *J Korean Med Sci,* 22**,** 943-5.

LEE, Y. C., TSAI, Y. S., HUNG, S. Y., LIN, T. M., LIN, S. H., LIOU, H. H., LIU, H. C., CHANG, M. Y., WANG, H. H., HO, L. C., CHEN, Y. T., CHEN, H. P., FAN, H. A., LIU, K. W., KUNG, Y. T., WANG, H. K. & CHIOU, Y. Y. 2014. Shorter daily dwelling time in peritoneal dialysis attenuates the epithelial-to-mesenchymal transition of mesothelial cells. *BMC Nephrol,* 15**,** 35.

LEYPOLDT, J. K. 2002. Solute Transport Across the Peritoneal Membrane. *Journal of the American Society of Nephrology,* 13**,** S84-S91.

LI, C., REN, Y., JIA, X., LIANG, P., LOU, W., HE, L., LI, M., SUN, S. & WANG, H. 2012. Twist overexpression promoted epithelial-to-mesenchymal transition of human peritoneal mesothelial cells under high glucose. *Nephrol Dial Transplant,* 27.

LI, P., ZHANG, R., SUN, H., CHEN, L., LIU, F., YAO, C., DU, M. & JIANG, X. 2013a. PKH26 Can Transfer to Host Cells In Vitro and Vivo. *Stem Cells and Development,* 22**,** 340-344.

LI, W. & KANG, Y. 2016. Probing the Fifty Shades of EMT in Metastasis. *Trends in Cancer,* 2**,** 65-67.

LI, Y., LUA, I., FRENCH, S. W. & ASAHINA, K. 2016. Role of TGF-beta signaling in differentiation of mesothelial cells to vitamin A-poor hepatic stellate cells in liver fibrosis. *Am J Physiol Gastrointest Liver Physiol,* 310**,** G262-72.

LI, Y., WANG, J. & ASAHINA, K. 2013b. Mesothelial cells give rise to hepatic stellate cells and myofibroblasts via mesothelial–mesenchymal transition in liver injury. *Proceedings of the National Academy of Sciences of the United States of America,* 110**,** 2324-2329.

LIANG, Z., XIE, W., WU, R., GENG, H., ZHAO, L., XIE, C., LI, X., HUANG, C., ZHU, J., ZHU, M., ZHU, W., WU, J., GENG, S. & ZHONG, C. 2015. ERK5 negatively regulates tobacco smoke-induced pulmonary epithelial-mesenchymal transition. *Oncotarget,* 6**,** 19605-18.

LIN, C. Y., KIFT-MORGAN, A., MOSER, B., TOPLEY, N. & EBERL, M. 2013. Suppression of pro-inflammatory T-cell responses by human mesothelial cells. *Nephrol Dial Transplant,* 28**,** 1743-50.

LITTLE, M. H. & TAKASATO, M. 2015. Generating a self-organizing kidney from pluripotent cells. *Curr Opin Organ Transplant,* 20**,** 178-86.

LIU, Q., MAO, H., NIE, J., CHEN, W., YANG, Q., DONG, X. & YU, X. 2008. TRANSFORMING GROWTH FACTOR β1 INDUCES EPITHELIAL-MESENCHYMAL TRANSITION BY ACTIVATING THE JNK-SMAD3 PATHWAY IN RAT PERITONEAL MESOTHELIAL CELLS. *Peritoneal Dialysis International,* 28**,** S88-S95.

LIU, S., ZHOU, J., ZHANG, X., LIU, Y., CHEN, J., HU, B., SONG, J. & ZHANG, Y. 2016. Strategies to Optimize Adult Stem Cell Therapy for Tissue Regeneration. *Int J Mol Sci,* 17.

LIU, Y., DONG, Z., LIU, H., ZHU, J., LIU, F. & CHEN, G. 2015. Transition of mesothelial cell to fibroblast in peritoneal dialysis: EMT, stem cell or bystander? *Perit Dial Int,* 35**,** 14-25.

LIU, Y., PETREACA, M., YAO, M. & MARTINS-GREEN, M. 2009. Cell and molecular mechanisms of keratinocyte function stimulated by insulin during wound healing. *BMC Cell Biology,* 10**,** 1-15.

LOBO, S., WICZER, B. M., SMITH, A. J., HALL, A. M. & BERNLOHR, D. A. 2007. Fatty acid metabolism in adipocytes: functional analysis of fatty acid transport proteins 1 and 4. *J Lipid Res,* 48**,** 609-20.

LÓPEZ-CABRERA, M. 2014. Mesenchymal Conversion of Mesothelial Cells Is a Key Event in the Pathophysiology of the Peritoneum during Peritoneal Dialysis. *Advances in Medicine,* 2014**,** 17.

LOUREIRO, J., AGUILERA, A., SELGAS, R., SANDOVAL, P., ALBAR-VIZCAINO, P., PEREZ-LOZANO, M. L., RUIZ-CARPIO, V., MAJANO, P. L., LAMAS, S., RODRIGUEZ-PASCUAL, F., BORRAS-CUESTA, F., DOTOR, J. & LOPEZ-CABRERA, M. 2011. Blocking TGF-beta1 protects the peritoneal membrane from dialysate-induced damage. *J Am Soc Nephrol,* 22**,** 1682-95.

LOUREIRO, J., SCHILTE, M., AGUILERA, A., ALBAR-VIZCAINO, P., RAMIREZ-HUESCA, M., PEREZ-LOZANO, M. L., GONZALEZ-MATEO, G., AROEIRA, L. S., SELGAS, R., MENDOZA, L., ORTIZ, A., RUIZ-ORTEGA, M., VAN DEN BORN, J., BEELEN, R. H. & LOPEZ-CABRERA, M. 2010. BMP-7 blocks mesenchymal conversion of mesothelial cells and prevents peritoneal damage induced by dialysis fluid exposure. *Nephrol Dial Transplant,* 25**,** 1098-108.

LUA, I. & ASAHINA, K. 2016. The Role of Mesothelial Cells in Liver Development, Injury, and Regeneration. *Gut and Liver,* 10**,** 166-176.

LUA, I., LI, Y., PAPPOE, L. S. & ASAHINA, K. 2015. Myofibroblastic Conversion and Regeneration of Mesothelial Cells in Peritoneal and Liver Fibrosis. *Am J Pathol,* 185**,** 3258-73.

LUA, I., LI, Y., ZAGORY, J. A., WANG, K. S., FRENCH, S. W., SÉVIGNY, J. & ASAHINA, K. 2016. Characterization of hepatic stellate cells, portal fibroblasts, and mesothelial cells in normal and fibrotic livers. *Journal of Hepatology,* 64**,** 1137-1146.

LUO, W., LI, S., PENG, B., YE, Y., DENG, X. & YAO, K. 2013. Embryonic Stem Cells Markers SOX2, OCT4 and Nanog Expression and Their Correlations with Epithelial-Mesenchymal Transition in Nasopharyngeal Carcinoma. *PLoS ONE,* 8**,** e56324.

MAN, L., LEWIS, E., EINBINDER, T., ROGACHEV, B., CHAIMOVITZ, C. & DOUVDEVANI, A. 2003. Major involvement of CD40 in the regulation of chemokine secretion from human peritoneal mesothelial cells. *Kidney Int,* 64**,** 2064-71.

MARCHETTI, A., COLLETTI, M., COZZOLINO, A. M., STEINDLER, C., LUNADEI, M., MANCONE, C. & TRIPODI, M. 2008. ERK5/MAPK is activated by TGFbeta in hepatocytes and required for the GSK-3beta-mediated Snail protein stabilization. *Cell Signal,* 20**,** 2113-8.

MARGETTS, P. J., BONNIAUD, P., LIU, L., HOFF, C. M., HOLMES, C. J., WEST-MAYS, J. A. & KELLY, M. M. 2005. Transient overexpression of TGF-{beta}1 induces epithelial mesenchymal transition in the rodent peritoneum. *J Am Soc Nephrol,* 16**,** 425-36.

MERIKALLIO, H., PÄÄKKÖ, P., SALMENKIVI, K., KINNULA, V., HARJU, T. & SOINI, Y. 2013. Expression of snail, twist, and Zeb1 in malignant mesothelioma. *APMIS,* 121**,** 1-10.

MICHAILOVA, K., WASSILEV, W. & WEDEL, T. 1999. Scanning and transmission electron microscopic study of visceral and parietal peritoneal regions in the rat. *Ann Anat,* 181**,** 253-60.

MORISHITA, Y., OOKAWARA, S., HIRAHARA, I., MUTO, S. & NAGATA, D. 2016. HIF-1alpha mediates Hypoxia-induced epithelial-mesenchymal transition in peritoneal mesothelial cells. *Ren Fail,* 38**,** 282-9.

MUBARAK, K. K., MONTES-WORBOYS, A., REGEV, D., NASREEN, N., MOHAMMED, K. A., FARUQI, I., HENSEL, E., BAZ, M. A., AKINDIPE, O. A., FERNANDEZ-BUSSY, S., NATHAN, S. D. & ANTONY, V. B. 2012. Parenchymal trafficking of pleural mesothelial cells in idiopathic pulmonary fibrosis. *Eur Respir J,* 39**,** 133-40.

MUNDER, M. 2009. Arginase: an emerging key player in the mammalian immune system. *British Journal of Pharmacology,* 158**,** 638-651.

MUTSAERS, S. E., BIRNIE, K., LANSLEY, S., HERRICK, S. E., LIM, C. B. & PRELE, C. M. 2015. Mesothelial cells in tissue repair and fibrosis. *Front Pharmacol,* 6**,** 113.

MUTSAERS, S. E. & WILKOSZ, S. 2007. Structure and function of mesothelial cells. *Cancer Treat Res,* 134**,** 1-19.

NAGY, J. A., SHOCKLEY, T. R., MASSE, E. M., HARVEY, V. S., HOFF, C. M. & JACKMAN, R. W. 1995. Systemic delivery of a recombinant protein by genetically modified mesothelial cells reseeded on the parietal peritoneal surface. *Gene Ther,* 2**,** 402-10.

NAGYOVA, M., SLOVINSKA, L., BLASKO, J., GRULOVA, I., KURICOVA, M., CIGANKOVA, V., HARVANOVA, D. & CIZKOVA, D. 2014. A comparative study of PKH67, DiI, and BrdU labeling techniques for tracing rat mesenchymal stem cells. *In Vitro Cell Dev Biol Anim,* 50**,** 656-63.

NASREEN, N., MOHAMMED, K. A., MUBARAK, K. K., BAZ, M. A., AKINDIPE, O. A., FERNANDEZ-BUSSY, S. & ANTONY, V. B. 2009. Pleural mesothelial cell transformation into myofibroblasts and haptotactic migration in response to TGF-β1 in vitro. *American Journal of Physiology - Lung Cellular and Molecular Physiology,* 297**,** L115-L124.

NIETO, M. A. 2002. The snail superfamily of zinc-finger transcription factors. *Nat Rev Mol Cell Biol,* 3**,** 155-66.

OFFNER, F. A., FEICHTINGER, H., STADLMANN, S., OBRIST, P., MARTH, C., KLINGLER, P., GRAGE, B., SCHMAHL, M. & KNABBE, C. 1996. Transforming growth factor-beta synthesis by human peritoneal mesothelial cells. Induction by interleukin-1. *Am J Pathol,* 148**,** 1679-88.

OJI, Y., TATSUMI, N., KOBAYASHI, J., FUKUDA, M., UEDA, T., NAKANO, E., SAITO, C., SHIBATA, S., SUMIKAWA, M., FUKUSHIMA, H., SAITO, A., HOJO, N., SUZUKI, M., HOSHIKAWA, T., SHIMURA, T., MORII, E., OKA, Y., HOSEN, N., KOMATSU, K. & SUGIYAMA, H. 2015.

Wilms' tumor gene WT1 promotes homologous recombination-mediated DNA damage repair. *Mol Carcinog,* 54**,** 1758-71.

ONITSUKA, I., TANAKA, M. & MIYAJIMA, A. 2010. Characterization and Functional Analyses of Hepatic Mesothelial Cells in Mouse Liver Development. *Gastroenterology,* 138**,** 1525-1535.e6.

PENG, X., CUFF, L. E., LAWTON, C. D. & DEMALI, K. A. 2010. Vinculin regulates cell-surface E-cadherin expression by binding to β-catenin. *Journal of Cell Science,* 123**,** 567-577.

PERIN, L., GIULIANI, S., JIN, D., SEDRAKYAN, S., CARRARO, G., HABIBIAN, R., WARBURTON, D., ATALA, A. & DE FILIPPO, R. E. 2007. Renal differentiation of amniotic fluid stem cells. *Cell Prolif,* 40**,** 936-48.

PEZ-CABRERA, M. 2014. Mesenchymal Conversion of Mesothelial Cells Is a Key Event in the Pathophysiology of the Peritoneum during Peritoneal Dialysis. *Advances in Medicine,* 2014**,** 17.

PROGATZKY, F., DALLMAN, M. J. & LO CELSO, C. 2013. From seeing to believing: labelling strategies for in vivo cell-tracking experiments. *Interface Focus,* 3**,** 20130001.

QUE, J., WILM, B., HASEGAWA, H., WANG, F., BADER, D. & HOGAN, B. L. 2008. Mesothelium contributes to vascular smooth muscle and mesenchyme during lung development. *Proc Natl Acad Sci U S A,* 105**,** 16626-30.

RAK-RASZEWSKA, A., HAUSER, P. V. & VAINIO, S. 2015. Organ In Vitro Culture: What Have We Learned about Early Kidney Development? *Stem Cells International,* 2015**,** 16.

RAK-RASZEWSKA, A., MARCELLO, M., KENNY, S., EDGAR, D., SEE, V. & MURRAY, P. 2012. Quantum dots do not affect the behaviour of mouse embryonic stem cells and kidney stem cells and are suitable for short-term tracking. *PLoS One,* 7**,** e32650.

RANGHINI, E., MORA, C. F., EDGAR, D., KENNY, S. E., MURRAY, P. & WILM, B. 2013. Stem Cells Derived from Neonatal Mouse Kidney Generate Functional Proximal Tubule-Like Cells and Integrate into Developing Nephrons <italic>In Vitro</italic>. *PLoS ONE,* 8**,** e62953.

REID, G. 2015. MicroRNAs in mesothelioma: from tumour suppressors and biomarkers to therapeutic targets. *J Thorac Dis,* 7**,** 1031-40.

RINKEVICH, Y., MORI, T., SAHOO, D., XU, P.-X., BERMINGHAM, J. R. & WEISSMAN, I. L. 2012. Identification and prospective isolation of a mesothelial precursor lineage giving rise to smooth muscle cells & fibroblasts for mammalian internal organs, and their vasculature. *Nature cell biology,* 14**,** 1251-1260.

ROSSI, D. J., BRYDER, D., SEITA, J., NUSSENZWEIG, A., HOEIJMAKERS, J. & WEISSMAN, I. L. 2007. Deficiencies in DNA damage repair limit the function of haematopoietic stem cells with age. *Nature,* 447**,** 725-9.

ROUGIER, J. P., GUIA, S., HAGEGE, J., NGUYEN, G. & RONCO, P. M. 1998. PAI-1 secretion and matrix deposition in human peritoneal mesothelial cell cultures: transcriptional regulation by TGF-beta 1. *Kidney Int,* 54**,** 87-98.

RYMER, C., PAREDES, J., HALT, K., SCHAEFER, C., WIERSCH, J., ZHANG, G., POTOKA, D., VAINIO, S., GITTES, G. K., BATES, C. M. & SIMS-LUCAS, S. 2014. Renal blood flow and oxygenation drive nephron progenitor differentiation. *Am J Physiol Renal Physiol,* 307**,** F337-45.

SAVAGNER, P. 2015. Chapter Eight - Epithelial–Mesenchymal Transitions: From Cell Plasticity to Concept Elasticity. *In:* ALPHA, S. Y. (ed.) *Current Topics in Developmental Biology.* Academic Press.

SHANDILYA, J. & ROBERTS, S. G. 2015. A role of WT1 in cell division and genomic stability. *Cell Cycle,* 14**,** 1358-64.

SIEGEL, N., ROSNER, M., UNBEKANDT, M., FUCHS, C., SLABINA, N., DOLZNIG, H., DAVIES, J. A., LUBEC, G. & HENGSTSCHLAGER, M. 2010. Contribution of human amniotic fluid stem cells to renal tissue formation depends on mTOR. *Hum Mol Genet,* 19**,** 3320-31.

SIERSBAEK, R., NIELSEN, R. & MANDRUP, S. 2010. PPARgamma in adipocyte differentiation and metabolism--novel insights from genome-wide studies. *FEBS Lett,* 584**,** 3242-9.

SON, Y., CHEONG, Y.-K., KIM, N.-H., CHUNG, H.-T., KANG, D. G. & PAE, H.-O. 2011. Mitogen-Activated Protein Kinases and Reactive Oxygen Species: How Can ROS Activate MAPK Pathways? *Journal of Signal Transduction,* 2011**,** 6.

STRIPPOLI, R., BENEDICTO, I., FORONDA, M., PEREZ-LOZANO, M. L., SÁNCHEZ-PERALES, S., LÓPEZ-CABRERA, M. & DEL POZO, M. Á. 2010. p38 maintains E-cadherin expression by modulating TAK1–NF-κB during epithelial-to-mesenchymal transition. *Journal of Cell Science,* 123**,** 4321-4331.

STRIPPOLI, R., BENEDICTO, I., PEREZ LOZANO, M. L., CEREZO, A., LOPEZ-CABRERA, M. & DEL POZO, M. A. 2008. Epithelial-to-mesenchymal transition of peritoneal mesothelial cells is regulated by an ERK/NF-kappaB/Snail1 pathway. *Dis Model Mech,* 1**,** 264-74.

STRIPPOLI, R., BENEDICTO, I., PEREZ LOZANO, M. L., PELLINEN, T., SANDOVAL, P., LOPEZ-CABRERA, M. & DEL POZO, M. A. 2012. Inhibition of transforming growth factor-activated kinase 1 (TAK1) blocks and reverses epithelial to mesenchymal transition of mesothelial cells. *PLoS One,* 7**,** e31492.

STRIPPOLI, R., LOUREIRO, J., MORENO, V., BENEDICTO, I., PEREZ LOZANO, M. L., BARREIRO, O., PELLINEN, T., MINGUET, S., FORONDA, M., OSTESO, M. T., CALVO, E., VAZQUEZ, J., LOPEZ CABRERA, M. & DEL POZO, M. A. 2015. Caveolin-1 deficiency induces a MEK-ERK1/2-Snail-1-dependent epithelial-mesenchymal transition and fibrosis during peritoneal dialysis. *EMBO Mol Med,* 7**,** 102-23.

STRIPPOLI, R., MORENO-VICENTE, R., BATTISTELLI, C., CICCHINI, C., NOCE, V., AMICONE, L., MARCHETTI, A., DEL POZO, M. A. & TRIPODI, M. 2016. Molecular Mechanisms Underlying Peritoneal EMT and Fibrosis. *Stem Cells International,* 2016**,** 11.

SUZUKI, T., KONO, T., BOCHIMOTO, H., HIRA, Y., WATANABE, T. & FURUKAWA, H. 2015. An injured tissue affects the opposite intact peritoneum during postoperative adhesion formation. *Sci Rep,* 5**,** 7668.

TAKASATO, M., ER, P. X., BECROFT, M., VANSLAMBROUCK, J. M., STANLEY, E. G., ELEFANTY, A. G. & LITTLE, M. H. 2014. Directing human embryonic stem cell differentiation towards a renal lineage generates a self-organizing kidney. *Nat Cell Biol,* 16**,** 118-26.

TAKEICHI, M., NIMURA, K., MORI, M., NAKAGAMI, H. & KANEDA, Y. 2013. The transcription factors Tbx18 and Wt1 control the epicardial epithelial-mesenchymal transition through bi-directional regulation of Slug in murine primary epicardial cells. *PLoS One,* 8**,** e57829.

TAM, W. L. & WEINBERG, R. A. 2013. The epigenetics of epithelial-mesenchymal plasticity in cancer. *Nat Med,* 19**,** 1438-49.

TAO, R., SUN, T. J., HAN, Y. Q., XU, G., LIU, J. & HAN, Y. F. 2014. Optimization of in vitro cell labeling methods for human umbilical cord-derived mesenchymal stem cells. *Eur Rev Med Pharmacol Sci,* 18**,** 1127-34.

TETI, G., SALVATORE, V., FOCAROLI, S., DURANTE, S., MAZZOTTI, A., DICARLO, M., MATTIOLI-BELMONTE, M. & ORSINI, G. 2015. In vitro osteogenic and odontogenic differentiation of human dental pulp stem cells seeded on carboxymethyl cellulose-hydroxyapatite hybrid hydrogel. *Frontiers in Physiology,* 6**,** 297.

THAYER, T. C. & WONG, F. S. 2016. Tracking Immunological Responses of Islet Antigen-Specific T Cells in the Nonobese Diabetic (NOD) Mouse Model of Type 1 Diabetes. *Methods Mol Biol*.

TOPLEY, N., BROWN, Z., JORRES, A., WESTWICK, J., DAVIES, M., COLES, G. A. & WILLIAMS, J. D. 1993. Human peritoneal mesothelial cells synthesize interleukin-8. Synergistic induction by interleukin-1 beta and tumor necrosis factor-alpha. *Am J Pathol,* 142**,** 1876-86.

UHLENHAUT, N. H. & TREIER, M. 2008. Transcriptional regulators in kidney disease: gatekeepers of renal homeostasis. *Trends in Genetics,* 24**,** 361-371.

UNBEKANDT, M. & DAVIES, J. A. 2010. Dissociation of embryonic kidneys followed by reaggregation allows the formation of renal tissues. *Kidney Int,* 77**,** 407-16.

VAN TUYN, J., ATSMA, D. E., WINTER, E. M., VAN DER VELDE-VAN DIJKE, I., PIJNAPPELS, D. A., BAX, N. A., KNAAN-SHANZER, S., GITTENBERGER-DE GROOT, A. C., POELMANN, R. E., VAN DER LAARSE, A., VAN DER WALL, E. E., SCHALIJ, M. J. & DE VRIES, A. A. 2007. Epicardial cells of human adults can undergo an epithelial-to-mesenchymal transition and obtain characteristics of smooth muscle cells in vitro. *Stem Cells,* 25**,** 271-8.

VARGHA, R., ENDEMANN, M., KRATOCHWILL, K., RIESENHUBER, A., WICK, N., KRACHLER, A. M., MALAGA-DIEGUEZ, L. & AUFRICHT, C. 2006. Ex vivo reversal of in vivo transdifferentiation in mesothelial cells grown from peritoneal dialysate effluents. *Nephrol Dial Transplant,* 21.

VAUGHAN, M. R. & QUAGGIN, S. E. 2008. How Do Mesangial and Endothelial Cells Form the Glomerular Tuft? *Journal of the American Society of Nephrology,* 19**,** 24-33.

VILLAREJO, A., CORTES-CABRERA, A., MOLINA-ORTIZ, P., PORTILLO, F. & CANO, A. 2014. Differential role of Snail1 and Snail2 zinc fingers in E-cadherin repression and epithelial to mesenchymal transition. *J Biol Chem,* 289**,** 930-41.

VON GISE, A., ZHOU, B., HONOR, L. B., MA, Q., PETRYK, A. & PU, W. T. 2011. WT1 regulates epicardial epithelial to mesenchymal transition through β-catenin and retinoic acid signaling pathways. *Developmental biology,* 356**,** 421-431.

WAGHRAY, A., SAIZ, N., JAYAPRAKASH, ANITHA D., FREIRE, ANA G., PAPATSENKO, D., PEREIRA, C.-F., LEE, D.-F., BROSH, R., CHANG, B., DARR, H., GINGOLD, J., KELLEY, K., SCHANIEL, C., HADJANTONAKIS, A.-K. & LEMISCHKA, IHOR R. 2015. Tbx3 Controls Dppa3 Levels and Exit from Pluripotency toward Mesoderm. *Stem Cell Reports,* 5**,** 97-110.

WALLACE, P. K., TARIO, J. D., FISHER, J. L., WALLACE, S. S., ERNSTOFF, M. S. & MUIRHEAD, K. A. 2008. Tracking antigen-driven responses by flow cytometry: Monitoring proliferation by dye dilution. *Cytometry Part A,* 73A**,** 1019-1034.

WANG, H. Y., YANG, S. L., LIANG, H. F. & LI, C. H. 2014. HBx protein promotes oval cell proliferation by up-regulation of cyclin D1 via activation of the MEK/ERK and PI3K/Akt pathways. *Int J Mol Sci,* 15**,** 3507-18.

WANG, L., LIU, N., XIONG, C., XU, L., SHI, Y., QIU, A., ZANG, X., MAO, H. & ZHUANG, S. 2015. Inhibition of EGF Receptor Blocks the Development and Progression of Peritoneal Fibrosis. *J Am Soc Nephrol*.

WANG, X. Q., DUAN, X. M., LIU, L. H., FANG, Y. Q. & TAN, Y. 2005. Carboxyfluorescein diacetate succinimidyl ester fluorescent dye for cell labeling. *Acta Biochim Biophys Sin (Shanghai),* 37**,** 379-85.

WARN, R., HARVEY, P., WARN, A., FOLEY-COMER, A., HELDIN, P., VERSNEL, M., ARAKAKI, N., DAIKUHARA, Y., LAURENT, G. J., HERRICK, S. E. & MUTSAERS, S. E. 2001. HGF/SF induces mesothelial cell migration and proliferation by autocrine and paracrine pathways. *Exp Cell Res,* 267**,** 258-66.

WILM, B., IPENBERG, A., HASTIE, N. D., BURCH, J. B. & BADER, D. M. 2005. The serosal mesothelium is a major source of smooth muscle cells of the gut vasculature. *Development,* 132**,** 5317-28.

WITOWSKI, J., JÖRRES, A., COLES, G. A., WILLIAMS, J. D. & TOPLEY, N. 1996. Superinduction of IL-6 synthesis in human peritoneal mesothelial cells is related to the induction and stabilization of IL-6 mRNA. *Kidney International,* 50**,** 1212-1223.

XINARIS, C., BENEDETTI, V., RIZZO, P., ABBATE, M., CORNA, D., AZZOLLINI, N., CONTI, S., UNBEKANDT, M., DAVIES, J. A., MORIGI, M., BENIGNI, A. & REMUZZI, G. 2012. In vivo

maturation of functional renal organoids formed from embryonic cell suspensions. *J Am Soc Nephrol,* 23**,** 1857-68.

XU, J., LAMOUILLE, S. & DERYNCK, R. 2009. TGF-[beta]-induced epithelial to mesenchymal transition. *Cell Res,* 19**,** 156-172.

XU, Z.-G., KIM, K. S., PARK, H. C., CHOI, K. H., LEE, H. Y., HAN, D. S. & KANG, S.-W. 2003. High glucose activates the p38 MAPK pathway in cultured human peritoneal mesothelial cells. *Kidney International,* 63**,** 958-968.

YAMANOUCHI, K., OHTA, T., LIU, Z., OJI, Y., SUGIYAMA, H., SHRIDHAR, V., MATSUMURA, S., TAKAHASHI, T., TAKAHASHI, K. & KURACHI, H. 2014. The Wilms' Tumor Gene WT1 – 17AA/− KTS Splice Variant Increases Tumorigenic Activity Through Up-Regulation of Vascular Endothelial Growth Factor in an In Vivo Ovarian Cancer Model. *Translational Oncology,* 7**,** 580-589.

YÁÑEZ-MÓ , M., LARA-PEZZI , E., SELGAS , R., RAMÍREZ-HUESCA , M., DOMÍNGUEZ-JIMÉNEZ , C., JIMÉNEZ-HEFFERNAN , J. A., AGUILERA , A., SÁNCHEZ-TOMERO , J. A., BAJO , M. A., ÁLVAREZ , V., CASTRO , M. A., DEL PESO , G., CIRUJEDA , A., GAMALLO , C., SÁNCHEZ-MADRID , F. & LÓPEZ-CABRERA , M. 2003. Peritoneal Dialysis and Epithelial-to-Mesenchymal Transition of Mesothelial Cells. *New England Journal of Medicine,* 348**,** 403-413.

YOSHIZAWA, H., MORISHITA, Y., WATANABE, M., ISHIBASHI, K., MUTO, S., KUSANO, E. & NAGATA, D. 2015. TGF-beta(1)-siRNA delivery with nanoparticles inhibits peritoneal fibrosis. *Gene Ther,* 22**,** 333-40.

YU, M. A., SHIN, K. S., KIM, J. H., KIM, Y. I., CHUNG, S. S., PARK, S. H., KIM, Y. L. & KANG, D. H. 2009. HGF and BMP-7 ameliorate high glucose-induced epithelial-to-mesenchymal transition of peritoneal mesothelium. *J Am Soc Nephrol,* 20.

YUNG, S. & CHAN, T. M. 2007. Mesothelial cells. *Perit Dial Int,* 27 Suppl 2**,** S110-5.

ZHANG, C. & KLYMKOWSKY, M. W. 2009. Unexpected functional redundancy between Twist and Slug (Snail2) and their feedback regulation of NF-kappaB via Nodal and Cerberus. *Dev Biol,* 331**,** 340-9.

ZHANG, J., TIAN, X. J., ZHANG, H., TENG, Y., LI, R., BAI, F., ELANKUMARAN, S. & XING, J. 2014. TGF-beta-induced epithelial-to-mesenchymal transition proceeds through stepwise activation of multiple feedback loops. *Sci Signal,* 7**,** ra91.

ZHANG, L., LIU, F., PENG, Y., SUN, L. & CHEN, G. 2013. Changes in expression of four molecular marker proteins and one microRNA in mesothelial cells of the peritoneal dialysate effluent fluid of peritoneal dialysis patients. *Exp Ther Med,* 6**,** 1189-1193.

ZHANG, W., FREICHEL, M., VAN DER HOEVEN, F., NAWROTH, P. P., KATUS, H., KÄLBLE, F., ZITRON, E. & SCHWENGER, V. 2016. Novel Endothelial Cell-Specific AQP1 Knockout Mice Confirm the Crucial Role of Endothelial AQP1 in Ultrafiltration during Peritoneal Dialysis. *PLoS ONE,* 11**,** e0145513.

ZHOU, B., MA, Q., RAJAGOPAL, S., WU, S. M., DOMIAN, I., RIVERA-FELICIANO, J., JIANG, D., VON GISE, A., IKEDA, S., CHIEN, K. R. & PU, W. T. 2008. Epicardial progenitors contribute to the cardiomyocyte lineage in the developing heart. *Nature,* 454**,** 109-13.

ZHOU, Q. & YU, X. 2016. Isolation and Propagation of Rat Peritoneal Mesothelial Cells. *Methods Mol Biol,* 1397**,** 25-34.

ZOLAK, J. S., JAGIRDAR, R., SUROLIA, R., KARKI, S., OLIVA, O., HOCK, T., GUROJI, P., DING, Q., LIU, R.-M., BOLISETTY, S., AGARWAL, A., THANNICKAL, V. J. & ANTONY, V. B. 2013. Pleural Mesothelial Cell Differentiation and Invasion in Fibrogenic Lung Injury. *The American Journal of Pathology,* 182**,** 1239-1247.